Title
Calibration of *CalME* models using WesTrack Performance Data

Authors
Ullidtz, Per
Harvey, John
Tsai, Bor-Wen
et al.

Publication Date
2006-11-01

November 2006
Research Report: UCPRC-RR-2006-14

Calibration of CalME Models Using WesTrack Performance Data

Authors:
Per Ullidtz, Dynatest Consulting Inc
John Harvey, UC Davis
Bor-Wen Tsai, UC Berkeley
Carl Monismith, UC Berkeley

This work was completed as part of Partnered Pavement Research Program Strategic Plan Element 4.1:
"Development of the First Version of a Mechanistic-Empirical Pavement Rehabilitation, Reconstruction and New Pavement Design Procedure for Rigid and Flexible Pavements (pre-Calibration of AASHTO 2002)"

PREPARED FOR:

California Department of Transportation
Division of Research and Innovation Office of Roadway Research

PREPARED BY:

University of California
Pavement Research Center
Berkeley and Davis

DOCUMENT RETRIEVAL PAGE	**Report No.:** UCPRC-RR-2006-14

Title: Calibration of *CalME* models using WesTrack Performance Data

Authors: Per Ullidtz, Dynatest Consulting Inc.; John Harvey, UC Davis; Bor-Wen Tsai, UC Berkeley; and Carl Monismith, UC Berkeley

Prepared for: California Department of Transportation Division of Research and Innovation Office of Roadway Research	**FHWA No.:** CA081081A	**Date**: November 2006
Contract number: UCPRC-RR-2006-14	**Client Reference No:** UCPRC-RR-2006-14	**Status:** Stage 6 approved version

Abstract: Since 2000 the UCPRC has been developing a mechanistic-empirical (M-E) pavement design method for Caltrans. The software associated with the flexible pavement design methodology is termed *CalME*. This report presents the results of a validation and calibration study for the *CalME* software using the performance data from the FHWA's WesTrack accelerated pavement test (APT) program. This APT was conducted in the period between March 1996 and February 1999 at a site near Carson City, Nevada; all 26 initial test sections were used in the study. These sections, constructed with Superpave-type hot-mix asphalt (HMA) consisting of a single source for the aggregate and asphalt binder (PG64-28), were subjected up to approximately 5 million ESALs. HMA variables included: aggregate gradation, asphalt content, and degree of compaction.

The calibration procedure used both falling weight deflectometer (FWD) field test data and laboratory-measured properties of all the mixes. Laboratory-measured characteristics included: mix stiffness, flexural fatigue characteristics, and rutting response as determined in the SHRP-developed shear test.

Results of this *CalME* validation and calibration exercise using the WesTrack data indicated that the models selected are able to predict the performance observed on this full-scale APT experiment using actual trucks and environmental conditions at this site in western Nevada. Differences between actual and predicted performance were identified and recommendations for reducing these differences were made; e.g., modifications to laboratory testing and to shift factors relating laboratory data to field performance.

Keywords: Calibration, fatigue cracking, flexible pavement, full-scale accelerated pavement testing, Mechanistic-empirical, pavement performance, performance, response, rutting, WesTrack, calibration.

Proposals for implementation:

Related documents:

- Epps, J.A., A. Hand, S. Seeds, T. Scholz, S. Alavi, C. Ashmore, C.L. Monismith, J.A. Deacon, J.T. Harvey and R.B. Leahy, "Recommended Performance-Related Specifications for Hot-Mix Asphalt Construction," NCHRP Report 455, National Cooperative Highway Research Program, Transportation Research Board, National Research Council, Washington, D.C., 2002, 496 pp.
- Monismith, C.L., J. A. Deacon, and J.T. Harvey, WesTrack: Performance Models for Permanent Deformation and Fatigue, Pavement Research Center, Institute of Transportation Studies, University of California, Berkeley, June 2000, 373 pp.
- Ullidtz, P., J. Harvey, B.-W. Tsai, and C. L. Monismith. "Calibration of Incremental-Recursive Flexible Damage Models in *CalME* Using HVS Experiments." University of California Pavement Research Center, Davis and Berkeley. April 2006. (UCPRC-RR-2005-06)

Signatures:

P. Ullidtz **Principal Author**	J. Harvey **Co-principal Investigator**	C. L. Monismith **Co-principal Investigator**	D. Spinner **Editor**	M. Samadian **Caltrans Contract Mgr.**

DISCLAIMER

The contents of this report reflect the views of the authors who are responsible for the facts and accuracy of the data presented herein. The contents do not necessarily reflect the official views or policies of the State of California or the Federal Highway Administration. This report does not constitute a standard, specification, or regulation.

PROJECT OBJECTIVES

This study is a part of the University of California Pavement Research program to develop a mechanistic empirical (ME) pavement design method for use by Caltrans to replace existing design procedures which have been in use for the past approximately 50 years.

The overall objective of the study was to use the flexible pavement performance data from the initial 26 test sections of the FHWA's WesTrack Accelerated Pavement Test project to calibrate and validate the Classical and Incremental-Recursive models in the *CalME* software.

Executive Summary

In 2005, the California Department of Transportation (Caltrans) approved an issue memo titled "Adoption of Mechanistic-Empirical (ME) Pavement Design Method," which calls for the adoption of ME pavement design methodology to replace existing pavement design methods which have been in place since the early 1960s.

Since 2000 the University of California Pavement Research Center (UCPRC) has been supporting the Caltrans effort to adopt ME pavement design by working on a series of tasks assigned in Partnered Pavement Research Center Strategic Plan Element 4.1. This work is under the technical guidance of the Caltrans Pavement Standards Team, with the Division of Design in the lead. One of the tasks is to develop and calibrate ME flexible pavement design and models for new pavements and rehabilitation. These models have been incorporated into a draft software program called *CalME*.

The validation and calibration of the models in *CalME* was first performed using performance data from Heavy Vehicle Simulator (HVS) tests completed by the UCPRC between 1995 and 2004. The results of that work are documented in a separate report titled "Calibration of Incremental-Recursive Flexible Damage Models in *CalME* Using HVS Experiments."

The purpose of this report is to present the results of a validation and calibration study performed by the UCPRC using performance data from the Federal Highways Administration (FHWA) project commonly referred to as "WesTrack." WesTrack was an experiment performed on a closed-circuit test road facility constructed at the Nevada Automotive Test Center (NATC) near Fallon, Nevada; the experiment was named "Accelerated Field Test of Performance-Related Specifications for Hot-Mix Asphalt Construction" (Contract No. DTFH61-94-C-00004).

The WesTrack experiment had two primary objectives. The first was to continue developing performance-related specifications for hot-mix construction by evaluating how deviations from material and construction property design values impact pavement performance in a full-scale, accelerated field test. Because the WesTrack site typically experiences less than 100 mm of precipitation per year and no frost penetration, it was well suited for evaluating the direct effects of deviations of materials and construction properties on performance under traffic loading. The second was to provide some early field verification of the Superpave™ mix design procedures.

WesTrack was constructed as a 2.9-km oval loop incorporating twenty-six 70-m long experimental sections on the two tangents. The pavement cross sections consisted of various asphalt concrete (AC) mixes placed on a design thickness of 300 mm (12 in.) of aggregate base, with a thick layer of "engineered fill" below, sometimes referred to as the subgrade. The design thickness of the AC layer in all sections was 150 mm (6 in.), placed in two 75-mm lifts.

Construction was completed in October 1995, and trafficking was carried out between March 1996 and February 1999. During this period, four triple-trailer combinations composed of a tandem axle, Class 8 tractor, and a lead semi-trailer followed by two single-axle trailers, operated on the track at a speed of 64 km/h (40 mph), providing 10.3 equivalent single-axle load (ESAL) applications per vehicle pass.

The experimental variables were in the AC mix design and construction and included asphalt content, in-place (i.e., field-mixed, field-compacted) air-void content, and aggregate gradation; the main response variables were rut depth and percentage of the wheelpath area with fatigue cracking. Approximately 4.95 million ESALs were applied during the trafficking period. Several original sections failed early in the experiment; they were replaced with a mix design that duplicated the coarse-graded mix experiment in the original construction, but changed from the crushed gravel used in the original sections to a more angular, quarried andesite aggregate. The replacement sections were constructed in June 1997, after the application of approximately 2.85 million ESALs. The total experiment yielded clearly differentiated levels of permanent deformation and fatigue cracking among the experimental sections.

All 26 of the initial WesTrack test sections used the same aggregate source and conventional asphalt binder in the asphalt concrete. The experiment included three mixes with different aggregate gradations referred to as Fine, Coarse, and Fine Plus. The Fine mixes had a Superpave aggregate gradation that passed above the "Restricted Zone" in the Superpave mix design system. The Fine Plus mixes had a gradation that

was slightly finer than Fine gradation. The Coarse mixes had a gradation that passed below the Restricted Zone. For each mix type there were sections with High, Medium, and Low asphalt content, and with High, Medium, and Low air-void content with target values of 4, 8, and 12 percent, respectively. Only a few sections had replicates.

Measurements taken during the WesTrack experiment and used in this study included Falling Weight Deflectometer (FWD) deflections (in the right wheelpath and between the wheelpaths), pavement temperatures at several depths in the asphalt concrete, and pavement distress condition surveys following the FHWA Long-Term Pavement Performance protocol.

Overall, the Fine mixes had the best performance with respect to rutting. The first half-million ESALs applied to the test sections caused about twice as much rutting in the Coarse mixes as in the Fine mixes, and approximately one-third more in the Fine Plus than in the Fine mixes. The Fine Plus mixes had the best performance with respect to cracking. The Coarse mix had about five times more cracking than the Fine Plus mixes (even though the tests were of shorter duration) and the Fine mixes had about two times more cracking than the Fine Plus mixes.

The lateral traffic wander pattern on the WesTrack project was not well defined for some periods in the experiment, particularly on sections where rutting developed, which caused the trailers to follow a different path than the programmed path followed by the tractor. This is at least partly responsible for differences between measured and predicted values from *CalME*.

The validation and calibration of *CalME* using WesTrack data was performed in 2005 and 2006, after the validation and calibration of *CalME* models with HVS data.

The performance models in *CalME* are described in detail in the previous report documenting calibration of *CalME* models with HVS data[1].Two sets of models in the *CalME* software were calibrated with WesTrack data. The first, used for what is called the "Classical" mechanistic-empirical design method, is largely based on the Asphalt Institute method. This method uses a standard ESAL for the traffic load, one temperature to characterize the entire range of temperatures the asphalt concrete layer will experience, and the Asphalt Institute fatigue and unbound layers rutting equations, with an adjustment for air-void content and binder content in the asphalt concrete.

The second are used for what is called the "Incremental-Recursive" design method. In this set of models the materials properties for the pavement are updated in terms of damage as the simulation of the pavement life progresses. The Incremental-Recursive approach was used for the simulations included in this report, and is the only approach that can provide an accurate indication of pavement condition at different points during the pavement's life.

The models included in the Classical design method and the Incremental-Recursive design method in the current software were validated and calibrated in this study using WesTrack data. The research team proposes that pavement designers should begin their designs by applying either an existing Caltrans method or the Classical method. In *CalME* both of these options perform a "design" function, calculating and presenting pavement structures that meet design requirements for a predetermined number of traffic loads. Then, the lowest-cost alternatives in the set of candidate pavement structures meeting the design requirements with either of these methods should be checked by the designer with the more comprehensive and precise Incremental-Recursive method to be certain that the lowest-cost alternatives meet the design requirements. Once a final design has been selected, its Incremental-Recursive output can be used to provide a prediction of the pavement's condition across its entire life.

For calibration of the Classical method, initial layer moduli were backcalculated from Falling Weight Deflectometer (FWD) data taken very soon after the beginning of trafficking. A nonlinear subgrade was assumed in the backcalculation to obtain reasonable results for the aggregate base and subgrade moduli. The reference temperature used was 15.4ºC, which is the approximate mean annual asphalt temperature at WesTrack (corresponding to a mean annual air temperature of about 11ºC), following the approach in the Asphalt Institute method. The backcalculated moduli for the asphalt concrete were compared with laboratory

[1] Ullidtz, P., J. Harvey, B. W. Tsai, C. Monismith, "Calibration of Incremental-Recursive Flexible Damage Models in CalME Using HVS Experiments," Research Report UCPRC-RR-2005-06, University of California Pavement Research Center, Davis and Berkeley, June, 2006 (FHWA No.: F/CA/RR/2006/49).

modulus testing performed by the University of Nevada, Reno (UNR) using indirect tension and the University of California, Berkeley (UCB) using flexural beams, and it was found that the values were similar, after adjustment for different test temperatures. The backcalculated aggregate base and subgrade moduli were compared with triaxial test results, and it was found that the backcalculated moduli were within the range of values obtained from the laboratory tests.

Correlations were found between the stiffness of the aggregate base and subgrade, and the bending resistance of the layers above them, particularly the aggregate base and the asphalt concrete above it. When the asphalt concrete was stiffer, primarily due to colder temperatures, the backcalculated stiffness of the aggregate base increased. This is counter to common wisdom, which says that as the asphalt concrete becomes stiffer the confining stresses in the aggregate base are reduced and the aggregate base stiffness is therefore reduced. The hypothesis is that the stiffer asphalt concrete acts as a stiff plate that provides greater confinement to the aggregate base. This observation will continue to be checked in the future with additional calibration cases.

The service life for rutting was calculated using the Asphalt Institute's subgrade criterion equation. In the equation, the vertical strain at the top of the subgrade is used as an indicator of the structural capacity of the pavement system and does not necessarily imply that rutting should take place at the subgrade level. In the case of WesTrack, however, most of the rutting occurred in the asphalt layer and it is unlikely that the Asphalt Institute criterion would be fully applicable.

The results, presented in one table and several figures in the report, showed that the service life based on the subgrade criterion using FWD backcalculated moduli at the reference temperature was overestimated in a number of cases. Comparison of the calculated and measured rutting showed that the sections where the subgrade criterion overpredicted the rutting life were primarily those with high voids filled with asphalt values. This indicates that the shorter-than-predicted lives of the field sections were related to asphalt mix design more than the overall pavement rutting that the subgrade criterion is intended to predict. For those sections that did not have high asphalt contents or Coarse gradations, and therefore did not have severe rutting in the asphalt concrete early in the experiment, the comparison between the calculated pavement rutting life and the measured rutting was much better.

Calculation of the typical difference between the measured and calculated rutting service lives indicated that the variance between the observed and predicted number of loads to failure using the Asphalt Institute subgrade rutting criterion for the WesTrack was consistent with the variance observed when it was compared with the AASHO Road Test results during its calibration in the early 1980s.

Cracking of more than 5 percent of the wheelpath was observed on 9 of the original 26 WesTrack sections by the end of the experiment. The left wheelpath tended to have more cracking than the right wheelpath.

The predicted cracking life of the sections was determined using the Asphalt Institute criterion from the initial moduli at a reference temperature of 15.4ºC. This relation was originally calibrated using laboratory flexural beam fatigue tests. A shift factor between laboratory fatigue tests and observed cracking of 18.4 was used, based on the original field calibration correlated to 40 percent observed cracking in the wheelpaths at the AASHO Road Test. The service life for cracking was calculated with and without a factor related to compaction and mix design (referred to as the C factor) in the Asphalt Institute method that calculates reduced fatigue life for lower Voids Filled with Asphalt (VFA). Lower VFA occurs with lower asphalt contents and/or greater air voids in the compacted mix.

The observed fatigue lives on the WesTrack sections were all longer than those predicted using the Asphalt Institute fatigue criterion. This was true even when the mixes are assumed to have very good compaction, calculated using the C factor. This occurs, even though the Asphalt Institute fatigue criterion is for 40 percent of the wheelpath cracked, and was compared using WesTrack data with observed cracking set at 10 percent of the wheelpath cracked. This implies a great deal of conservatism in the design criterion compared to the WesTrack results. Setting aside the question of the number of environmental cycles, this is to be expected because the Asphalt Institute fatigue criterion was calibrated with a great deal of conservatism. The conservatism of the fatigue criterion will be addressed in another report discussing the use of *CalME* for design and reliability.

The number of load applications to 10 percent cracking would have been predicted quite well if the Asphalt Institute criterion were used without the C factor, so that the effects of volume of binder and volume of voids were accounted for through their effects on the modulus only. The prediction would have been

conservative, corresponding to a reliability of 92 percent with the standard deviation from the AASHO Road Test (98 percent with the actual standard deviation of WesTrack).

As the first step in the comparison of the Incremental-Recursive method with measured results from the WesTrack experiment, the moduli of the asphalt concrete mixes measured by different methods were compared. The measured moduli were then compared with predicted moduli calculated using the equations in the *Guide for Mechanistic-Empirical Design of New and Rehabilitated Pavement Structures* (MEPDG) that use laboratory binder test data and mix volumetric information. Laboratory results included indirect tension tests performed by UNR, and flexural beam and simple shear tests performed by UCB. Moduli were also backcalculated from FWD deflection data. A detailed comparison was made for one section, and more general comparisons with the remaining sections. The results indicated general agreement between the various measured values, with the flexural frequency sweeps somewhat lower than the other laboratory and field measured results.

Master curves, which predict asphalt concrete moduli for a wide range of temperatures and load durations were fit through the data, and also calculated using the MEPDG equation using binder test results and mix volumetrics.

The results showed that the MEPDG equation for predicting the master curve from binder data and mix volumetrics predicted stiffnesses that were greater than those backcalculated from FWD data and laboratory testing. An earlier version of the MEPDG equation (Witczak and Fontana) produced a master curve that was closer to the measured values, as shown in two figures in the report.

Age hardening of the mix was evaluated from moduli backcalculated from FWD deflections measured outside the wheelpaths. Age hardening was observed over the duration of the experiment as shown in one figure in the report. The measured aging was checked against the MEPDG age hardening models. While the intermediate results in the calculation sometimes did not appear reasonable, the final predicted age hardening matched fairly well with the measured results. Asphalt moduli measured in the laboratory on cores taken just after construction and at later times in the experiment did not show consistent results.

Aggregate base moduli backcalculated from FWD deflections taken across the duration of the experiment showed an opposite trend compared to moduli calculated from triaxial results and calculated bulk stresses, as shown in two figures. The backcalculated moduli showed greater moduli in the winter when asphalt temperatures were colder, whereas the triaxial results and calculated bulk stresses showed a decrease in moduli during the winter. Backcalculated subgrade moduli generally matched subgrade moduli calculated from triaxial results.

Incremental-Recursive damage equations were fit using flexural fatigue beam data for fatigue cracking, and using Repeated Simple Shear Test at Constant Height (RSST-CH) data for rutting of the asphalt mix. Same laboratory-to-field shift factors were used for all sections, in the first set of simulations. Based on these results the Coarse mix sections were rerun with a shift factor of 5. For some sections, laboratory compacted specimens compacted to the as-built air-void content were used. These tended to give parameters that overestimated the field rutting performance compared with parameters from trafficked field cores. Some of the asphalt mixes, particularly those with High air-voids (12 percent target air-voids) had significant densification in the first several months of trafficking. The vertical rut depth caused by this densification was included in the total rut depth. In practice, for asphalt mixes compacted to 8 percent or less air-voids there should not be significant rut depth due to densification.

Parameters for rutting of the unbound layers were taken from previous HVS calibrations. Incremental-Recursive simulations were run for all sections using actual temperatures and traffic loading. The results are "incremental" in that the materials properties are updated based on damage after each period of time for the duration of the experiment.

Results are presented for the simulations of each of the original 26 WesTrack sections. The parameters used for each section are shown in tables. The results include comparison of measured and calculated values across the duration of the experiment for each section:

- Deflections under the loading plate in the wheelpath,
- Damage calculated in the asphalt concrete versus damage measured from backcalculated temperature-corrected moduli from FWD deflections versus cracking observed on the pavement surface,

- Downward rut depth in the right wheelpath calculated versus measured,
- Maximum rut depth in both wheelpaths calculated versus measured, and
- Calculated IRI versus measured in the right and left wheelpaths.

The agreement between the measured and calculated response during the duration of the WesTrack trafficking on each section, in terms of the deflection under the load plate of the FWD, was seen to be very good in most cases. The results are shown in several figures and one table in the report. The calculated deflection is a function of the following factors which are considered in *CalME*:

- The estimated asphalt temperature during the FWD test,
- The asphalt modulus versus reduced time relationship,
- The moduli of the unbound materials (aggregate base and subgrade),
- The hardening of the asphalt material as a function of post compaction and aging, and
- The damage to the asphalt caused by fatigue.

Figures in the report for each WesTrack section compare the damage, ω, predicted by *CalME*, based on the laboratory fatigue data, to the damage estimated from the FWD tests in the right wheelpath. A summary figure in the report shows the damage for all sections as predicted by *CalME* and estimated from the FWD tests. As explained above the FWD backcalculated asphalt moduli were corrected for the effects of (estimated) temperature and hardening, due to aging and decrease in air-void content. The difference between the adjusted modulus and the modulus calculated from the modulus-versus-reduced time model was then assumed to be due to damage.

On average the Fine, Coarse, and Fine Plus mixes all have less damage predicted by *CalME* than estimated from the FWD. The Coarse mix shows the largest difference, with the FWD-estimated damage being 2.2 times that of the *CalME*-predicted damage. For the Fine and the Fine Plus mixes the ratio is 1.3 and 2.0, respectively. This indicates that the shift factor of 15 is too large for the Fine and Fine Plus mixes and that the shift factor of 5 for the Coarse mix is still too high, It also shows that the shift factor should be a function of mix type. This is quite reasonable as the influence of rest periods on the fatigue life is likely to be different for different mixes.

There is also some indication that mixes with a high binder content should have a lower shift factor than mixes with a low binder content, and that mixes with a low air-void content should have a lower shift factor than mixes with a high air-void content. This would indicate that the asphalt under in situ loading is less affected by the binder and air-void content than in the laboratory fatigue tests, but it should be recalled that the uncertainties on the damage estimated from the FWD tests are very large.

The measured cracking is compared with calculated damage in one figure, which also indicates that the shift factor of 5 was too large for the Coarse mixes.

One table and one figure in the report show the mean difference between the measured down rut in the right wheelpath and the predicted permanent deformation, as well as the Root Mean Square (RMS) difference value. For comparison it may be noted that the difference between the rutting in the right and the left wheelpaths was often 3–4 mm with an RMS value of 4–5 mm.

For the sections where the required RSST-CH data were available for traffic-compacted cores, the prediction of the permanent deformation was seen to be quite good.

For the four sections where untrafficked cores were used to obtain the required RSST-CH data, prediction of the permanent deformation was greatly overestimated compared to the measured values. These simulations have not been included in the report. However, it was seen that when the as-constructed air-void content is Low or Medium the calculated and measured values are much closer than when the as-constructed air-void content is High. This suggests that the initial rapid densification applied by traffic is important to obtaining good RSST-CH parameters, and that laboratory prepared specimens should be prepared at an air-void content that is similar to that after initial trafficking, not the as-constructed air-void content.

The results of the *CalME* validation and calibration exercise using the WesTrack data indicate that the models are able to predict actual performance on this full-scale accelerated pavement testing experiment using actual trucks and actual environment. Major differences between actual and predicted performance have been

identified, the reasons have been noted, and recommendations for reducing the differences have been proposed. Examples of these recommendations include details of laboratory testing, shift factors, and need for further investigation.

CalME has now been compared to HVS testing under controlled loading and environment, and to WesTrack with its semi-controlled loading and three years of uncontrolled environment. The next steps in the validation and calibration of *CalME* are to simulate additional HVS and test track cases with different kinds of pavements and distresses, and to obtain field data from California mainline highway sections for simulation and comparison of results. Currently underway is simulation of HVS tests on thin overlays with modified binders and overlay of PCC. Data is being collected for simulation of MnROAD and NCAT Pavement Test Track sections and mainline highway sections in California.

TABLE OF CONTENTS

List of Figures

List of Tables

1 Introduction

1.1 Purpose

In 2005, the California Department of Transportation (Caltrans) approved an issue memo titled "Adoption of Mechanistic-Empirical (ME) Pavement Design Method," which calls for the adoption of ME pavement design methodology to replace existing pavement design methods that have been in place since the early 1960s.

The University of California Pavement Research Center (UCPRC) has been supporting the Caltrans effort to implement ME pavement design by working on a series of tasks assigned in Partnered Pavement Research Center Strategic Plan Element 4.1 since 2000. This work is under the technical guidance of the Pavement Standards Team, with the Division of Design in the lead. One of those tasks is to develop and calibrate ME flexible pavement design models. These models have been incorporated into a draft software program called *CalME.*

The validation and calibration of the models in *CalME* was first performed using performance data from Heavy Vehicle Simulator (HVS) tests completed by the UCPRC between 1995 and 2004. The results of that work are documented in a separate report titled "Calibration of Incremental-Recursive Flexible Damage Models in *CalME* Using HVS Experiments" (1).

The purpose of this report is to present the results of a validation and calibration study performed by the UCPRC using performance data from the Federal Highways Administration project commonly referred to as "WesTrack." The validation and calibration of *CalME* using WesTrack data was performed in 2005 and 2006, after the validation and calibration of *CalME* models with HVS data.

1.2 Background

The first step in creating a Mechanistic-Empirical (ME) pavement design or evaluation is to calculate pavement response — in terms of stresses, strains, and/or displacements — using a mathematical (or mechanistic) model. In the second step, the calculated response is used as a variable in empirical relationships to predict structural damage (decrease in moduli or cracking) and functional damage (rutting and roughness) to the pavement.

Both of these steps must be reasonably correct. If the calculated response bears little resemblance to the pavement's actual response, there is no point in trying to use the calculation to predict future damage to the pavement with the empirical relationship. In other words, only if the calculated response is reasonably correct does it make sense to try to relate the damage to the pavement response.

1.2.1 *CalME* Performance Models

The performance models in *CalME* are described in detail in Reference (1). *CalME* software provides the user with three approaches for evaluating or designing a flexible pavement structure:

- Caltrans current methods, the R-value method for new flexible structures, and the deflection reduction method for overlay thickness design for existing flexible structures.
- "Classical" mechanistic-empirical design, largely based on the Asphalt Institute method. This method uses a standard Equivalent Single Axle Load (ESAL) for the traffic load, one temperature to characterize the entire range of temperatures the asphalt concrete layer will experience, and the Asphalt Institute fatigue and unbound layers rutting equations, with an adjustment for air-void content and binder content in the asphalt concrete.
- An Incremental-Recursive method in which the materials properties of the pavement layers are updated in terms of damage as the simulation of the pavement life progresses. The Incremental-Recursive approach was used for the simulations included in this report, and is the only approach that can provide an accurate indication of pavement condition at different points during the pavement's life.

Previous versions of *CalME* included an Incremental Method, using the typical Miner's Law approach, permitting damage calculation for the axle-load spectrum and expected temperature regimes, but with no updating of materials properties through the life of the project. This is similar to the approach included in the NCHRP 1-37A Design Guide (2), also referred to as the Mechanistic-Empirical Pavement Design Guide (MEPDG). This type of approach is calibrated against an end failure state, such as 25 percent cracking of the wheelpath, and it assumes a linear accumulation of damage to get to that state. The Incremental Method has been removed from *CalME* because it does not offer many advantages over the Incremental-Recursive Method, and it is more difficult to calibrate using HVS, test track, Pavement Management System (PMS), and Long-Term Pavement Performance (LTPP) data because it requires that a pavement fail before it can be included in the calibration data set. Also, calibration of damage between pavement construction and failure cannot be performed using Miner's Law in the Incremental Method.

The models included in the Classical Method and the Incremental-Recursive Method in the current software were calibrated in this study using WesTrack data. The research team proposes that pavement designers should begin their design process by using either an existing Caltrans method or the Classical method. In *CalME* both of these options perform a "design" function, calculating and presenting pavement structures that meet design requirements for a predetermined number of traffic loads. Then, the lowest cost alternatives in the set of candidate pavement structures meeting the design requirements with either of these methods should be checked by the designer with the more comprehensive and precise Incremental-Recursive method to be certain that those structures meet the design requirements. Once a final design has been selected, its Incremental-Recursive output can be used to provide a prediction of the pavement's condition across its entire life.

1.2.2 WesTrack Experiment and Performance Results

Details of the WesTrack experiment and results are available in Reference (3). The following is a brief summary of the experiment and results to provide background for the modeling of the performance of the WesTrack sections using *CalME*, taken primarily from Reference 3.

WesTrack refers to an experimental test road facility constructed at the Nevada Automotive Test Center (NATC) near Fallon, Nevada, under the Federal Highway Administration (FHWA) project "Accelerated Field Test of Performance-Related Specifications for Hot-Mix Asphalt Construction" (Contract No. DTFH61-94-C-00004). The project was conducted by the WesTrack team, a consortium of seven public- and private-sector organizations lead by the NATC and including Granite Construction Co.; Harding Lawson and Associates; Nichols Consulting Engineers, Chtd.; Oregon State University; the University of California, Berkeley; and the University of Nevada, Reno.

The WesTrack experiment had two primary objectives. The first was to continue development of performance-related specifications (PRS) for HMA construction by evaluating the impact of deviations in materials and construction properties from design values on pavement performance in a full-scale, accelerated field test. The second was to provide some early field verification of the Superpave™ mix design procedures. Because the WesTrack site typically experiences less than 100 mm of precipitation per year and no frost penetration, it was well suited for evaluating the direct effects of deviations of materials and construction properties on performance.

WesTrack was constructed as a 2.9-km (1.8 mi) oval loop incorporating twenty-six 70-m (230 ft) long experimental sections on the two tangents. The pavement cross sections consisted of various asphalt concrete mixes placed on a design thickness of 300 mm (12 in.) of aggregate base, with a thick layer of "engineered fill" below, sometimes referred to as the subgrade in this report. The design thickness of the AC layer in all sections was 150 mm (6 in.), placed in two 75-mm lifts.

Construction was completed in October 1995; trafficking was carried out between March 1996 and February 1999. During this period, four triple-trailer combinations composed of a tandem axle, Class 8 tractor, and a lead semi-trailer followed by two single-axle trailers, operated on the track at a speed of 64 km/h (40 mph), providing 10.3 equivalent single-axle load (ESAL) applications per vehicle pass. The use of autonomous (driverless) vehicle technology provided an exceptional level of operational safety and permitted loading to occur up to 22 hours per day, 7 days per week.

The experimental variables were in the asphalt concrete mixes, and included asphalt content, in-place (i.e., field-mixed, field-compacted) air-void content, and aggregate gradation; the main response variables were rut depth and percentage of the wheelpath area with fatigue cracking. Approximately 4.95 million ESALs were applied during the trafficking period. Several original sections failed early in the experiment; they were replaced with a mix design that duplicated the coarse-graded mix experiment in the original construction, but changed from the crushed gravel used in the original sections to a more angular, quarried andesite aggregate. The replacement sections were constructed in June 1997, after the application of approximately 2.85 million ESALs. The total experiment yielded clearly differentiated levels of permanent deformation and fatigue cracking among the experimental sections.

All of the initial 26 test sections used the same aggregate source and binder in the asphalt concrete. The WesTrack experiment had three different mixes: Fine (F), Coarse (C), and Fine Plus (P), referring to the aggregate gradation. The Fine mixes had a Superpave aggregate gradation that passed above the "Restricted Zone" in the Superpave mix design system. The Fine Plus mixes had a gradation that was slightly finer than Fine gradation. The Coarse mixes had a gradation that passed below the Restricted Zone. For each mix type there were sections with high (H), medium (M), and low (L) asphalt content with target values of 4.7, 5.4, and 6.1 percent, respectively for Fine and Fine Plus mixes and 5.0, 5.7, and 6.4 percent for the Coarse mix, and with high (H), medium (M), and low (L) air-void contents with target values of 4, 8, and 12 percent, respectively.

In the naming system used for each section in this report, "FML" indicates a section with a Fine mix with a medium AC content, and a low air-void content (a 1 or 2 following the mix name would indicate whether the section was the first or the second of replicate sections).

Measurements taken during the WesTrack experiment and used in this study included Falling Weight Deflectometer (FWD) deflections, pavement temperatures at several depths in the asphalt concrete, and pavement distress condition surveys following the LTPP protocol.

Overall, the Fine mixes had the best performance with respect to rutting. The first half-million equivalent single axle loads (ESALs) applied to the test sections caused about twice as much rutting in the Coarse mixes as in the Fine mixes, and approximately one-third more in the Fine Plus than in the Fine mixes. The Fine Plus mixes had the best performance with respect to cracking. The Coarse mix had about five times more cracking than the Fine Plus mixes (even though the tests were of shorter duration) and the Fine mixes had about two times more cracking than the Fine Plus mixes.

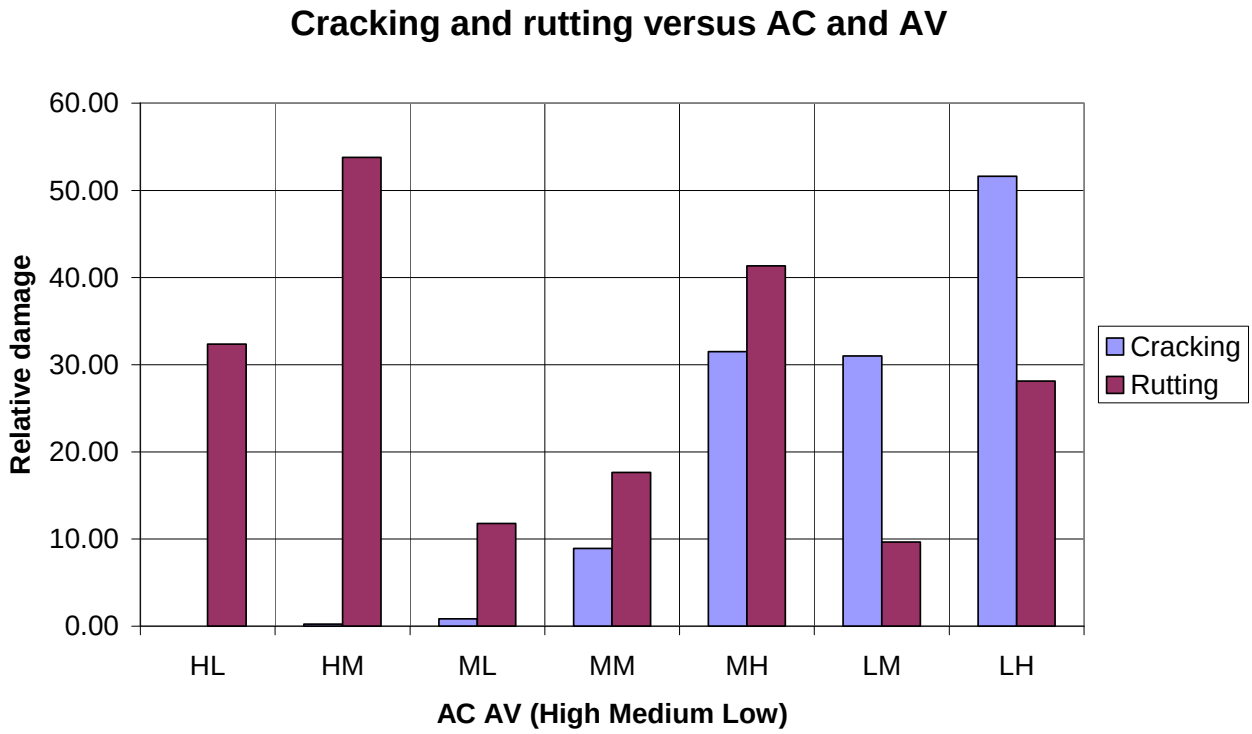

Figure 1. Average relative damage as a function of asphalt content (AC) and air voids (AV).

Figure 1 shows a relative damage index, adjusted for the differences between the mix types, to highlight the influence of binder content and air voids. Not surprisingly the high binder content results in high rutting but little cracking and the low binder content results in a large amount of cracking. For the medium binder content an increase in air voids is detrimental both with respect to cracking and to rutting.

Laboratory performance test data on the WesTrack mixes was used in this study. This primarily consisted of flexural fatigue beam and simple shear test data performed by the UCPRC during the WesTrack project. The details of those results are described in detail in Reference (4). These data are taken from the UCPRC database of WesTrack laboratory testing results.

1.3 Scope of this Report

This report describes a study using the results of the WesTrack project to calibrate the Mechanistic-Empirical (ME) models in *CalME*. The first section deals primarily with the "Classical" design method, mostly based on the Asphalt Institute's procedure, and the second part with predictions made using *CalME*'s incremental-recursive procedure. The first section, however, also has some comments on FWD testing, traffic loads, and other details, which are relevant for the incremental-recursive modeling in the second part.

2 Classic ME Design Procedure

2.1 Backcalculation of Layer Moduli

Layer moduli were backcalculated from the first FWD session in early March 1996 using *Elmod5* (5), with results shown in Table 1. At that point in time the accumulated number of ESALs was about 4,500 (431 laps), so some damage could already have occurred. To avoid the transition zone between test sections on the track only test points with section chainages between 30 m and 65 m were used. To get the initial, undamaged moduli the tests done between the wheelpaths (files named "F1") were used.

The asphalt concrete (AC) layer thicknesses were obtained from the table "Avg_In_place AV and Thickness (UNR)" in the WesTrack database (3), shown in Table 1. The thickness of the aggregate base (AB) was assumed to be 300 mm. The subgrade was assumed to be non-linear elastic following Equation 1:

$$E = C \times \left(\frac{\sigma_1}{p} \right)^n$$

Equation 1. Nonlinear model for subgrade.

where σ_1 is the major principal stress,
p is a reference stress (0.1 MPa ≈ atmospheric pressure), and
C and n are constants (n was kept at -0.2 in all of the backcalculations).

If the subgrade is treated as a linear elastic material the modulus of the subgrade will be overestimated and that of the aggregate base will be underestimated. This problem is well known, and is sometimes referred to as the "inverted layer effect." It can be seen, for example, in Table 149, page 232 of the NCHRP 455 report (3), where the modulus of the subgrade is larger than the modulus of the aggregate base.

During the FWD tests the asphalt surface temperature was recorded. This temperature was used with the BELLS equation to determine the AC temperature at a depth of 50 mm. The previous day's average air temperature (required as an input to BELLS equation) was obtained from the "DailyWeather (NCE)" table in the WesTrack database.

The temperature was also measured with thermocouples at test sections 12 and 25, at a number of depths, and the temperature at 50 mm depth was determined by interpolation. Unfortunately thermocouple data is missing for some of the points in time where FWD tests were carried out.

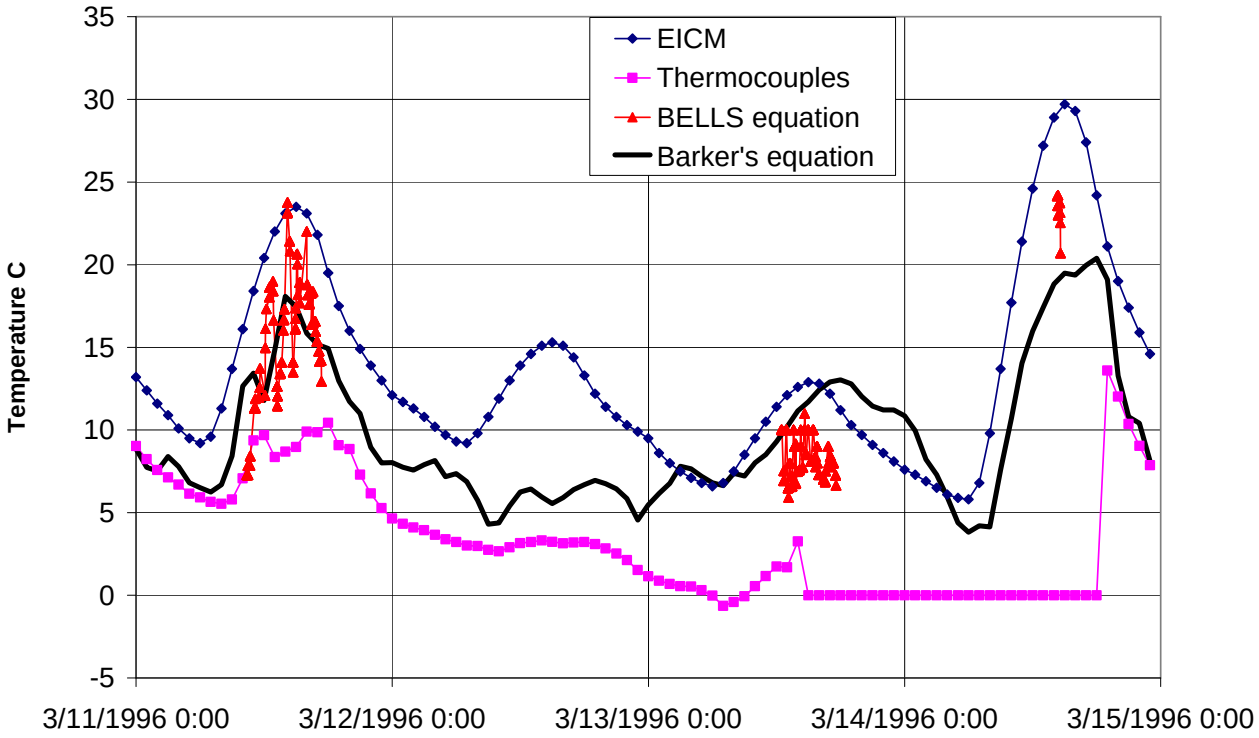

Figure 2. Temperature at 50 mm depth during the first FWD session.

For most of the testing shown in Figure 2 the temperatures recorded by the thermocouples are significantly lower than the temperatures calculated from BELLS equation. Figure 2 also shows the temperature at a depth of 50 mm calculated with the Enhanced Integrated Climate Model (EICM) and with Barker's equation for asphalt temperature as a function of air temperature during daytime (6):

$$T_{asphalt} = 1.2 \times T_{air} + 3.2\ ^{\circ}C$$

Equation 2. Barker's equation for asphalt temperature as a function of surface temperature.

During the first two-and-a-half days the thermocouples recorded a lower temperature than the other three methods. After the break in thermocouple recording on March 14–15, the values appeared to be much closer to the other methods.

At Test Section 6 (Coarse mix/Medium AC content/High voids content, CMH) the BELLS temperature was calculated as about 21ºC and the temperature recorded by the thermocouples was about 9ºC.

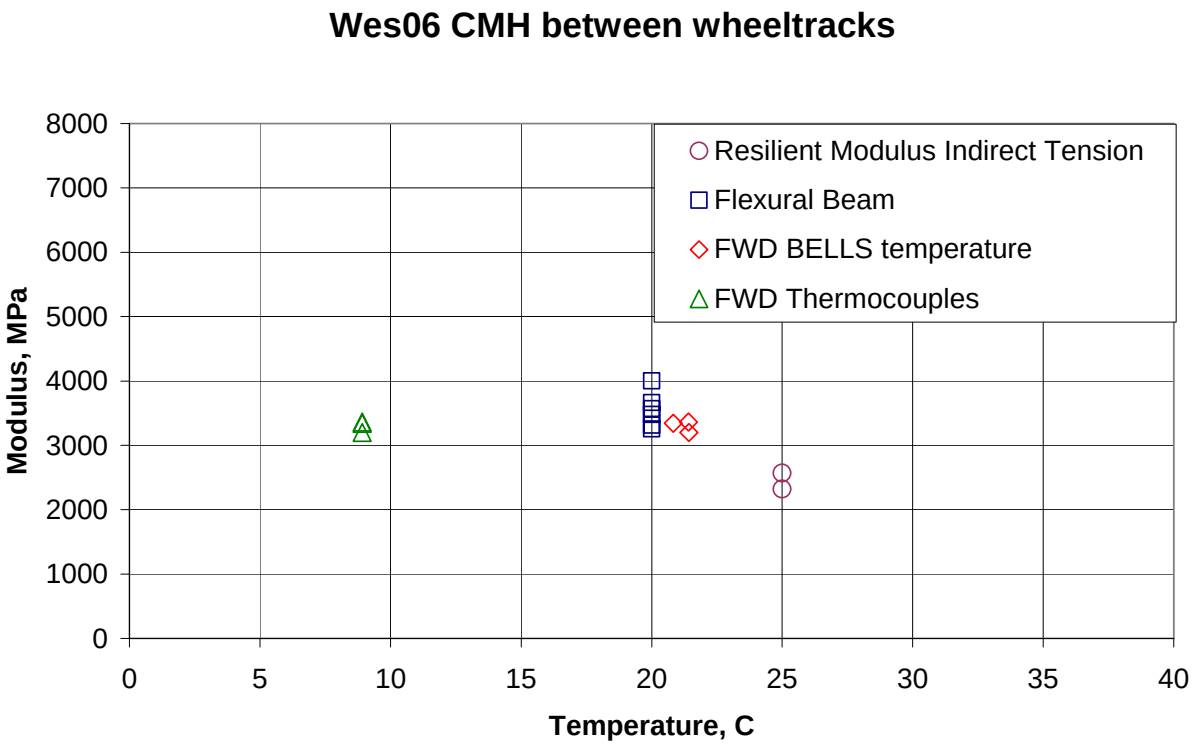

Figure 3. Modulus versus temperature for Section 6.

The resilient modulus of the mix at Section 6, see Figure 3**,** was determined at 25ºC by the University of Nevada, Reno [Table "Avg_Res Modulus – HMA (UNR)" in the WesTrack database, from indirect tensile tests]. The legend "Flexural Beam" is for initial modulus determined during bending beam fatigue testing at University of California, Berkeley (from the UCPRC database, "Fatigue_RSST.mdb"). The fatigue testing was done at 20ºC.

The backcalculated moduli from FWD testing during Session 1 are also shown in Figure 3, plotted at the BELLS temperature and at the thermocouple temperature. The backcalculated moduli are in much better agreement with the laboratory moduli at the BELLS temperature than at the thermocouple temperature.

An explanation could be that the thermocouples were not recording the correct temperature during the first part of the experiment, and may have been recalibrated during the break in thermocouple recording.
The temperature adjustment for Table 1 was done using a simple exponential relationship:

$$E(t) = E(t_{ref}) \times \exp(a \times [t - t_{ref}])$$

Equation 3. Modulus versus temperature relationship.

where $E(t)$ is the modulus at temperature tºC,
t_{ref} is a reference temperature, and
a is a constant.

The reference temperature used was 15.4ºC which is the approximate mean annual asphalt temperature at WesTrack (corresponding to a mean annual air temperature of about 11ºC), following the approach in the Asphalt Institute method (7). The constant a was -0.06322 for the Fine mix (F), -0.07 for the Coarse mix (C), and -0.08 for the Fine Plus mix (P). These values were estimated from resilient modulus and bending beam tests on the mixes.

Table 1. Backcalculated Layer Moduli

Section	Mix	AC, mm	E AC, MPa	At Temp, ºC	E AC at 15.4ºC	E AB, MPa	E SG, MPa
1	FMM1	160	5127	8.1	3239	219	72
2	FLM	157	5662	12.5	4729	224	78
3	FLH1	163	4074	18.5	4957	99	74
4	FML	155	6401	12.2	5226	234	88
5	CMM1	153	3895	16.7	4255	217	70
6	CMH	150	3301	21.2	4962	102	61
7	CHM	154	4030	16.6	4379	130	63
8	CLM	152	4142	18.6	5185	117	62
9	PHL2	155	3428	22.5	6062	119	71
10	PLH	147	2704	17.9	3312	98	78
11	PMM2	155	4136	17.9	5045	148	82
12	PML	150	5579	15.4	5559	176	82
13	PHM	157	4122	13.9	3651	174	78
14	FHM	155	7970	7.2	4757	198	109
15	FMM2	155	6704	6.4	3783	217	110
16	FLH2	160	4549	6.7	2631	123	82
17	FMH	160	5169	7.4	3109	119	79
18	FHL	155	9661	7.6	5894	375	126
19	PMM1	157	7715	7.7	4176	157	96
20	PMH	157	4788	8.5	2761	115	76
21	PHL1	160	8909	8.1	4974	185	93
22	PLM	152	7241	8.2	4081	144	102
23	CML	147	8159	7.3	4631	155	70
24	CMM2	170	6009	7.0	3344	108	57
25	CHL	154	8437	8.2	5108	170	80
26	CLH	170	4012	7.1	2245	101	61

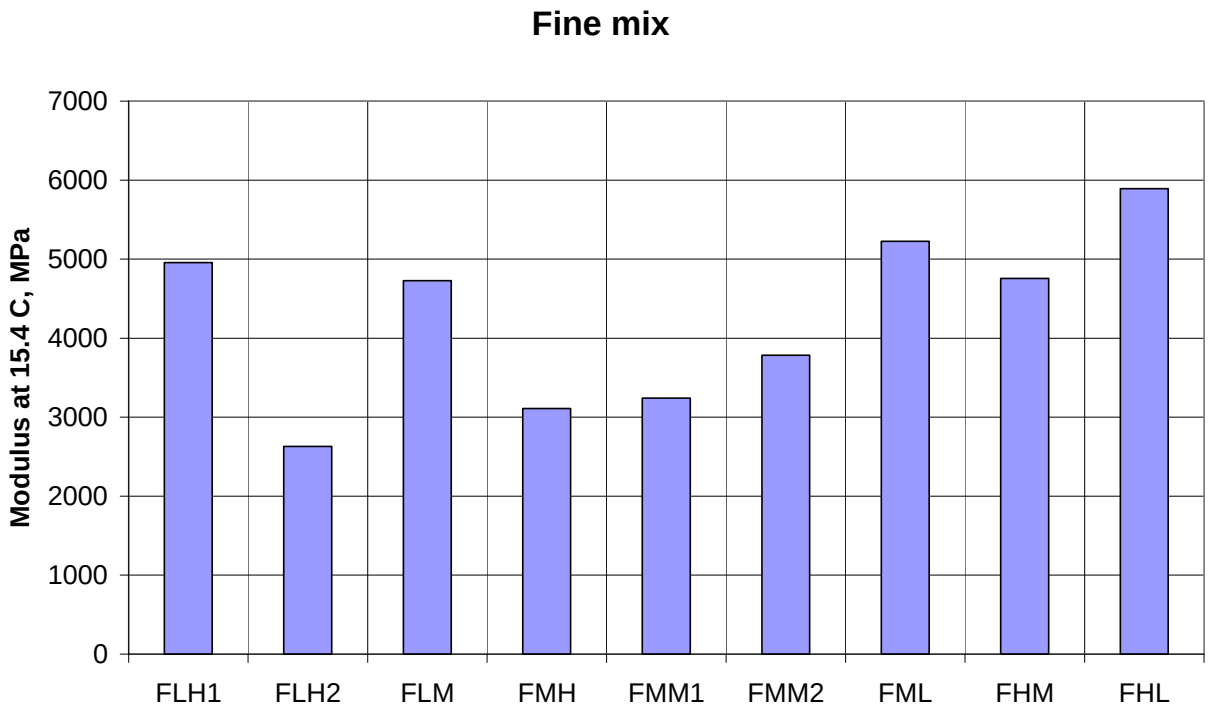

Figure 4. Backcalculated moduli of Fine mix sections.

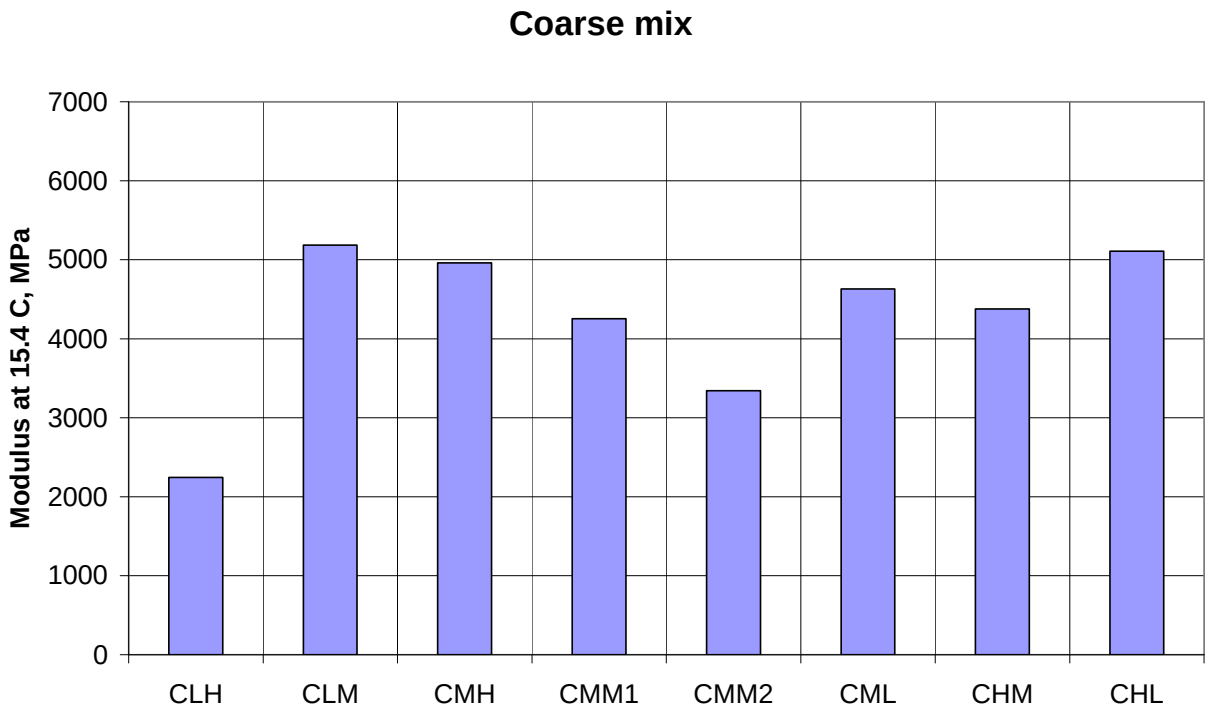

Figure 5. Backcalculated moduli of Coarse mix sections.

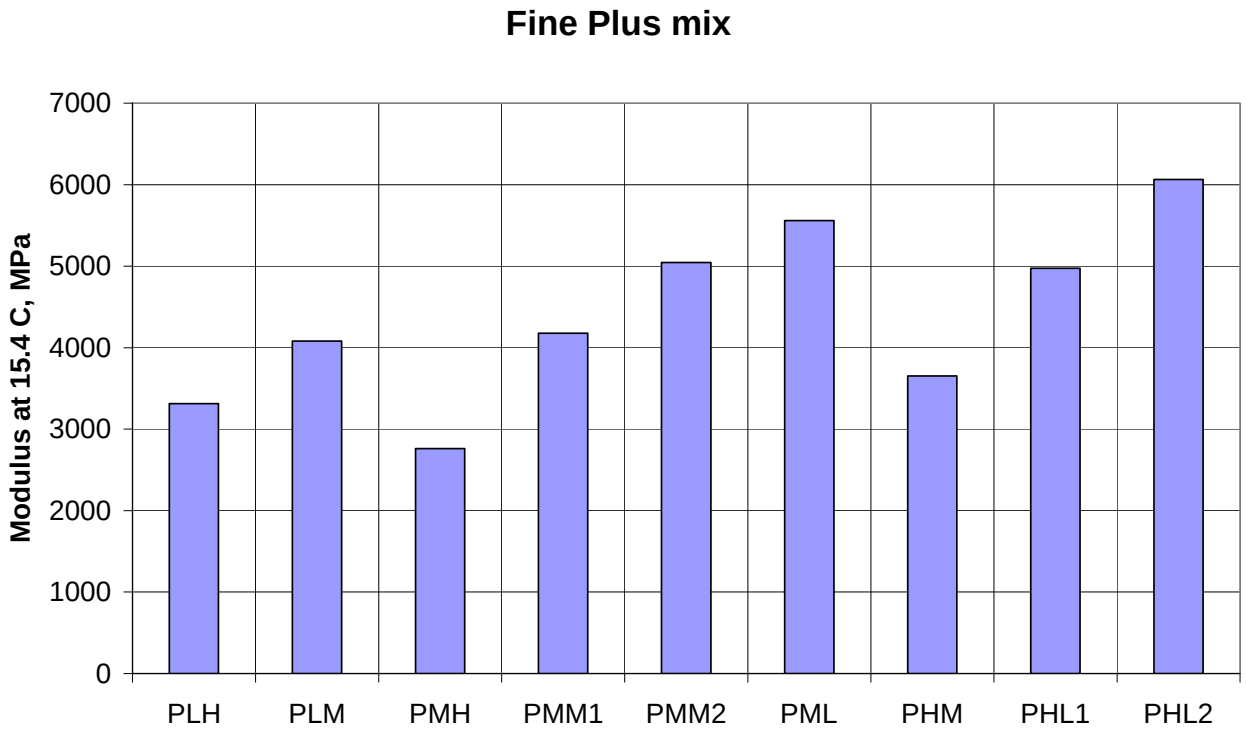

Figure 6. Backcalculated moduli of Fine Plus mix sections.

The Fine mix and the Fine Plus mix both have a clear trend with increasing modulus for decreasing voids content.

Only the AC modulus was adjusted for temperature, although the moduli of the unbound materials also showed a clear trend with temperature. There was considerable scatter in the backcalculated moduli, particularly for the AB. To characterize the moduli of the unbound layers as a function of the layers above [AC above the AB; AC and AB above the subgrade (SG)], the following relations were developed:

$$E_{AB} = 257\,MPa \times \left(1 - \left[1 - \frac{S}{3500^3}\right] \times 0.73\right),\ R^2 = 0.28,\ SEE = 52\,MPa$$

$$E_{SG} = 62\,MPa \times \left(1 - \left[1 - \frac{S}{3500^3}\right] \times 0.32\right),\ R^2 = 0.53,\ SEE = 11\,MPa$$

$$S = \left(\sum_{1}^{n-1} h_i \times \sqrt[3]{E_i}\right)$$

Equation 4. Moduli of unbound layers as a function of stiffness of layers above.

where h_i is the thickness of layer i above the layer of interest, in mm, and
E_i is the modulus of layer i above the layer of interest in MPa.

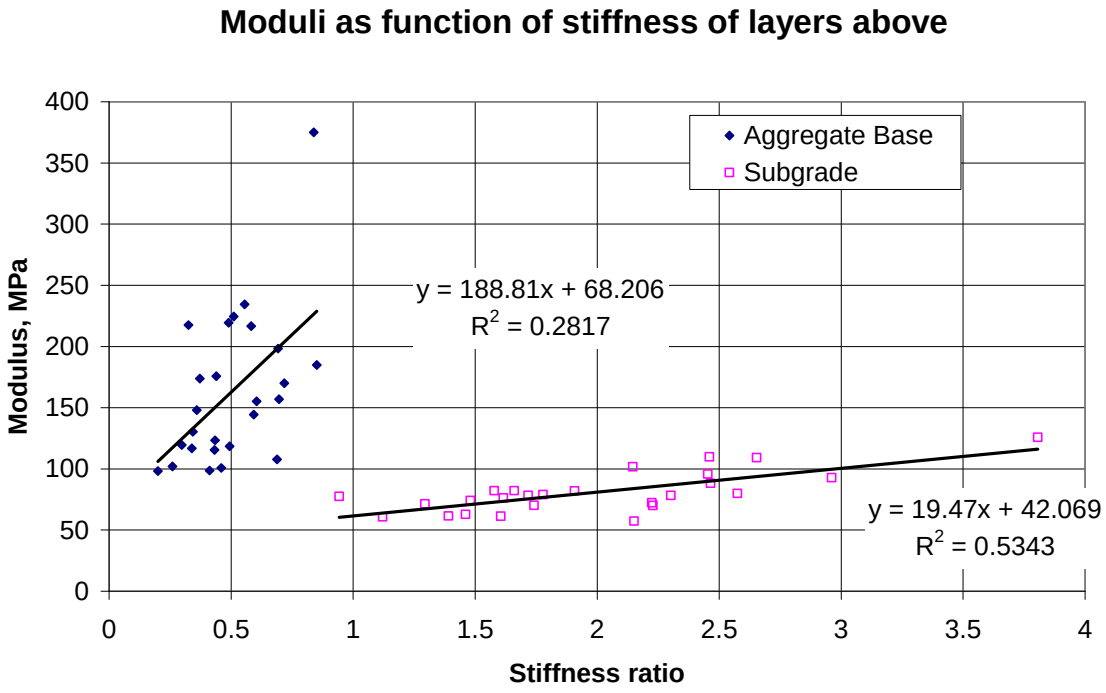

Figure 7. Correlation between moduli of unbound layers and stiffness ratio of layer above to given layer (S/35003 in Equation 4), all sections.

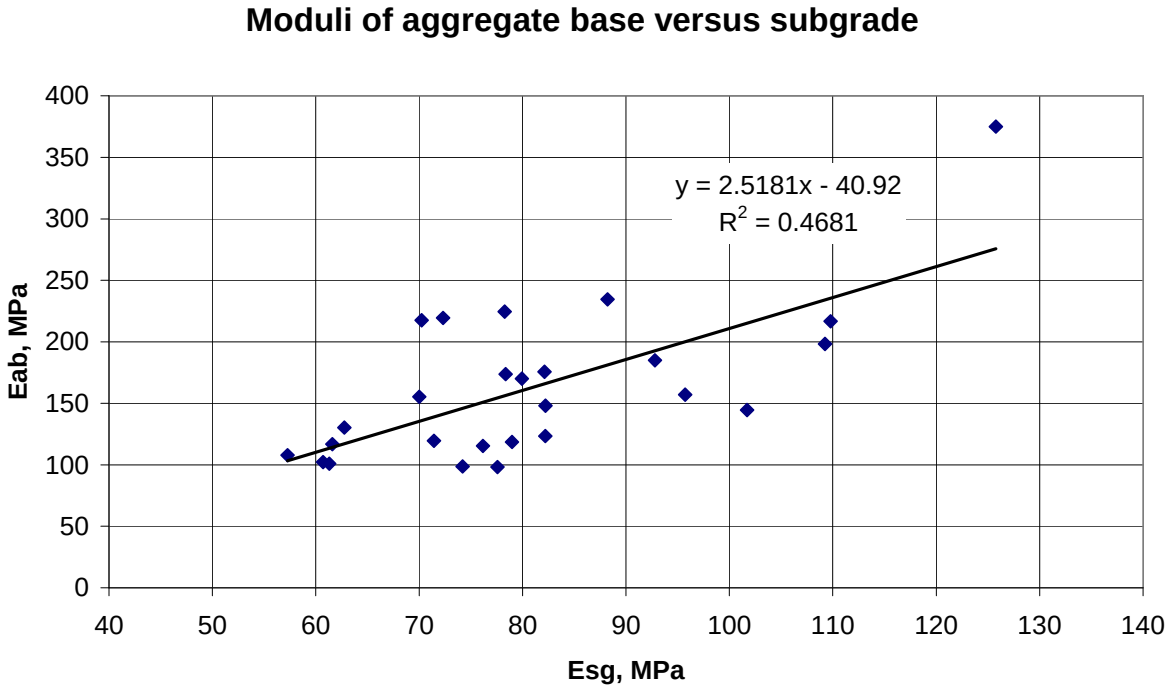

Figure 8. Moduli of aggregated base as a function of the moduli of the subgrade (March 1996).

Figure 8 indicates that the modulus of the AB is also a function of the modulus of the subgrade.

For comparison, resilient moduli from triaxial testing on samples of the AB (Figure 43) range between 70 and 230 MPa, depending upon bulk stress applied in the test. Subgrade resilient moduli (Figure 44) from triaxial testing range between 20 and 160 MPa, depending upon deviator stress applied in the test. FWD tests done directly on the subgrade gave moduli of 103 to 113 MPa in October 1994; 33 to 40 MPa in February 1995; and 25 to 69 MPa in April 1995.

2.2 Loads

The trucks used at WesTrack had a steering wheel (single tire) with an axle load of 53 kN (12,000 lbs) and 7 axles loaded to 89 kN (20,000 lbs) with dual wheels. Two of these were in a tandem axle, but they have been treated as two individual axles. The tire pressure was 0.69 MPa (100 psi) for all wheels. For the dual wheels a distance of 300 mm (12 in.) was assumed between tire centers. The passage of one truck corresponds to 10.48 ESALs, with a power of 4.

The wander pattern of the wheels is shown in Figure 9, Figure 10, Figure 11, and Figure 12 (8). The locations are given in 1-inch increments, i.e., 1R is one inch to the right of the wire embedded in the pavement to guide the trucks. "Off" means that the antenna was off and the position is not known.

For the first 480,000 ESALs a little less than half of the loads were in the center of the wheelpath. During the next two periods, during which 1,320,000 ESALs were applied, the wheels were located far to the left and the right of the track center, and in the last period, during which 3,150,000 ESALs were applied, the wander pattern was more widely distributed. This succession of wander patterns may have had an influence on the development of rutting, as indicated by Figure 13, which shows the downward permanent deformation in the wheelpath below the original pavement surface (neglecting upward bulging of material at the sides of the wheelpath; see next section on measured rut depth). During the first period, where a large proportion of the loads are in the centerline, there is a steep increase in rutting. In the second and third period (combined in Figure 13) the rutting progressed very slowly, possibly because the wheels were positioned on the upward humps at the sides of the wheelpath created during the first period. In the last period the rutting again started increasing, even though this was during winter, when little rutting is expected.

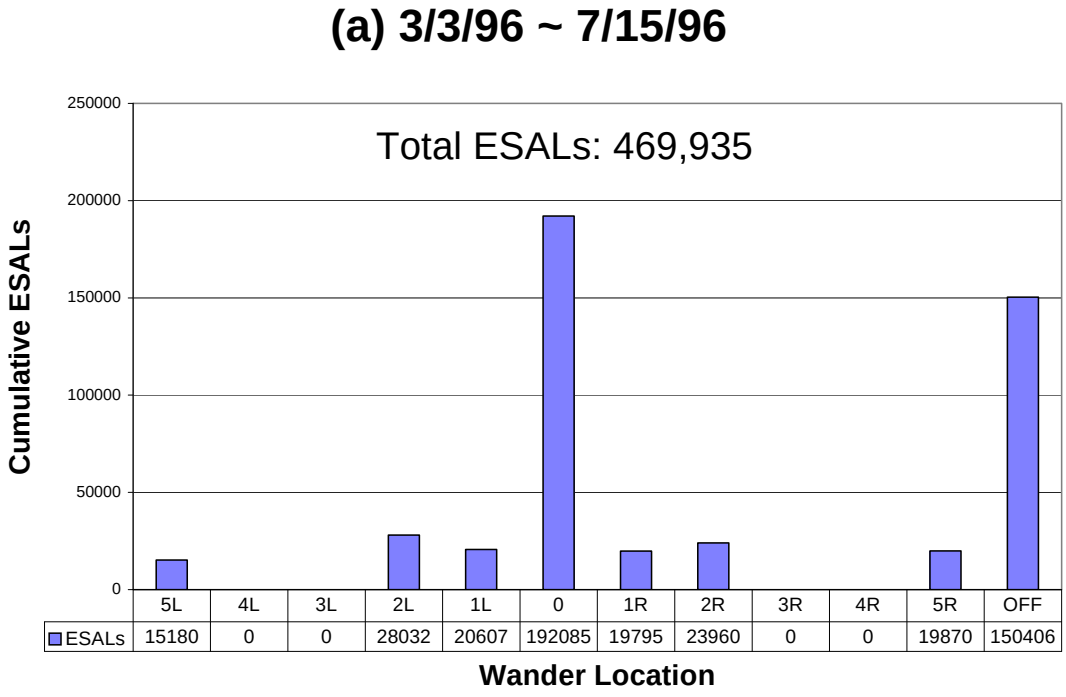

Figure 9. Wheel locations from March 3 to July 15, 1996.

(b) 7/16/96 ~ 12/14/96

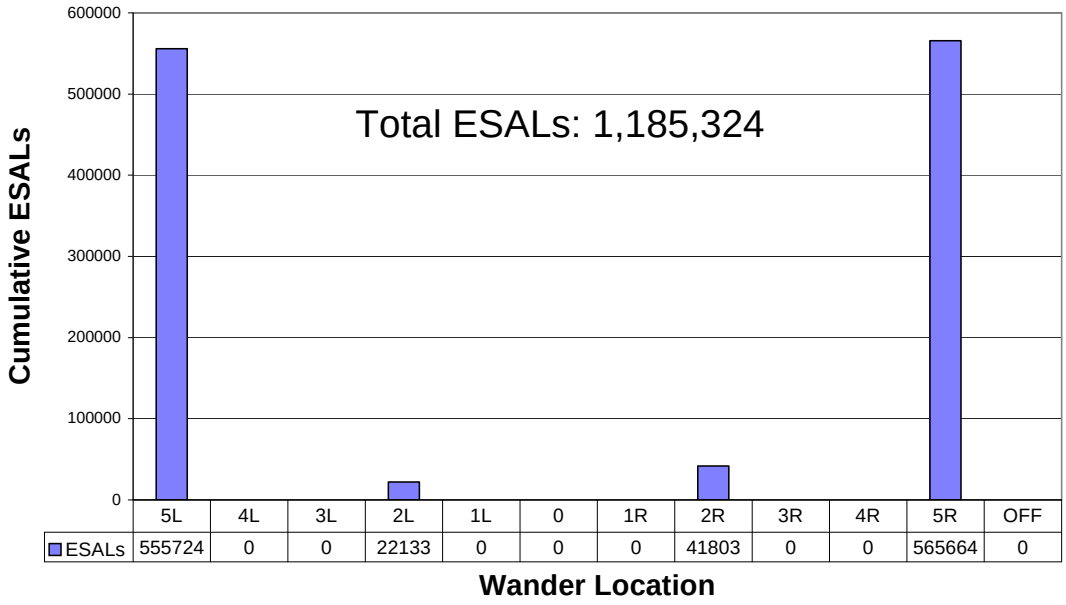

Figure 10. Wheel locations from July 16 to December 14, 1996.

(c) 12/15/96 ~ 2/18/97

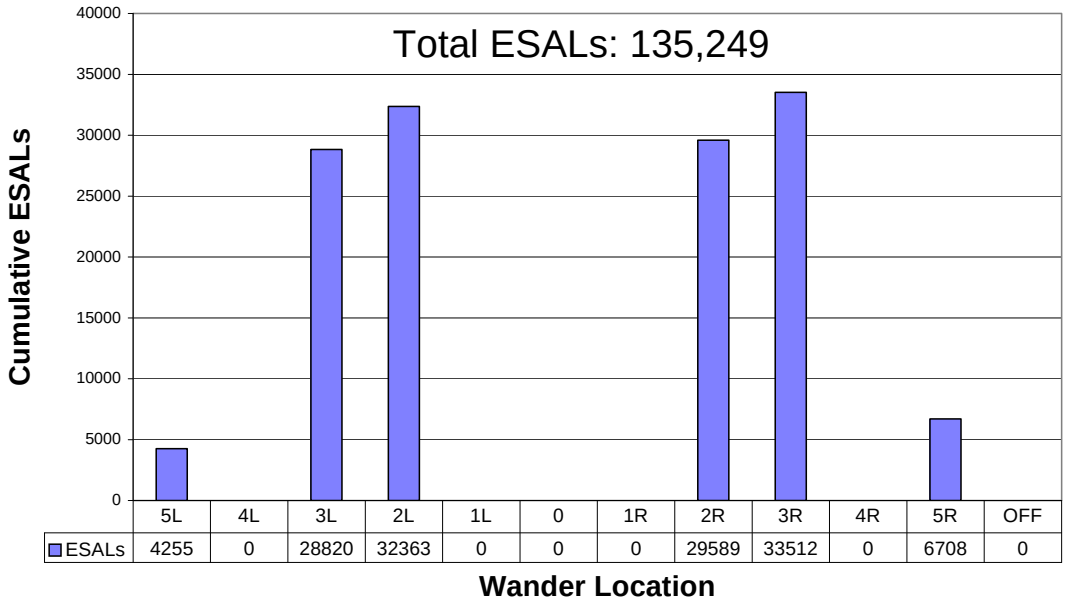

Figure 11. Wheel locations from December 15, 1996, to February 18, 1997.

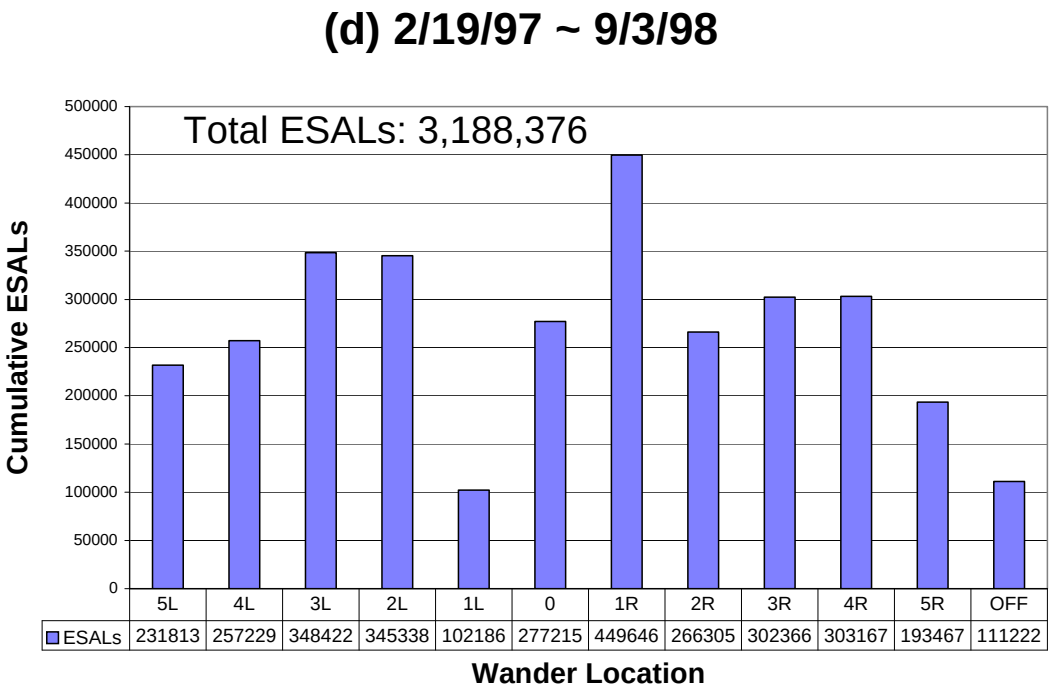

Figure 12. Wheel locations from February 19, 1997, to March 9, 1998.

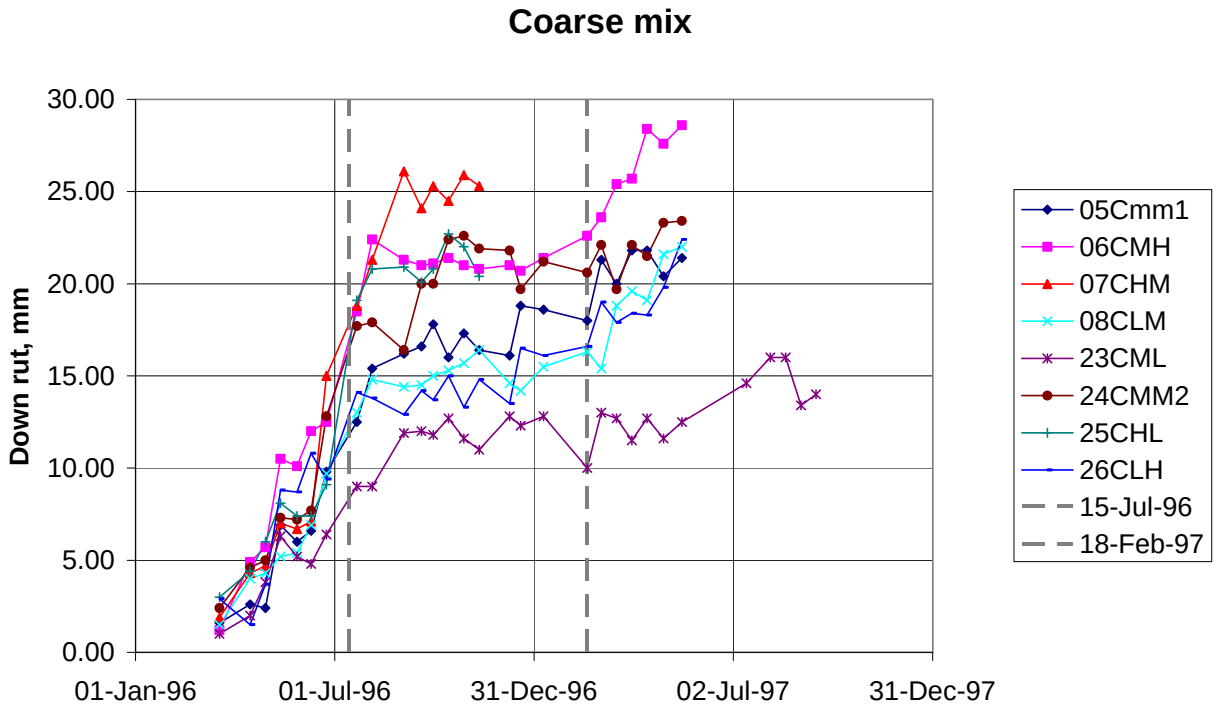

Figure 13. Downward rut below original pavement surface on the Coarse mix sections during the periods with different wander patterns.

The wander patterns shown above are for the antenna positions. The wheels of the trucks did not always follow the antenna position as shown in Figure 14 from Reference 3.

The following is a quote from NCHRP Report 455 (3) regarding Figure 14:

> …shows the path that WesTrack Truck 1 (WT-1) with its front axle centered, followed down the south tangent on August 9, 1997. These data indicate that the truck had a tendency to weave rather than follow the guidewire and that the rear antenna (located on the third trailer's rear axle) was always offset down the cross-slope of the pavement. This off-set between the front antenna (front or steering axle of tractor) and the rear antenna (rear axle of third trailer) is of the order of 200 mm (8 in.) to 250 mm (10 in.). Similar sets of data collected on the other trucks at WesTrack is reported in WesTrack Technical Report NCE-6 (57) and indicates a varying amount of cross-slope induced antenna offset. Because the trucks and their guidance systems were essentially identical, it was assumed that the difference in cross-slope induced wander (offset) was due to differences in the front antenna locations relative to the wheelpath rutting.

In addition to this observation, it has been observed that once the ruts start forming there is a tendency for the wheels to track in the wheelpaths. The Classical procedure does not explicitly consider wander.

In the first simulations of WesTrack with the *CalME* Incremental-Recursive procedure (described in the next chapter) it was assumed that the wheels would be at the centerlines of the wheelpaths once the rut depth exceeded 6 mm (0.25 inches). Because of these uncertainties it was eventually decided to not consider any wander in the Incremental-Recursive simulations. This decision had little influence on the results because 6 mm of rutting is reached very early for most sections, normally within the first four months, during which time there was little programmed wander for the trucks.

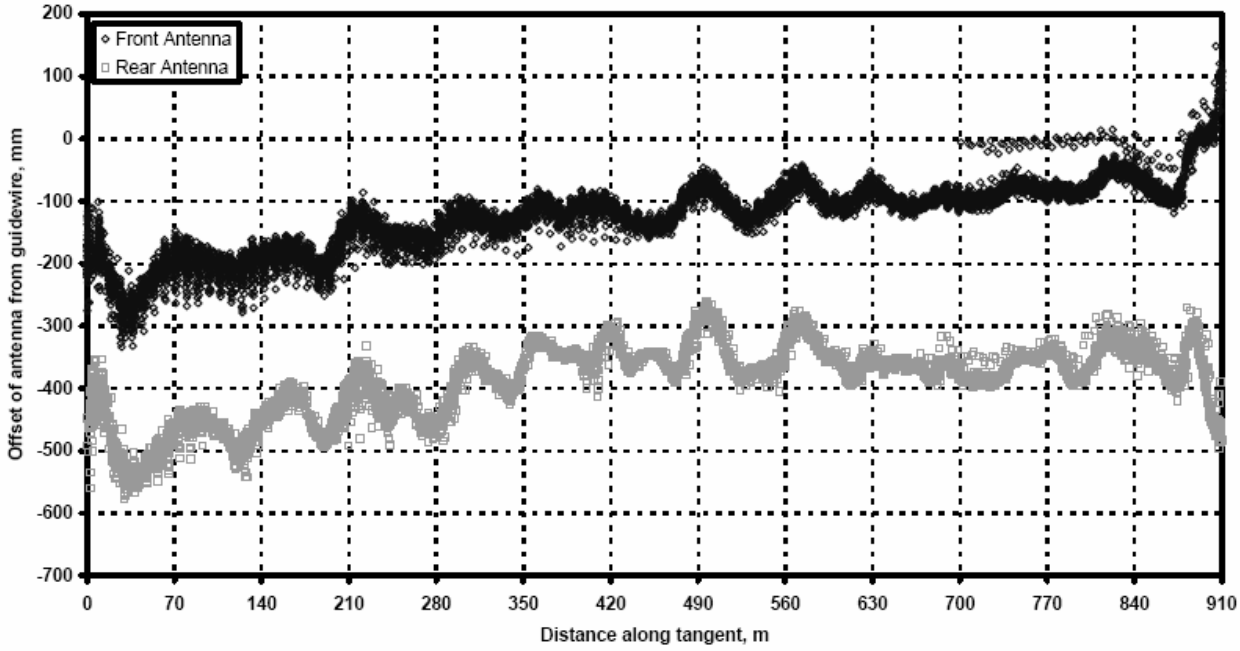

Truck path down south tangent (WT-1, antenna centered, date 8/9/97) (1 in. = 25.4 mm).

Figure 14. Positions of front and rear axles, with the antenna in the centerline (3).

2.3 Measured Rut Depth

The table "Avg_Down Rutting (NCE)" from the WesTrack database was used. The table contains the averaged downward rut below the original pavement surface in the right wheelpath, referred to after this as the

"down rut." The table "Avg_Max Rutting (NCE)" shows that there may be large differences in the rutting measured in the two wheelpaths, but the variation appears to be random.

The down rut is shown versus time for all of the original mixes in Figure 15 to Figure 17. It can be seen that all of the Coarse mixes and some of the Fine Plus mixes were severely rutted by the end of six months of trafficking, and were removed from service before the end of the experiment. This means that the temperature regimes across the life of the different sections were different, which may be of importance when comparing to the "Classical" prediction of service life. For a normal classical design the service life would be more than 10 years, therefore the performance of these sections is outside the data set used for calibration of the classical design. A key difference would be the environmental conditions to which these WesTrack sections were exposed, part of one annual cycle, versus those of the sections used to calibrate the method that were exposed to numerous cycles.

It may also be noted that for those sections that remained in service to the end of the experiment, most of the rutting occurred during the first spring and summer.

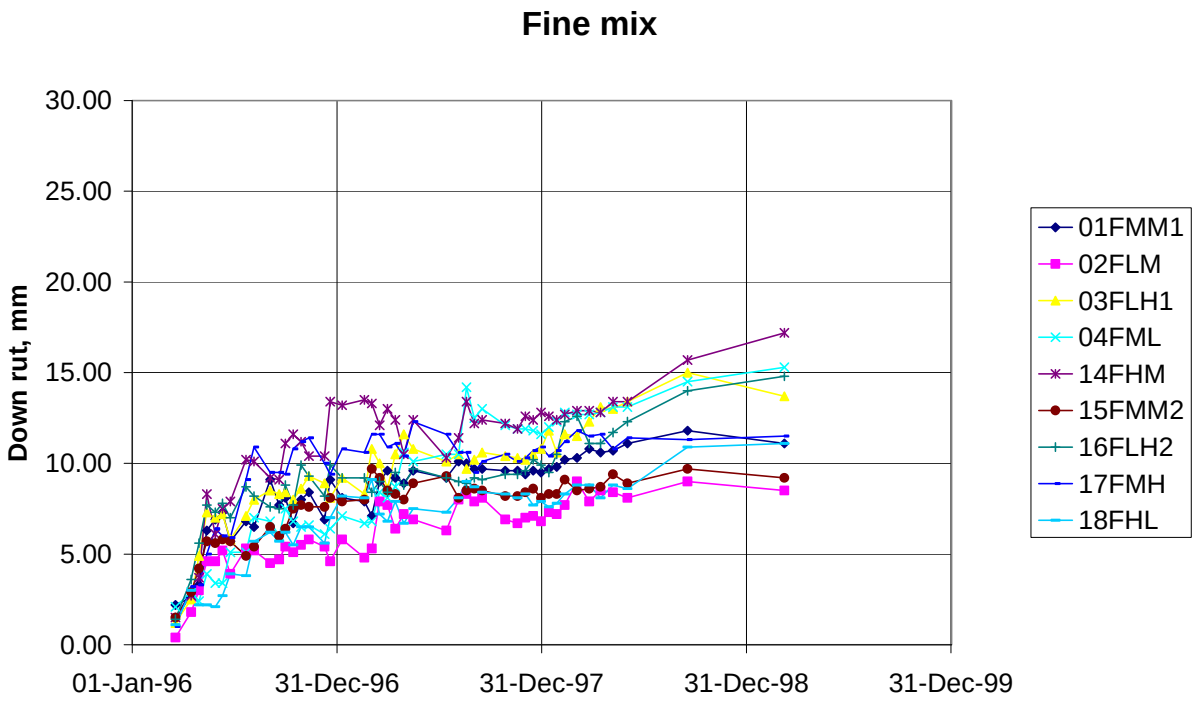

Figure 15. Down rut for Fine mixes.

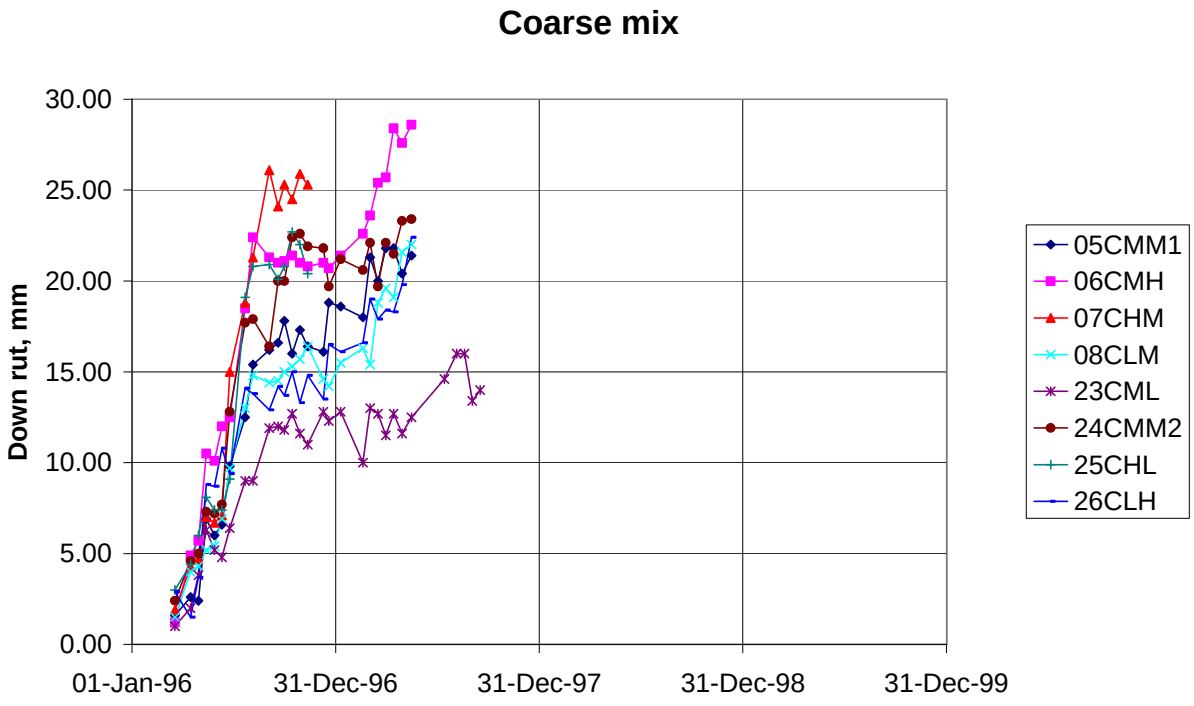

Figure 16. Down rut for Coarse mixes.

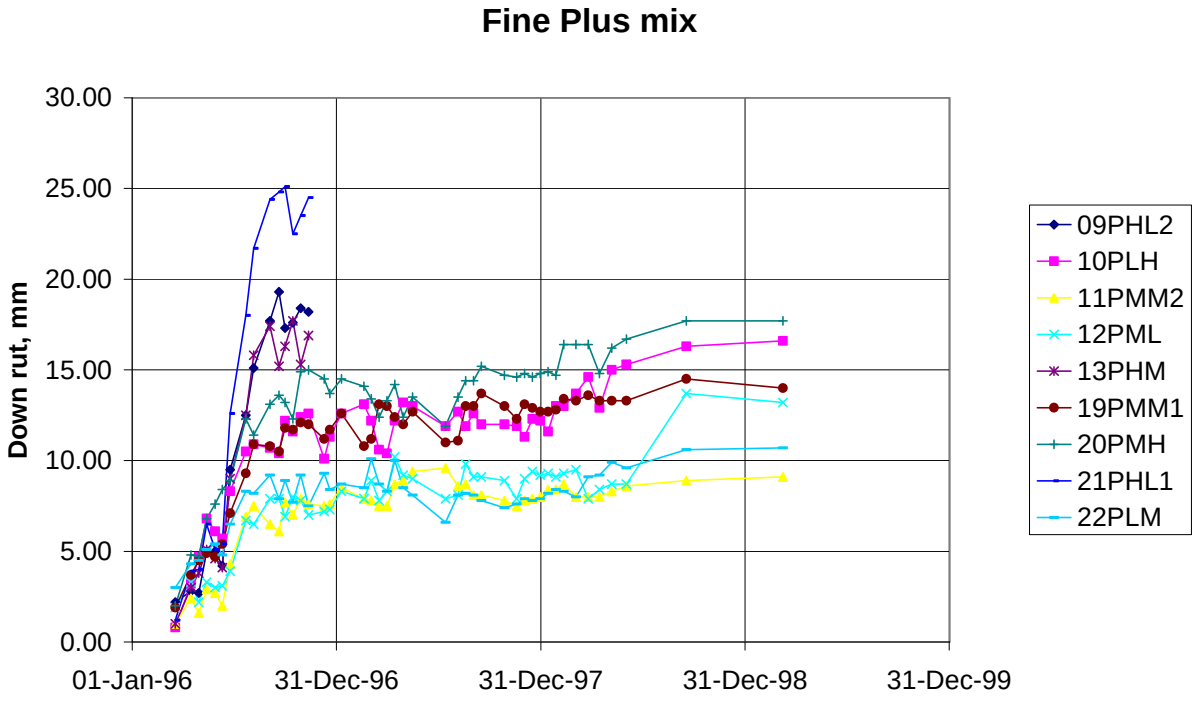

Figure 17. Down rut for Fine Plus mixes.

It may also be seen from Figure 15 to Figure 17 that there is a considerable amount of scatter in the measurements. In order to determine the number of loads to a specific amount of rutting the data was fitted with a power function as shown in Figure 18**.** The power function was then used to predict the number of loads, in million ESALs (MESALs), to a down rut of 10 mm, assumed to correspond to a total rut depth of 12.5 mm.

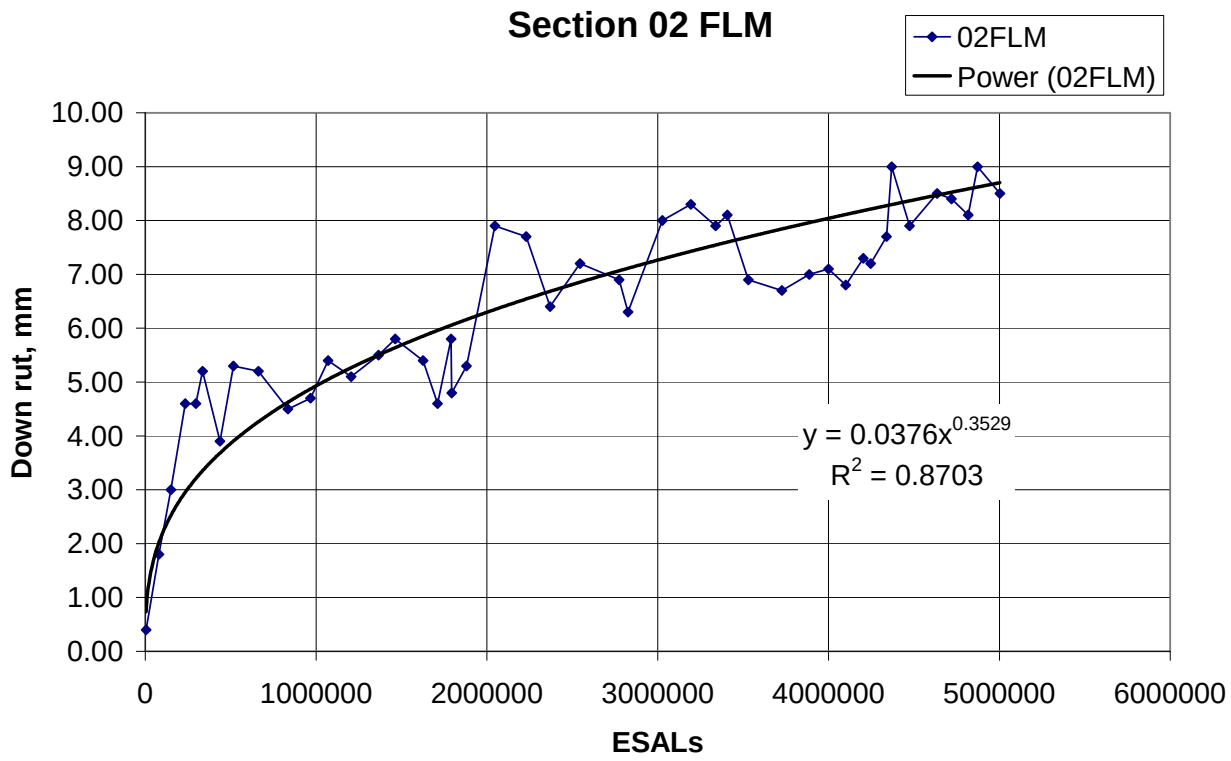

Figure 18. Example of power function fitted to the measured down rut at Section 2.

2.4 Calculated Service Life for Rutting

The service life for rutting was calculated using the Asphalt Institute's subgrade criterion:

$$\varepsilon_{z,p} = 482\,\mu strain \times MN^{-0.223}$$

Equation 5. Asphalt Institute subgrade criterion.

where $\varepsilon_{z,p}$ is the permissible vertical strain at the top of the subgrade, and
MN is the number of load repetitions in millions.

The vertical strain at the top of the subgrade is used as an indicator of the structural capacity of the pavement system and does not necessarily imply that rutting should take place at the subgrade level (7). In the case of WesTrack, however, most of the rutting occurred in the asphalt layer and it is unlikely that the Asphalt Institute criterion would be fully applicable.

The loading was composed of 14.3 percent single wheels at 53 kN (steering wheel) and 85.7 percent dual wheels at 89 kN.

The strains were calculated for the initial, temperature adjusted moduli shown in Table 1

.Table 2 shows the power function parameters for all of the measured down ruts for the original test sections, the R^2 value, the number of loads (in MESALs) to a down rut of 10 mm, and the number of MESALs predicted from the subgrade criterion using the initial moduli determined from FWD testing. Figure 19 through Figure 21 show the MESALs to 10 mm down rut depth versus the same value predicted from the subgrade criterion for each section, for the Fine, Coarse, and Fine Plus mixes, respectively.

Table 2. Measured and Calculated Service Life for Rutting

Section	Mix	A	Alpha	R^2	MESALs to 10 mm Down Rut	MESALs from Subgrade Criterion (FWD Moduli)
1	FMM1	0.2650	0.240	0.87	3.71	2.44
2	FLM	0.0376	0.353	0.87	7.40	4.88
3	FLH1	0.1230	0.301	0.90	2.22	2.44
4	FML	0.0570	0.348	0.86	2.81	6.91
5	CMM1	0.0149	0.495	0.89	0.51	2.71
6	CMH	0.0215	0.490	0.96	0.28	1.19
7	CHM	0.0135	0.530	0.86	0.26	1.48
8	CLM	0.0283	0.444	0.93	0.55	1.57
9	PHL2	0.0201	0.472	0.74	0.52	3.05
10	PLH	0.0744	0.347	0.87	1.36	0.81
11	PMM2	0.0507	0.341	0.82	5.37	3.56
12	PML	0.1180	0.288	0.82	4.95	4.26
13	PHM	0.0068	0.552	0.89	0.55	2.44
14	FHM	0.1350	0.305	0.87	1.35	7.18
15	FMM2	0.2350	0.241	0.91	5.74	5.69
16	FLH2	0.2700	0.244	0.83	2.68	1.22
17	FMH	0.1120	0.308	0.85	2.16	1.35
18	FHL	0.0485	0.341	0.88	6.12	27.09
19	PMM1	0.1530	0.296	0.90	1.36	3.74
20	PMH	0.2160	0.283	0.90	0.77	0.95
21	PHL1	0.0050	0.599	0.87	0.33	6.32
22	PLM	0.8110	0.158	0.72	8.03	3.05
23	CML	0.0251	0.429	0.93	1.15	1.84
24	CMM2	0.0509	0.419	0.90	0.30	1.10
25	CHL	0.0579	0.414	0.81	0.25	3.32
26	CLH	0.0582	0.393	0.76	0.49	0.60

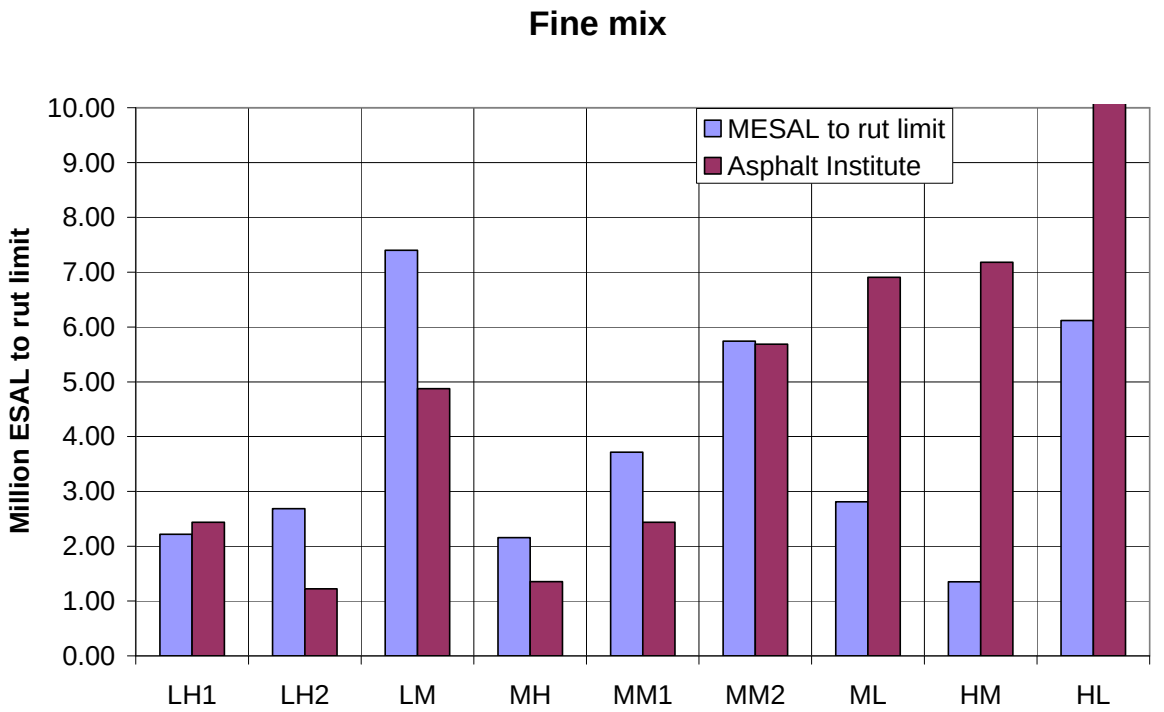

Figure 19. Million ESALs to 10 mm down rut, Fine mix.

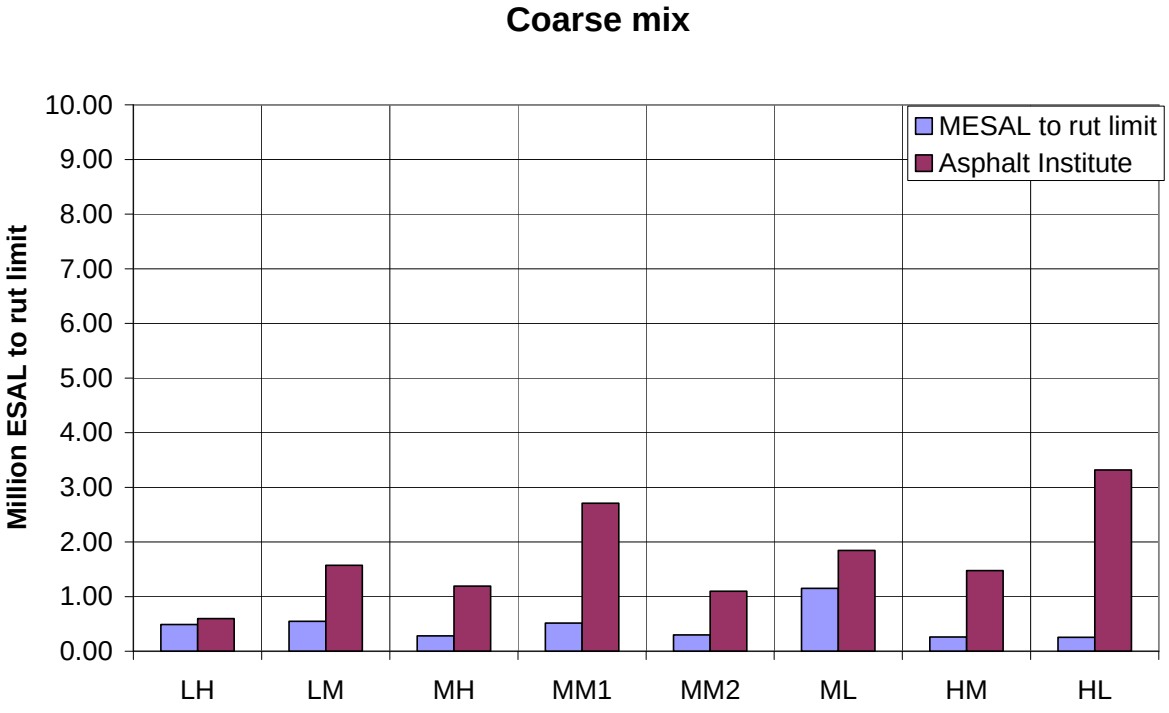

Figure 20. Million ESALs to 10 mm down rut, Coarse mix.

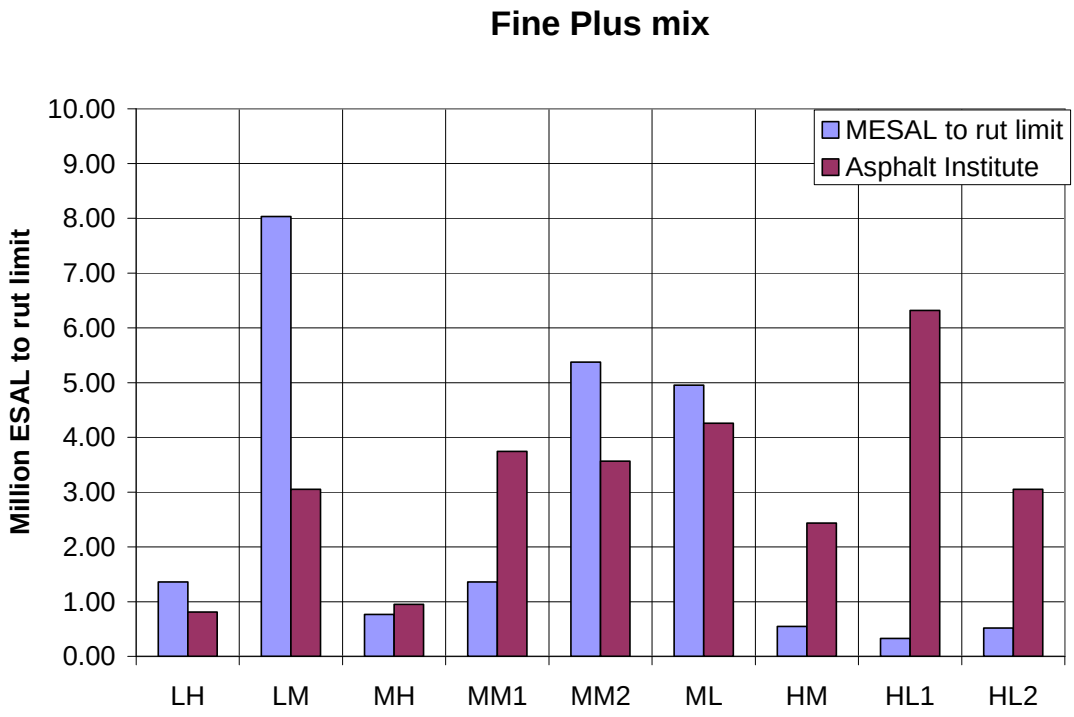

Figure 21. Million ESALs to 10 mm down rut, Fine Plus mix.

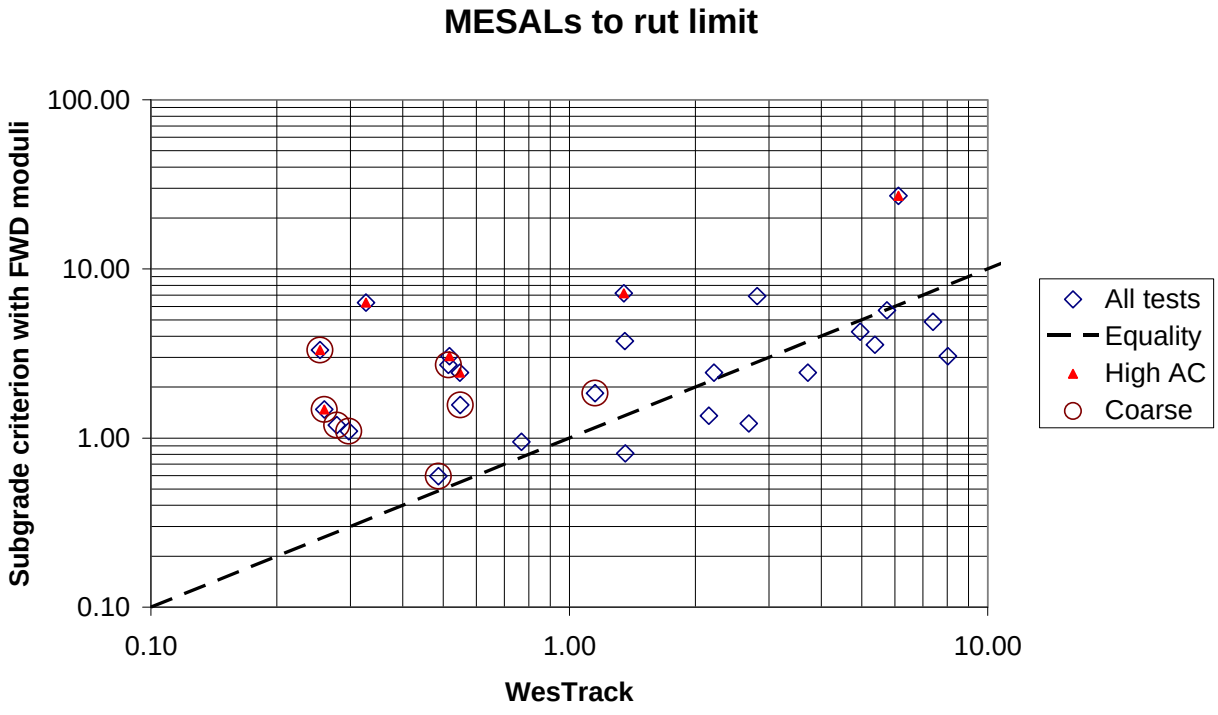

Figure 22. Measured and calculated service life for rutting. (Note: High AC indicates high asphalt content; Coarse indicates coarse gradation mixes.)

Table 2 and Figure 22 show that the service life based on the subgrade criterion using FWD backcalculated moduli at the reference temperature is overestimated in a number of cases. For all of the mixes with a high asphalt content the service life is overestimated and also for most of the Coarse mixes.

As mentioned above the duration of WesTrack was only three years and some of the tests lasted considerably less than that. For those sections the mean weighted asphalt temperature of 15.4ºC is probably too low. The temperature should be weighted with respect to damage (rutting potential) and if much of the damage occurs during an early warm period the mean temperature could be considerably higher. A calculation for Section 5 showed that increasing the mean weighted asphalt temperature to 30ºC reduced the predicted service life by a factor of 2.5.

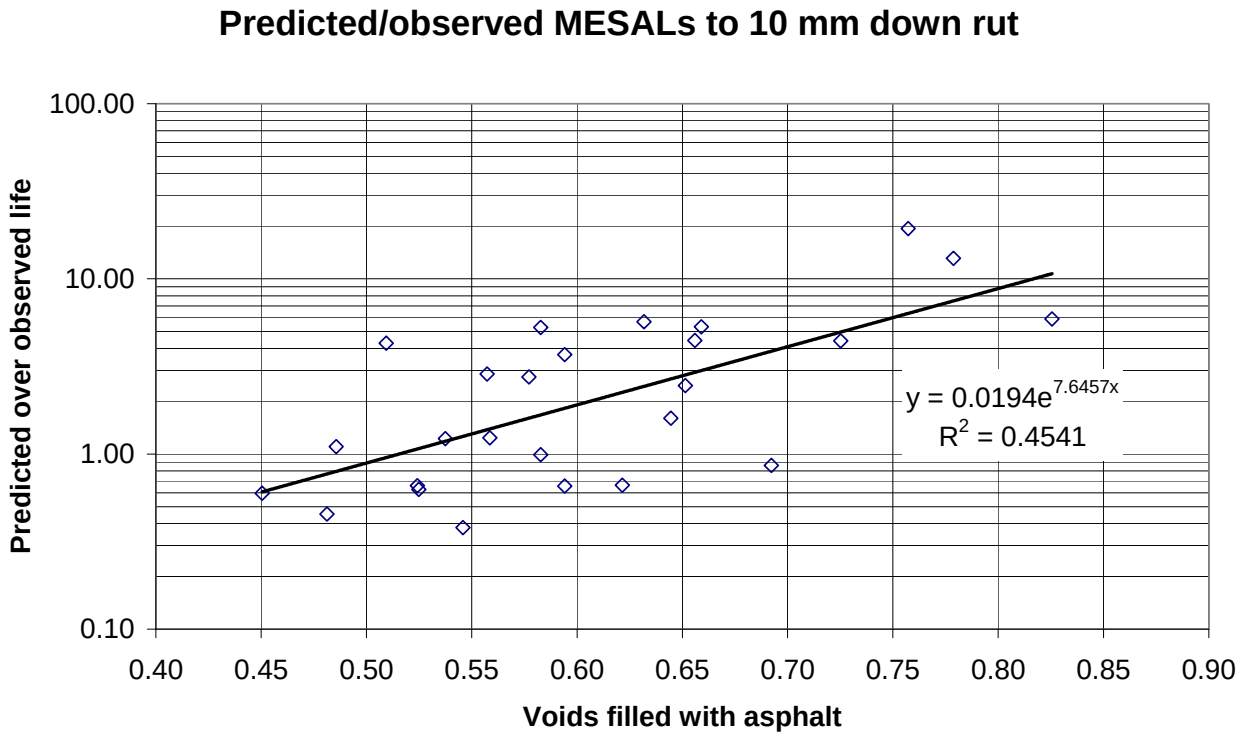

Figure 23. Predicted/observed rut life as a function of voids filled with asphalt.

Figure 23 shows the ratio of predicted versus observed life, with respect to rutting, as a function of the voids filled with asphalt (3). This comparison shows that the sections where the subgrade criterion overpredicted the rutting life were primarily those with high voids filled with asphalt values, indicating that the shorter-than-predicted lives of the field sections were related to asphalt mix design more than the overall pavement rutting that the subgrade criterion is intended to predict.

During the AASHO Road Test the number of load applications to a certain amount of damage (or failure) was observed to follow a logarithmic normal distribution. The standard deviation on the difference between the logarithms of the observed (Nt) and the predicted (Wt) number of loads to failure using the Asphalt Institute subgrade rutting criterion [$\delta = \log(Nt)-\log(Wt)$] was found to be 0.44 for flexible pavements. For all of the tests in Figure 22 the standard deviation is 0.47. This is reduced to 0.35 if the sections with high AC content are excluded, and to 0.24 for the Fine mix with medium or low AC content. This indicates that the variance between the observed and predicted number of loads to failure using the Asphalt Institute subgrade rutting criterion for WesTrack was consistent with the variance observed at the AASHO Road Test.

2.5 Observed Cracking

Fatigue cracking was obtained from the table "Avg_Fatigue Cracking (NCE)" in the WesTrack database. The final recorded cracking for the Left Wheel Path (LWP) and for the Right Wheel Path (RWP) are shown in percent in Table 3.

Table 3. Terminal Cracking in Percent of Wheelpath Cracked

Section	Mix	LWP	RWP
1	FMM1	0	0
2	FLM	57	18
3	FLH1	74	41
4	FML	0	0
5	CMM1	81	18
6	CMH	90	81
7	CHM	0	0
8	CLM	100	93
9	PHL2	0	0
10	PLH	88	34
11	PMM2	7	0
12	PML	5	0
13	PHM	0	0
14	FHM	0	0
15	FMM2	0	0
16	FLH2	6	51
17	FMH	15	3
18	FHL	0	0
19	PMM1	0	0
20	PMH	0	0
21	PHL1	0	0
22	PLM	0	0
23	CML	0	0
24	CMM2	0	0
25	CHL	0	0
26	CLH	100	32

Most of the cracking was in the left wheelpath (except for Section 16). In some cases the left wheelpath had reached 100 percent cracking before any cracking was observed in the right wheelpath. The mean value of the two wheelpaths was used to estimate the number of loads to cracking in 10 percent of the wheelpath.

An example (from Section 16) is shown in Figure 24.

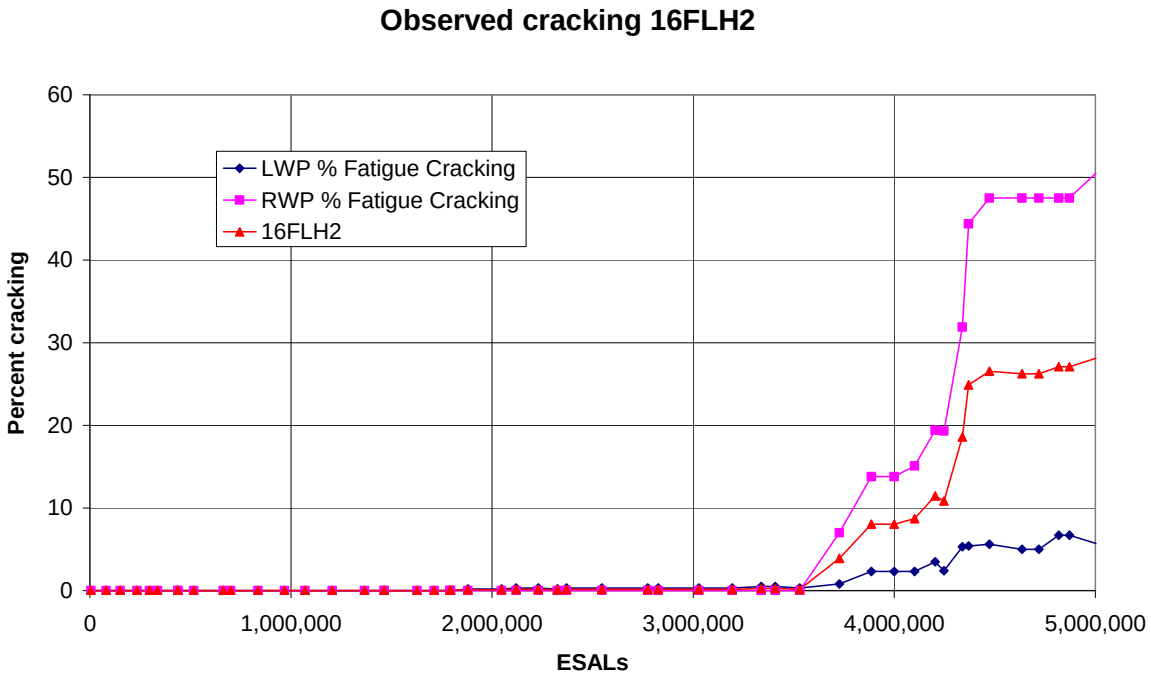

Figure 24. Example of observed cracking, Section 16.

The first cracks were observed at 3.5 MESALs (million ESALs). At the end of the test (5 MESALs) the average cracking had reached 28 percent of the wheelpath cracked. A linear interpolation between these two points results in 10 percent cracking at 4.04 MESALs.

Cracking was observed on 11 of the original 26 WesTrack sections, although it was very low, 2 to 3 percent, on Sections 11PMM2 and 12PML, so that the extrapolation to 10 percent cracking is rather uncertain. The authors have observed in pavement management system data that when the extent of cracking is less than 5 percent of the wheelpath, it often does not progress for a long time. The two sections with less than 5 percent cracking were, therefore, not included in the analysis.

The predicted cracking life of the sections was determined using the Asphalt Institute criterion (Equation 6) from the initial moduli at a reference temperature of 15.4ºC.

$$\mu\varepsilon_{permissible} = 98.2\,\mu strain \times C \times \left(\frac{MN}{18.4}\right)^{-.304} \times \left(\frac{E}{3000\,MPa}\right)^{-0.259}$$

$$C = 10^{\left(1.47 \times \left(\frac{Vb}{Vb+Vv} - 0.69\right)\right)}$$

Equation 6. Asphalt Institute permissible tensile strain at bottom of asphalt layer (7).

where $\mu\varepsilon_{permissible}$ is the permissible tensile strain at the bottom of the asphalt layer,
MN is the number of load applications in millions,
E is the modulus of the asphalt.
18.4 is the shift factor between laboratory fatigue tests and observed cracking,
C is a constant determined from Vb the volume percent binder and Vv the volume of voids (air).

The criterion is derived from controlled stress and controlled strain fatigue testing, to a 50 percent decrease in modulus, and correlated to 40 percent observed cracking in the wheelpaths (through the shift factor) at the AASHO Road Test. Figure 25 through Figure 27 show the MESALs to 10 percent of the wheelpath cracked for each WesTrack section, the predicted MESALs to 40 percent of the wheelpath cracked using the Asphalt Institute Criterion using the actual C factor for each section, and the predicted MESALs to 40 percent of the wheelpath cracked assuming that the C factor is 1, for the Fine, Coarse, and Fine Plus mixes, respectively. The C factor in the Asphalt Institute fatigue cracking criterion is equal to one when the asphalt content is 5 percent (by mass of mix) and the air-void content is 6 percent.

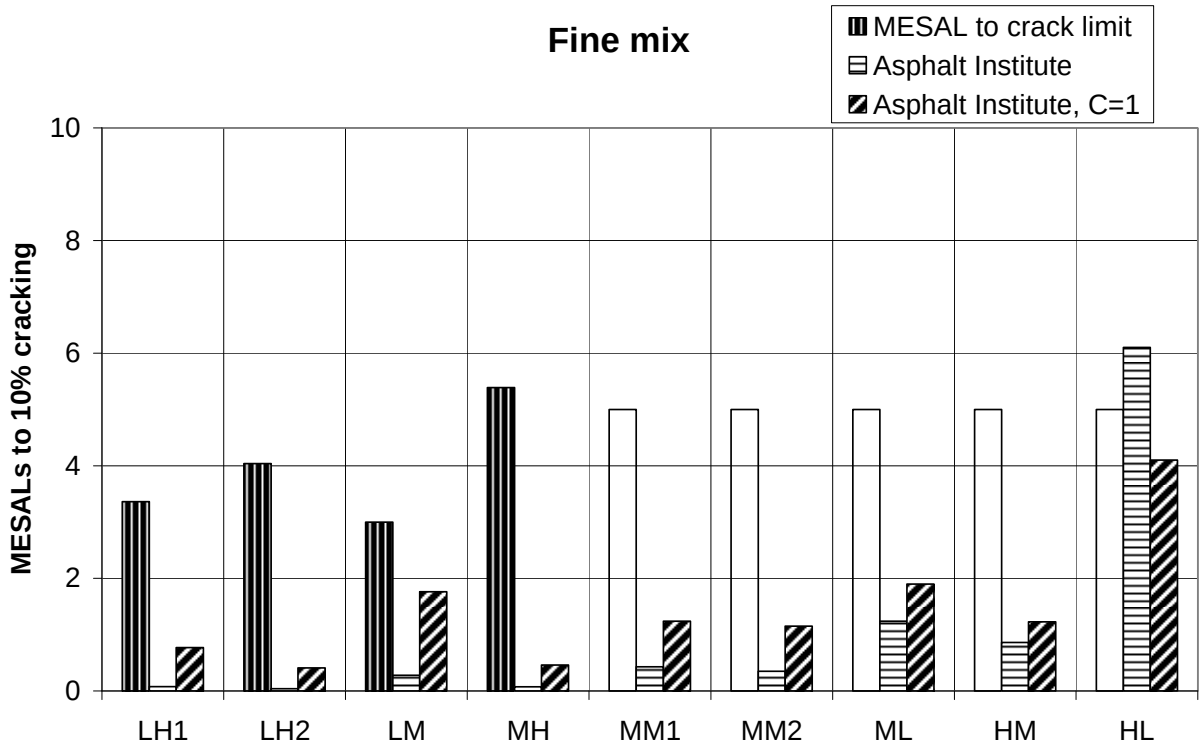

Figure 25. Million ESALs to 10% cracking, Fine mix.

In Figure 25 empty bars are shown for sections where no cracking was observed. The length of the bar indicates the duration of the test.

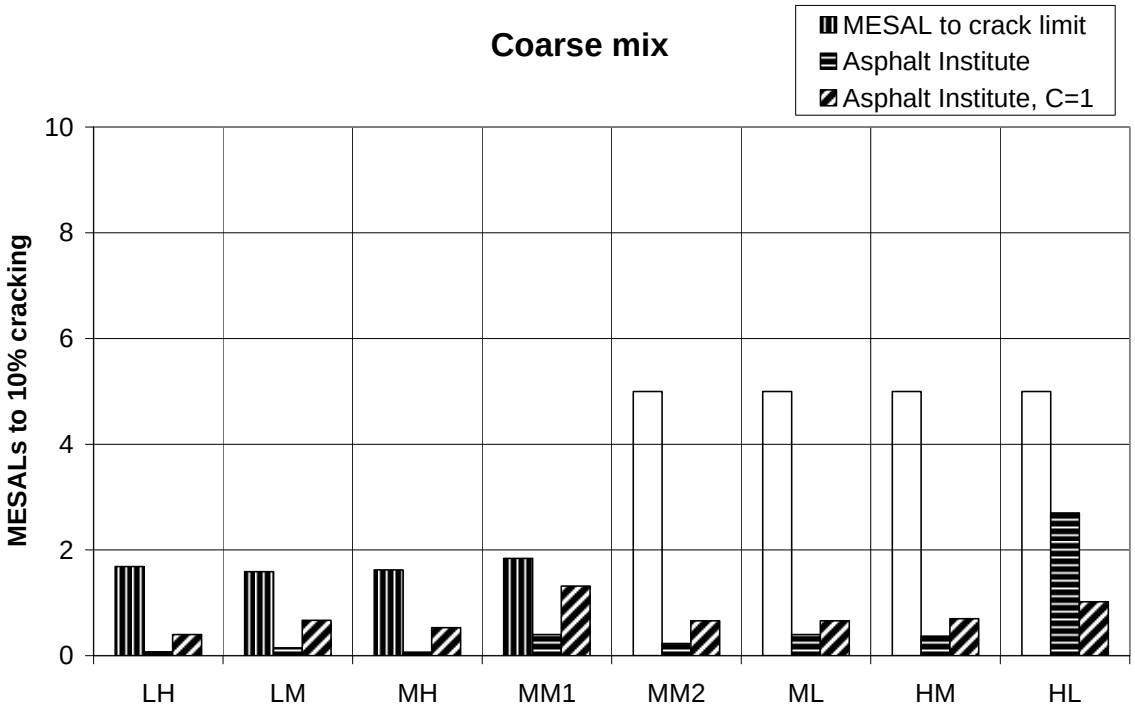

Figure 26. Million ESALs to 10% cracking, Coarse mix.

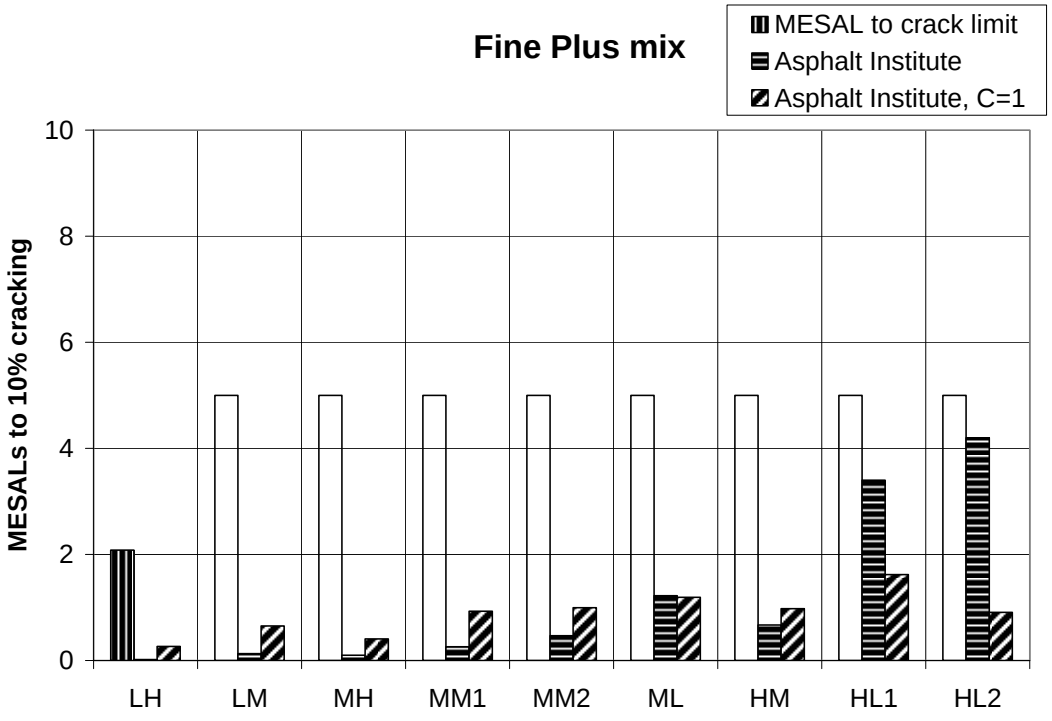

Figure 27. Million ESALs to 10% cracking, Fine Plus mix.

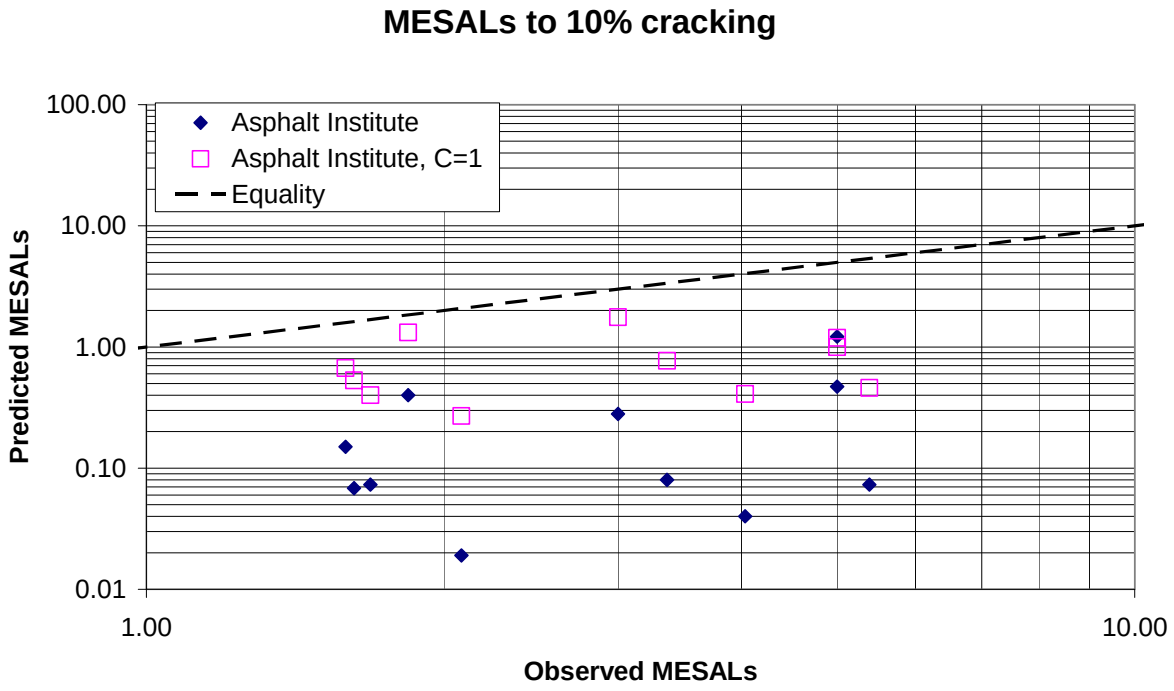

Figure 28. Observed and predicted life for fatigue cracking.

The observed fatigue lives on the WesTrack sections are all longer than those predicted using the Asphalt Institute fatigue criterion, as shown in Figure 28**.** This is true even when the mixes are assumed to have very good compaction (C equals 1). This occurs, even though the Asphalt Institute fatigue criterion is for 40 percent of the wheelpath cracked, and the observed cracking is to 10 percent of the wheelpath cracked. This implies a great deal of conservatism in the design criterion compared to the WesTrack results. Setting aside the question of the number of environmental cycles, this is to be expected, because the Asphalt Institute fatigue criterion was calibrated with a great deal of conservatism. The conservatism of the fatigue criterion will be addressed in another report discussing the use of *CalME* for design and reliability.

Figure 29 shows the number of loads to 10 percent cracking as a function of the voids filled with asphalt. For the sections where cracking was observed, the number of loads to 10 percent cracking is not well correlated with voids filled with asphalt, $R^2 = 0.104$.

The Asphalt Institute criterion, where the effects of volume of binder and volume of voids are included, shows a high correlation with voids filled with asphalt, whereas the criterion with C = 1 is much closer to the observed performance. This indicates that the effects of volume of binder and volume of voids are accounted for through the modulus term in the criterion and that the term C should not be used.

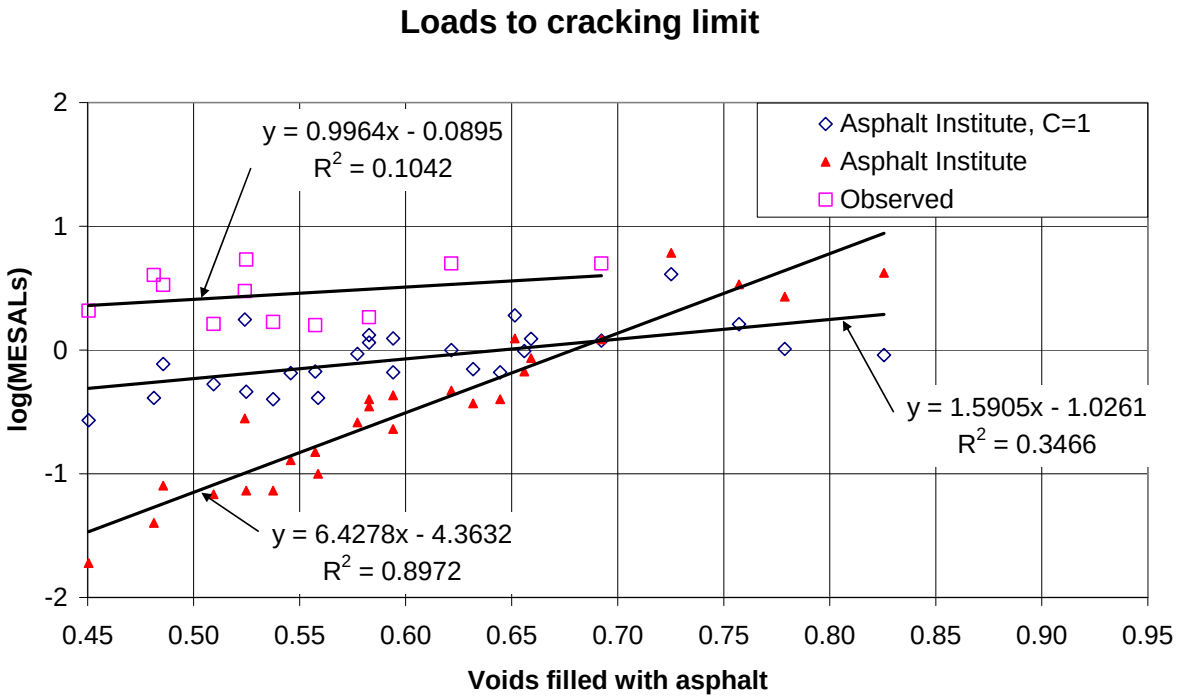

Figure 29. "Cracking life" as a function of voids filled with asphalt.

2.6 Summary of Classical Model Results

The WesTrack project is not very well suited for calibrating classical mechanistic-empirical models, partly because the test was accelerated (less than three years) and partly because a number of rather unusual mixes were tested. Nevertheless the two criteria used in the Asphalt Institute flexible pavement design method are to some extent confirmed by the project.

Had the service life of the pavements been predicted based on moduli backcalculated from FWD tests carried out at the outset of the experiment, the number of loads to 10 mm of downward rut would have been predicted quite well, as seen in Figure 22, except for the mixes with a high asphalt content and some of the coarse mixes, where the contribution of the asphalt layers to the overall rutting was larger than for "usual" pavements.

The number of load applications to 10 percent cracking would also have been predicted quite well, as shown in Figure 28, if the Asphalt Institute criterion were used with a C value of 1, so that the effects of volume of binder and volume of voids were accounted for through their effects on the modulus only. The prediction would have been conservative, corresponding to a reliability of 92 percent with the standard deviation from the AASHO Road Test (98 percent with the actual standard deviation of WesTrack).

3 *CalME* Incremental-Recursive Models

In this chapter, Section 18, a fine mix section with high asphalt content and low air-void content (FHL) was chosen as the first example because it showed no cracking during the experiment and because it had little hardening over time. The example for Section 18 shows development of all inputs, comparison of inputs, simulation, and comparison of the results from the simulation with observed performance. Inputs and results for all other sections are then summarized, sorted by mix type.

3.1 Section 18 Example, Inputs and Models Used, Comparison with MEPDG Inputs and Models, and Simulation Results

3.1.1 Measured Asphalt Modulus

The mean values of the moduli for different mixes were obtained from the table "Avg_Res Modulus – HMA (UNR)" in the WesTrack database.

3.1.1.1 Resilient Modulus from Indirect Tensile Tests

Indirect tensile resilient modulus tests were performed by the University of Nevada, Reno, at "Time Zero Construction" and at "12 Months Traffic," at a haversine loading time of 0.1 sec, and a temperature of 25ºC. Figure 30 shows the results for the Fine mix. A few data points were also available for "Time Zero Traffic" but they showed no hardening compared to "Time Zero Construction," although several months passed between construction and commencement of trafficking.

Repeated Simple Shear Tests at Constant Height (RSST-CH) were performed by the University of California Pavement Research Center (UCPRC) laboratory at the University of California, Berkeley (UCB) Richmond Field Station on the original asphalt and after trafficking (post mortem). The ratio between the hardened shear modulus (Gpm) and the original shear modulus (Go) from the one-hundredth repetition of the RSST-CH tests is shown in Table 4. The hardening is quite similar to that shown in Figure 30.

Table 4. Hardening from RSST-CH Tests, Fine Mix

Mix	Gpm/Go
LH	2.59
LM	1.72
MH	2.73
MM	1.90
ML	1.16
HM	2.03
HL	0.55

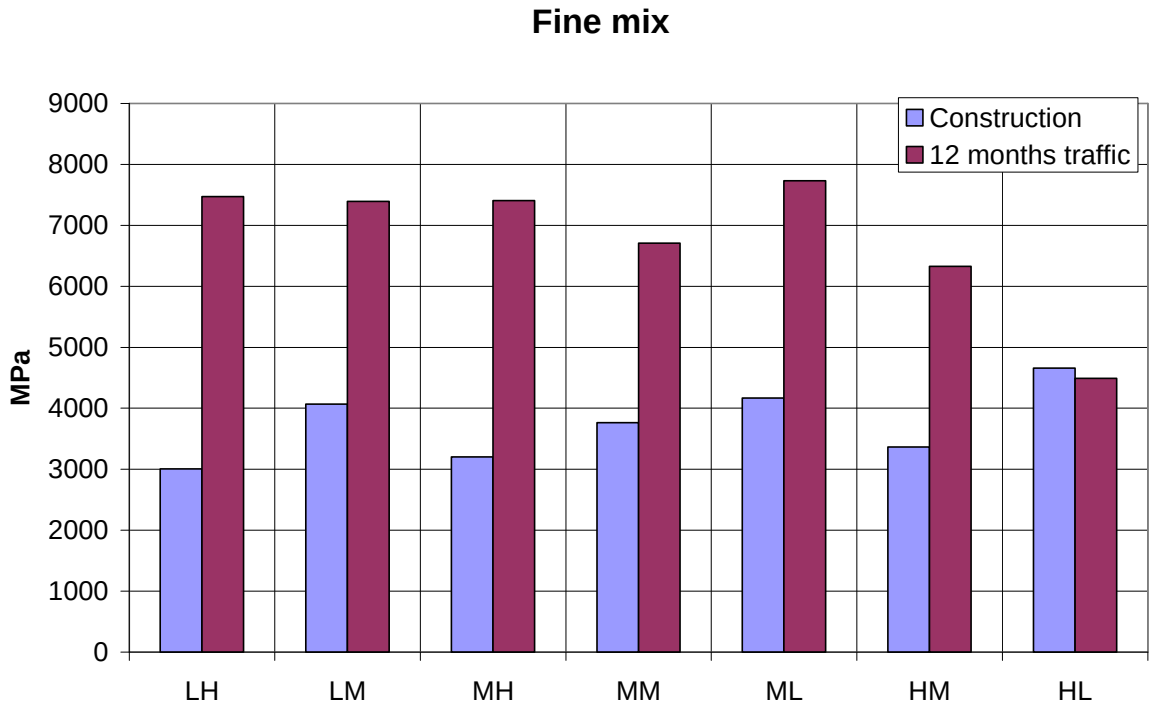

Figure 30. Mean resilient moduli of Fine mix, at construction and after 12 months traffic.

3.1.1.2 Frequency Sweep Tests

Frequency sweep tests on flexural beams were performed by UCB but only for one sample of each of the Fine, Coarse, and Fine Plus mixes. For the Fine mix the sample was from Section 04 (FML). Shear frequency sweeps were performed by the UCB, only for the Coarse mix.

The table "Avg_Freq Sweep (FHWA)" in the FHWA WesTrack database has shear frequency sweep data for Section 18, at 10 Hz and temperatures of 40, 50, and 60ºC.

3.1.1.3 Fatigue Beam Tests

The initial modulus (fiftieth repetition) from flexural fatigue beam testing by UCB was available for six samples from Section 18.

3.1.1.4 Moduli Backcalculated from FWD Tests

The moduli backcalculated from FWD tests performed between the wheelpaths were used for determining the moduli of the undamaged asphalt. The assumption that there was no damage between the wheelpaths may not be correct, as may be seen for some of the test sections, where the deflections increased more between the wheelpaths than they did in the right wheelpath. This could be due to problems of getting a good contact between the FWD loading plate and the pavement surface once rutting started to form. The FWD that was used did not have a split loading plate to accommodate the rutting. In some cases the operator had to move the loading plate about 100 mm to the left or to the right of the wheelpath center to get a reasonably good contact.

In the UCB report (4) layer moduli were backcalculated from FWD tests. For the asphalt layer the modulus was given as a function of the surface temperature determined from thermocouples in Section 12:

$$E_1 = \exp(A_0 + A_1 T)$$

Equation 7. AC modulus as function of surface temperature.

The asphalt modulus is given in psi and the temperature inºC. Values for A_0 and A_1 are given in Table 2.3 of the UCB report. For Section 18 the constants are: A_0 = 15.30039 and A_1 = -0.0587 [the latter coefficient value presented as being applicable for all sections in the UCB report (4)]. In the comparisons made below, the asphalt temperature has been calculated from the surface temperature using Equation 2.

Asphalt moduli were also backcalculated using *Elmod5*.

3.1.1.5 Asphalt Temperature

Figure 31 shows the asphalt temperature, at a depth of 50 mm, during FWD tests on Section 18. The temperature calculated from BELLS equation, temperature measured with the thermocouples at Section 12 and Section 25, and the temperature calculated with the Enhanced Integrated Climate Model (EICM) (9) are shown.

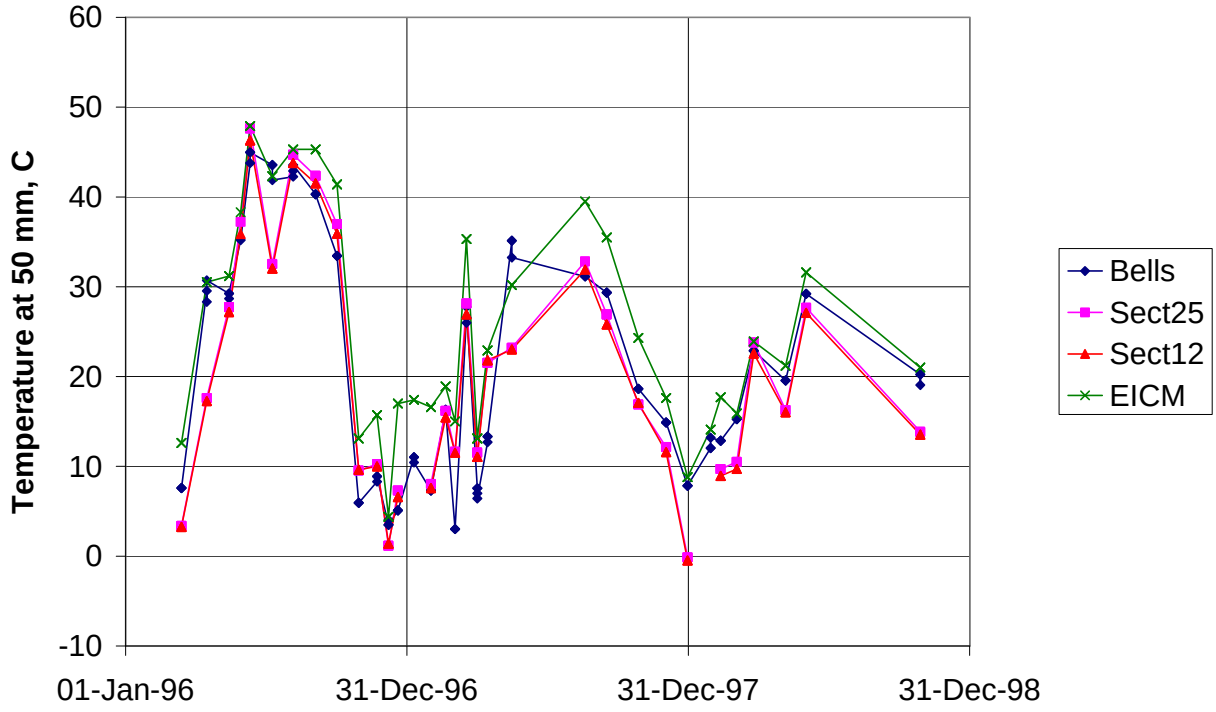

Figure 31. Asphalt temperature during FWD tests at Section 18.

The differences in temperature are surprisingly large, sometimes 10ºC or more. On average the BELLS temperatures and the thermocouples are similar, whereas the EICM temperature is approximately 5ºC higher.

For the moduli backcalculated with *Elmod5* the asphalt temperature was assumed to be the mean value of the thermocouple at Section 12 and EICM and the same values were used for the simulation in *CalME* (BELLS temperature is only available during FWD tests, so it could not be used in the simulations).

3.1.2 Comparison of Asphalt Moduli from Different Tests

Equation 14 in Chapter 4 of Reference 2 was also used in the comparison. An asphalt content of 6.2 percent and an air-void content of 4.3 percent were used. Different sources give different values for the air-

void content but 4.3 percent appears to be a reasonable value at the start of the test (dropping to about 2.1 percent toward the end of the experiment).

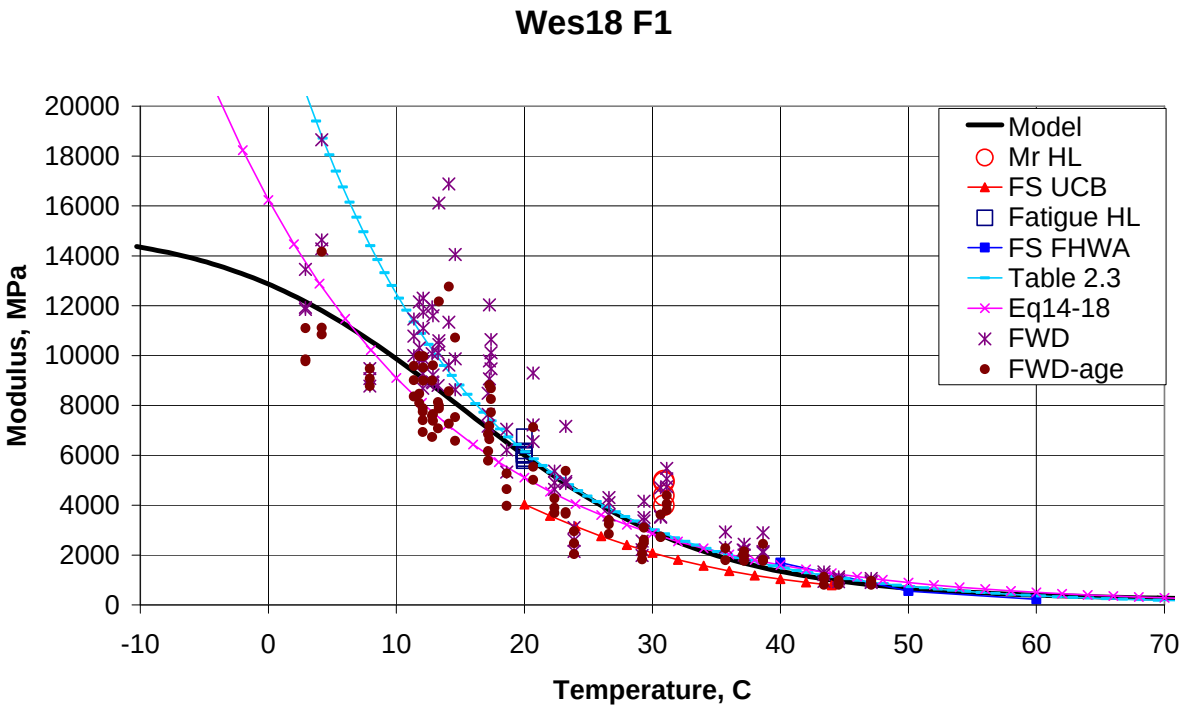

Figure 32. Asphalt modulus (linear) as a function of temperature.

Figure 32 and Figure 33 compare the moduli determined by the different means, on a linear and a logarithmic scale, respectively. The legends are: "Mr HL" — initial resilient modulus from indirect tensile tests (University of Nevada, Reno; UNR), "FS UCB" flexural frequency sweep data from UCB, "Fatigue HL" — moduli from fatigue beams (UCB), "FS FHWA" — shear frequency sweep data from Federal Highway Administration (FHWA), "Table 2.3" — FWD backcalculated moduli from the UCB report, "Eq 14-18" — from the NCHRP report (with asphalt content and air voids for Section 18), "FWD" — moduli backcalculated with *Elmod5* and "FWD-age" the same moduli adjusted for hardening (discussed later).

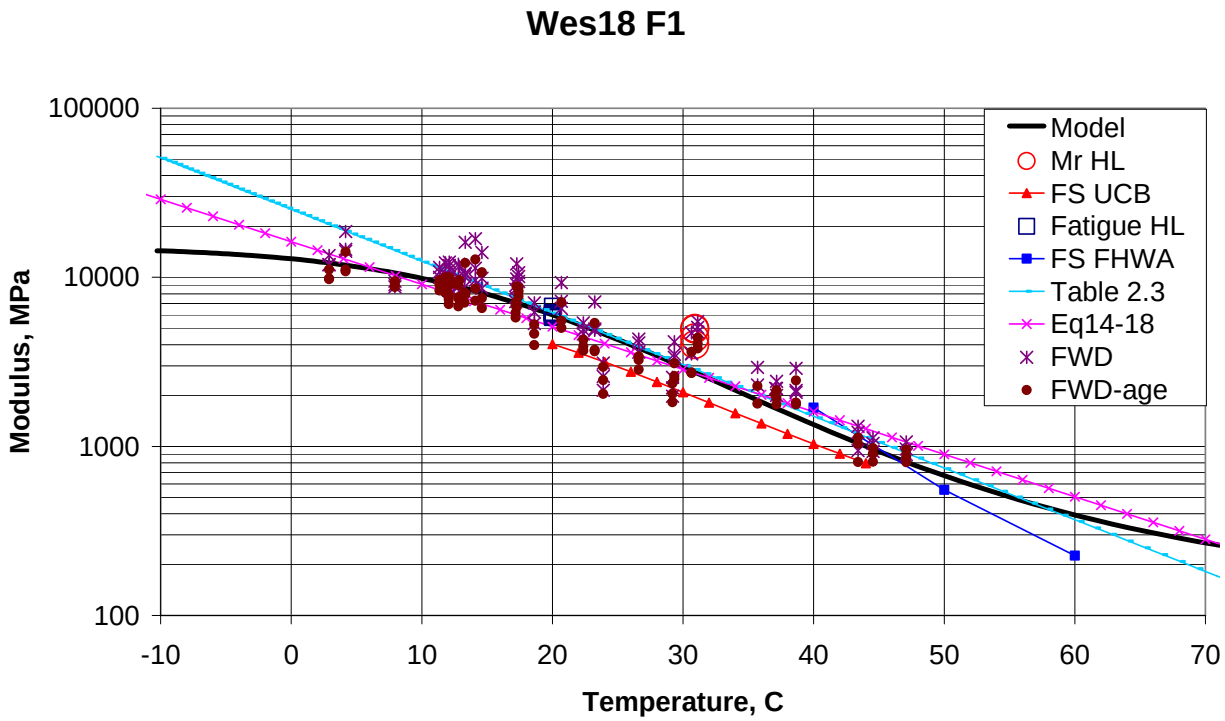

Figure 33. Asphalt modulus (logarithmic) as a function of temperature.

3.1.3 Master Curve Models

The "Model" shown in Figure 32 and Figure 33 is the master curve equation used in *CalME*. It has the same format as the MEPDG master curve equation (2), and was fitted using the various kinds of laboratory data and backcalculated FWD data shown in the figures.

$$\log(E_i) = \delta + \frac{\alpha}{1 + \exp(\beta + \gamma \log(tr))}$$

Equation 8. MEPDG AC modulus versus reduced time.

where E_i is the modulus of intact asphalt in MPa,
tr is reduced time in sec,
α, β, γ, and δ are constants, and
logarithms are to base 10.

Reduced time is found from:

$$tr = lt \times \left(\frac{visc_{ref}}{visc} \right)^{aT}$$

Equation 9. Reduced time as function of loading time and viscosity of binder.

where lt is the loading time (in sec)
$visc_{ref}$ is the binder viscosity at the reference temperature,
$visc$ is the binder viscosity at the present temperature, and
aT is a constant.

For Section 18 the model parameters are:

Table 5. Master Curve Parameters for Section 18

Parameter	Value
α	2.1761
β	-0.8842
γ	0.5526
δ	2.0000
aT	1.3000

The master curve has a minimum modulus of 100 MPa and a maximum of 15,000 MPa.
The viscosity is found from:

$$\log(\log(visc\,cPoise)) = A + VTS * \log(t_K)$$

Equation 10. Binder viscosity, cPoise, as a function of temperature.

where t_K is the temperature (in °K), and
A and VTS are constants.

For all of the asphalt materials in this report a value of A = 10.0406 (10.98 in ºR) and VTS = -3.68 were used. These values correspond according to the MEPDG, (2) to a PG64-22. A given mix modulus versus temperature relationship can, however, be fitted quite well with a number of different viscosity-versus-temperature relationships.

NCHRP Report 455 provides the following information on viscosity (Tables 44 and 45, pages 80 and 81) for the WesTrack binder:

Table 6. Measured Viscosity

Aging	Test method	Temp C	Value	Lay-down viscosity cPoise
Original	Viscosity	135	0.37 Pa.sec	6.02E+02
Original	Viscosity	60	1897 Poise	3.59E+05
Original	Viscosity	135	362 cSt	5.89E+02
Original	Penetration	25	55.5 dmm	7.13E+08
Original	Penetration	4	20.2 dmm	6.77E+09
RTFOT	Viscosity	60	4641 Poise	4.64E+05

Viscosity is calculated from penetration by the equation (according to MEPDG):

$$\log(\eta) = 10.5012 - 2.2601 \times \log(Pen) + 0.00389 \times \log(Pen)^2$$

Equation 11. Viscosity from penetration.

where η is the viscosity in Poise, and
Pen is penetration in 0.1 mm (dmm).

Short-term hardening, corresponding to Rolling Thin Film Oven Test (RTFOT) is determined from:

$$\log(\log(\eta_0)) = a_0 + a_1 \times \log(\log(\eta_{orig}))$$
$$a_0 = 0.054405 + 0.004082 \times code$$
$$a_1 = 0.972035 + 0.010886 \times code$$

Equation 12. Short-term aging (RTFOT).

where η_0 is the mix/lay-down viscosity in cPoise,
η_{orig} is the original viscosity in cPoise, and
code is the hardening ratio code.

The hardening ratio code ranges from -1 for low hardening to 2 for high hardening (0 for average). A *code* of -1 was used for calculating the lay-down values in Table 6. The California Valley binder used at WesTrack has less aging than most binders used in the US. The same binder was used in all WesTrack mixes. It is unmodified and conventional steam-refined asphalt.

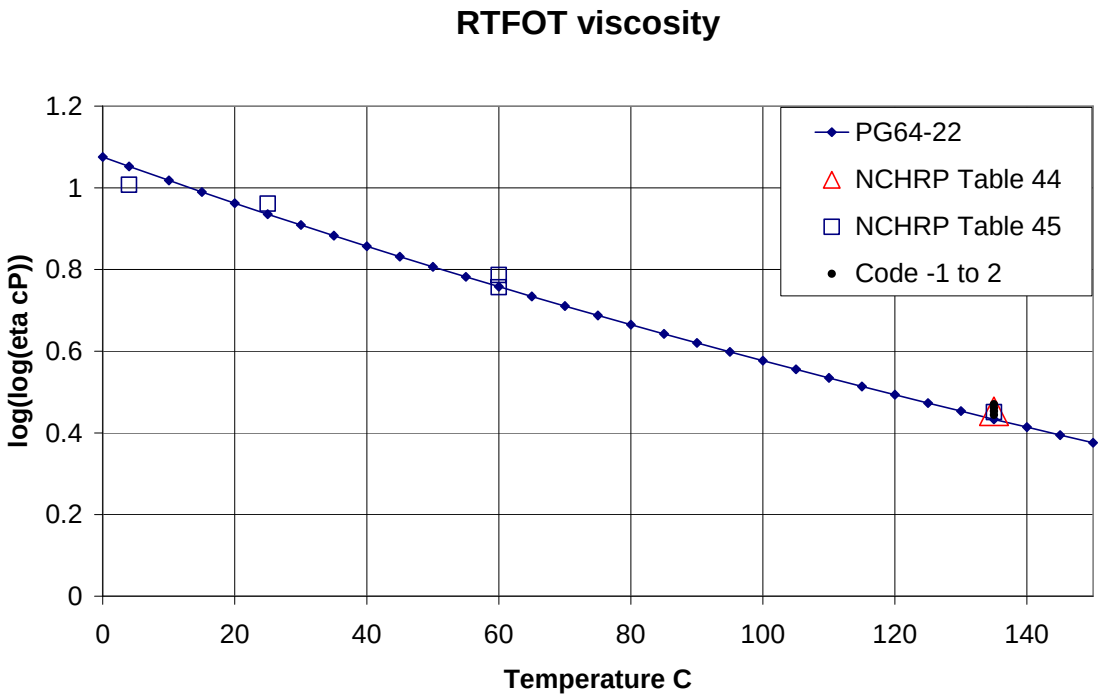

Figure 34. Lay-down viscosity, in cPoise, PG64-22 and measured viscosity, versus temperature. (Note: NCHRP refers to viscosity values from NCHRP Report 455, Reference 3.)

It may be seen that the hardening *code* has a limited influence on the lay-down viscosity. A *code* of -1 corresponds to the lowest of the values shown in Figure 34 and is in good agreement with the PG64-22 binder.

The model is shown for a loading time of 0.015 sec. This loading time corresponds to a creep test. For a sinusoidal vibration with a frequency *f* Hz the corresponding loading time is calculated as:

$$lt = \frac{1}{2 \times \pi \times f}$$

Equation 13. Relation between creep test loading time and frequency of sinusoidal vibration.

A loading time of 0.015 sec corresponds, roughly, to a frequency of 10 Hz and also to the equivalent creep test loading time of an FWD test. A haversine load of 0.1-sec duration corresponds to a loading time of 0.05 sec. The resilient modulus tests (UNR) were done at this load duration. To compare the results to those at 0.015 sec, the moduli are plotted at 30.9ºC instead of at the 25ºC of the test in Figure 32 and Figure 33.

Equation 8 may also be written in a simpler format as:

$$\log(E) = \delta + \frac{\alpha}{1 + \left(tr / tr_{ref} \right)^{\gamma'}} \quad where$$

$$\gamma' = \gamma / \ln(10) \quad and \quad tr_{ref} = \exp\left(-\beta / \gamma \times \ln(10) \right)$$

Equation 14. Alternative format of Equation 8.

With this format tr_{ref} may be used to shift the master curve left or right and γ' may be used to change the slope of the curve. For $tr = tr_{ref}$ one has $log(E) = \delta + \alpha/2$.

According to the MEPDG the master curve parameters may be determined from:

$$\log(E_i) = \delta + \frac{\alpha}{1 + \exp(\beta + \gamma \times \log(t_r))}$$

$$\delta = 3.750063 + 0.02932 \times \rho_{200} - 0.001767 \times \rho_{200}^2 - 0.002841 \times \rho_4 - 0.058097 \times V_a - 0.802208 \times \left[\frac{Vb_{eff}}{Vb_{eff} + V_a}\right]$$

$$\alpha = 3.871977 - 0.0021 \times \rho_4 + 0.003958 \times \rho_{38} - 0.000017 \times \rho_{38}^2 + 0.005470 \times \rho_{34}$$

$$\beta = -0.603313 - 0.393532 \times \log(\eta_{T_r})$$

$$\log(t_r) = \log(t) - c \times [\log(\eta) - \log(\eta_{T_r})]$$

$$\gamma = 0.313351$$

$$c = 1.255882$$

Equation 15. Initial modulus from volumetric data, MEPDG.

where E_i is the (dynamic) modulus in psi,
η is the viscosity in MPoise (10^6 Poise),
η_{Tr} is the viscosity at the reference temperature at RTFOT in MPoise,
T_r is the reference temperature,
t_r is the time of loading at the reference temperature in sec (reduced time),
t is the time of loading in sec,
V_a is air-void content percent,
V_{beff} is effective bitumen content, percent by volume,
ρ_{34} is cumulative percent retained on the 3/4 in sieve (19 mm),
ρ_{38} is cumulative percent retained on the 3/8 in sieve (9.5 mm),
ρ_4 is cumulative percent retained on the No. 4 sieve (4.76 mm),
ρ_{200} is percent passing the No. 200 sieve (0.075 mm)

An observation is that it is strange that β is a fixed function of the viscosity at the reference temperature, T_r. If the reference temperature is changed, then β must also be changed, but the required change is a function of γ, aT, and the viscosity-versus-temperature relationship in Equation 8, and not only of the viscosity at the reference temperature.

Information on the volumetric properties for the Fine mix of Section 18 is given in Tables 104 and 105, page 143, in NCHRP Report 455 (3):

Table 7. Volumetric Mix Properties, Section 18

Sieve Size		Fine Mix, Section 18	
mm	**US**	**Top Lift**	**Bottom Lift**
19	3/4-in	100	100
12.5	1/2-in	87.0	88.3
9.5	3/8-in	75.5	76.6
4.75	No.4	51.1	49.8
2.36	No.8	39.8	38.0
1.18	No.16	35.2	33.3
0.6	No.30	28.7	27.1
0.3	No.50	16.5	15.5
0.15	No.100	8.4	7.5
0.075	No.200	5.1	4.5

This results in the following input values:

Table 8. Volumetric Input Values

	Top Lift	**Bottom Lift**
ρ_{34}	0	0
ρ_{38}	24.5	23.3
ρ_{4}	48.9	50.2
ρ_{200}	5.1	4.5

The air-voids content and the volume percent of bitumen may be found from Tables 113 and 114 in Reference 2 for gyratory compacted specimens:

Table 9. Air Voids and Bitumen Percent

	Top Lift	Bottom Lift
V_a	2.7	3.1
Vb_{eff}	10.7	10.2

The parameters of Equation 15 are:

Table 10. Parameters of Equation 15

Parameter	Top Lift	Bottom Lift
δ	3.056213	3.050905
α	4.158888	4.155279
β	-1.2815	-1.2815
γ	0.313351	0.313351
c	1.255882	1.255882

This results in a very low minimum modulus (10^{δ}) of 8 MPa and a maximum modulus ($10^{\alpha+\delta}$) of more than 110,000 MPa. Both of these values are unrealistic, and the MEPDG master curve does not compare very well to the measured moduli, as seen in Figure 35 and Figure 36.

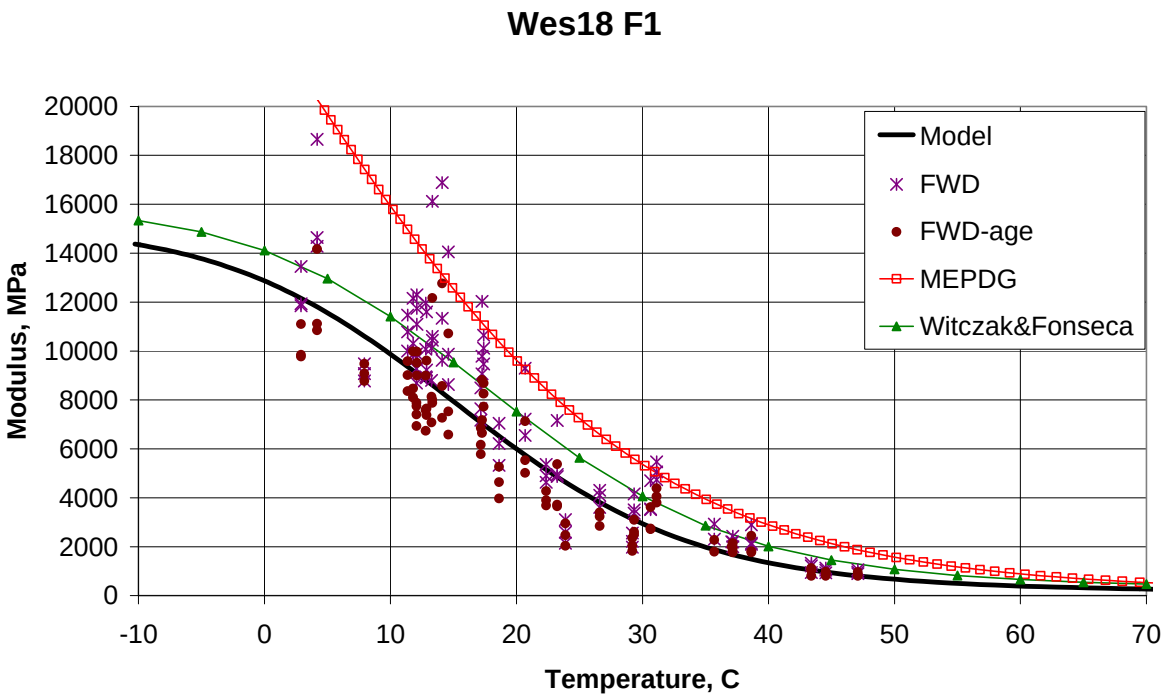

Figure 35. Section 18 Model (Equation 8) master curve compared to master curve estimated from volumetric data following MEPDG (Equation 15), linear.

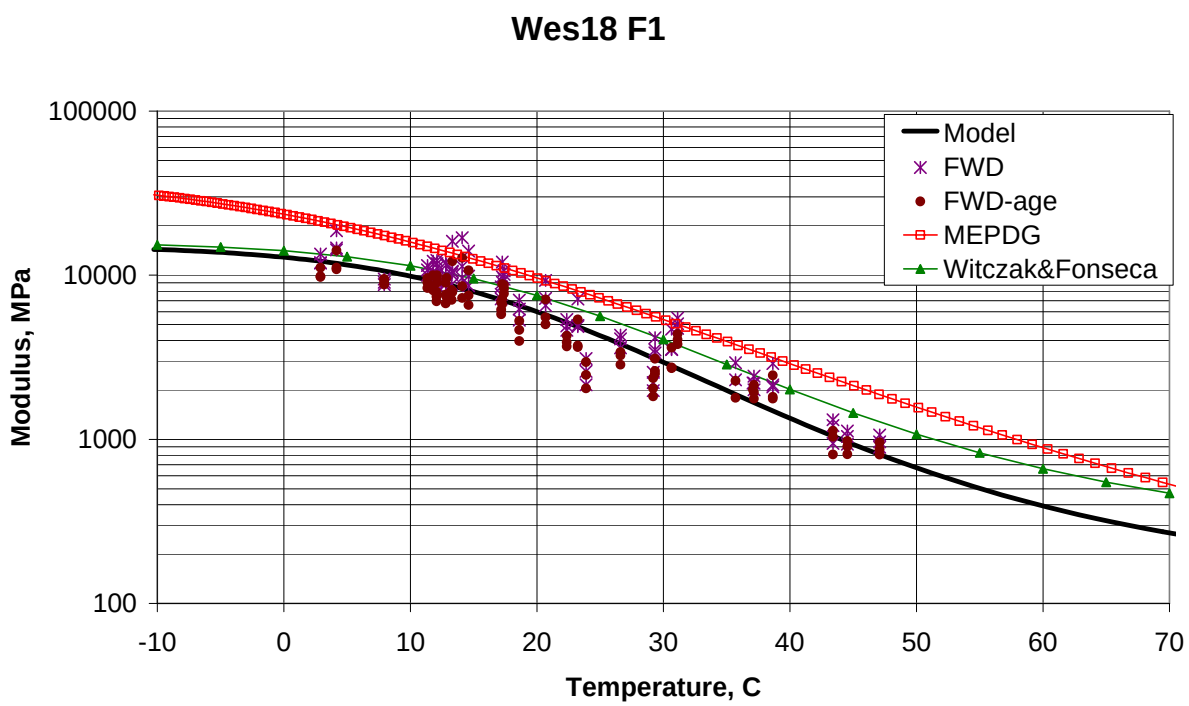

Figure 36. Section 18 Model (Equation 8) master curve compared to master curve estimated from volumetric data following MEPDG (Equation 15), logarithmic.

An older version of the MEPDG master curve is given by (10). This version is also shown in Figure 35 and Figure 36 and fits the measured data better than the master curve estimated from volumetric data following the MEPDG procedure.

3.1.4 Hardening/Aging

According to the resilient modulus tests from UNR there was no hardening of Section 18 during the experiment. On the other hand, the backcalculated moduli from FWD tests showed some hardening.

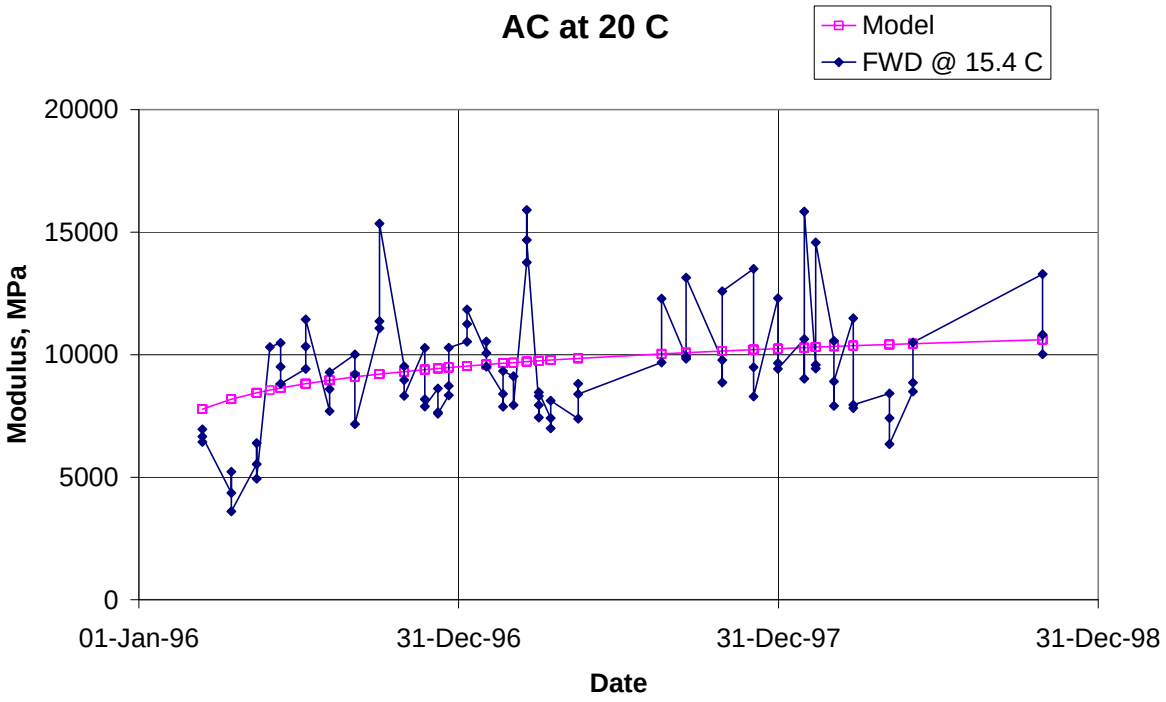

Figure 37. Temperature-adjusted asphalt modulus at Section 18.

In Figure 37 the FWD modulus has been adjusted to a fixed temperature of 20ºC. It can be seen that there is some increase in the temperature-adjusted modulus with time.

The hardening model included in *CalME*, and shown with open squares in Figure 37, has the format:

$$E(d1) = E(d0) \times \frac{AgeA \times \ln(d1) + AgeB}{AgeA \times \ln(d0) + AgeB}$$

Equation 16. Model for hardening of asphalt included in CalME.

where $E(d)$ is the modulus after d days, and
$AgeA$ and $AgeB$ are constants.

For Section 18, coefficients that fit the FWD backcalculated moduli well were: $AgeA$ = 0.112 and $AgeB$ = 0.3391. The reference modulus $E(d0)$ was assumed to correspond to an age of 72 days.

In the MEPDG the long-term viscosity aging at the surface is determined from:

$$\log(\log(\eta_t)) = \frac{\log(\log(\eta_0)) + A \times t}{1 + B \times t}$$

$$A = -0.004166 + 1.41213 \times C + C \times \log(Maat) + D \times \log(\log(\eta_0))$$

$$B = 0.197725 + 0.068384 \times \log(C)$$

$$C = 10^{274.4946 - 193.831 \times \log(T_R) + 33.9366 \times \log(T_R)^2}$$

$$D = -14.5521 + 10.47662 \times \log(T_R) - 1.88161 \times \log(T_R)^2$$

Equation 17. MEPDG model for effect of long-time aging on viscosity at the surface.

where η_t is aged viscosity at t months in cPoise,
η_0 is viscosity at mix/lay-down in cPoise,
$Maat$ is the mean annual air temperature, ºF,
T_R is temperature in Rankine, and
t is time in months.

The *Maat* at Reno, Nevada, is about 11ºC (corresponding to a mean asphalt temperature of about 16ºC).

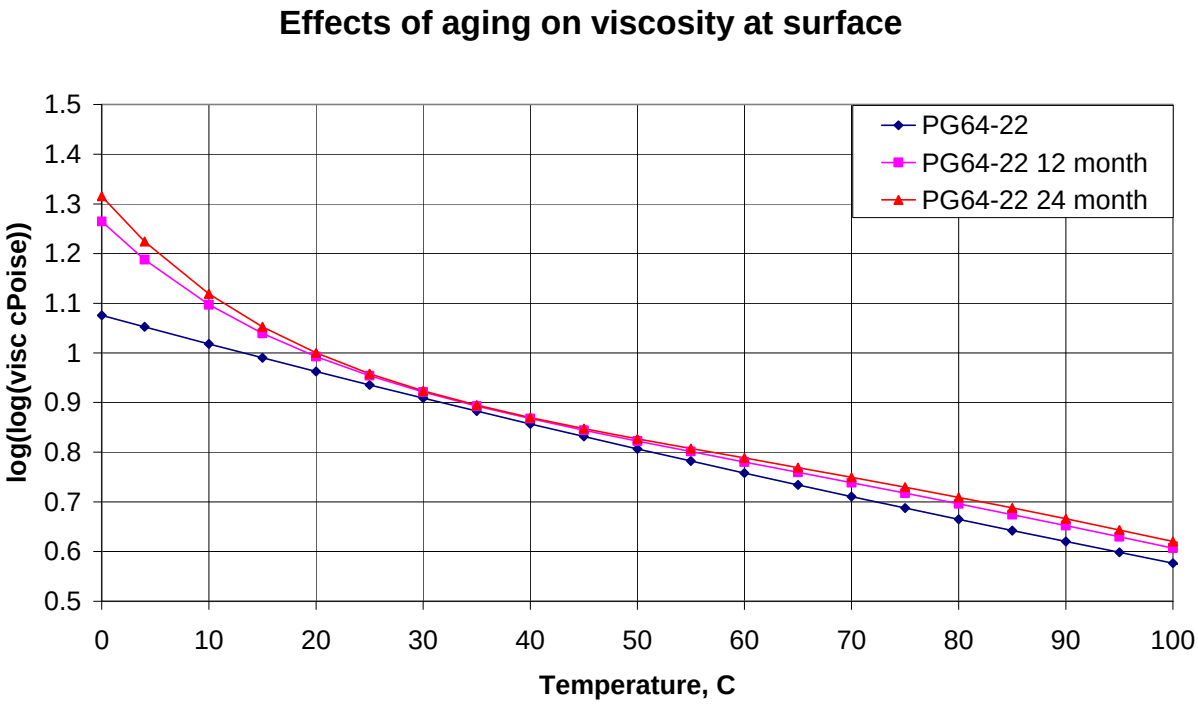

Figure 38. Viscosity at pavement surface versus temperature as a function of aging using MEPDG aging model.

The binder viscosity following Equation 17 is shown plotted for the WesTrack binder properties in Figure 38, including the original binder, and the binder after 12 and 24 months of aging . The viscosity versus-age-relationship in Equation 17 shows large effects at low temperatures and very little effect at temperatures of 30 to 50ºC, which is not the expected behavior for an unmodified asphalt. The relationship for the aged viscosity is no longer linear in a log(log(viscosity)) versus temperature plot and cannot be described by Equation 10.

To correct Equation 17 for the effects of air-void content the MEPDG indicates that the aged log(log (viscosity)) should be multiplied by F_v:

$$F_v = \frac{1 + 1.0367 * 10^{-4} \times V_{at} \times t}{1 + 6.1798 \times 10^{-4} \times t}$$

$$V_{at} = \frac{V_{a0} + 0.011 \times t - 2}{1 + 4.24 \times 10^{-4} \times t \times Maat + 1.169 \times 10^{-3} \times \left(t / \eta_{0,77} \right)} + 2$$

Equation 18. MEPDG correction of log(log(viscosity)) for effects of air voids.

where V_{a0} is the initial air voids,
V_{at} is the air voids after t months,
t is time in months,
$\eta_{0,77}$ is the original binder viscosity at 77ºF (25ºC) in MPoise.

Assuming an air voids content of 4.3 percent (for the top lift) Equation 18 predicts a drop to 3.9 percent after 12 months and to 3.7 percent after 24 months. The actual air-void content at the end of the experiment was found to be 2.1 percent in the top lift, whereas the bottom lift dropped from 4.0 percent to 3.2 percent (Table 11 and Table 12) (11). With the low air-void content of Section 18 F_v is less than 1. F_v is 0.997 after 12 months and 0.994 after 24 months. These factors have already been applied in Figure 38 and Figure 39.

In the MEPDG the aged viscosity is also a function of depth as follows:

$$\eta_{t,z} = \frac{\eta_t \times (4 + E) - E \times \eta_0 \times (1 - 4 \times z)}{4 \times (1 + E \times z)}$$

Equation 19. Viscosity aging as a function of depth.

where $\eta_{t,z}$ is the aged viscosity at time t and depth z in MPoise,
η_t is the aged surface viscosity in MPoise,
z is depth in inch,
E is $23.83 \times \exp(-0.0308 \times Maat)$.

This equation will not be correct for a depth of z = 0 inch.

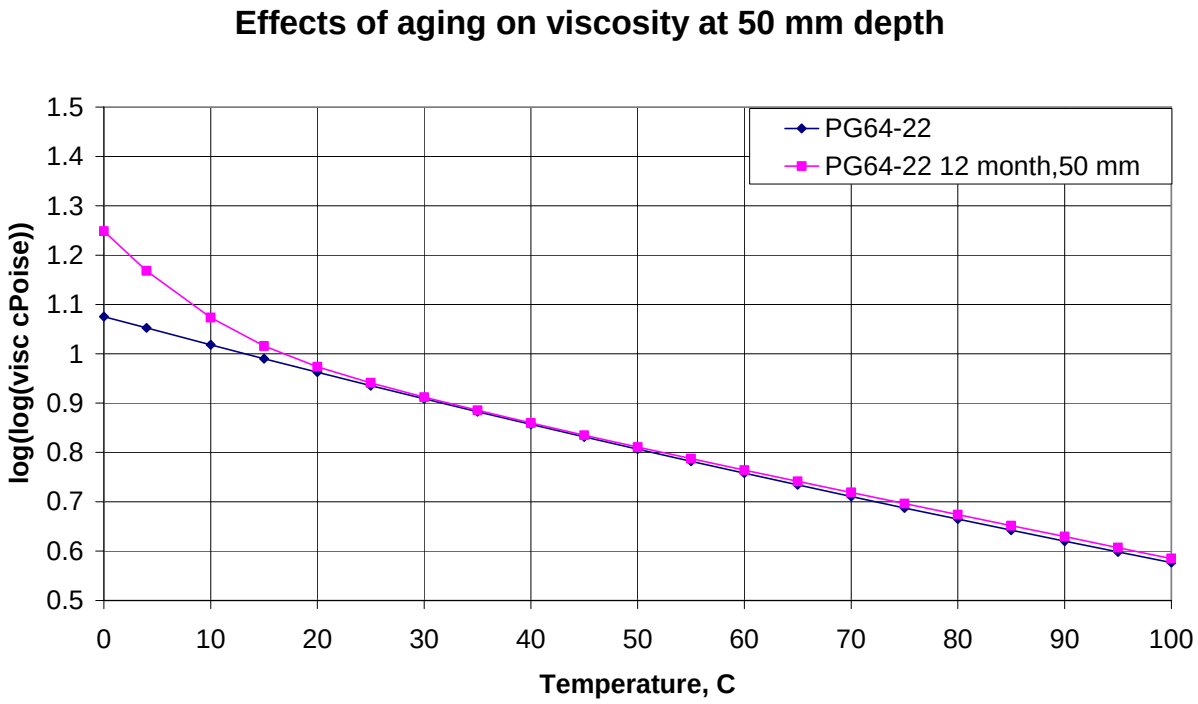

Figure 39. Viscosity at 50 mm depth as a function of aging using MEPDG model.

At most temperatures the MEPDG model indicates that there is very little change in viscosity at a depth of 50 mm, but at the reference temperature of 15.4ºC the change is noticeable, as shown in Figure 39. This will have an effect on β in Equation 15 and will cause the master curve to shift to the right, on a reduced time scale, resulting in a higher modulus at the same reduced time, or temperature, even though there is no increase in the viscosity of the binder.

Figure 40 shows the original modulus as calculated from Equation 15 and the modulus after 24 months of aging calculated using the MEPDG procedure described above. The increase in modulus shown by the MEPDG models of about 50 percent at a temperature of 20ºC is not unreasonable judging from the results of FWD testing, whereas the indirect tensile tests showed no increase at 25ºC, and the shear tests showed a decrease. The present hardening model in the MEPDG is, however, very complex and some of the intermediate results appear to be unreasonable.

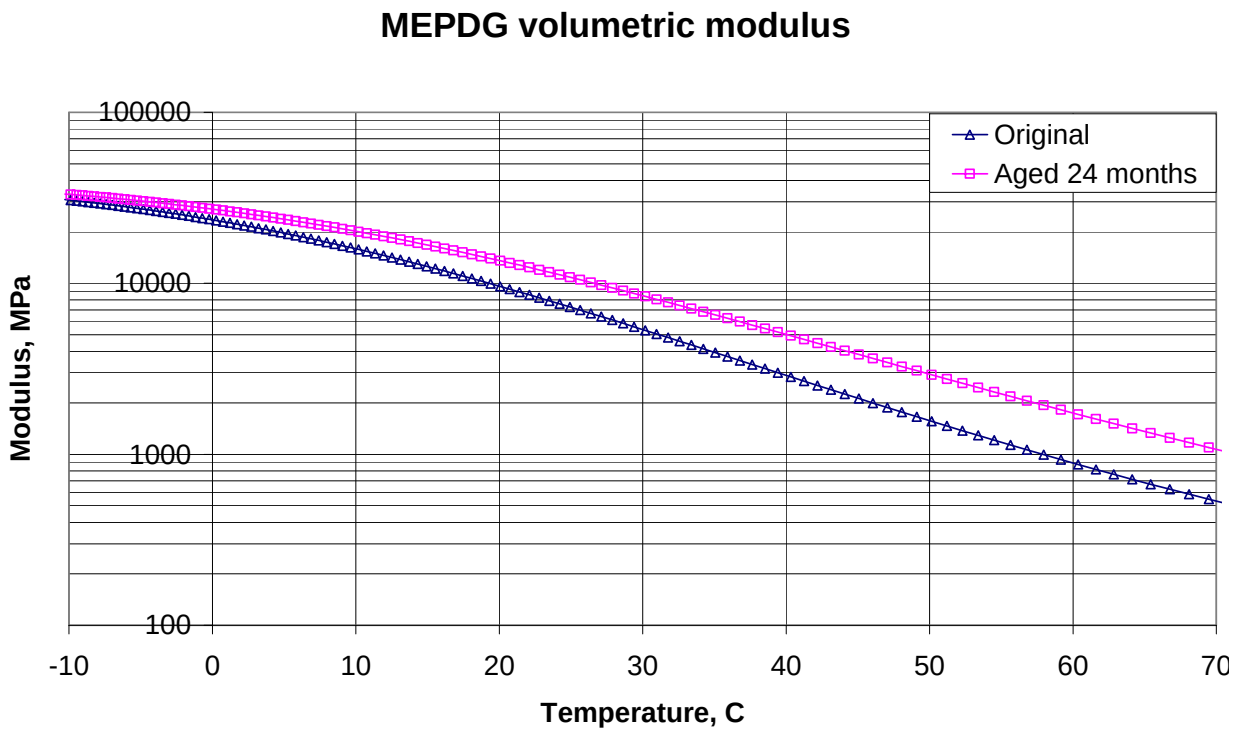

Figure 40. Effect of hardening on MEPDG modulus master curve.

3.1.5 Moduli of Unbound Layers

3.1.5.1 Moduli Backcalculated from FWD Tests between Wheelpaths

There was a tendency for the modulus of the aggregate base to increase with the modulus of the asphalt, although the correlation was not very good, as shown in Figure 41. The modulus of the aggregate base is calculated as follows in *CalME*:

$$E_{AB} = 317\,MPa \times \left(1 - \left[1 - \frac{S}{3500^3}\right] \times 0.31\right)$$

$$S = h_{AC}^3 \times E_{AC}$$

Equation 20. Modulus of aggregate base as a function of AC stiffness for Section 18.

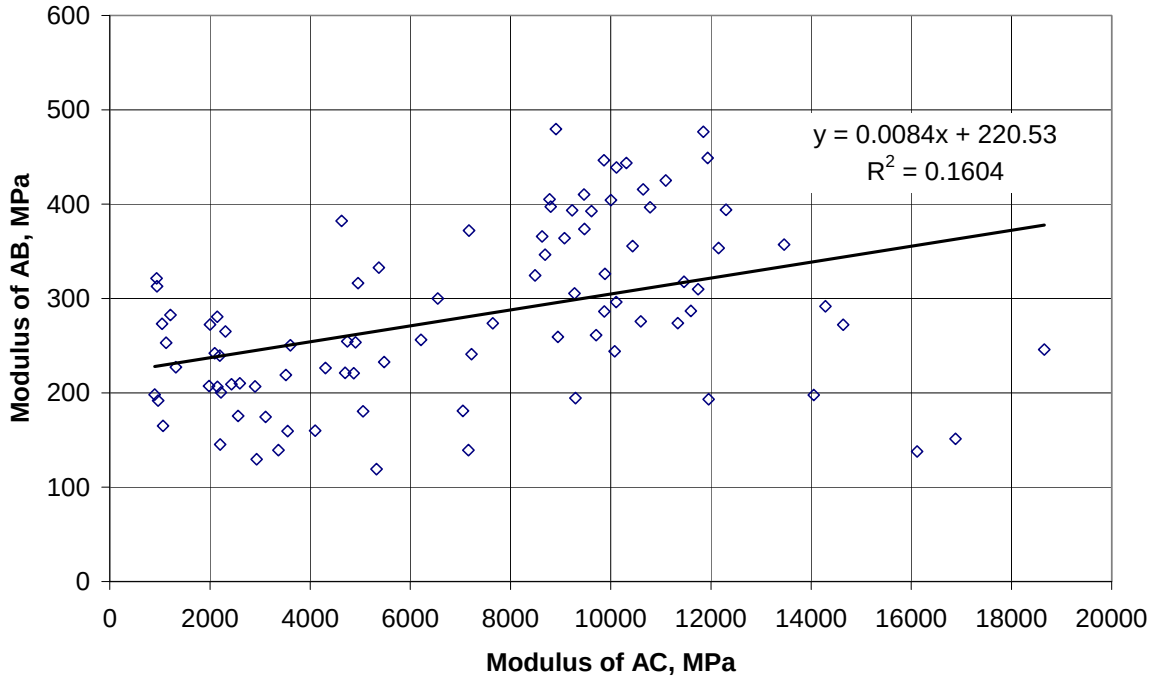

Figure 41. Modulus of aggregate base as a function of modulus of asphalt for Section 18 from backcalculation of FWD results.

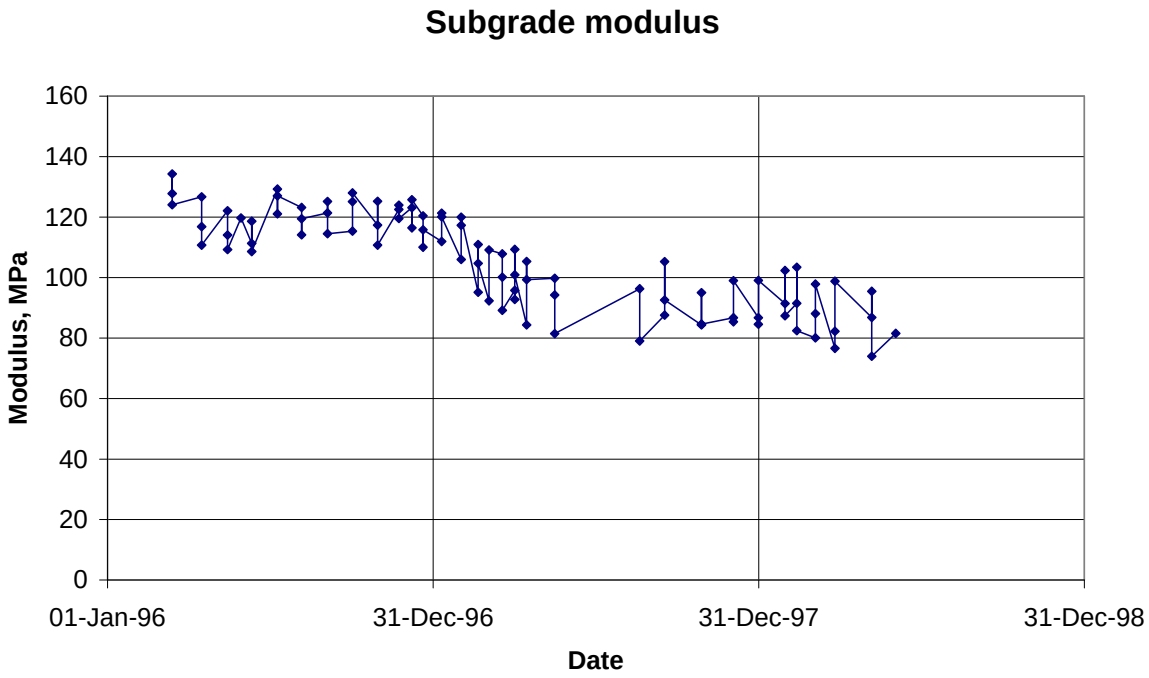

Figure 42. Modulus of subgrade for Section 18.

The subgrade modulus did not appear to be a function of the stiffness of the pavement layers, but it did vary during the experiment, as shown in Figure 42. The variation, which was probably associated with the

flooding of Carson River in early 1997, was not a systematic seasonal variation and cannot be modeled in the present version of *CalME*. Other sections also showed irregular variations of the moduli of both the aggregate base and subgrade that could not be modeled.

The aggregated base was assumed to increase in modulus with the bulk stress raised to a power of 0.6, and the subgrade was assumed to decrease in modulus with the deviator stress raised to -0.2.

3.1.5.2 Moduli from Triaxial Tests

Triaxial tests were available for the aggregate base and for some of the engineering fill lifts, but only for some of the test sections.

For the aggregate base the triaxial modulus was primarily a function of the bulk stress, $\theta = \sigma_1 + \sigma_2 + \sigma_3$, with the shear stress (or deviator stress) having very little effect on the modulus. The modulus could be calculated from:

$$Eab = 206\,MPa \times \left(\frac{\theta}{0.1\,MPa} \right)^{0.64}$$

Equation 21. Modulus of Aggregate Base from triaxial tests.

The agreement between the modulus measured in triaxial tests and the modulus calculated from Equation 21 is shown in Figure 43.

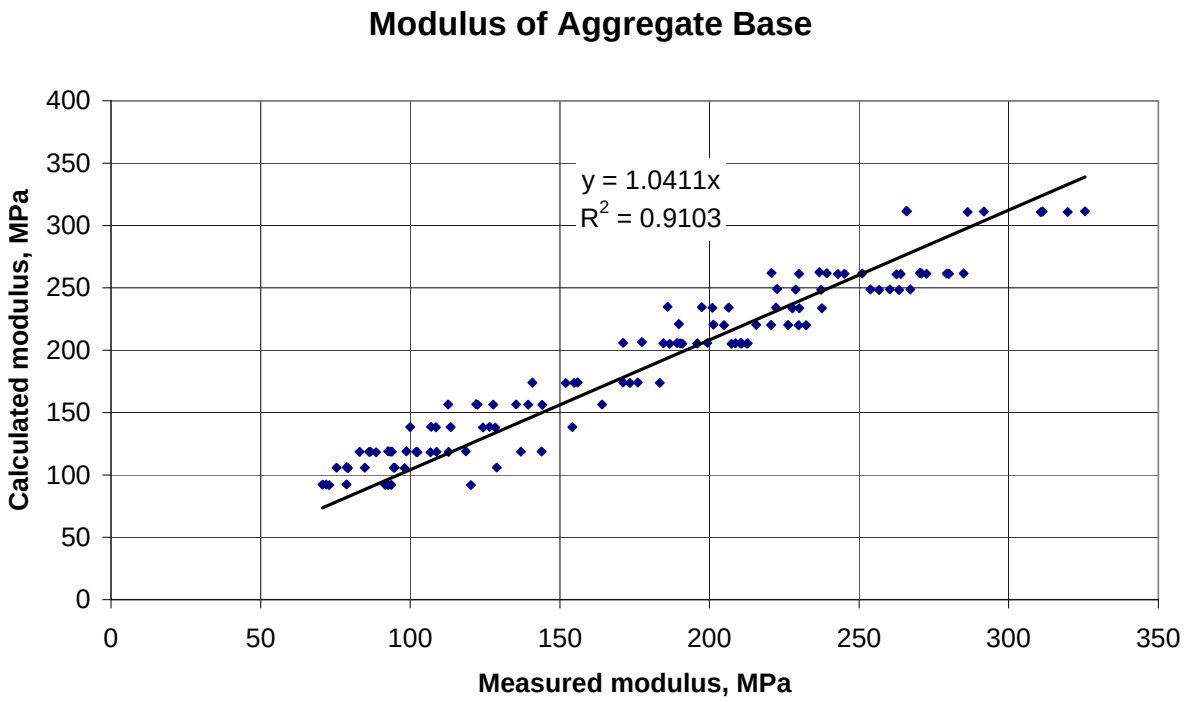

Figure 43. Moduli calculated from Equation 21 versus moduli from triaxial tests.

For the engineering fill the variation was very large from section to section and it was not possible to describe the modulus by a single relationship.

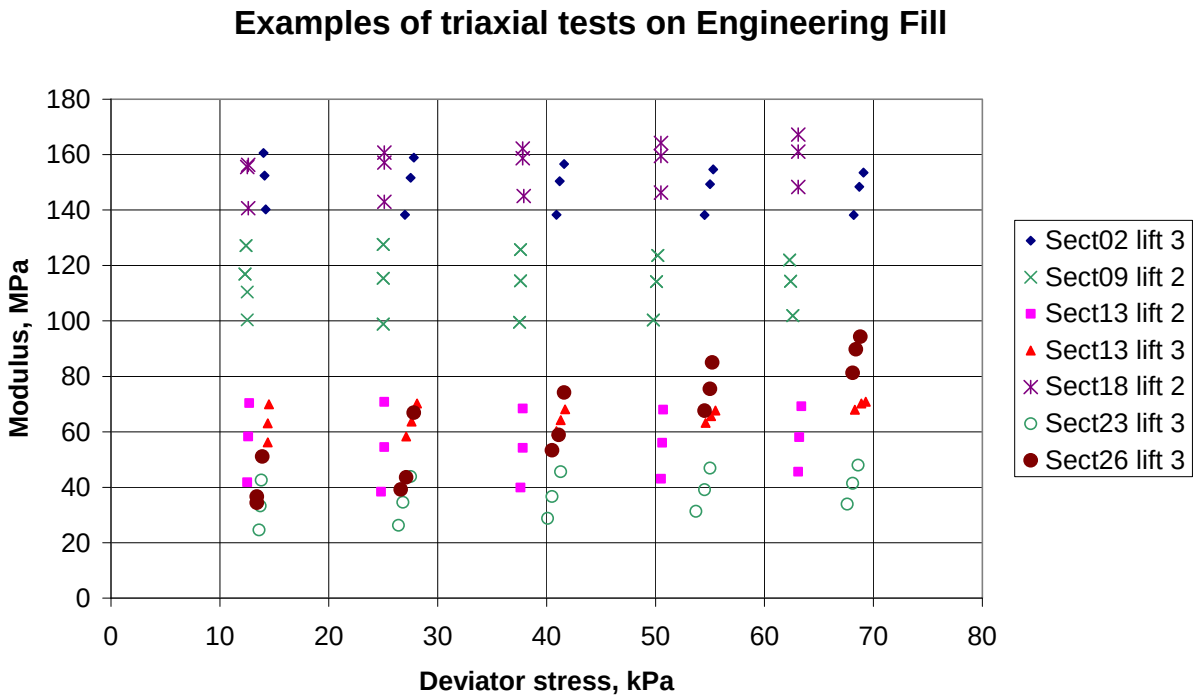

Figure 44. Examples of triaxial tests on engineering fill, at varying confining and deviator stresses.

Some examples of the results of triaxial tests on the subgrade material are shown in Figure 44. The modulus is shown as a function of the deviator stress and the vertical differences (within a test section) are due to differences in confining stress. It can be seen that the increased deviator stress can both cause an increase and a decrease in the modulus, depending on the section where the subgrade material was sampled.

3.1.5.3 Comparison of Backcalculated Moduli with Moduli Calculated Using Models

To relate the triaxial test results to the moduli under truck loading the bulk stress was calculated for the duration of the test for Section 18 using *CalME*. The bulk stress was calculated at depths of 50 mm below the surfaces of the aggregate base and subgrade (engineering fill), as shown in Figure 45.

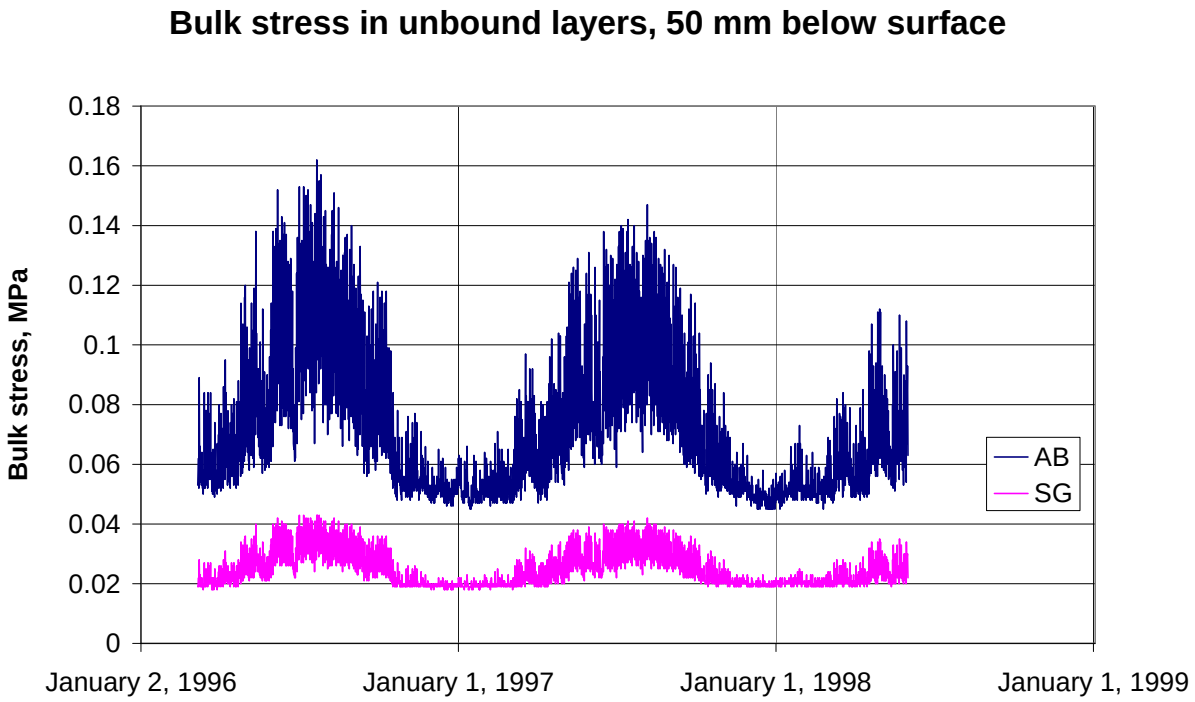

Figure 45. Bulk stress in aggregate base and in subgrade, 50 mm below the surface of the layers, Section 18, calculated using CalME.

For the aggregate base the bulk stress was used to calculate the modulus for the duration of the test. For the subgrade triaxial tests with a bulk stress of 0.02 to 0.04 MPa were used to determine the moduli.

Figure 46 shows the modulus of the AB, as calculated from the bulk stress using Equation 21 for triaxial tests and as determined from backcalculation of FWD data. During cold periods where the asphalt layer is stiff the bulk stress in the AB is low, resulting in a low triaxial modulus. The opposite is true for the FWD moduli, which is reflected by the function in Equation 20 showing aggregate base stiffness increasing with increased asphalt layer stiffness.

Figure 47 compares the moduli calculated by *CalME*, using the stiffness function in Equation 20 to the moduli backcalculated from FWD testing, indicating a much better match to the results than the triaxial based results shown in Figure 46.

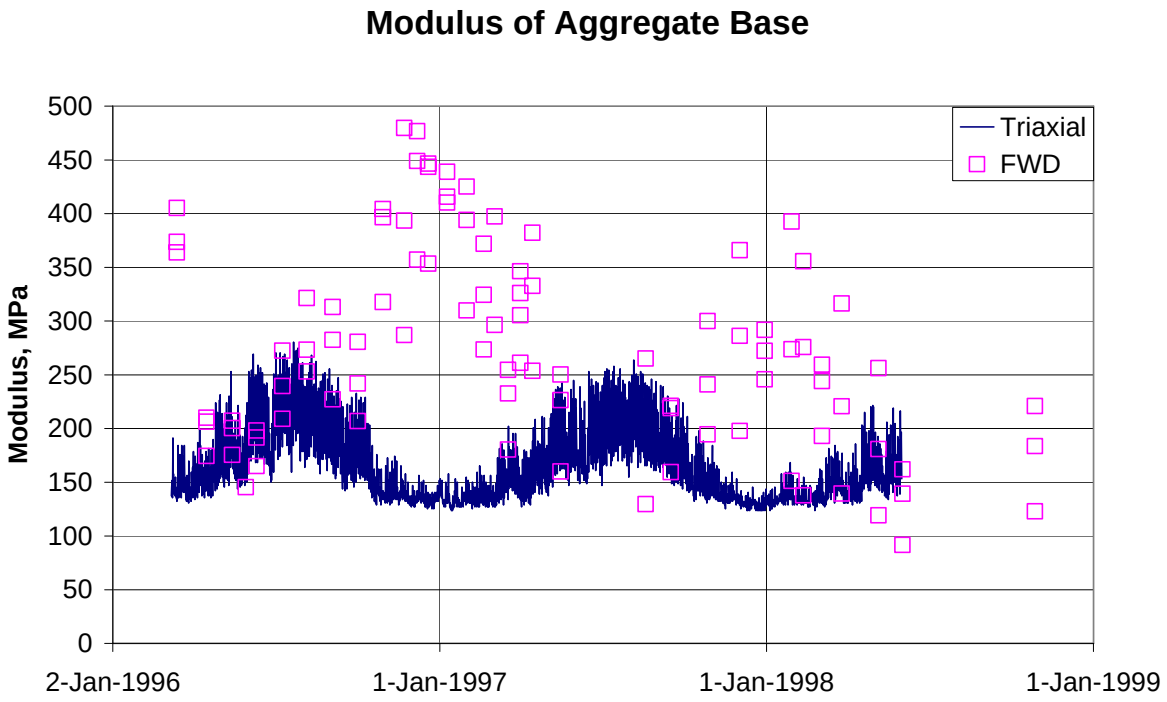

Figure 46. AB moduli at test Section 18, from triaxial tests and backcalculated from FWD.

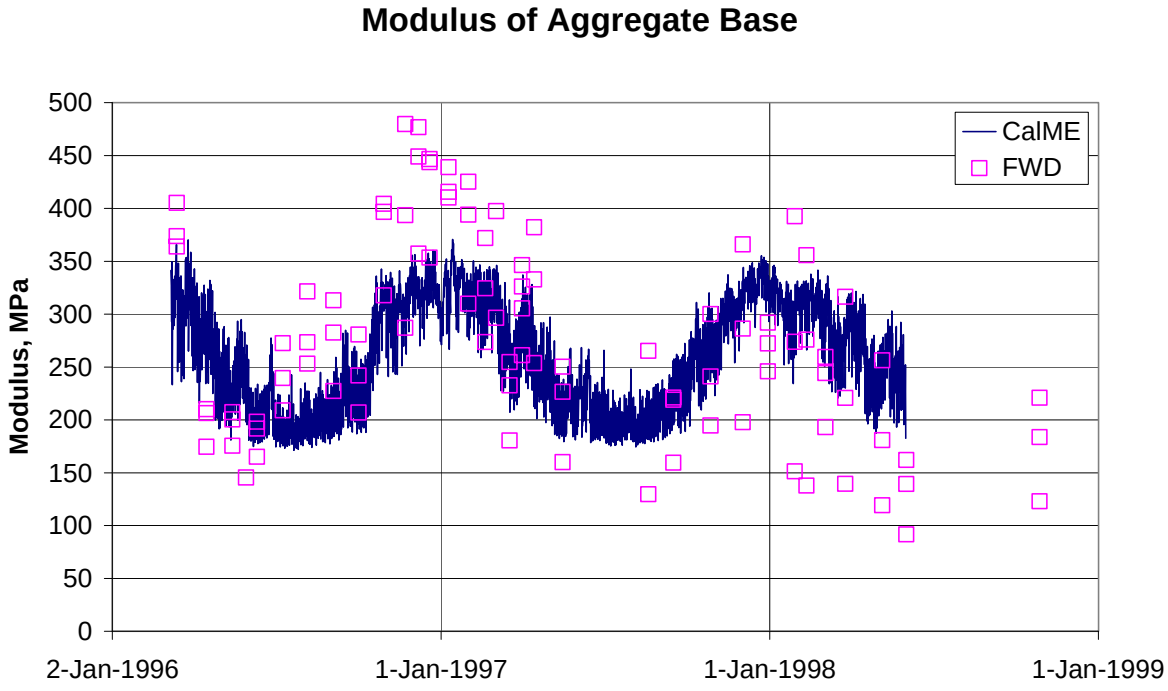

Figure 47. AB moduli calculated by CalME compared to FWD determined moduli.

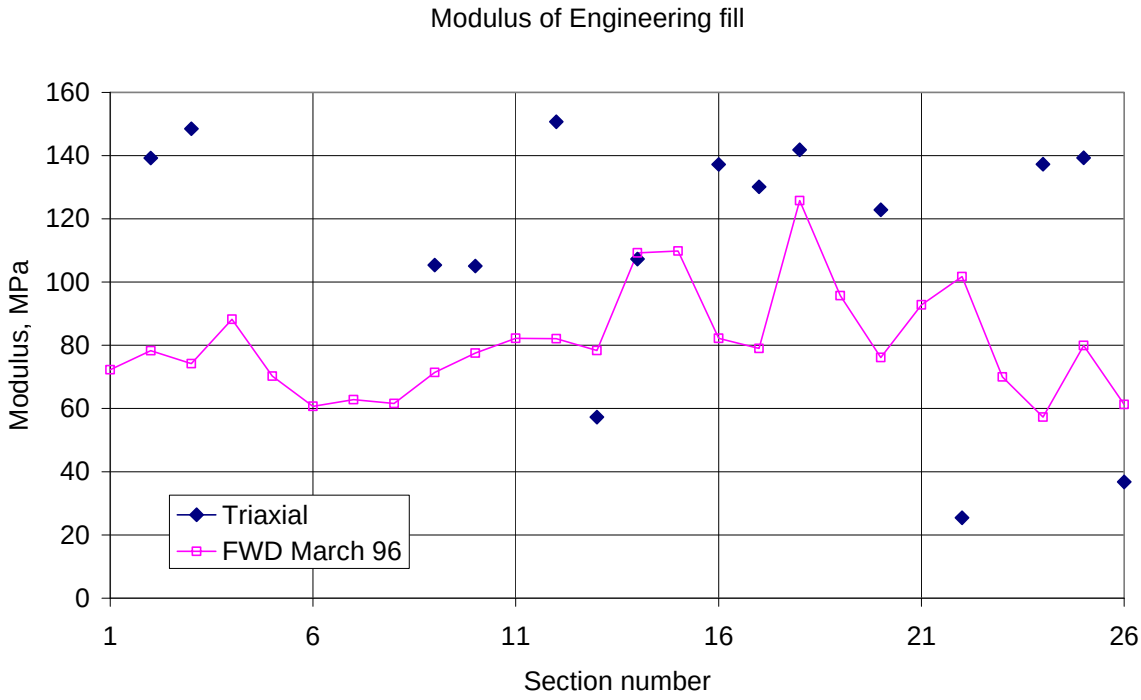

Figure 48. Modulus of subgrade from triaxial tests and from FWD backcalculation.

Figure 48 shows the moduli of different lifts of the engineering fill, as determined from triaxial testing at a bulk stress of 0.03 to 0.04 MPa, which is on the high side of the calculated bulk stress. As a comparison the moduli from the first FWD tests in March 1996 are shown. The average modulus from triaxial testing is 112 MPa. The average modulus from FWD tests is 81 MPa. Multiplying the FWD-derived subgrade moduli by a factor of 0.35, as recommended by the MEPDG, would clearly not be appropriate.

3.1.6 Asphalt Fatigue (Damage)

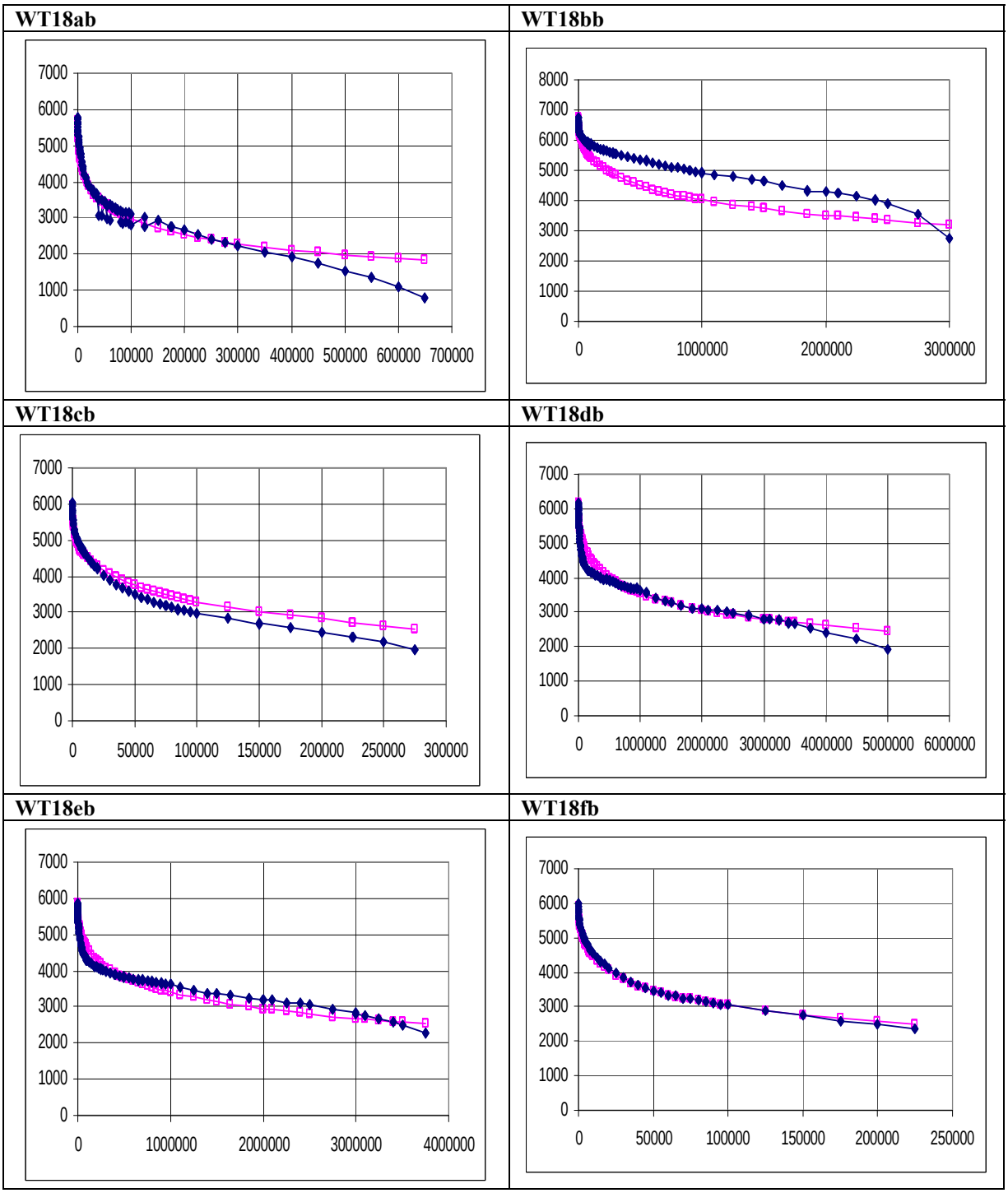

Figure 49. Modulus in MPa versus number of load applications during fatigue tests for Section 18. (Note: measured values are filled diamonds and calculated values are open squares. Specimen numbers are shown above each plot.)

The results of flexural fatigue controlled strain beam tests on Field Mixed, Field Compacted (FMFC) specimens at 20ºC and 10 Hz were used to calibrate the asphalt damage model in *CalME*. The fatigue tests are stored in the database *RSST_Fatigue.mdb*. The model for damaged asphalt modulus had the format:

$$\log(E) = \delta + \frac{\alpha \times (1-\omega)}{1+\exp(\beta+\gamma\log(tr))}$$

Equation 22. Modulus of damaged asphalt.

where the damage, ω, is calculated from:

$$\omega = A \times MN^{\alpha} \times \left(\frac{\mu\varepsilon}{200\ \mu strain}\right)^{\beta} \times \left(\frac{E}{3000\,MPa}\right)^{\gamma} \times \left(\frac{E_i}{3000\,MPa}\right)^{\delta}$$

Equation 23. Damage as a function of number of loads, strain, modulus and initial modulus.

where E_i is the modulus of intact material,
E is the modulus of damaged material,
MN is the number of load repetitions in millions ($N/10^6$),
$\mu\varepsilon$ is the strain at the bottom of the asphalt layer in μstrain, and
α, β, γ, and δ are constants (that are not related to the constants in Equation 8 or Equation 22).

The initial (intact) modulus, E_i, corresponds to a damage, ω, of 0 and the minimum modulus, $E_{min}=10^{\delta}$, to a damage of 1.

Equation 22 leads to:

$$\log(E) - \delta = (\log(E_i) - \delta) \times (1-\omega), \text{ or}$$

$$\frac{E}{E_i} = \left(\frac{E_{\min}}{E_i}\right)^{\omega}, \text{ or}$$

$$\omega = \frac{\log\left(E/E_i\right)}{\log\left(E_{\min}/E_i\right)}$$

Equation 24. Relations between moduli and damage.

Damage is sometimes defined as the relative decrease in modulus, $(E_i - E)/E_i = dE/E_i$. The MEPDG defines damage both through Equation 22 and as the relative decrease in modulus (2). These two definitions of damage used in MEPDG are incompatible with each other. If damage is defined through Equation 22 then the relative decrease in modulus will depend on the minimum modulus, E_{min}, and on the initial modulus, E_i, which again is a function of temperature and loading time. Figure 50 shows relative decrease in modulus on the y-axis, plotted against damage defined using Equation 22, for E_{min} = 100 MPa and different values of E_i.

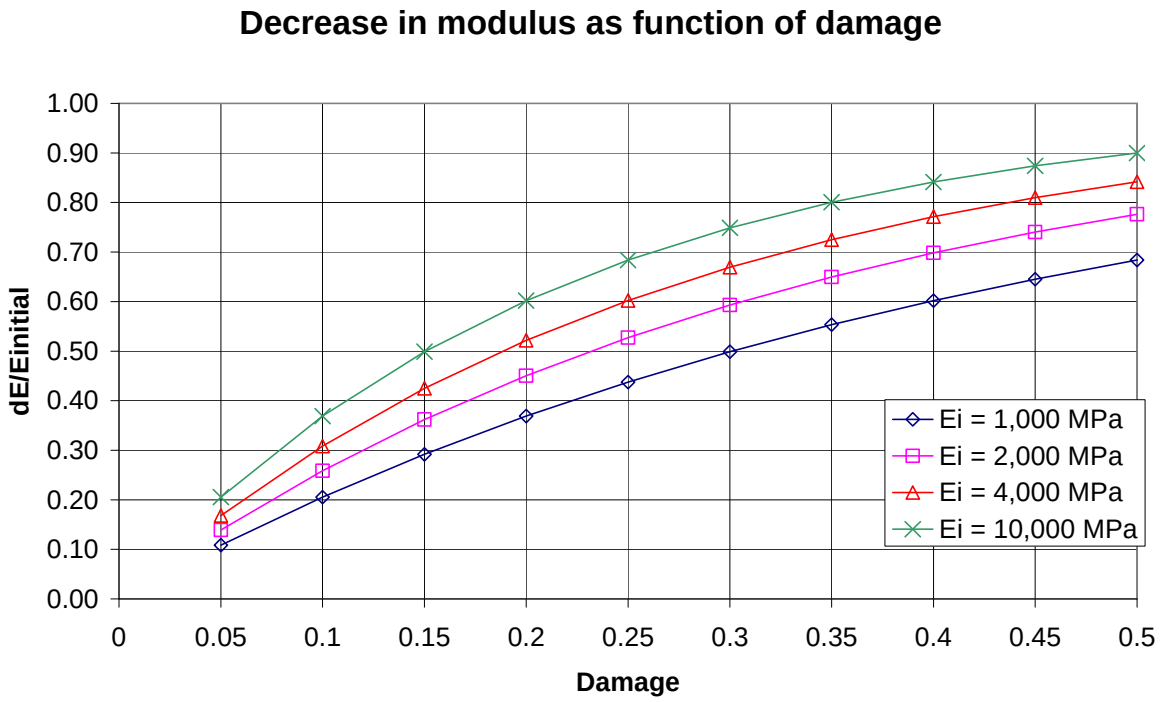

Figure 50. Relative decrease in modulus as a function of damage, for Emin = 100 MPa.

The parameters of Equation 23 were determined from time histories of the flexural fatigue tests in *Excel* by minimizing the Root Mean Square (RMS) difference between measured and calculated relative modulus (using "Solver") for the six beams tested for each section (two strain levels, three replicates at each strain level). The measured and calculated moduli for the six beams tested for Section 18 are shown in Figure 49. The power γ in Equation 23 was kept equal to $\beta/2$, making damage a function of the internal energy density (and reducing the number of parameters to be determined by one). The parameter δ was based on the parameter for initial asphalt moduli in the Asphalt Institute criterion for asphalt fatigue. With this criterion the damage will be proportional to the initial modulus raised to $-\alpha$ times -0.854 in Equation 23. This results in positive values of δ between 0.3 and 0.5.

Section 15FMM2 had fatigue tests at three different temperatures, 5, 20, and 30ºC. From these tests a value of δ = -1.9, for laboratory tests, may be derived. This value is in good agreement with values determined for AC materials used during HVS tests, but it will cause a very high rate of damage in a pavement structure at high temperatures. This was not a problem during the simulation of the HVS tests as all of the tests where damage could be determined from deflection measurements, with MDDs or RSD, were done at an almost constant temperature of 20ºC.

Figure 51 illustrates the problem. In this figure, damage has been calculated both for the fatigue relationship derived from the laboratory tests on Section 15FMM2, with δ = -1.9306, and for the relationship used in the simulations of WesTrack with *CalME*, where δ was 0.3788. The master curve determined for Section 15FMM2 is used for the modulus of the AC layer in the calculations. A 150mm thick AC layer resting on a granular base with a modulus of about 220 MPa was assumed. The structure was loaded by a 20 kN single wheel load with a tire pressure of 0.7 MPa. The tensile strain at the bottom of the AC layer was calculated using Odemark-Boussinesq's approach, and the damage was accumulated using an incremental-recursive procedure. The figure shows the accumulated damage after 200 load applications, at different temperatures (the temperature being kept constant during the 200 load applications).

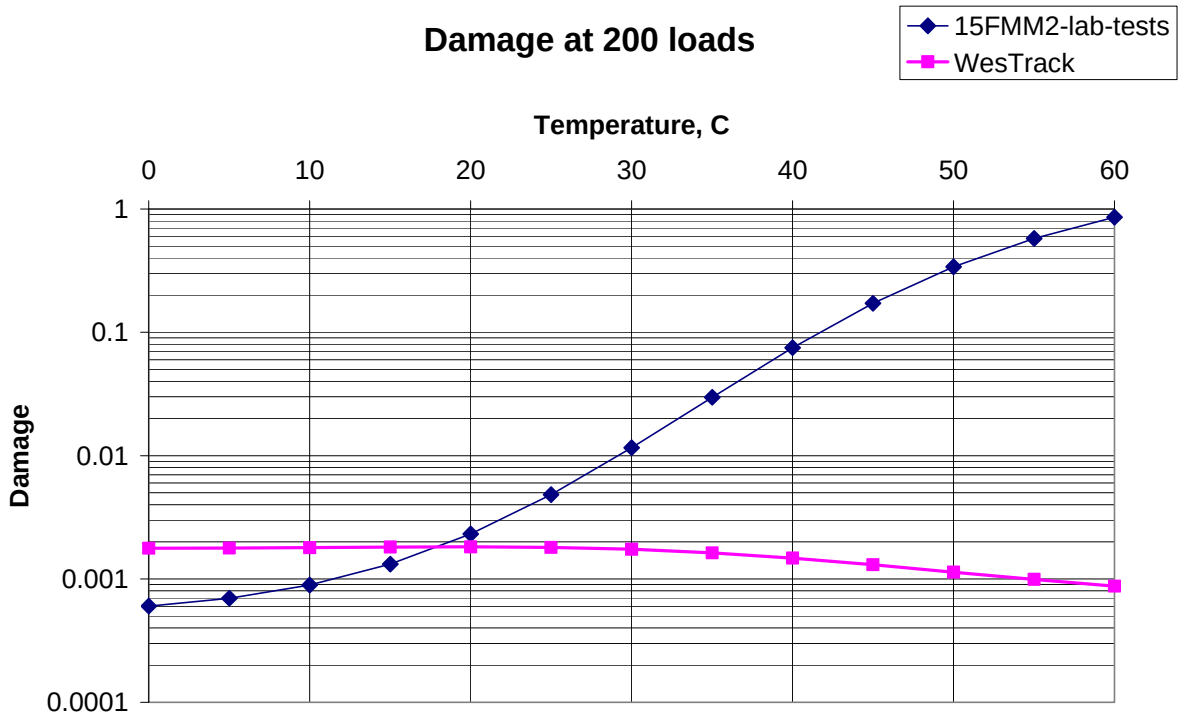

Figure 51. Damage calculated for laboratory value of δ and value used in WesTrack simulation.

The maximum temperatures at the WesTrack experiment were close to 60ºC. At this temperature 200 load applications (of a 20 kN load) would lead to complete failure, with a damage value close to 1. This creates two problems:

- One is that a very high shift factor must be used (a value of several hundred) to avoid simulations that result in premature failure of the sections. Such a high shift factor is unreasonable when compared to the simulations of the HVS tests where a factor of 3 was found.
- The other problem is that according to the simulations using the laboratory values the decrease in modulus would take place during the warm seasons. This is contrary to the change in moduli determined from FWD tests, which show a decrease in modulus during the cold seasons.

Because of these problems the value of δ in the damage relations was determined as described above. It should be noted that the stress conditions at the bottom of an asphalt layer at very high temperatures are quite different from those of a fatigue beam in the laboratory. In the laboratory test the first stress invariant is always tensile whereas the first stress invariant at the bottom of an asphalt layer will change with temperature and may become compressive at high temperatures.

3.1.7 Permanent Deformation

3.1.7.1 Rutting of Asphalt Layer

For rutting of the asphalt layer a shear based approach, developed by Deacon et al. (12), was used. In this approach, rutting in the asphalt is assumed to be controlled by shear deformation. The computed values of shear stress, τ, and elastic shear strain, γ^e, at a depth of 50 mm beneath the edge of the tire are used for the rutting estimates. Repeated Simple Shear Tests at Constant Height (RSST-CH) performed in the laboratory on WesTrack materials were used to determine the permanent deformation coefficients. RSST-CH tests were only performed on cores from the top lift of asphalt. Tests were performed on the following (4):

- Field cores from all sections prior to trafficking,

- Field cores taken in the wheelpath for sections 7, 9, 13, 21, and 25 after the first year of trafficking,
- Field cores taken in the wheelpath for all remaining original sections and the replacement sections at the end of trafficking, and
- From specimens mixed in the laboratory and compacted in the laboratory with rolling wheel compaction.

In *CalME*, rutting in the AC layer due to the shear deformation is determined from the following:

$$rd_{AC}\ mm = K \times 100 \times \gamma^{i} = K \times 100 \times A \times MN^{\alpha} \exp\left(\frac{\beta \times \tau}{resp_{ref}}\right) \times \left(\gamma^{e}\right)^{\gamma}$$

Equation 25. Rutting in AC from shear deformation.

where γ^{i} = permanent (inelastic) shear strain at 50 mm depth,
τ =shear stress determined at this depth using elastic analysis,
γ^{e} = corresponding elastic shear strain (m/m),
K is a value relating permanent shear strain to rut depth (mm), and
A, α, β, $resp_{ref}$, and γ are constants.

The variable $resp_{ref}$ was selected as atmospheric pressure (0.1 MPa) and γ was assumed to be 1. All the RSST-CH tests were done at a constant shear stress, therefore a value β of 1.03, determined from previous experiments, was used.

The AC layer was subdivided into three layers in the layer elastic calculation of elastic shear stress and strain to simulate the effects of temperature gradients on the mix stiffness, with thicknesses from top to bottom of 25 mm, 50 mm, and the remaining AC thickness as the third layer.

The permanent deformation was pro rated over the upper 100 mm of the asphalt layers (which is the reason for the factor 100 in Equation 25). Observation of trenched sections at WesTrack, and experience with high-temperature rutting tests with the Heavy Vehicle Simulator indicate that nearly all asphalt layer rutting typically occurs in the 100 mm nearest the surface. The shear stress is only calculated at the depth of 50 mm but the shear strain is determined in each asphalt sublayer, from the shear stress at 50 mm, and the shear modulus at the one-third depth of the sublayer. These values are used with Equation 25, substituting the factor 100 with the thickness of the layer in millimeters.

In addition to the permanent deformation caused by shearing, a certain amount of deformation was caused by the decrease in air-voids content (post compaction, see Table 11 and Table 12). A correlation analysis showed that for the top lift the air-void content dropped by 40 percent from initial to intermediate condition (one year later) and by 46 percent from initial to final condition. For the bottom lift the corresponding numbers were 33 percent and 44 percent respectively.

Table 11. Top Lift Air-void content (AVi = initial, AVint = intermediate, AVf = final)

Mix	Section	Target	AVi	AVint	AVf
FMM1	1	8	8.8		5.7
FLM	2	8	10.4	8.2	7.8
FLH1	3	12	12.4	6.4	7.2
FML	4	4	6.6	4.7	4.7
CMM1	5	8	8.1	4.5	replaced
CMH	6	12	10.8	5.3	replaced
CHM	7	8	6.9	High cracked	replaced
CLM	8	8	8.5	7.6	replaced
PHL2	9	4	3.9	High cracked	replaced
PLH	10	12	11.8	7.0	6.5
PMM2	11	8	7.9	4.5	2.2
PML	12	4	4.6	3.3	1.5
PHM	13	8	5.9	High cracked	replaced
FHM	14	8	9.0	4.4	2.1
FMM2	15	8	8.7	6.7	6.4
FLH2	16	12	12.2	9.1	8.2
FMH	17	12	11	6.9	6.5
FHL	18	4	4.3	2.1	2.1
PMM1	19	8	7.2	2.3	2.5
PMH	20	12	10.9	3.3	2.9
PHL1	21	4	4.2	High cracked	replaced
PLM	22	8	8.1	4.7	4.9
CML	23	4	4.9	2.1	2.7
CMM2	24	8	7.2	3.2	replaced
CHL	25	4	3.7	High cracked	replaced
CLH	26	12	11.0	9.0	replaced

Table 12. Bottom Lift Air-void content (AVi = initial, AVint = intermediate, AVf = final)

Mix	Section	Target	AVi	AVint	AVf
FMM1	1	8	8.8		5.0
FLM	2	8	10.0	6.1	3.7
FLH1	3	12	12	9.3	6.4
FML	4	4	6.1	5.0	4.7
CMM1	5	8	9.2	7.0	replaced
CMH	6	12	13.9	7.6	replaced
CHM	7	8	8.1	high cracked	replaced
CLM	8	8	8.4	7.2	replaced
PHL2	9	4	2.5	high cracked	replaced
PLH	10	12	12.7	9.5	7.7
PMM2	11	8	6.9	4.5	3.6
PML	12	4	5.4	2.7	3.0
PHM	13	8	6.5	high cracked	replaced
FHM	14	8	6.7	2.5	2.3
FMM2	15	8	7.5	5.1	5.5
FLH2	16	12	11.5	7.9	7.9
FMH	17	12	10.5	7.4	6.3
FHL	18	4	4	3.2	3.0
PMM1	19	8	7.2	3.4	3.2
PMH	20	12	8.8	4.6	3.3
PHL1	21	4	3.2	high cracked	replaced
PLM	22	8	8.1	6.4	5.8
CML	23	4	6.6	4.5	3.7
CMM2	24	8	9.2	6.8	replaced
CHL	25	4	4.6	high cracked	replaced
CLH	26	12	12.9	8.6	replaced

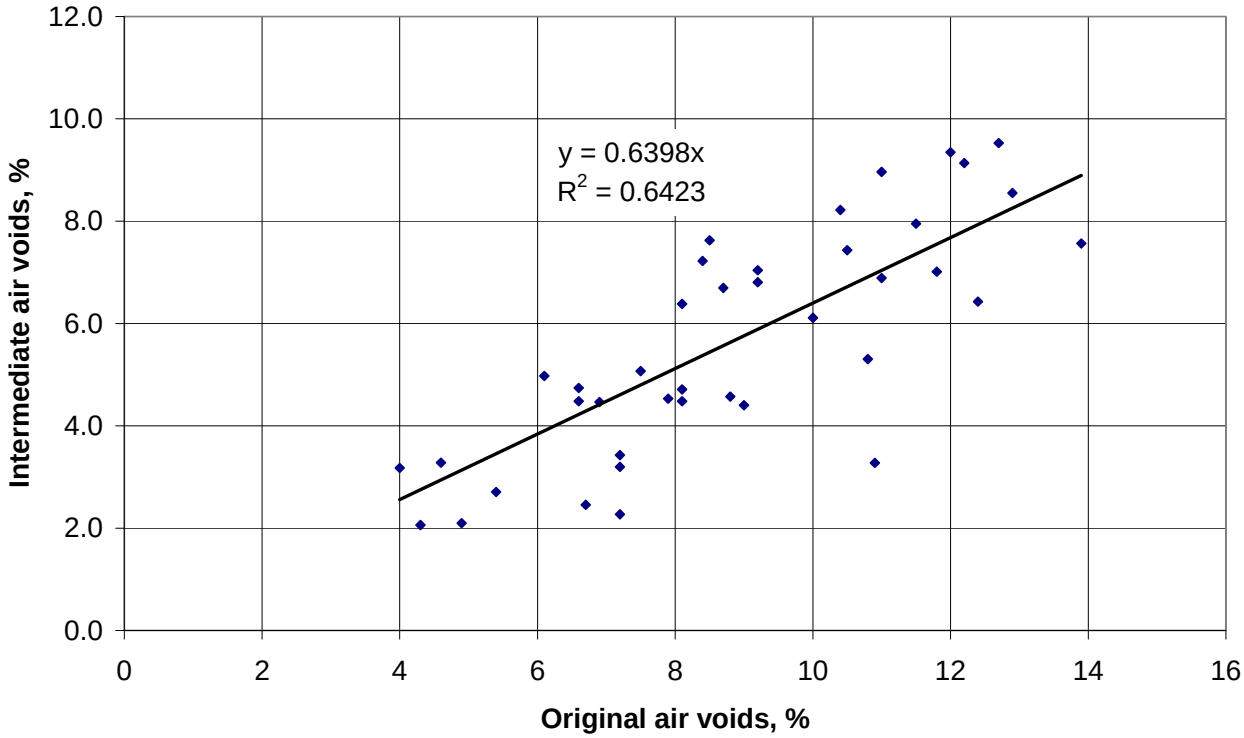

Figure 52. Air-voids of original mix and after intermediate traffic, top and bottom lifts combined.

Original and intermediate air-void contents are shown plotted against each other in Figure 52. The average decrease in air voids from the original to the intermediate state, ΔAV, for the top and bottom lifts combined, is:

$$\Delta AV = 0.36 \times AV_{original}$$

Equation 26. Average decrease in air voids.

This decrease was used in the simulations with *CalME*. It was assumed to occur over the first 60 days with traffic loading, and was distributed over the asphalt layers, proportional to the thickness of the layers. This last assumption may result in too large a contribution to the rut depth from the bottom layer.

From Figure 15, Figure 16, and Figure 17 it is evident that most of this post compaction to "intermediate condition" took place within the first few months of the experiment during the summer. It was therefore decided to use the samples from sections that had been under traffic for determining the parameters A and α in Equation 25. The parameters were determined by minimizing the RMS difference between the permanent shear strain measured in the RSST-CH test and that resulting from the permanent shear strain part of Equation 25. The best fit is shown in Figure 53 for Section 18 for the two replicate specimens tested.

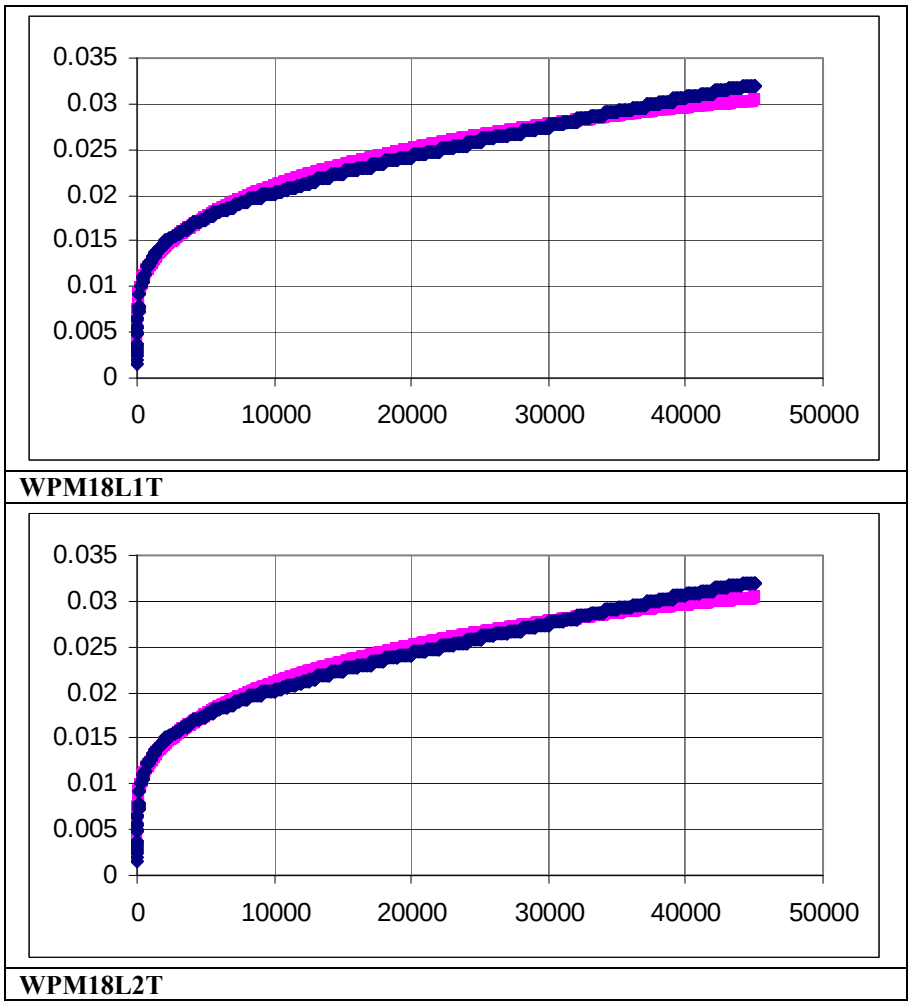

Figure 53. Permanent shear strain versus number of load applications, RSST-CH on Section 18.

The parameters obtained were A = 13.3 and α = 0.189.

3.1.7.2 Rutting of Unbound Layers

For permanent deformation, *dp*, of each of the unbound layers the following model was used for all sections (13):

$$dp\ mm = A \times MN^{\alpha} \times \left(\frac{\mu\varepsilon}{1000\ \mu strain} \right)^{\beta} \times \left(\frac{E}{40\ MPa} \right)^{\gamma}$$

Equation 27 Permanent deformation of unbound layers.

where $\mu\varepsilon$ is the vertical compressive strain at the top of the layer and

E is the modulus of the material.

A was 0.8 mm for aggregate base and 1.1 mm for subgrade. α = 0.333, β = 1.333 and γ = 0.333 were used for both layers. These are the same values as used for HVS calibration (1).

3.2 Roughness

Roughness was measured, in terms of the International Roughness Index (IRI), in both of the wheelpaths. In *CalME* simulations for WesTrack the increase in IRI, *ΔIRI*, was predicted from a simple subgrade strain model (13):

$$\Delta IRI\ m/km = A \times MN^{\alpha} \times \left(\frac{\mu\varepsilon}{1000\ \mu strain} \right)^{\beta} \times \left(\frac{E}{40\ MPa} \right)^{\gamma}$$

Equation 28. Roughness model for subgrade.

where $\mu\varepsilon$ is the elastic vertical compressive strain at the top of the subgrade and
E is the modulus of the material.

The parameters used were A = 0.64 m/km, α = 0.333, β = 1.333 and γ = 0.333.

3.2.1 Summary of Input Parameters for *CalME* for Section 18FHL

The input parameters in the *CalME* database used for the example simulation of Section 18 are shown in Table 13.

Table 13. Input Parameters for Section 18

Modulus	***α***	***B***	***γ***	***δ***	***aT***	***A***	***VTS***
AC	2.1761	-0.8842	0.5526	2.000	1.300	10.0406	-3.680
Unbound	*Eo*	*Stiffness factor*	*Power on load*	*Estart*			
AB	317 MPa	0.31	0.6	286 MPa			
Subgrade	100 MPa	0	-0.2	100 MPa			
Aging	*AgeA*	*AgeB*					
AC	0.112	0.3391					
Fatigue	*A*	*A*	*β*	*γ*	*δ*		
AC	0.08116	0.4741	2.0904	1.0452	0.4049		
Rutting	*A*	*A*	*β*	*γ*	*dVoids*		
AC	13.33	0.189	1.03	1	1.5		

3.3 Simulation of Section 18 with CalME

The simulation of Section 18 was performed with one-hour time steps for the entire WesTrack experiment, with the temperatures and loads recorded for that hour.

As mentioned earlier, each truck passage had a steering wheel (single tire) with an axle load of 53 kN and seven axles loaded to 89 kN with dual wheels. All the dual loads were treated as individual loads. As also mentioned previously, the wheel loads were initially assumed to be normally distributed laterally with a standard deviation of 300 mm at the beginning of the experiment decreasing linearly to 0 mm at a rut depth of 6 mm. Because of the uncertainties with respect to the actual distribution of the loads the wander was eventually abandoned. Because of the short period with wander during the initial assumptions (to a rut depth of 6 mm) this had little influence on the results.

The first step in the simulation process is to ensure that the mechanistic model predicts the resilient response reasonably well. The response measurements available for WesTrack are the FWD deflections. A shift factor of 15 was used for the asphalt damage to get a reasonably good agreement with the measured deflections for Fine and Fine Plus mixes. For Coarse mixes the shift factor was 5. This means that one load in

the laboratory fatigue test causes as much damage as 15 (or 5 for Coarse mix) in situ loads during WesTrack, at the same strain level and modulus. The shift factor used in the Asphalt Institute's criterion is 18.4, and that found from calibration of HVS data was 3.

Figure 54 shows the FWD deflection at the center of the loading plate in the wheelpath (F3) as a function of time. The deflections correspond to a peak load of approximately 40 kN (the actual load level was used both for measured and calculated values). The legends marked "M" are the measured values. The measured points are connected by fully drawn lines. The corresponding calculated deflections have legend "C" and the points are connected by dotted lines. Figure 54 shows results from four FWD positions within Section 18. "35_1" in the header of the figure indicates a test point between chainage 30 and 39.

The agreement between the measured and the calculated deflections is seen to be very good in this case. The mean difference between the four measured deflections in Figure 54 is 2 µm (10^{-6} m) and the Root Mean Square (RMS) difference is 55 µm. The mean difference between measured and calculated deflections is 3 µm and the RMS is 33 µm.

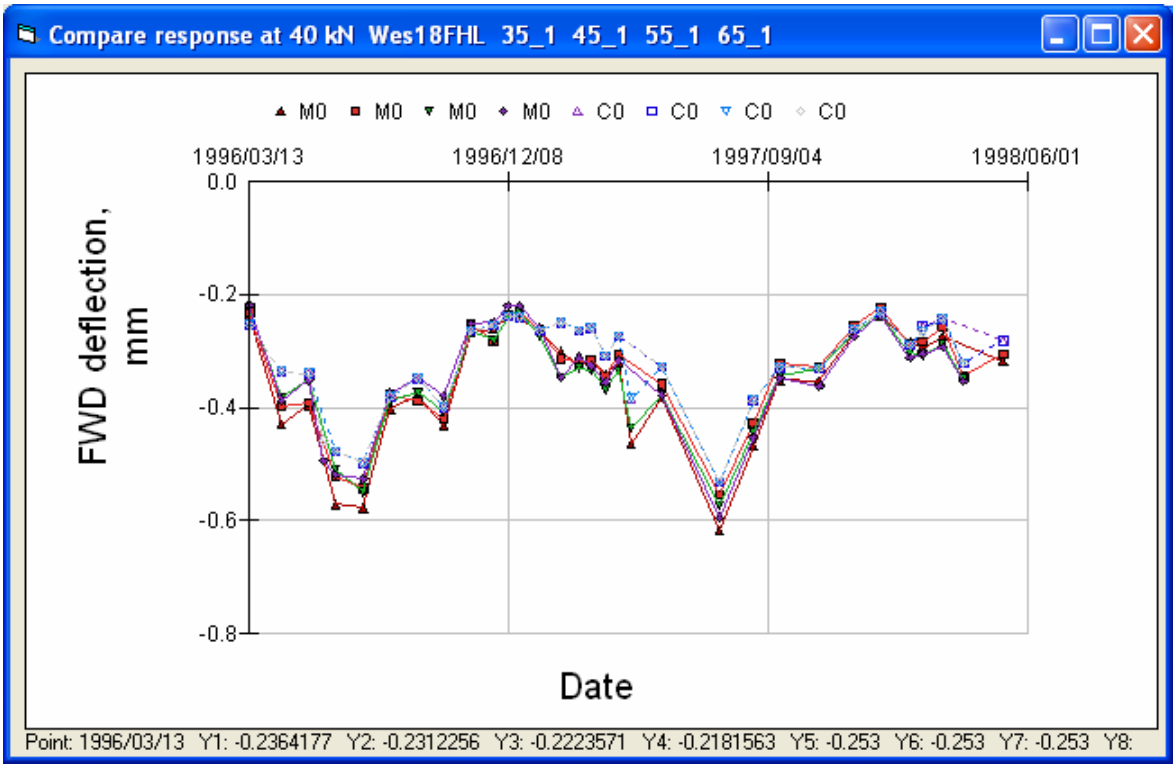

Figure 54. FWD deflections at Section 18 (in wheelpath, geophone under the loading plate).

Figure 55 shows the measured deflections between the wheelpaths, compared with the calculated deflections based on the damaged asphalt in the wheelpath (calculated deflections are identical to the calculated deflections of Figure 54). The figure clearly shows that the asphalt in the wheelpaths did suffer some damage, resulting in larger deflections, even though no visible fatigue cracking was recorded.

Figure 56 and Figure 57 show the deflections at a distance of 1,219 mm (geophone No. 6). This deflection is controlled almost entirely by the subgrade modulus. At the start of the experiment the calculated deflections are larger than the measured deflections, both in the wheelpath and between the wheelpaths, indicating that the subgrade modulus is underestimated. Towards the end of the experiment the measured deflections are larger than the calculated deflections, particularly in the wheelpath. This is in good agreement with the measured change in subgrade modulus shown in Figure 42. In the simulation the modulus was kept constant equal to 100 MPa.

The damage parameter, ω, of Equation 22 and Equation 23 is shown in Figure 58, as calculated by *CalME* (for the top 25 mm of the asphalt; for the lower layers the damage was a little less) and as determined from the FWD backcalculated asphalt moduli, adjusted for temperature and aging . The recorded fatigue cracking on the surface (zero in this case) is also shown.

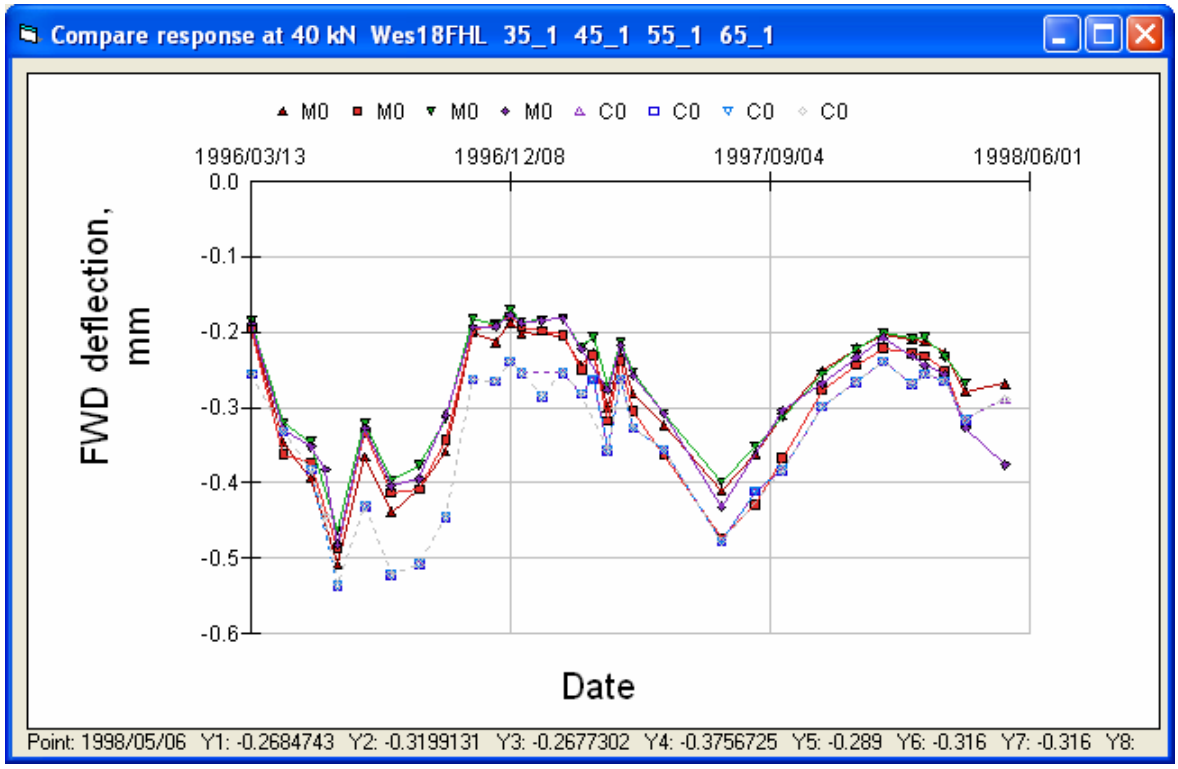

Figure 55. FWD deflections at Section 18 (between wheelpaths, geophone under load plate).

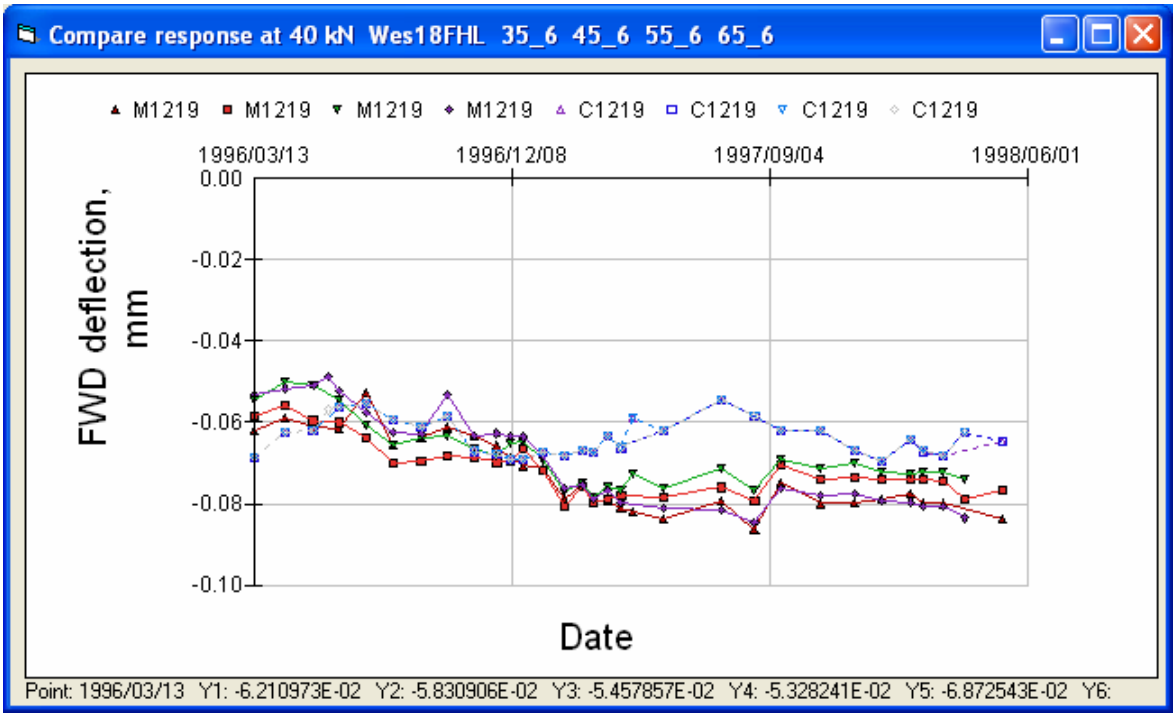

Figure 56. FWD deflections at Section 18 (in wheelpath, geophone at 1,219 mm from load plate).

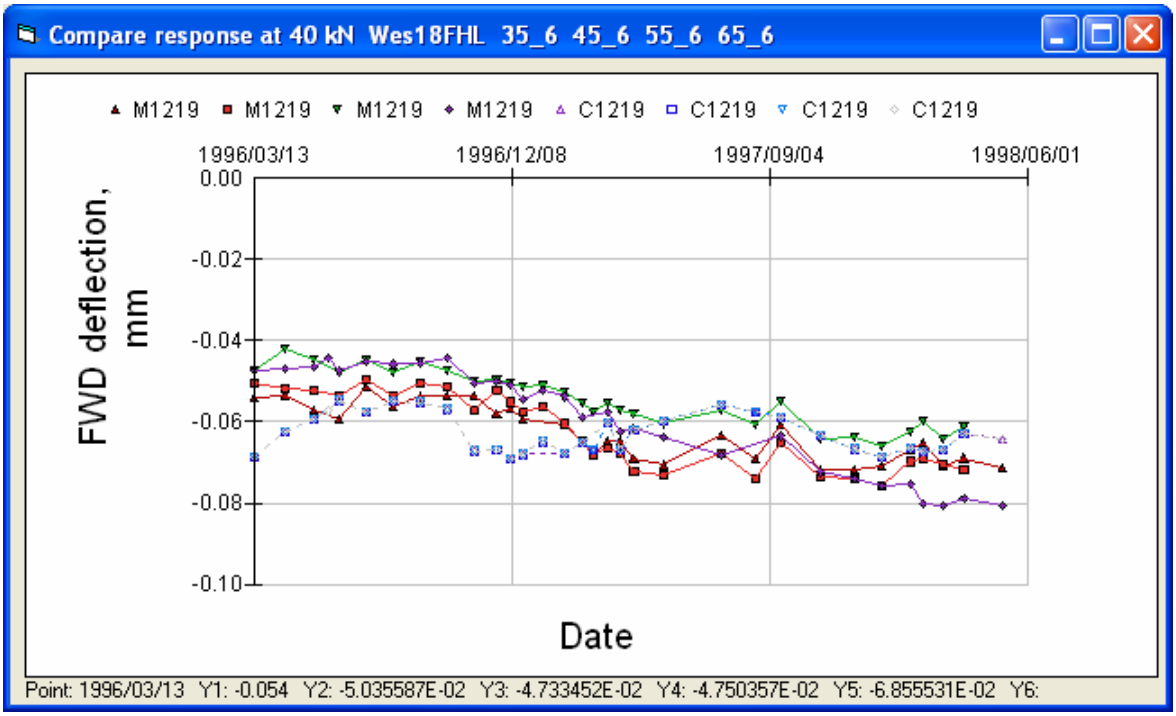

Figure 57. FWD deflections at Section 18 (between wheelpaths, geophone at 1,219 mm from load plate).

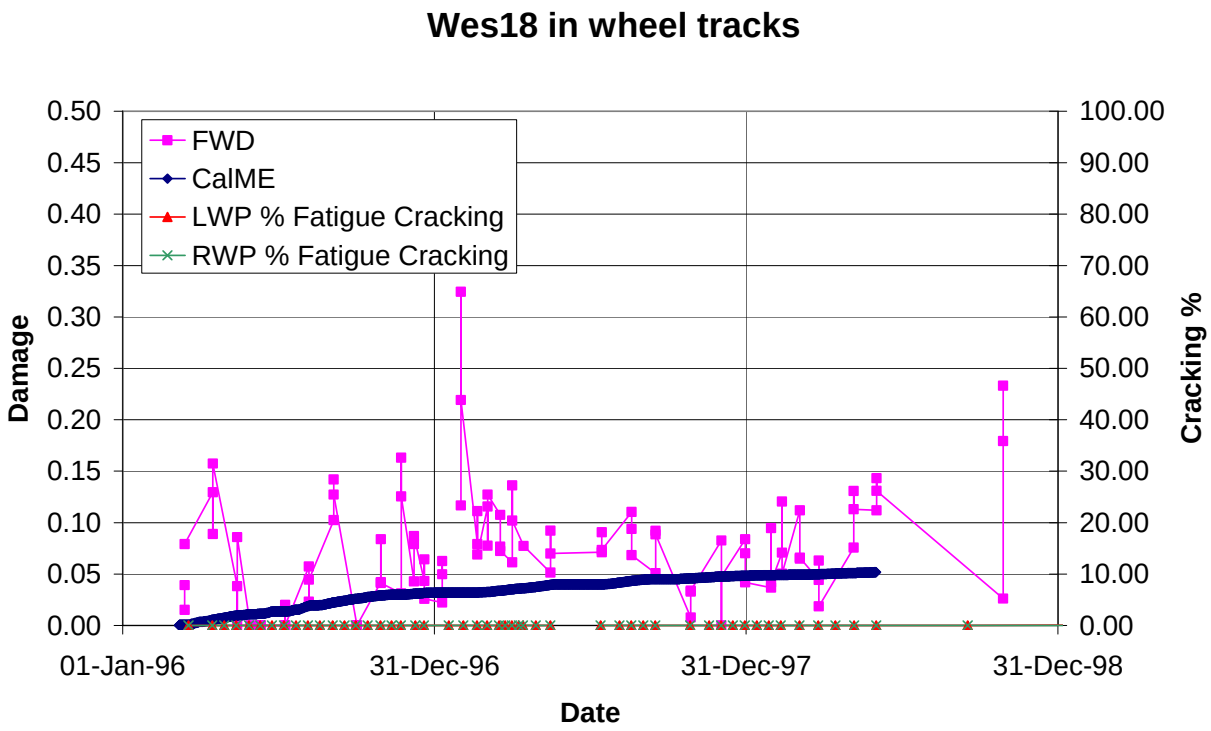

Figure 58. Damage in wheelpath of Section 18 (LWP = left wheelpath; RWP = right wheelpath).

To obtain a reasonably good agreement between the permanent deformation calculated with *CalME* and the measured down rut, a value of K = 0.9 (in Equation 25) was used (K should be multiplied by 100 in order to compare to the K value used by Deacon et al., 2002 (12). They reported a K value of 140 for an asphalt thickness of 150 mm increasing to 250 for a thickness of 300 mm, but this included the the rut depth caused by postconstruction compaction under traffic which is treated separately here). For the Coarse sections K was equal to 0.8. As mentioned above, a postconstruction compaction corresponding to 36 percent of the air-void content was assumed to take place within the first 60 days with traffic loading.

Figure 59 shows the down rut in the right wheelpath of Section 18. Again measured values are connected by a fully drawn line whereas the values calculated by *CalME* are connected by a dotted line.

In Figure 59 the mean difference between the measured down rut depth and the calculated permanent deformation is 0.9 mm and the RMS is 1.3 mm. Figure 60 shows the simulation results compared to the measured maximum rut depths in the right and leftwheelpaths. The mean difference between rutting in the left and the right wheelpath in Figure 60 is 2.7 mm and the RMS is 4.0 mm.

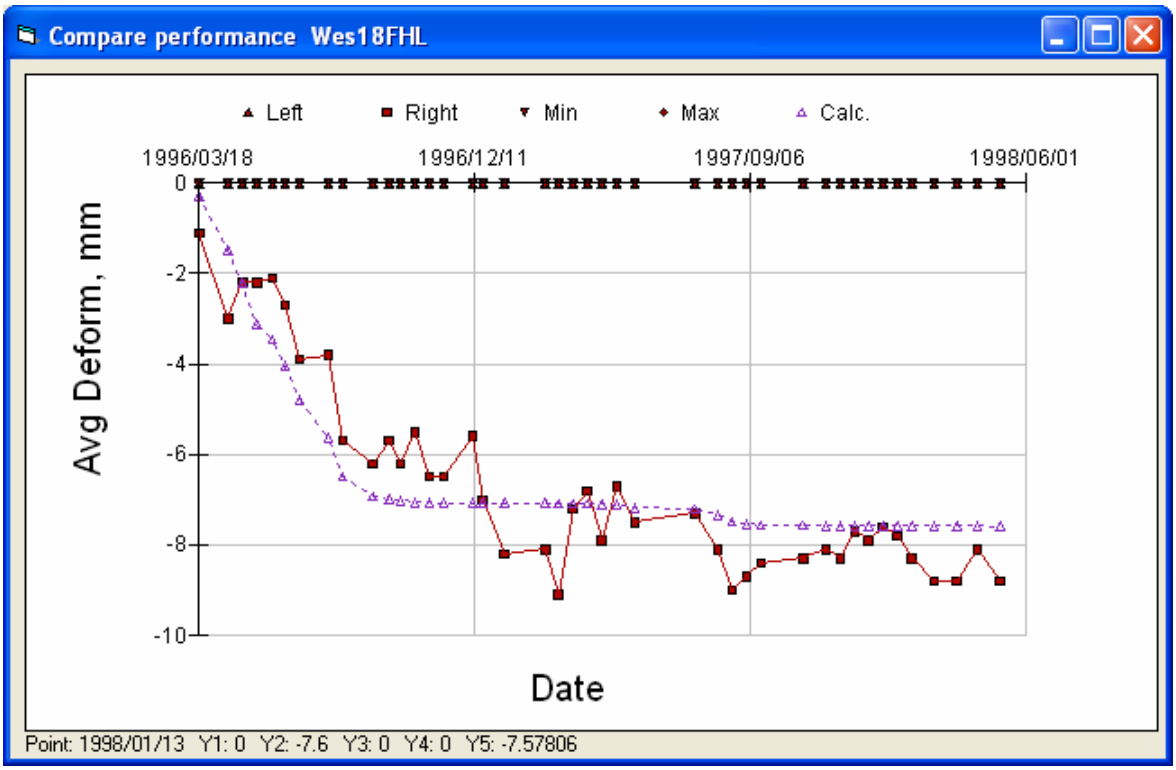

Figure 59. Down rut in right wheelpath at Section 18.

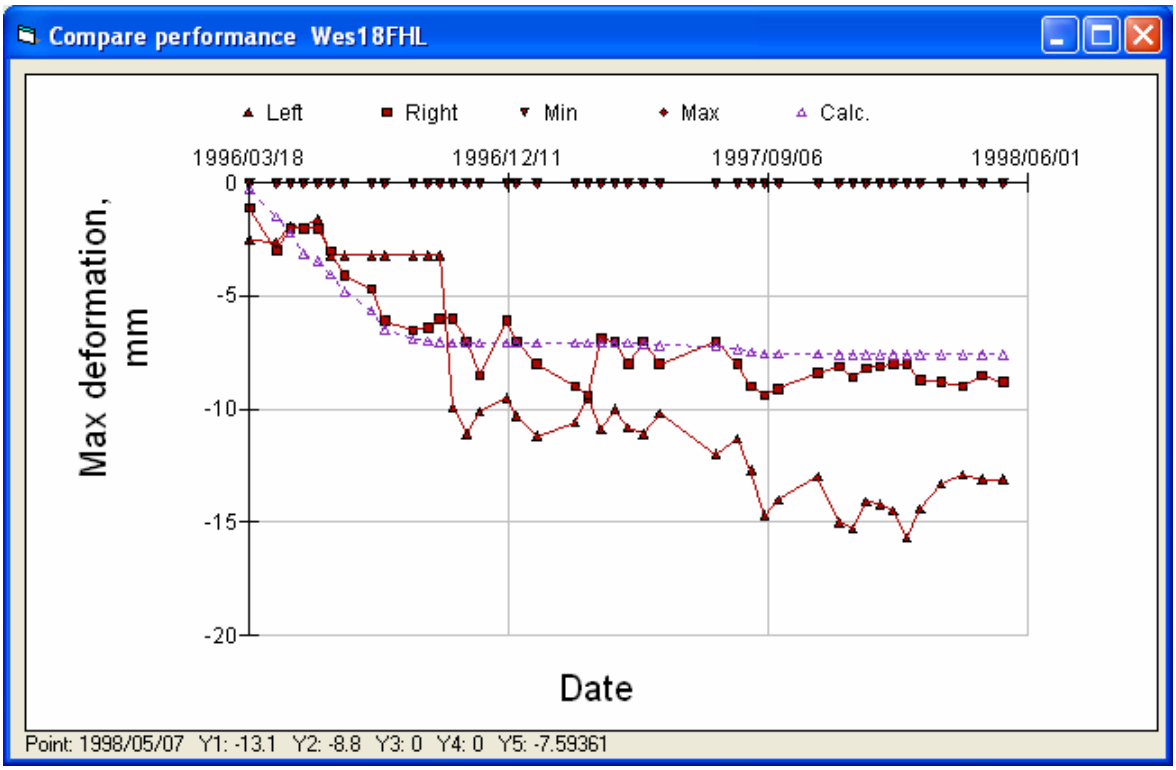

Figure 60. Maximum rutting in left and right wheelpaths at Section 18.

The maximum rut depth in the right wheelpath, shown in Figure 60, is not much different from the down rut shown in Figure 59, whereas the rutting in the left wheelpath is larger.

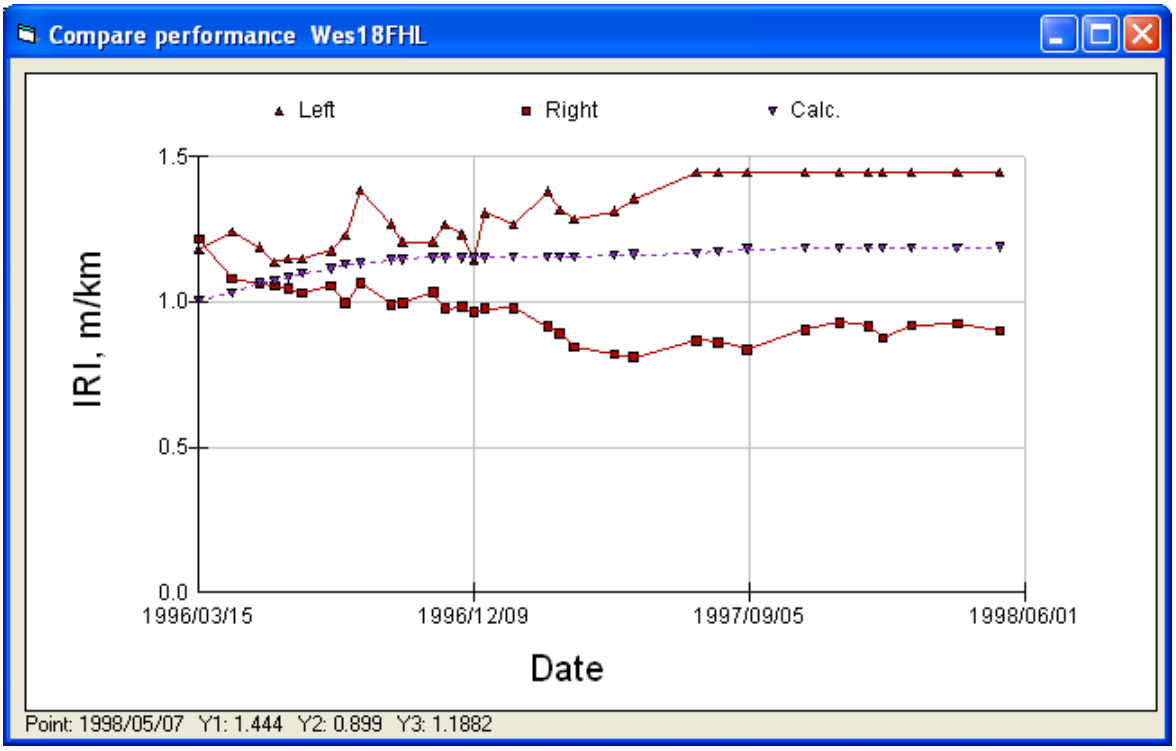

Figure 61. IRI in left and right wheelpaths at Section 18.

It is difficult to draw any conclusions from the roughness data at WesTrack shown in Figure 61 for Section 18. The roughness in the right wheelpath decreases during the first part of the experiment, whereas the roughness of the left wheelpath increases. The IRI values predicted by *CalME* are approximately midway between the measured values.

3.4 Simulation of Other Fine Mix Sections

For each of the WesTrack sections simulated, a table shows the input values in the *CalME* data used for the simulation of that section, followed by plots comparing measured and calculated FWD deflections, damage and fatigue cracking, rutting, and IRI.

3.4.1 Section 01FMM1

Table 14. Summary of Input Values for Section 01FMM1

Modulus	***α***	***β***	***γ***	***δ***	***aT***	***A***	***VTS***
AC	2.0792	-0.6908	0.6908	2.000	1.300	10.0406	-3.680
Unbound	*Eo*	*Stiffness factor*	*Power on load*	*Estart*			
AB	330 MPa	0.65	0.6	210 MPa			
Subgrade	70 MPa	0	-0.2	70 MPa			
Aging	*AgeA*	*AgeB*					
AC	0.277	-.6354					
Fatigue	*A*	*α*	*β*	*γ*	*δ*		
AC	0.3253	0.4872	2.0678	1.0339	0.4161		
Rutting	*A*	*α*	*β*	*γ*	*dVoids*		
AC	12.24	0.1350	1.03	1	3.2		

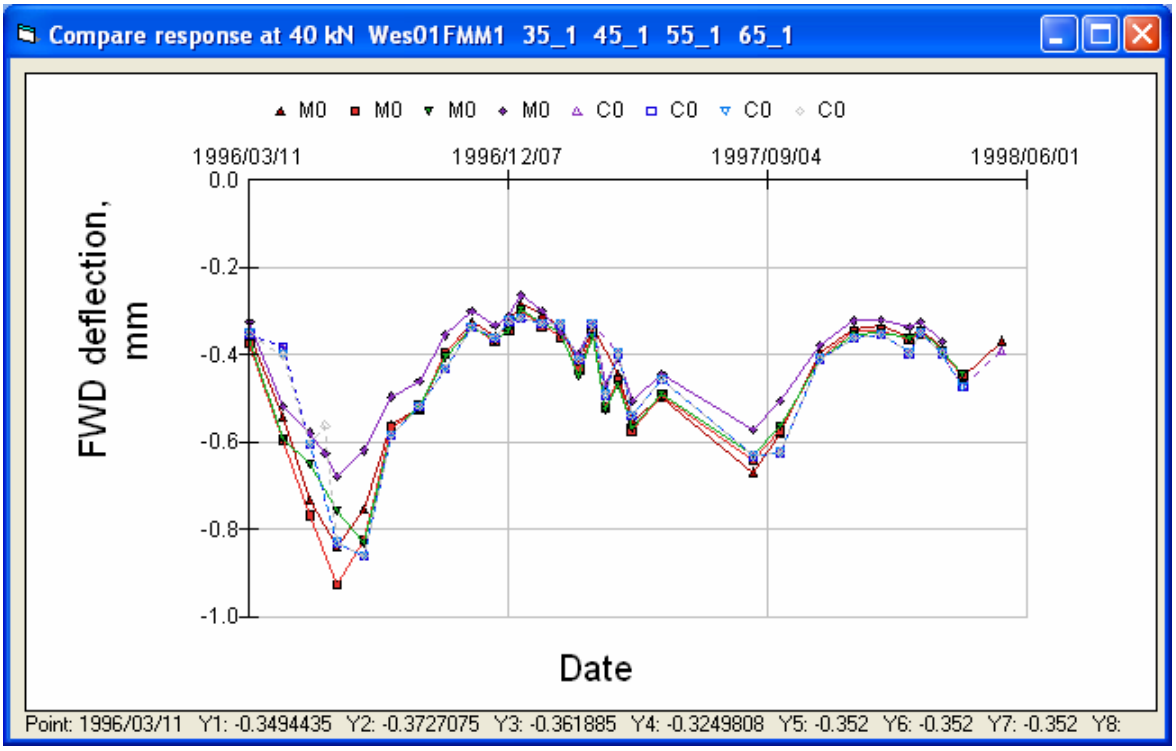

Figure 62. FWD deflections at Section 01 (in wheelpath, geophone under load plate).

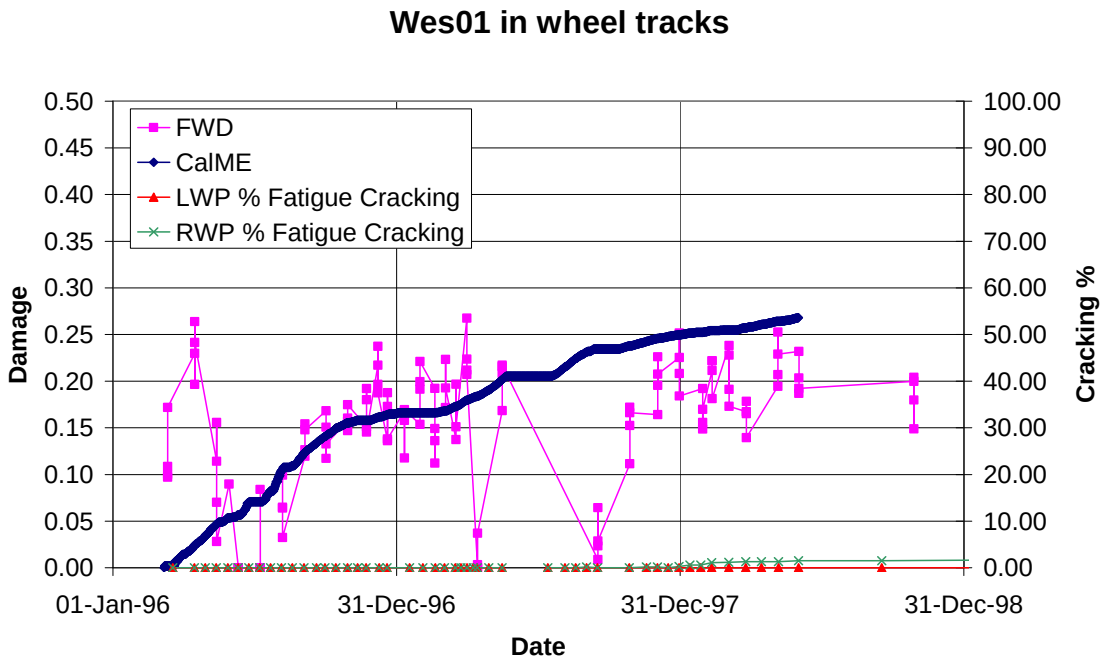

Figure 63. Damage in wheelpath of Section 01.

Both Figure 62 and Figure 63 indicate that *CalME* estimated the amount of damage to the asphalt of Section 01 quite well.

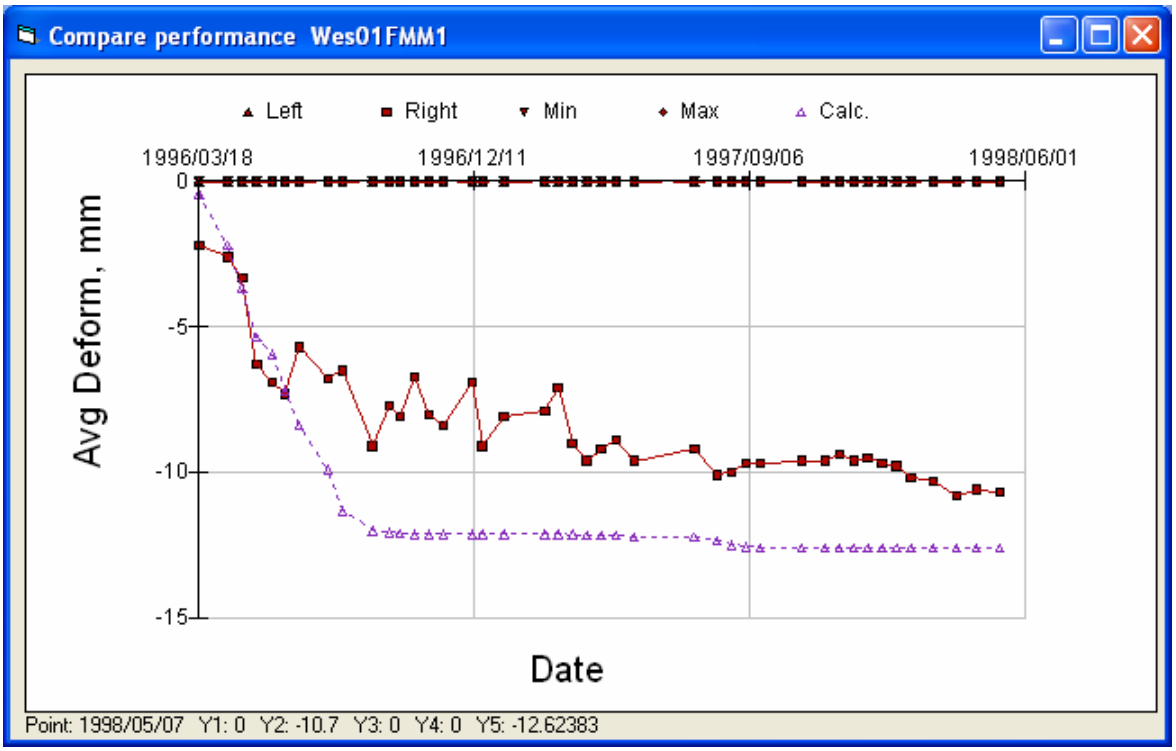

Figure 64. Down rut in right wheelpath at Section 01.

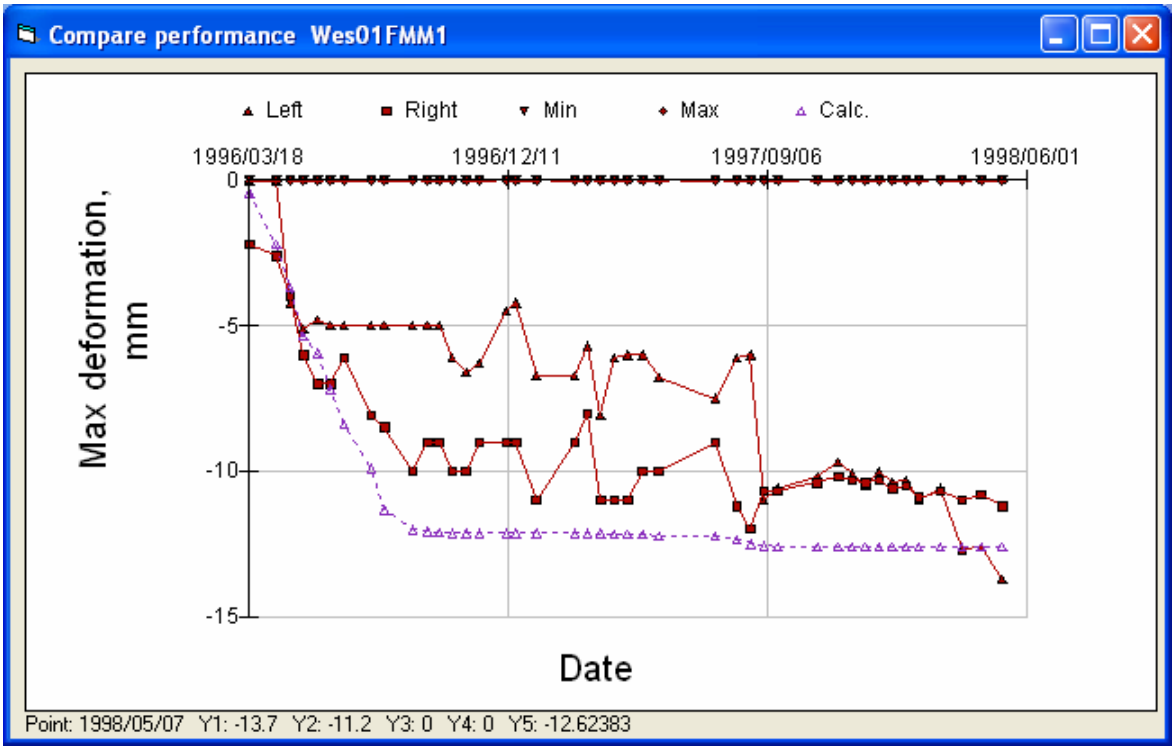

Figure 65. Maximum rutting in left and right wheelpaths at Section 01.

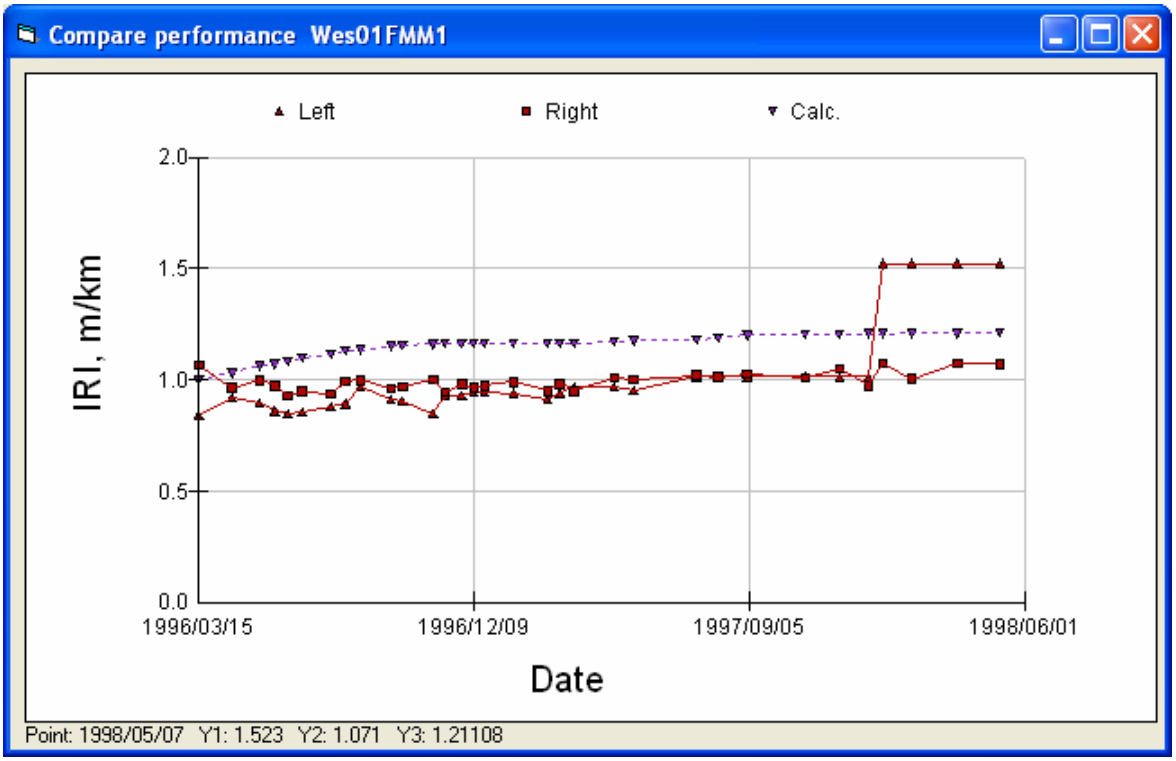

Figure 66. IRI in left and right wheelpaths at Section 01.

3.4.2 Section 02FLM

Table 15. Summary of Input Values for Section 02FLM

Modulus	*α*	*β*	*γ*	*δ*	*aT*	*A*	*VTS*
AC	2.0792	-0.8289	0.5526	2.000	1.300	10.0406	-3.680
Unbound	*Eo*	*Stiffness factor*	*Power on load*	*Estart*			
AB	219 MPa	0.42	0.6	184 MPa			
Subgrade	70 MPa	0	-0.2	70 MPa			
Aging	*AgeA*	*AgeB*					
AC	0.1912	-.1279					
Fatigue	*A*	*α*	*β*	*γ*	*δ*		
AC	0.1047	0.4470	2.2666	1.1333	0.3817		
Rutting	*A*	*α*	*β*	*γ*	*dVoids*		
AC	13.99	0.1430	1.03	1	3.7		

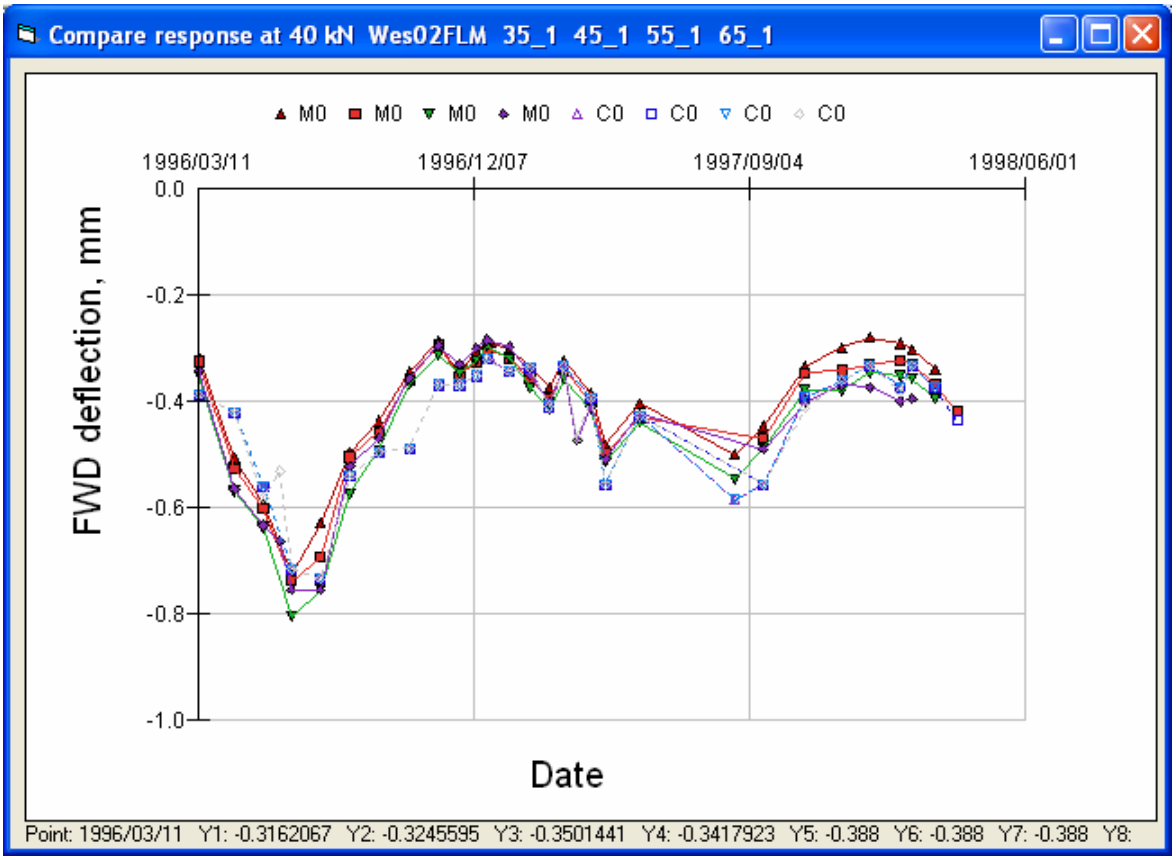

Figure 67. FWD deflections at Section 02 (in wheelpath, geophone under load plate).

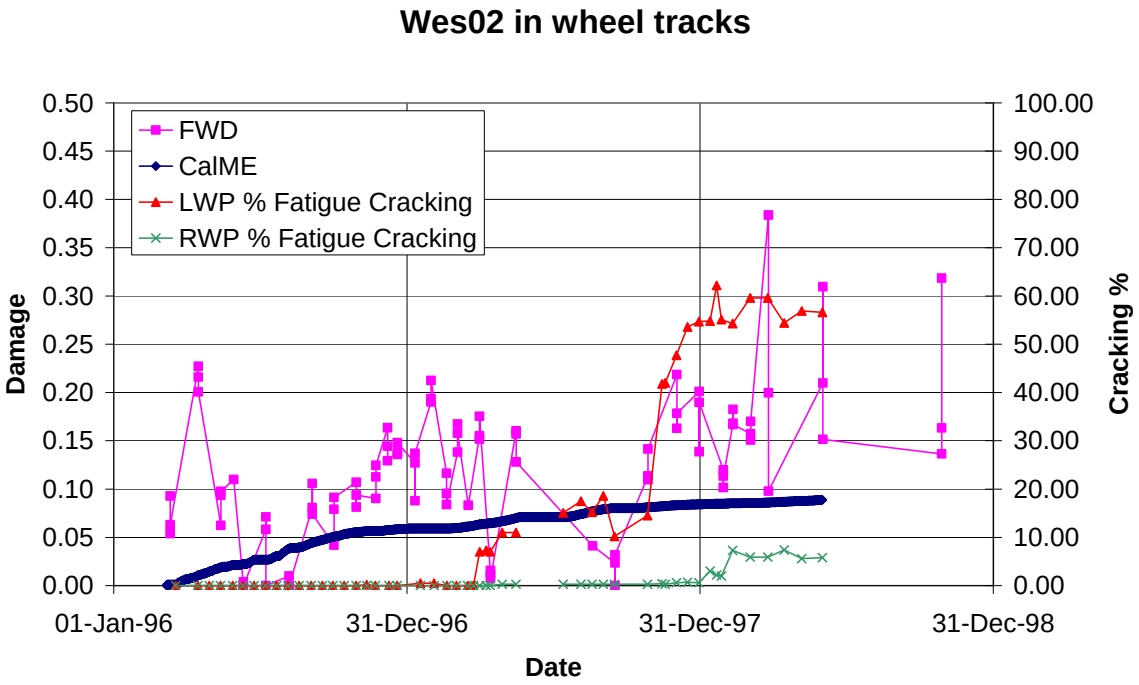

Figure 68. Damage in wheelpath of Section 02 (LWP = left wheelpath, RWP = right wheelpath).

The calculated damage appears to be in accordance with the measured FWD deflections. Although the calculated damage is less than half of the damage at Section 01 the amount of visible cracking is considerably higher.

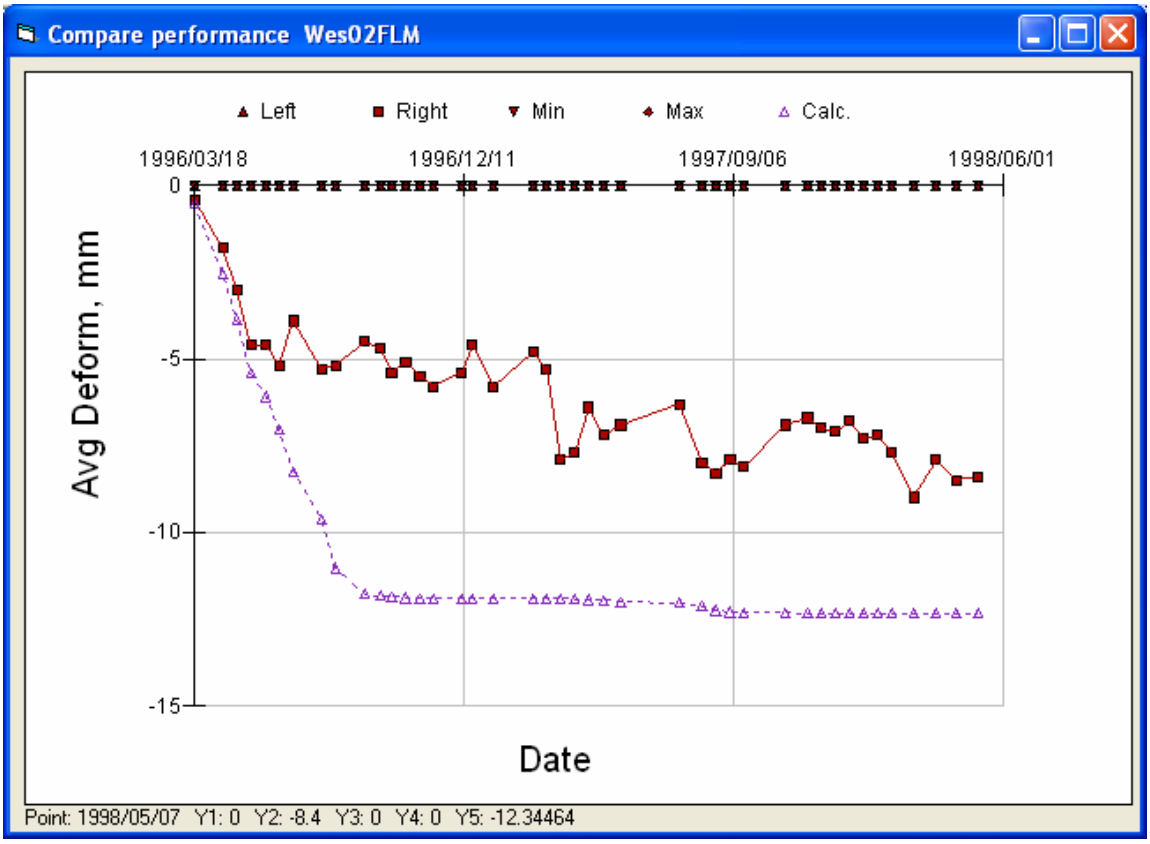

Figure 69. Down rut in right wheelpath at Section 02.

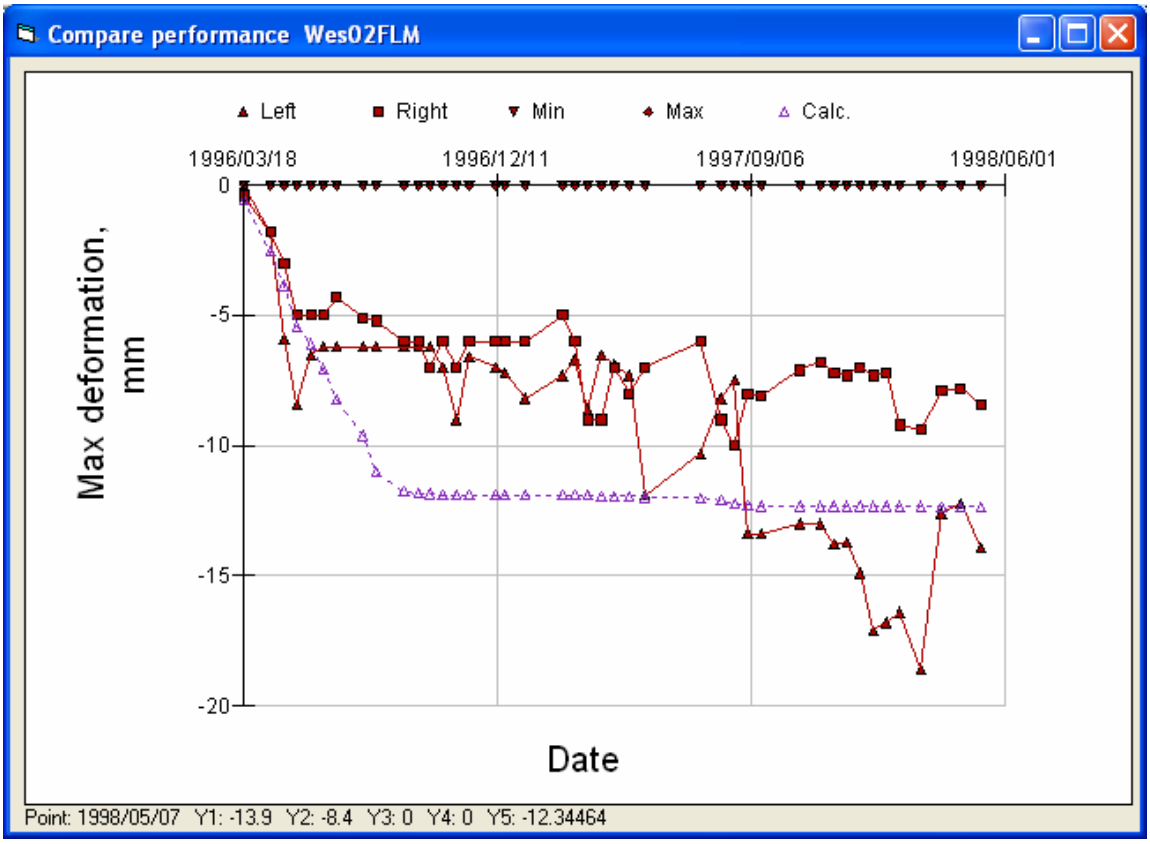

Figure 70. Maximum rutting in left and right wheelpaths at Section 02.

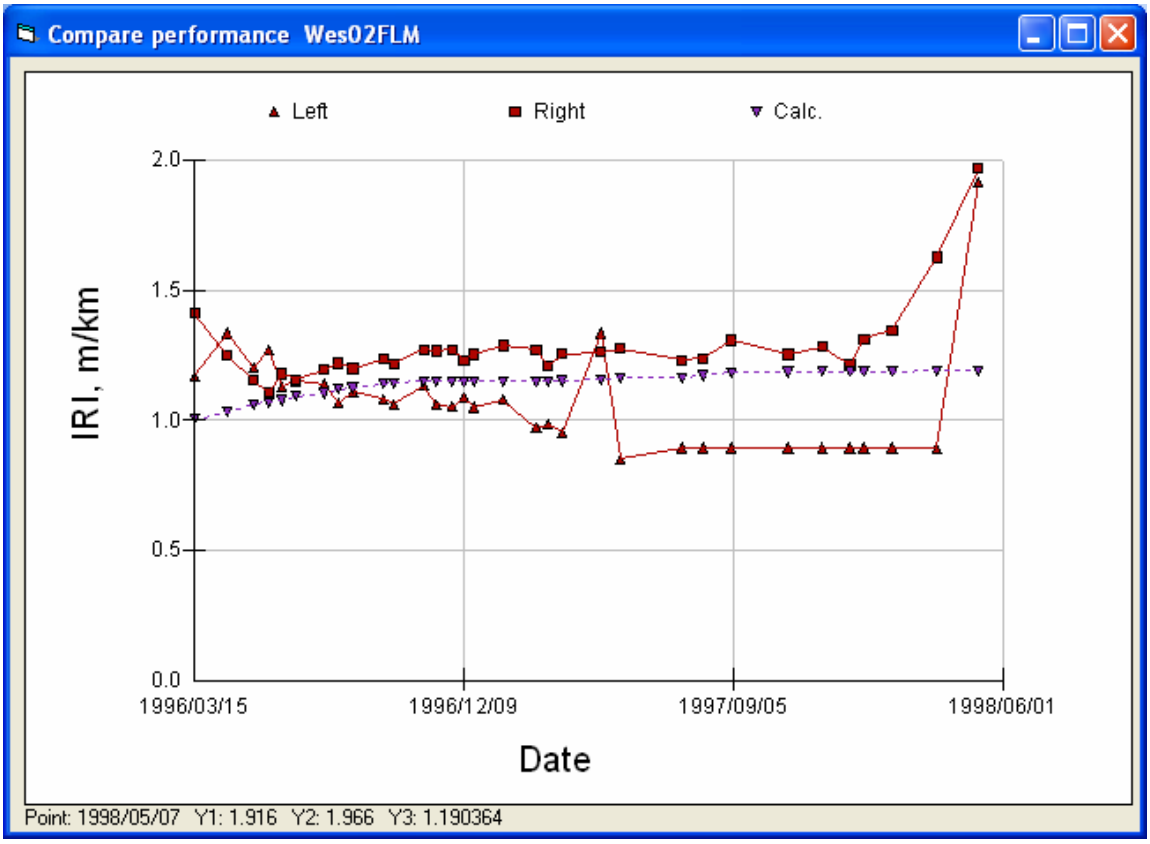

Figure 71. IRI in left and right wheelpaths of Section 02.

3.4.3 Section 03FLH1

Table 16. Summary of Input Values for Section 03FLH1

Modulus	*α*	*β*	*γ*	*δ*	*aT*	*A*	*VTS*
AC	2.0000	-0.6908	0.6908	2.000	1.300	10.0406	-3.680
Unbound	*Eo*	*Stiffness factor*	*Power on load*	*Estart*			
AB	214 MPa	0.60	0.6	158 MPa			
Subgrade	70 MPa	0	-0.2	70 MPa			
Aging	*AgeA*	*AgeB*					
AC	0.3840	-1.2656					
Fatigue	*A*	*α*	*β*	*γ*	*δ*		
AC	0.6447	0.5289	2.1371	1.0685	0.4517		
Rutting	*A*	*α*	*β*	*γ*	*dVoids*		
AC	12.11	0.0958	1.03	1	4.0		

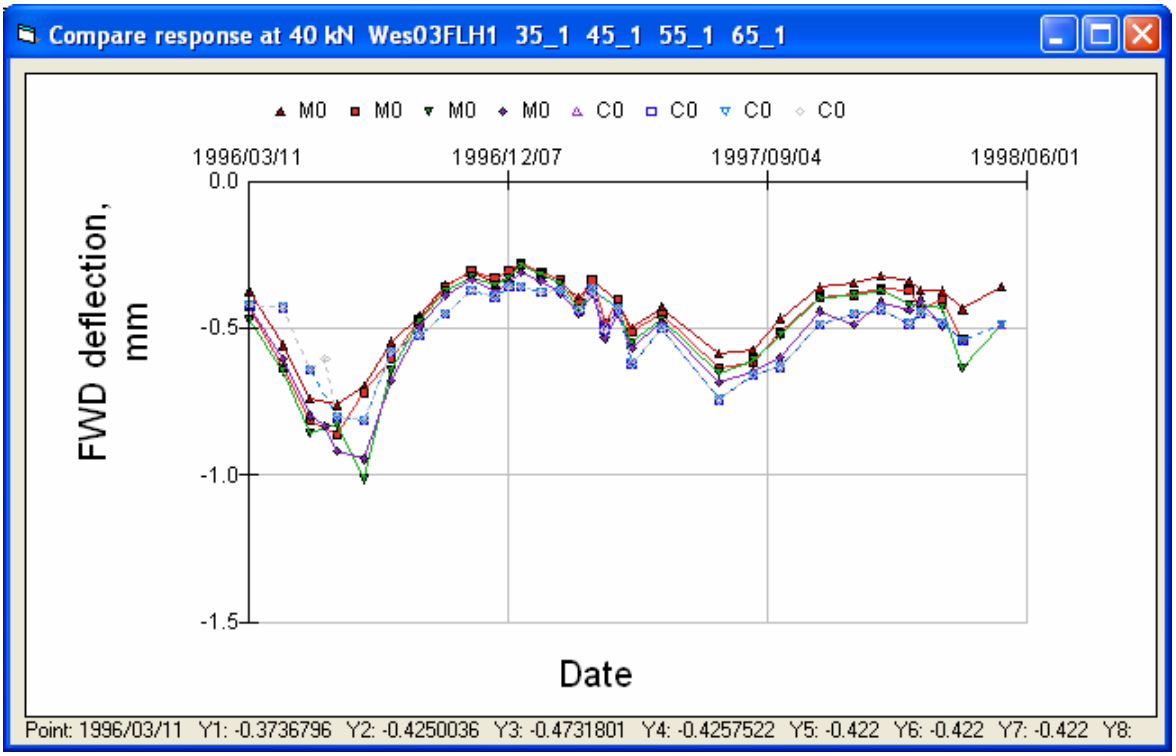

Figure 72. FWD deflections at Section 03 (in wheelpath, geophone under load plate).

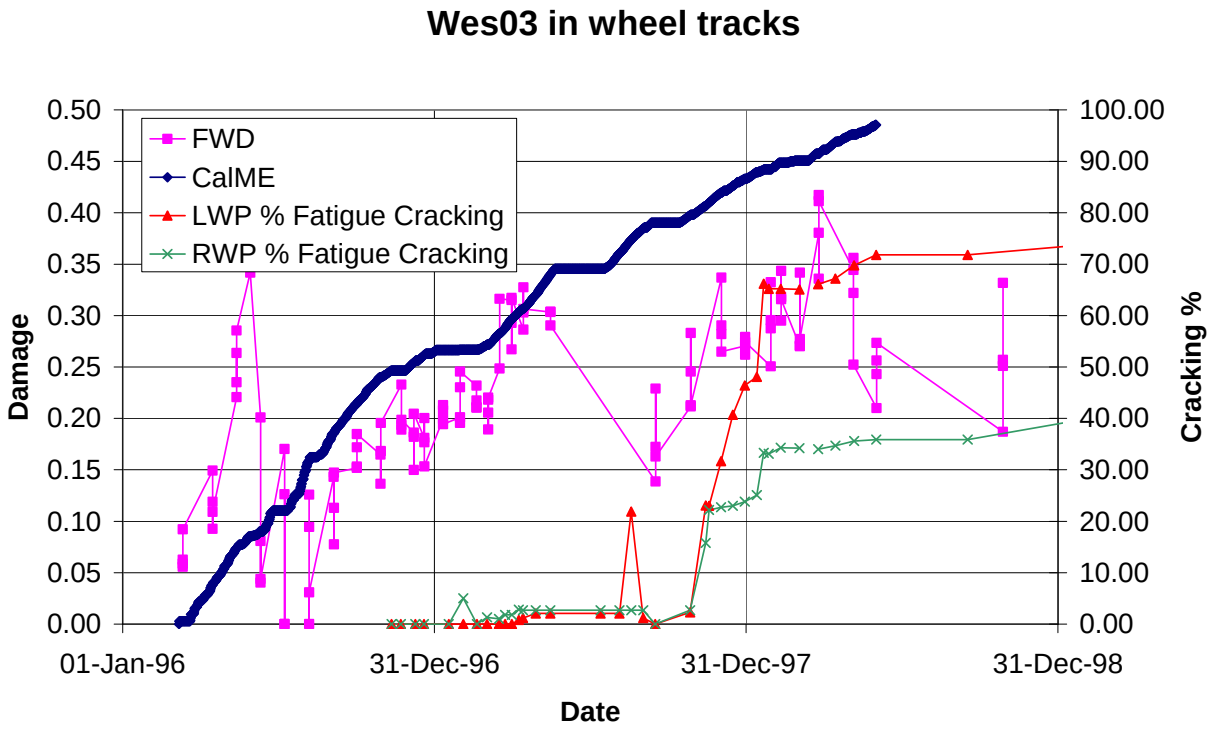

Figure 73. Damage in wheelpath of Section 03 (LWP = left wheelpath, RWP = right wheelpath).

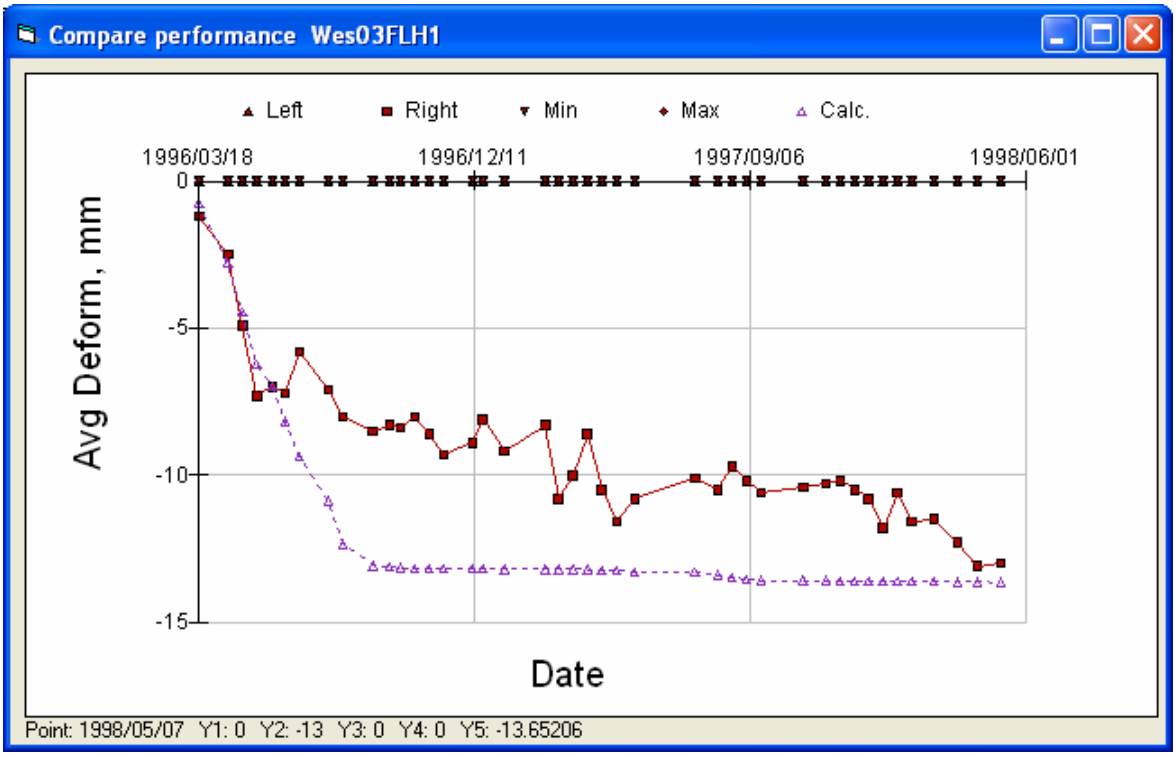

Figure 74. Down rut in right wheelpath at Section 03.

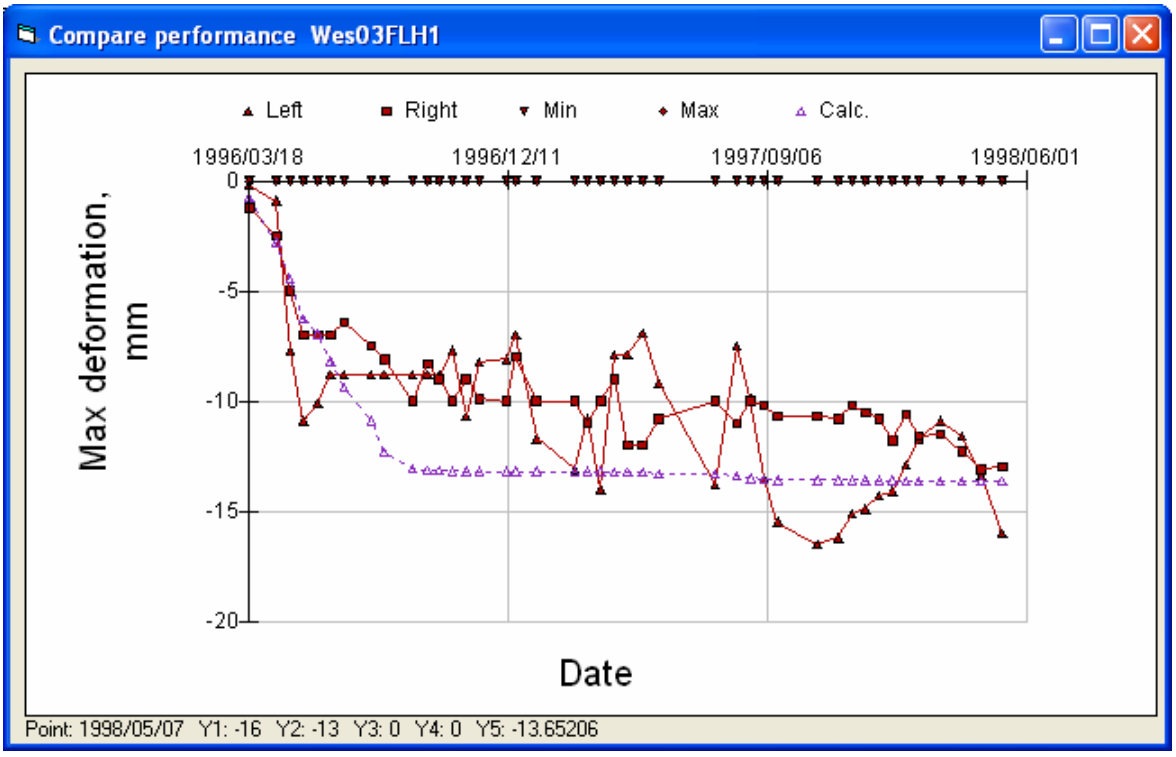

Figure 75. Maximum rutting in left and right wheelpaths at Section 03.

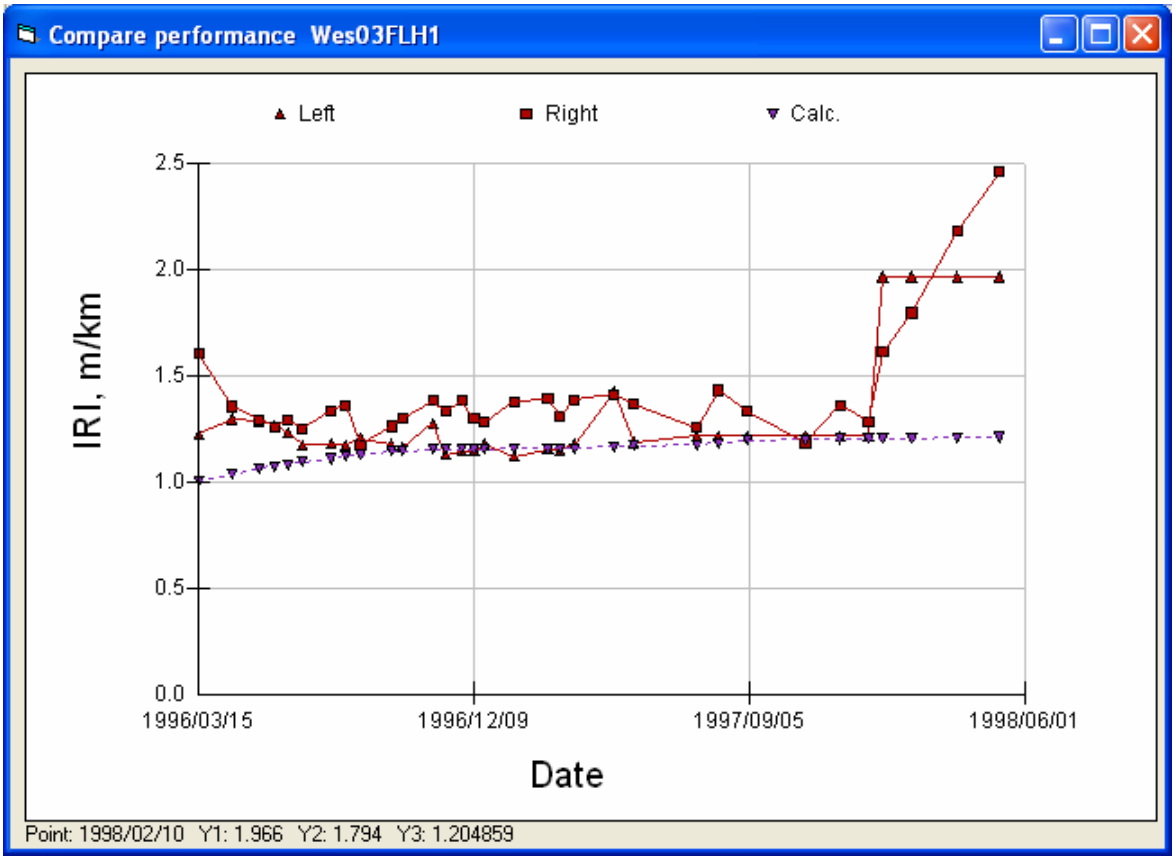

Figure 76. IRI in left and right wheelpaths of Section 03.

3.4.4 Section 04FML

It should be noted that the two RSST-CH samples from Section 04 showed very different results.

Table 17. Summary of Input Values for Section 04FML

Modulus	*α*	*β*	*γ*	*δ*	*aT*	*A*	*VTS*
AC	2.0792	-1.0362	0.6908	2.000	1.300	10.0406	-3.680
Unbound	*Eo*	*Stiffness factor*	*Power on load*	*Estart*			
AB	269 MPa	0.47	0.6	228 MPa			
Subgrade	82 MPa	0	-0.2	82 MPa			
Aging	*AgeA*	*AgeB*					
AC	0.2792	-0.6471					
Fatigue	*A*	*α*	*β*	*γ*	*δ*		
AC	0.1170	0.4746	2.8603	1.4301	0.4053		
Rutting	*A*	*α*	*β*	*γ*	*dVoids*		
AC	13.24	0.04597	1.03	1	2.3		

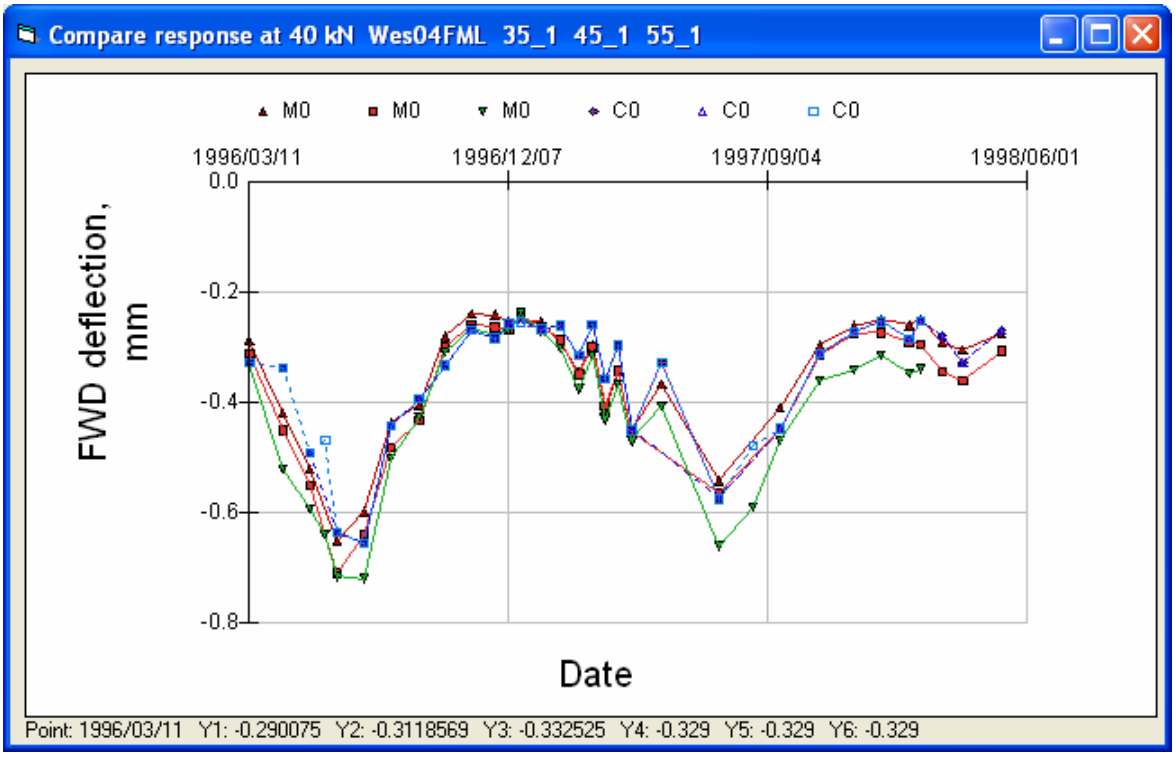

Figure 77. FWD deflections at Section 04 (in wheelpath, geophone under load plate).

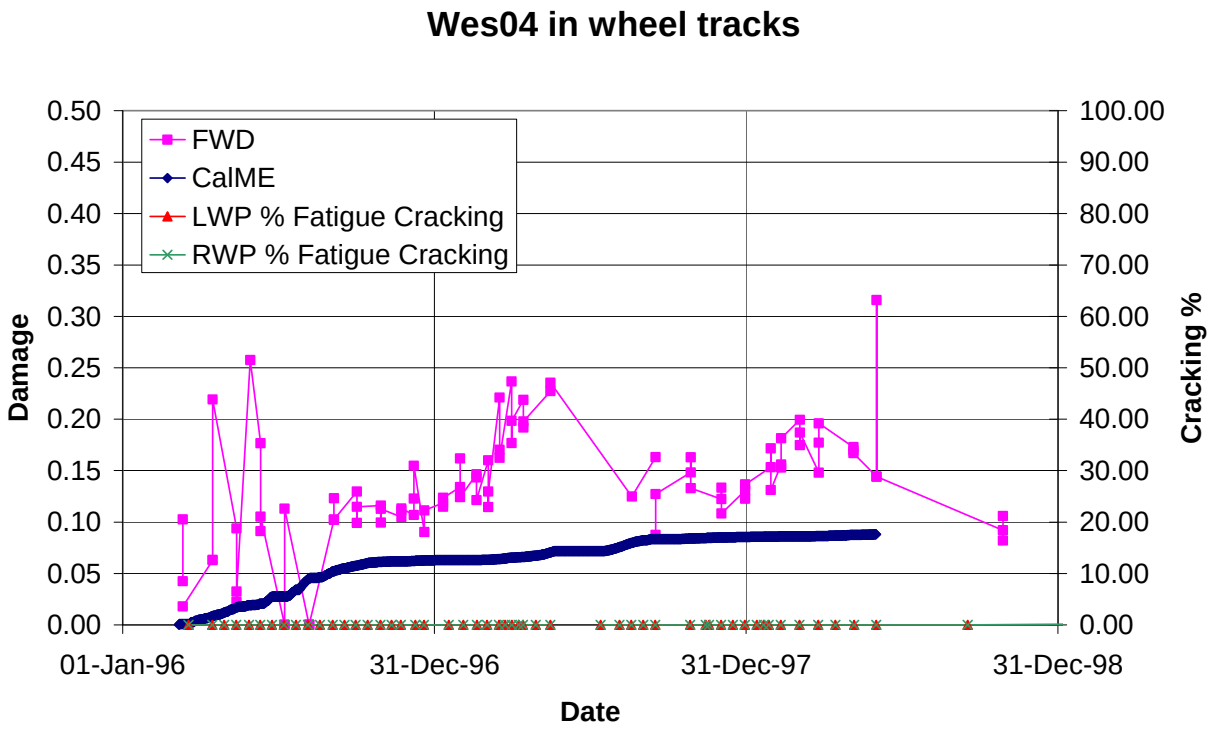

Figure 78. Damage in wheelpath of Section 04 (LWP = left wheelpath, RWP = right wheelpath).

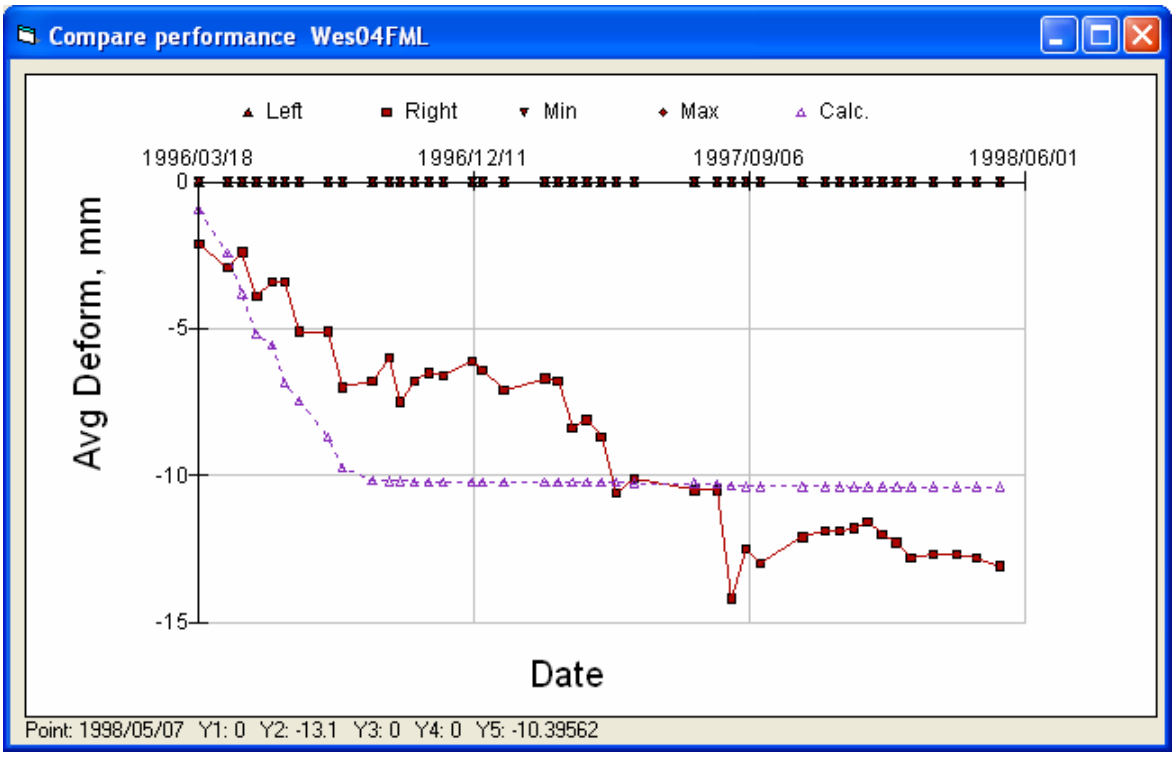

Figure 79. Down rut in right wheelpath at Section 04.

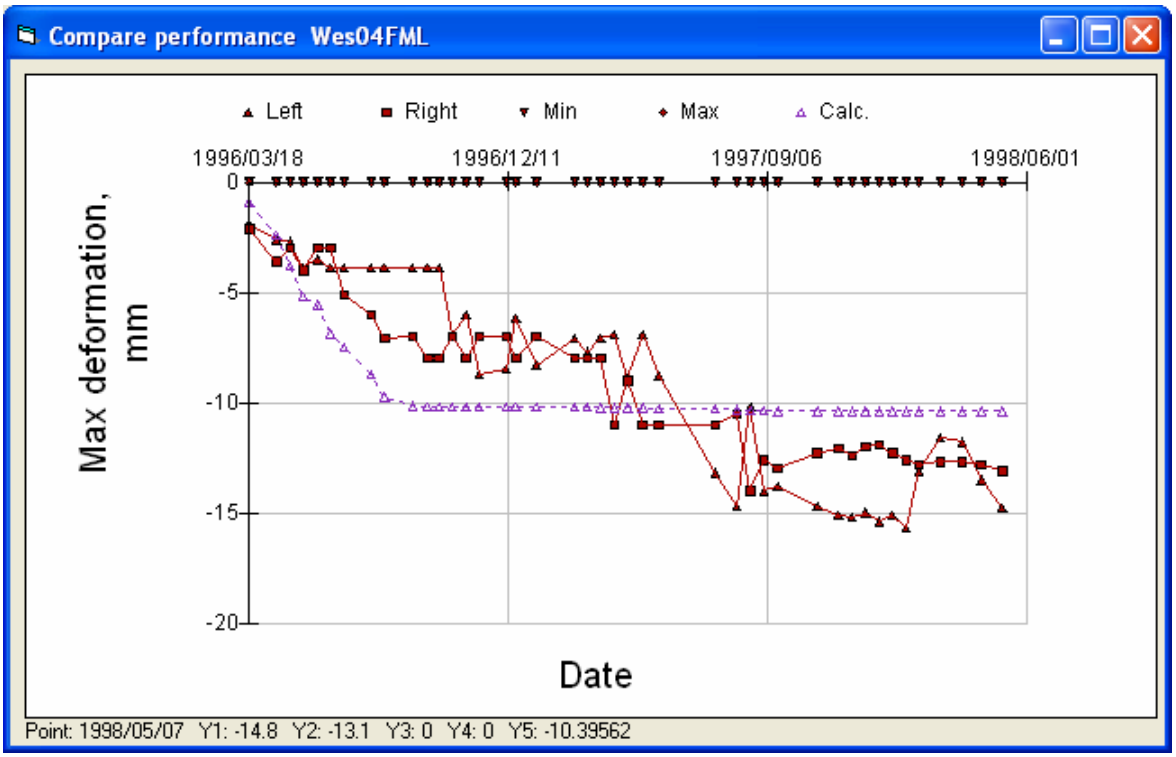

Figure 80. Maximum rutting in left and right wheelpaths at Section 04.

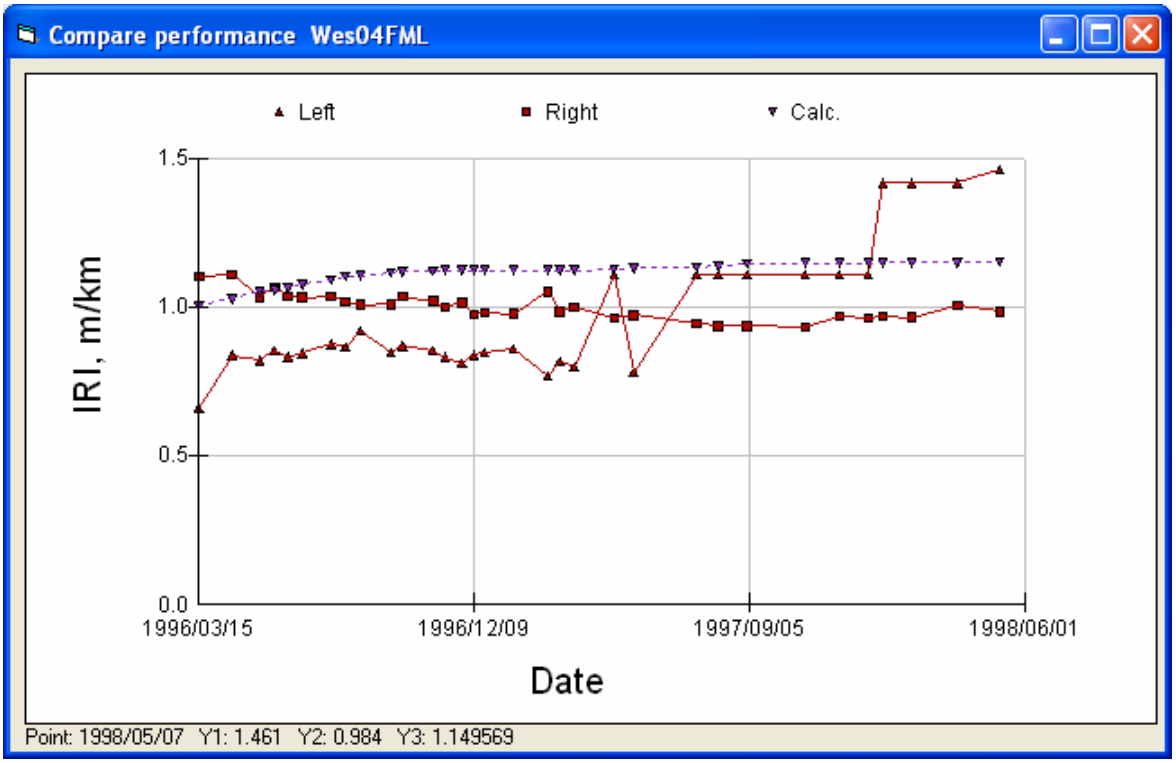

Figure 81. IRI in left and right wheelpaths of Section 04.

3.4.5 Section 14FHM

Table 18. Summary of Input Values for Section 14FHM

Modulus	*α*	*β*	*γ*	*δ*	*aT*	*A*	*VTS*
AC	2.0792	-1.0362	0.6908	2.000	1.300	10.0406	-3.680
Unbound	*Eo*	*Stiffness factor*	*Power on load*	*Estart*			
AB	213 MPa	0.40	0.6	176 MPa			
Subgrade	95 MPa	0	-0.2	95 MPa			
Aging	*AgeA*	*AgeB*					
AC	0.2885	-0.7021					
Fatigue	*A*	*α*	*B*	*γ*	*δ*		
AC	0.1677	0.4010	1.6609	0.8305	0.3424		
Rutting	*A*	*α*	*B*	*γ*	*dVoids*		
AC	12.64	0.1434	1.03	1	3.2		

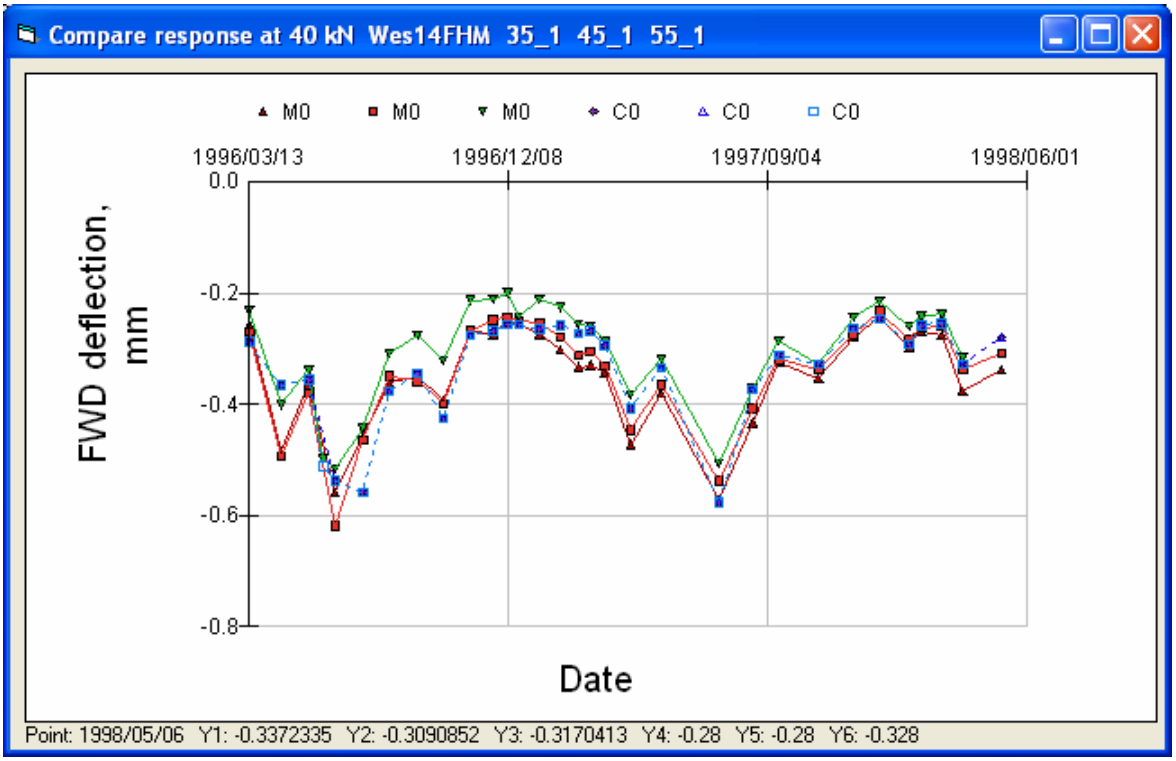

Figure 82. FWD deflections at Section 14 (in wheelpath, geophone under load plate).

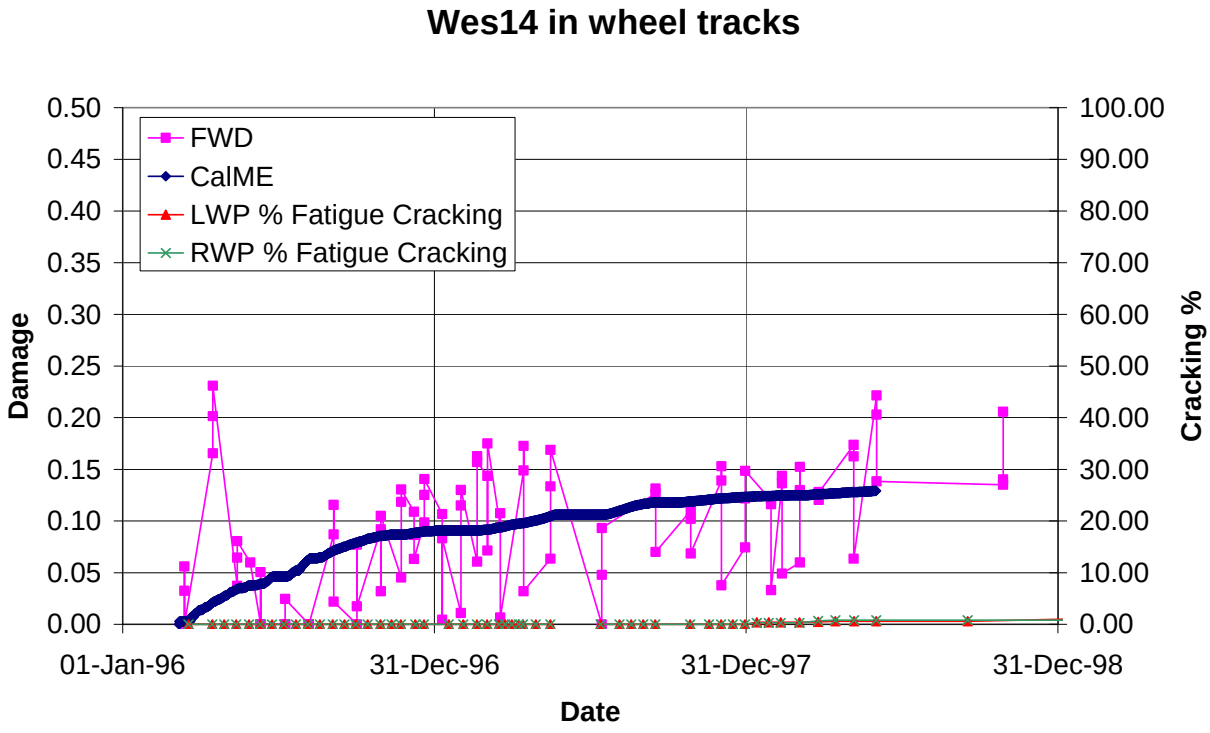

Figure 83. Damage in wheelpath of Section 14 (LWP = left wheelpath, RWP = right wheelpath).

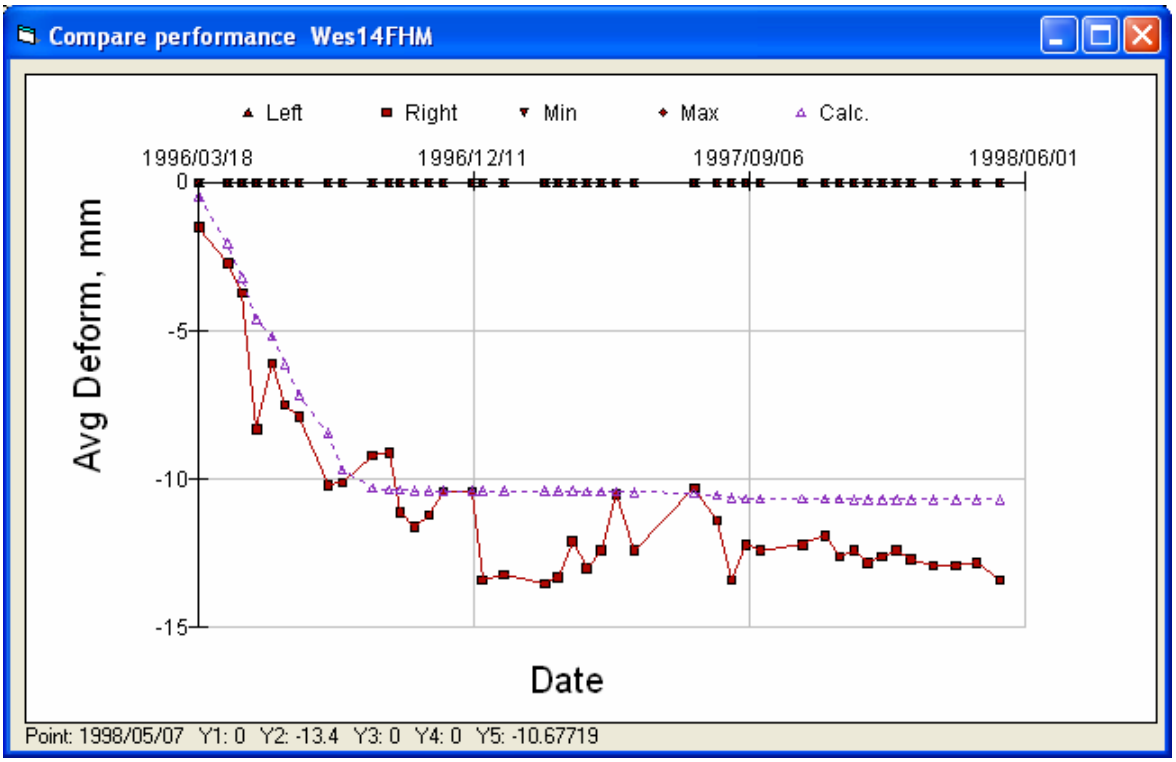

Figure 84. Down rut in right wheelpath at Section 14.

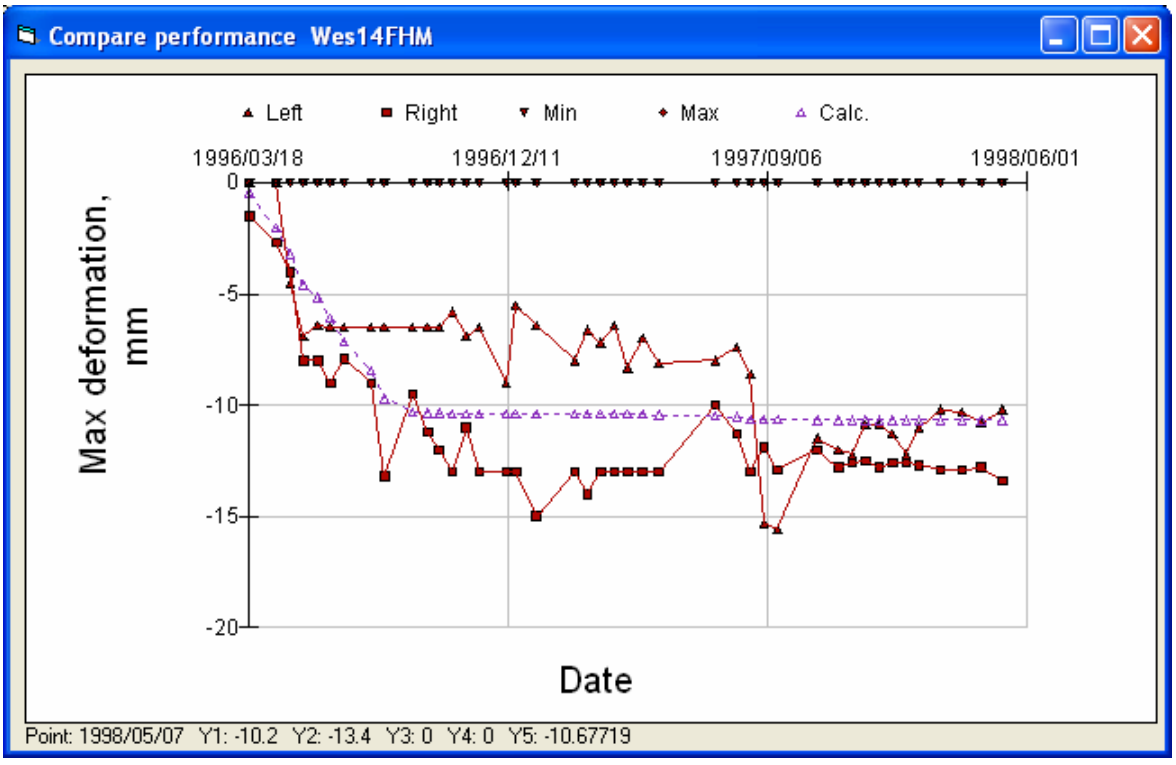

Figure 85. Maximum rutting in left and right wheelpaths at Section 14.

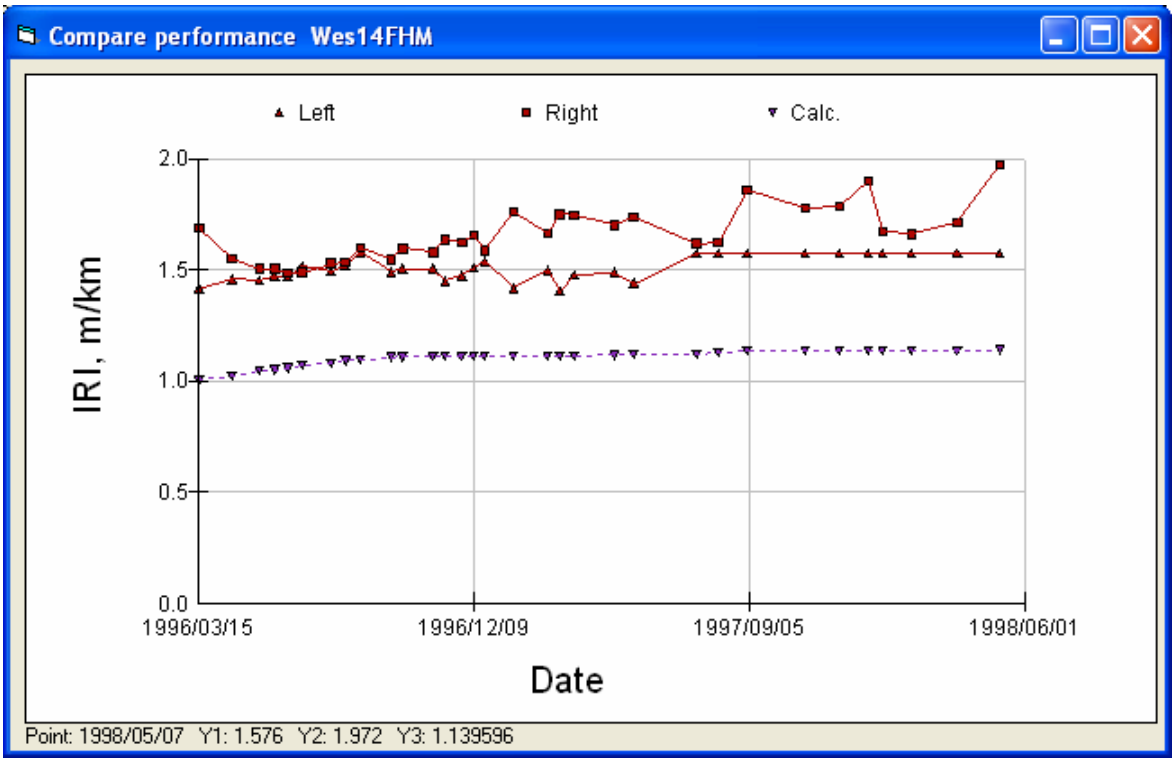

Figure 86. IRI in left and right wheelpaths at Section 14.

3.4.6 Section 15FMM2

Table 19. Summary of Input Values for Section 15FMM2

Modulus	*α*	*β*	*γ*	*δ*	*aT*	*A*	*VTS*
AC	2.0000	-1.0362	0.6908	2.000	1.300	10.0406	-3.680
Unbound	*Eo*	*Stiffness factor*	*Power on load*	*Estart*			
AB	186 MPa	0.43	0.6	151 MPa			
Subgrade	89 MPa	0	-0.2	89 MPa			
Aging	*AgeA*	*AgeB*					
AC	0.2627	-0.5502					
Fatigue	*A*	*α*	*β*	*γ*	*δ*		
AC	0.2117	0.4436	1.9107	0.9554	0.3788		
Rutting	*A*	*α*	*β*	*γ*	*dVoids*		
AC	10.88	0.1508	1.03	1	2.9		

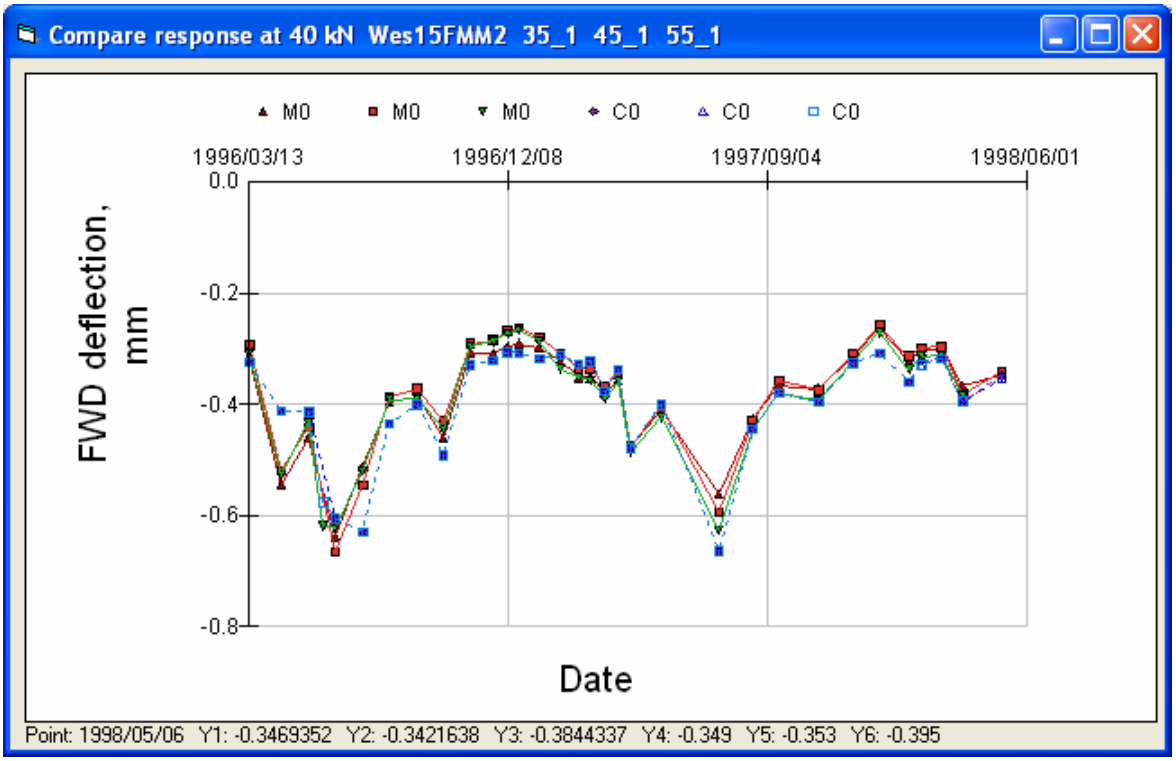

Figure 87. FWD deflections at Section 15 (in wheelpath, geophone under load plate).

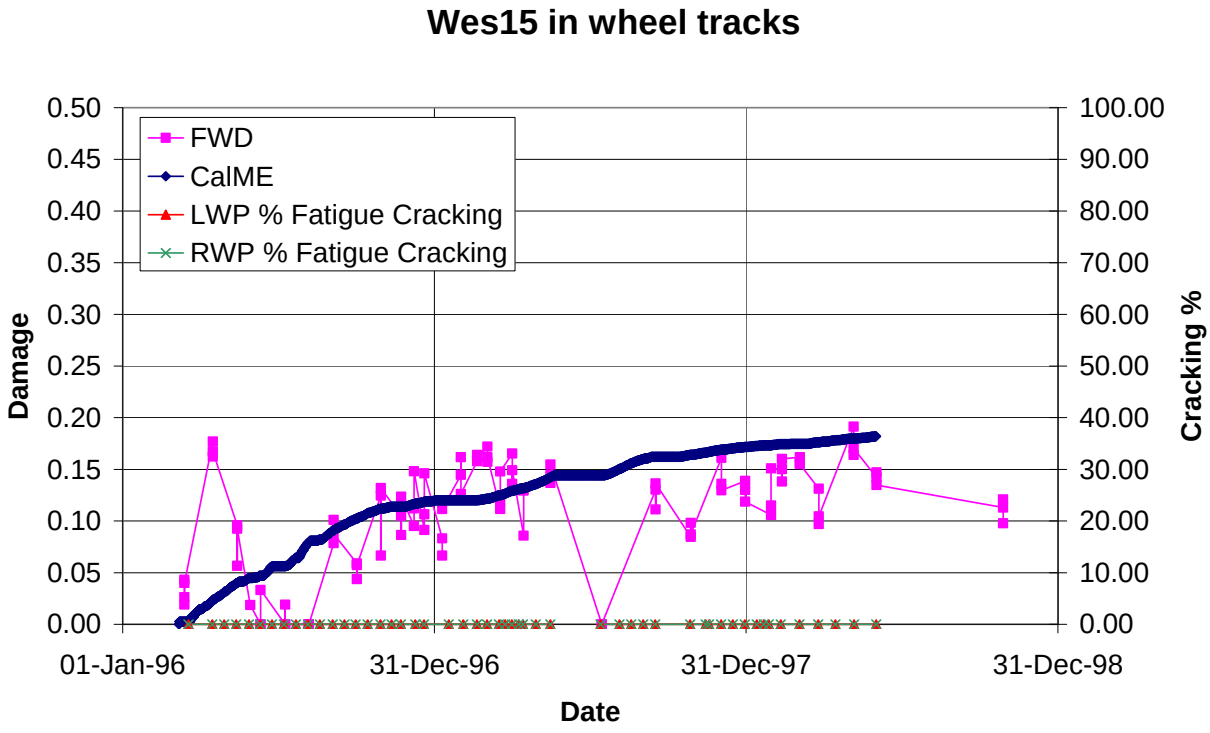

Figure 88. Damage in wheelpath of Section 15 (LWP = left wheelpath, RWP = rightwheelpath).

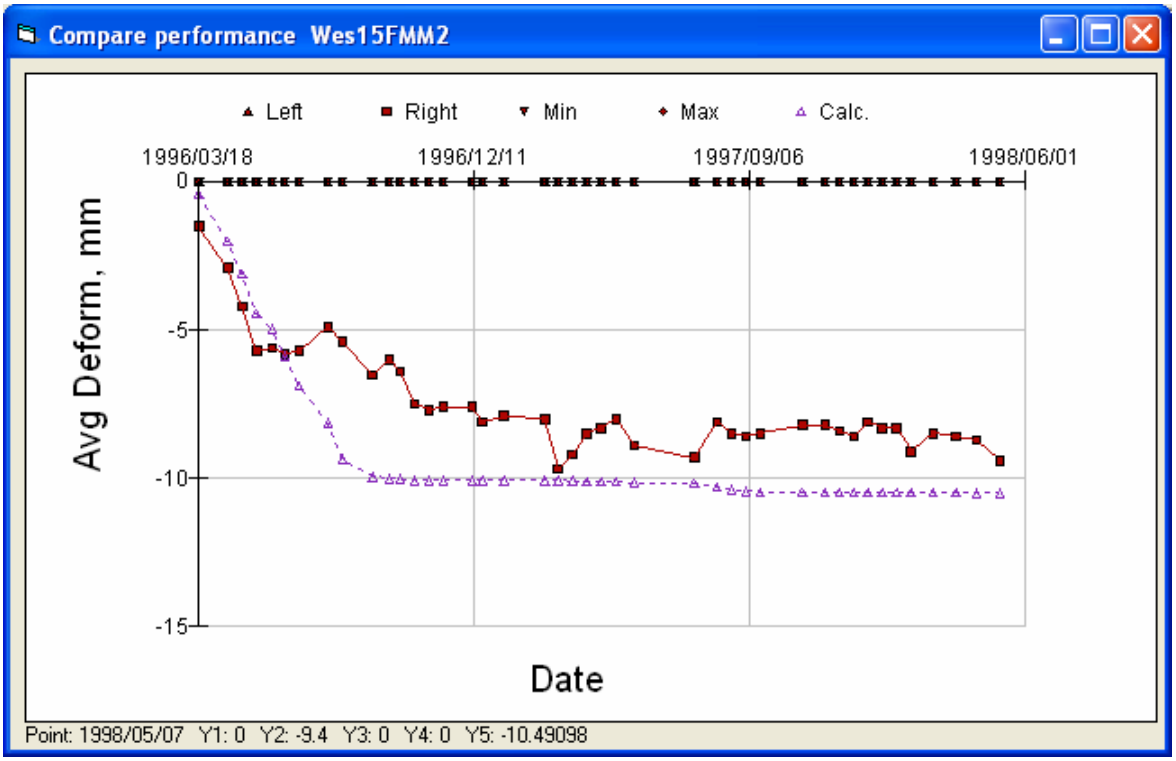

Figure 89. Down rut in right wheelpath at Section 15.

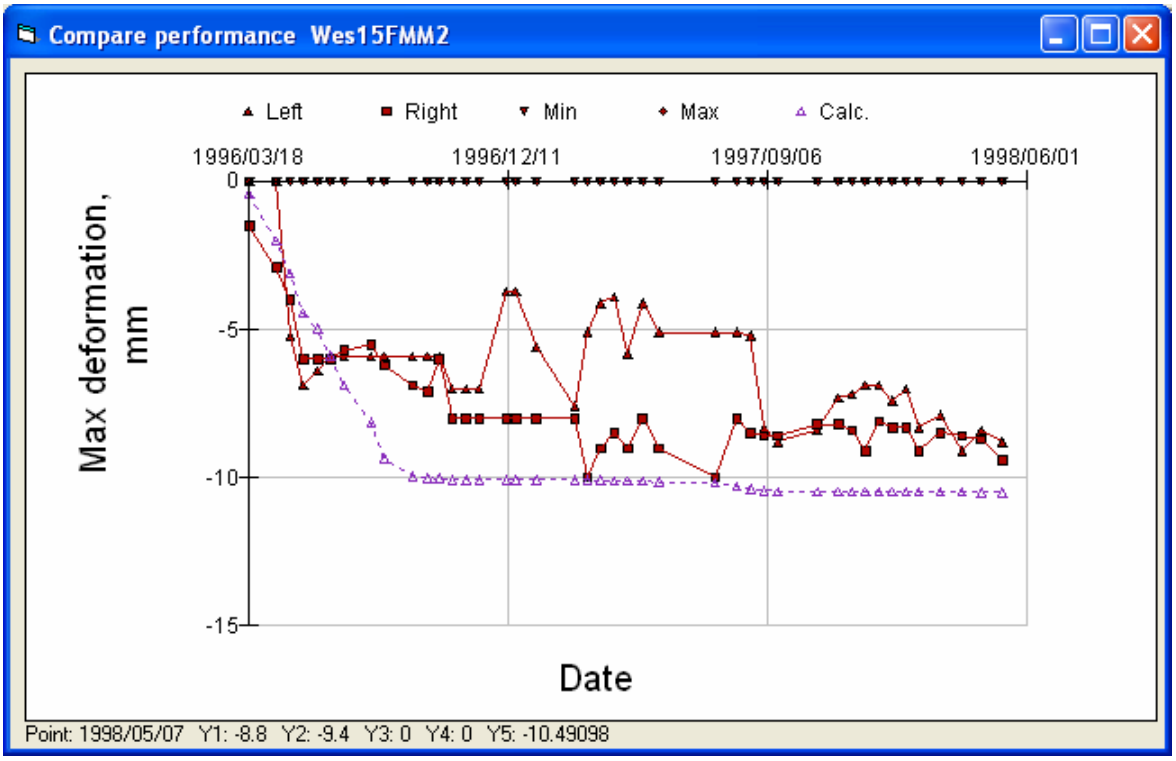

Figure 90. Maximum rutting in left and right wheelpaths at Section 15.

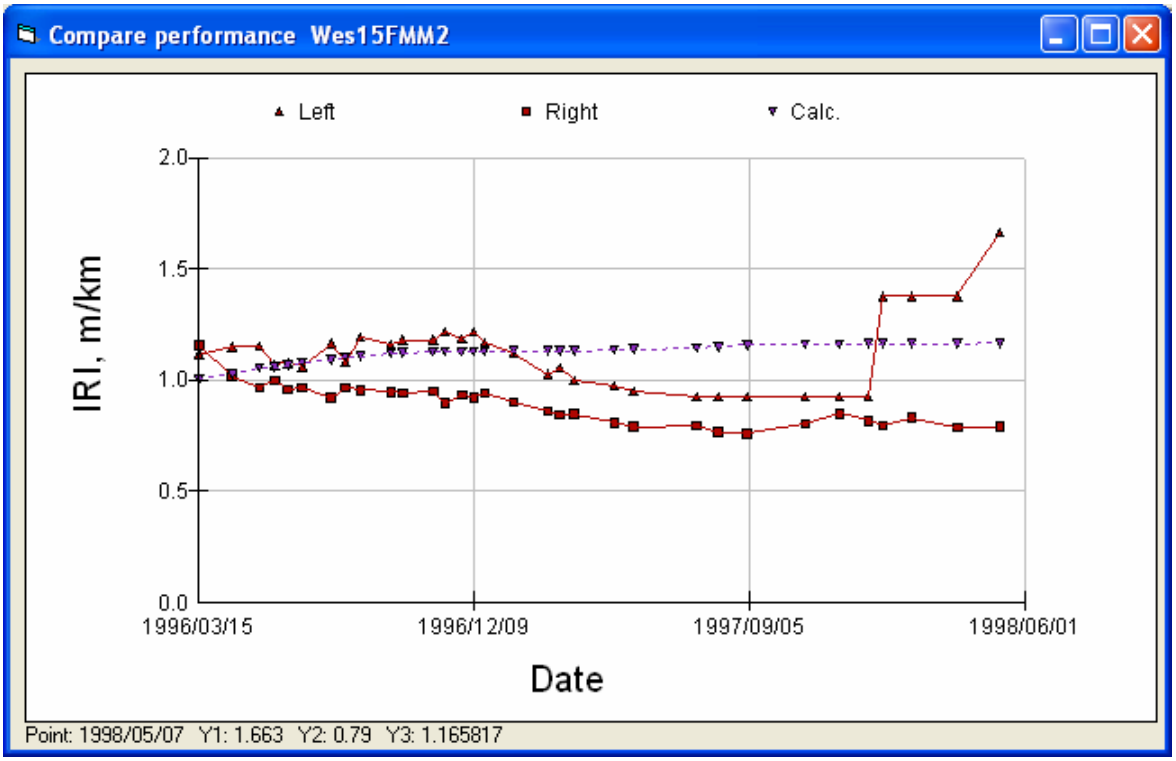

Figure 91. IRI in left and right wheelpaths at Section 15.

3.4.7 Section 16FLH2

Table 20. Summary of Input Values for Section 16LH2

Modulus	*α*	*β*	*γ*	*δ*	*aT*	*A*	*VTS*
AC	2.000	-0.842	0.5526	2.000	1.300	10.0406	-3.680
Unbound	*Eo*	*Stiffness factor*	*Power on load*	*Estart*			
AB	163 MPa	0.43	0.6	129 MPa			
Subgrade	77 MPa	0	-0.2	77 MPa			
Aging	*AgeA*	*AgeB*					
AC	0.3458	-1.0401					
Fatigue	*A*	*α*	*β*	*γ*	*δ*		
AC	0.3825	0.4738	2.0600	1.0300	0.4046		
Rutting	*A*	*α*	*β*	*γ*	*dVoids*		
AC	15.17	0.1322	1.03	1	4.3		

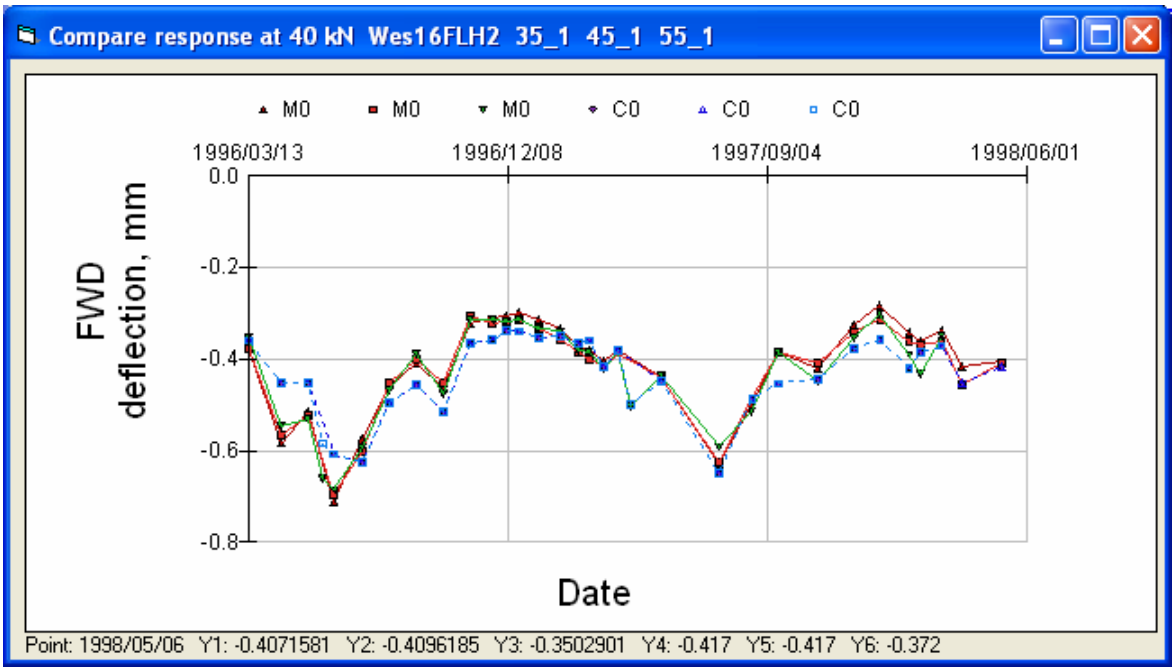

Figure 92. FWD deflections at Section 16 (in wheelpath, geophone under load plate).

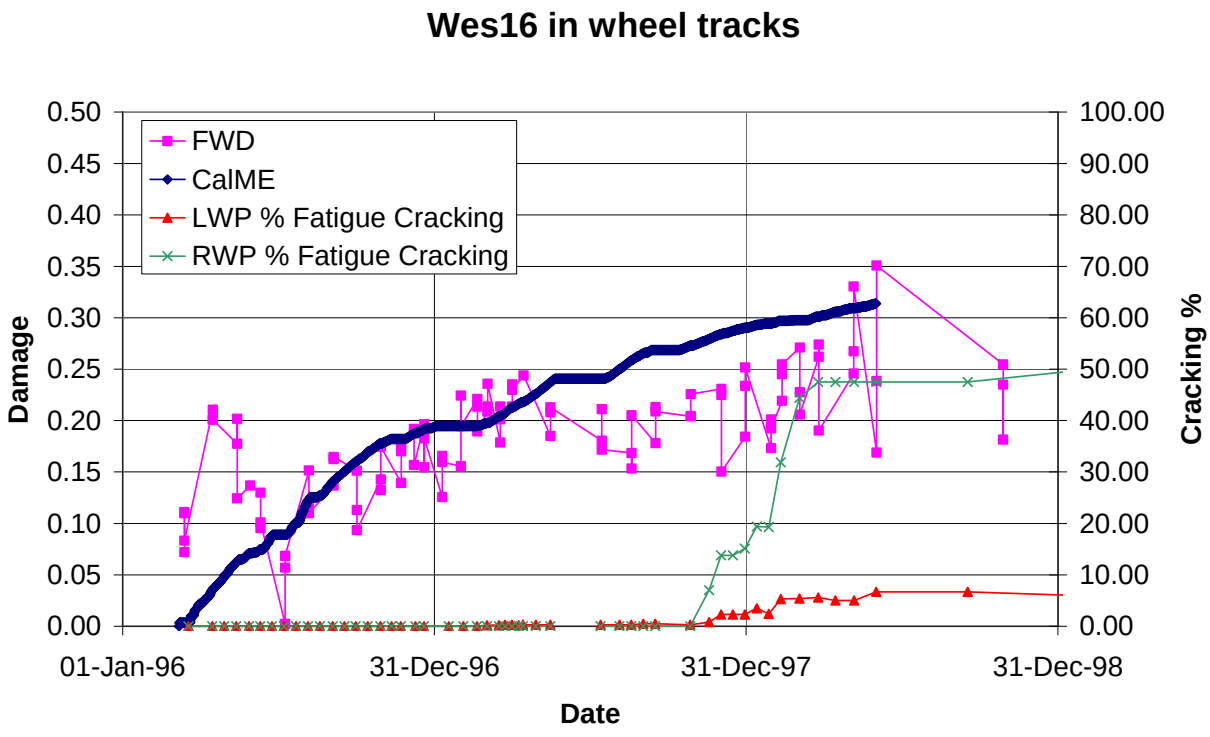

Figure 93. Damage in wheelpath of Section 16 (LWP = left wheelpath, RWP = right wheelpath).

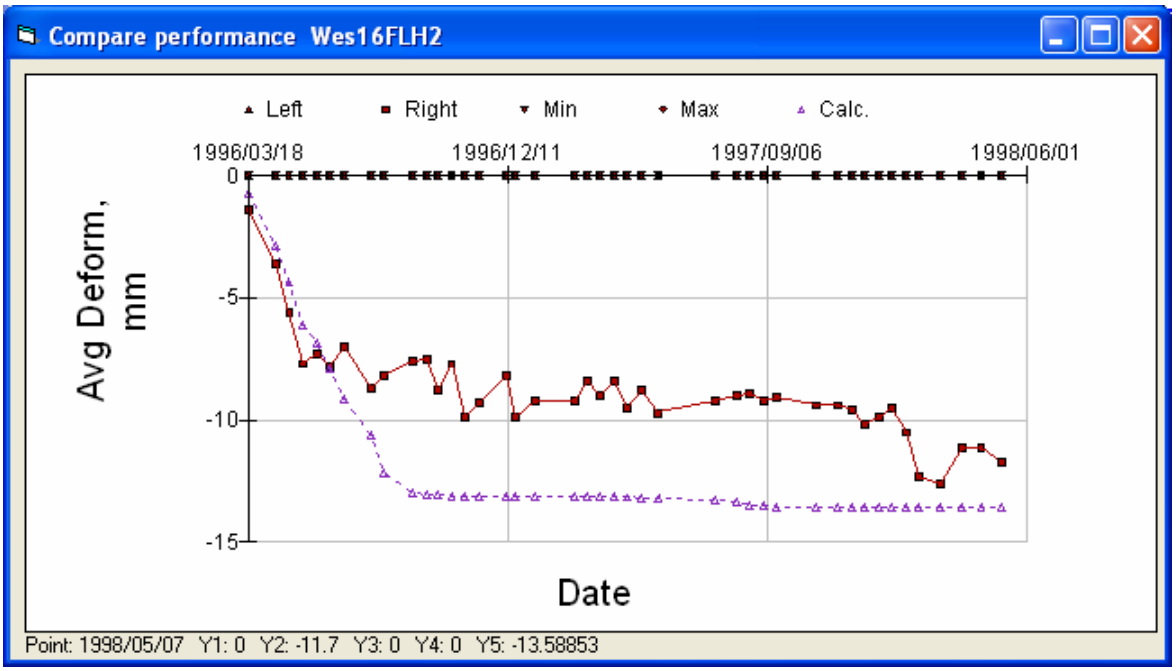

Figure 94. Down rut in right wheelpath at Section 16.

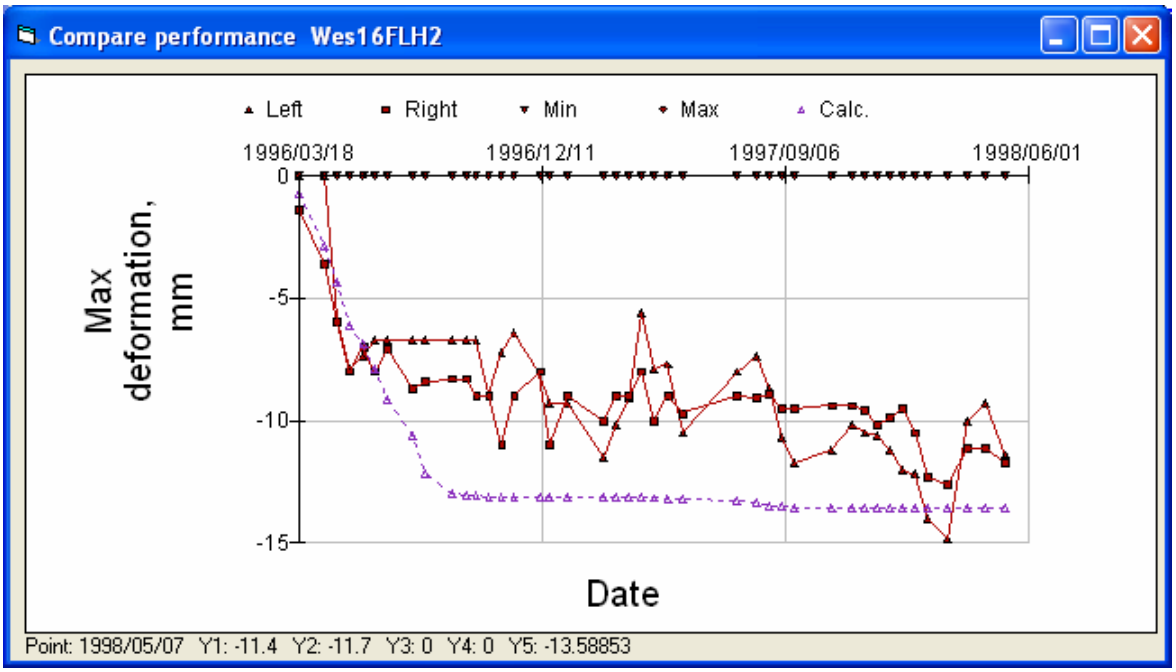

Figure 95. Maximum rutting in left and right wheelpaths at Section 16.

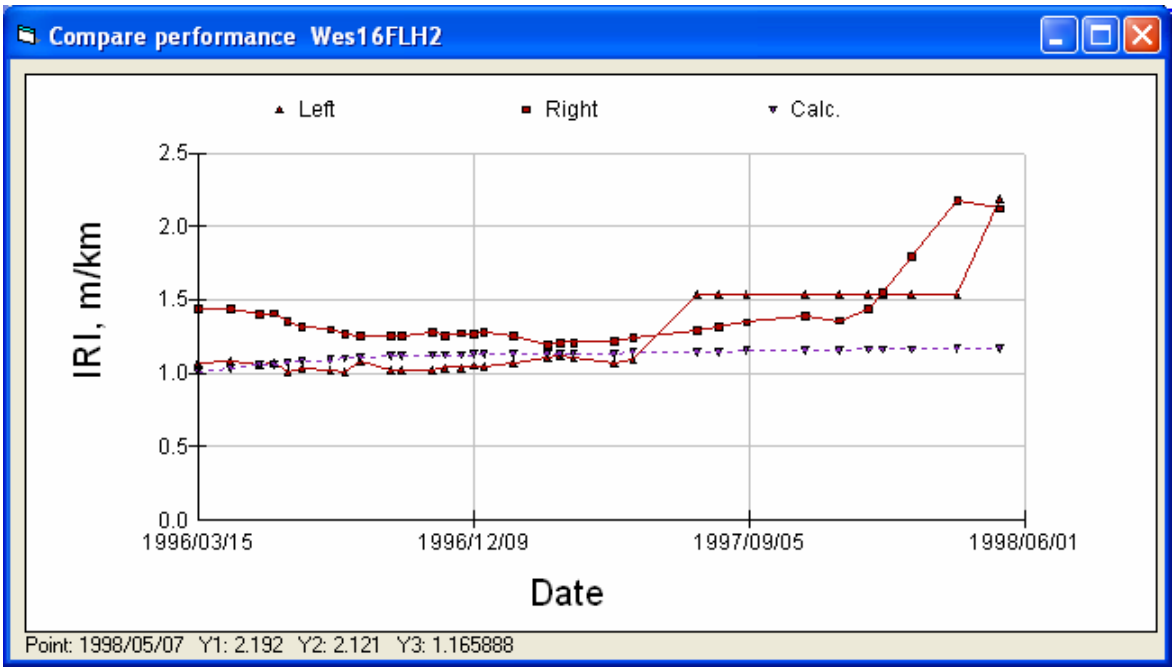

Figure 96. IRI in left and right wheelpaths at Section 16.

3.4.8 Section 17FMH

Table 21. Summary of Input Values for Section 17FMH

Modulus	*α*	*β*	*γ*	*δ*	*aT*	*A*	*VTS*
AC	2.000	-0.6447	0.6447	2.000	1.300	10.0406	-3.680
Unbound	*Eo*	*Stiffness factor*	*Power on load*	*Estart*			
AB	208 MPa	0.64	0.6	142 MPa			
Subgrade	75 MPa	0	-0.2	75 MPa			
Aging	*AgeA*	*AgeB*					
AC	0.3497	-1.0632					
Fatigue	*A*	*α*	*β*	*γ*	*δ*		
AC	0.2350	0.4481	1.9743	0.9871	0.3826		
Rutting	*A*	*α*	*β*	*γ*	*dVoids*		
AC	10.35	0.1269	1.03	1	3.9		

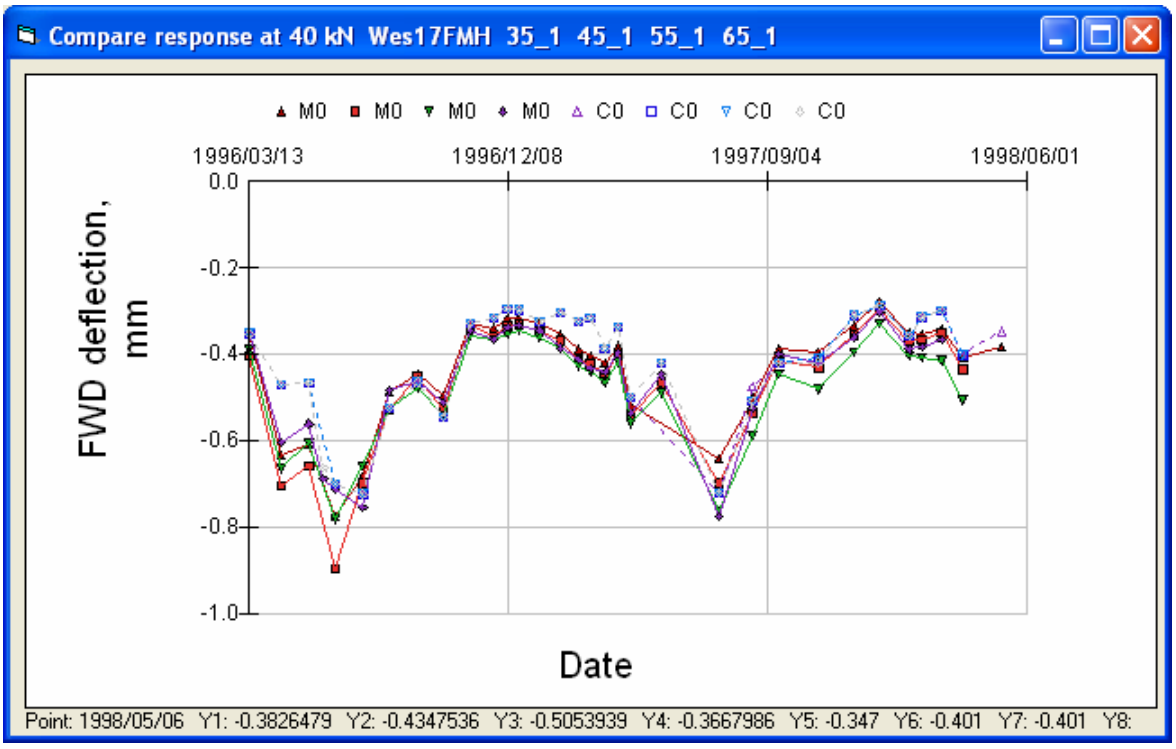

Figure 97. FWD deflections at Section 17 (in wheelpath, geophone under load plate).

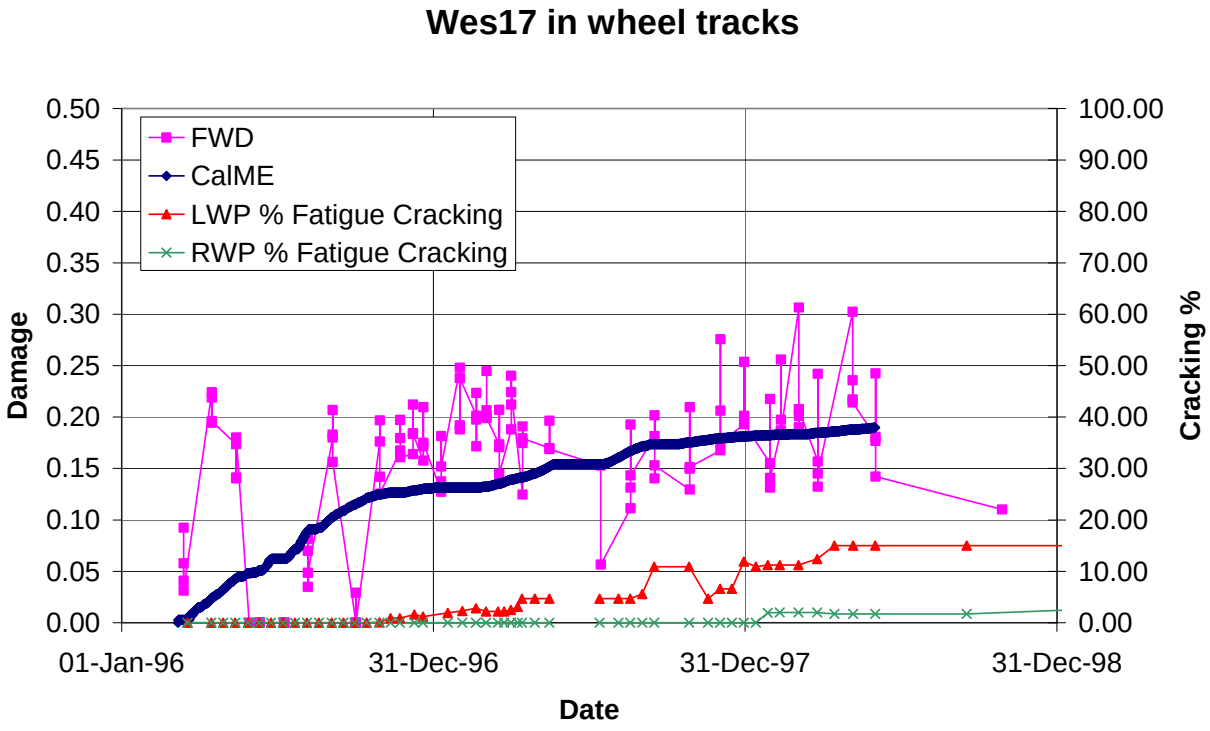

Figure 98. Damage in wheelpath of Section 17 (LWP = left wheelpath, RWP = right wheelpath).

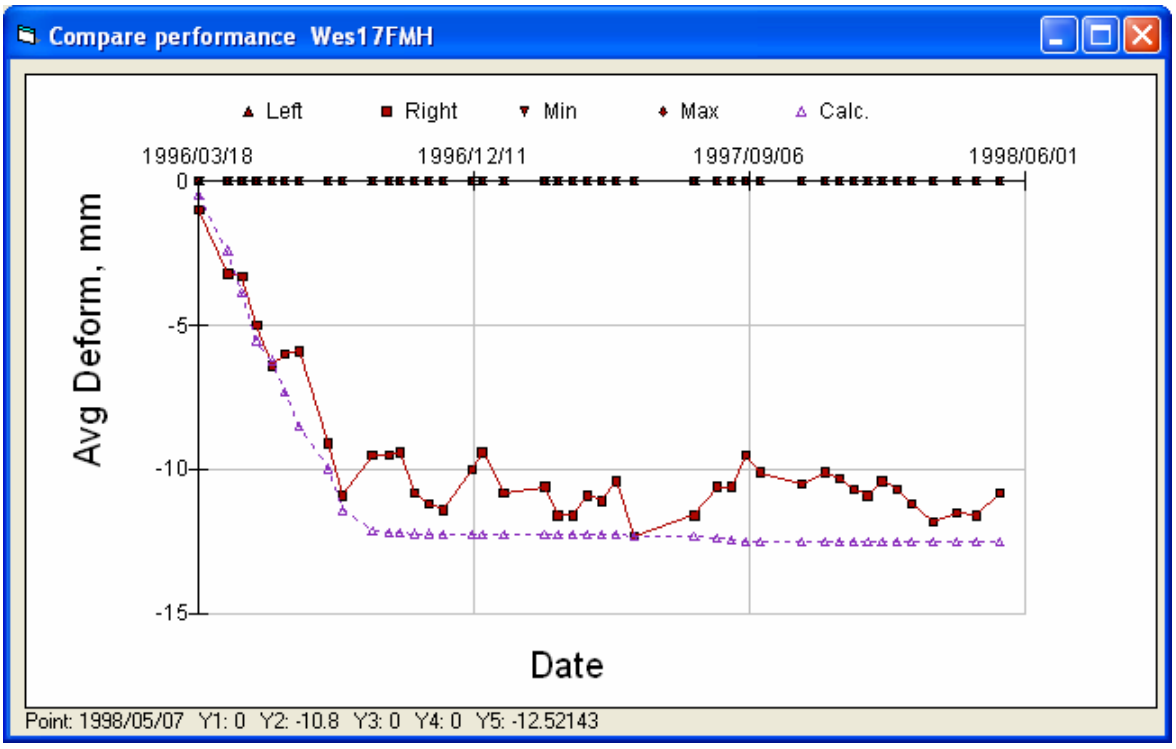

Figure 99. Down rut in right wheelpath at Section 17.

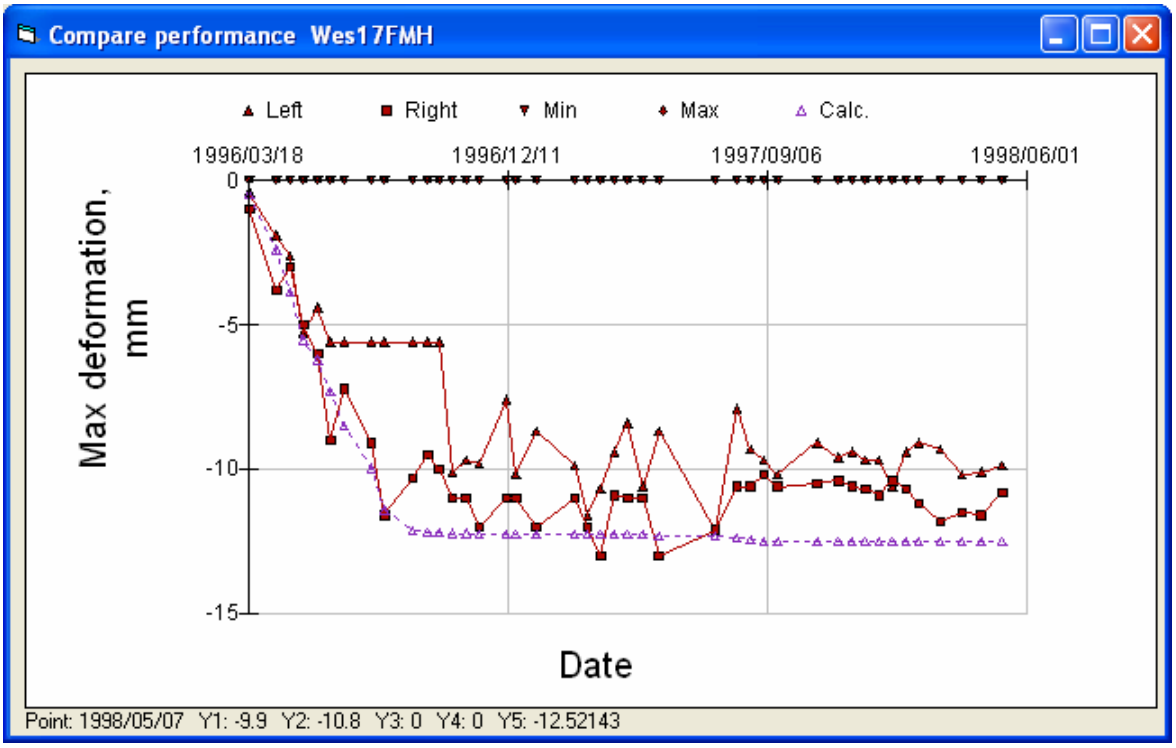

Figure 100. Maximum rutting in left and right wheelpaths at Section 17.

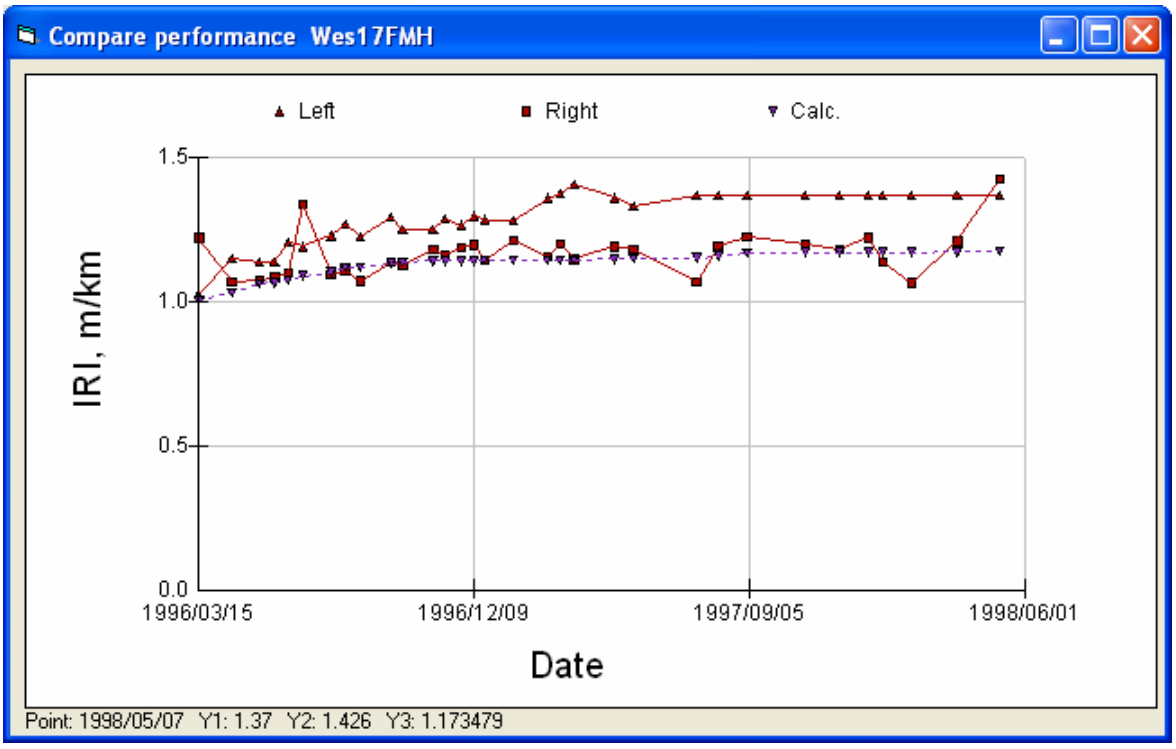

Figure 101. IRI in left and right wheelpaths at Section 17.

3.5 Simulation of Coarse Mix Sections

3.5.1 Notes on Simulations of Coarse Mix Sections

For each of the WesTrack sections simulated, a table shows the input values in the *CalME* database used for the simulation of that section, followed by plots comparing measured and calculated FWD deflections, damage and fatigue cracking, rutting, and IRI.

Development of inputs values, analysis, and plotting of results for the Coarse sections is the same as for the Fine mixes, except for handling of RSST-CH data for simulation of permanent deformation.

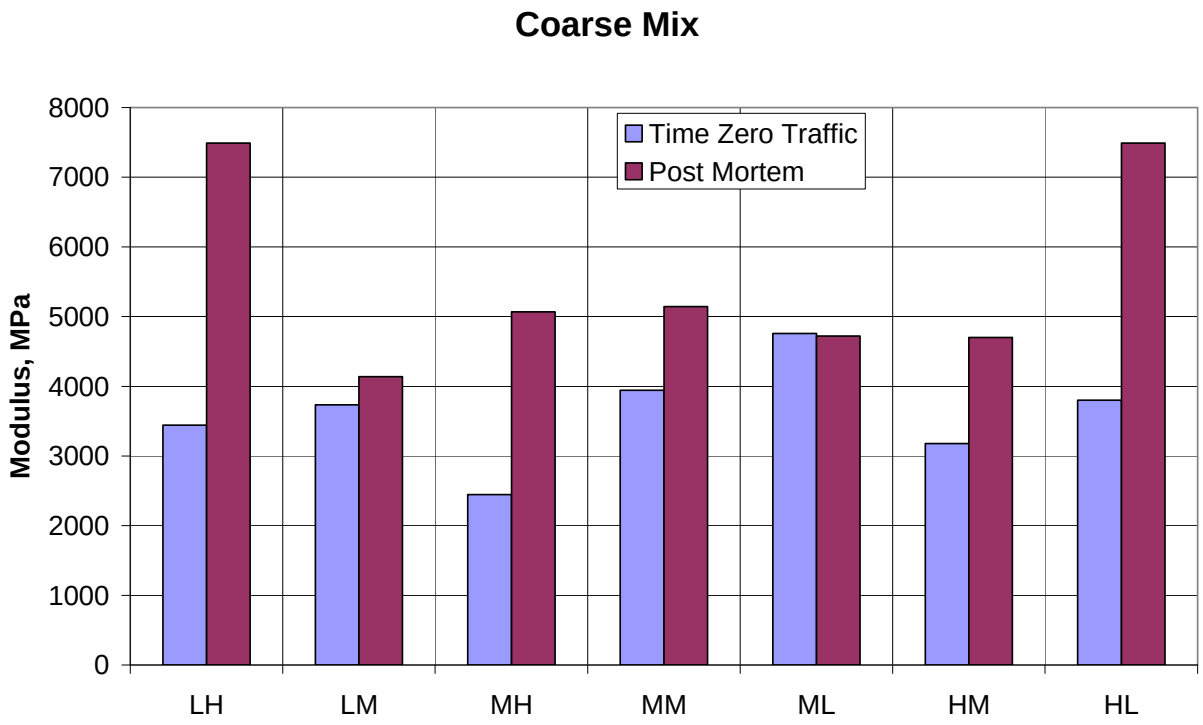

Figure 102. Mean Resilient Moduli from UNR indirect tensile tests of Coarse mix (MPa), at construction and post mortem.

Indirect tensile tests were performed by the University of Nevada, Reno, at "Time Zero Construction" and at "Post-Mortem." Many of the Coarse sections failed and were removed before the end of the WesTrack experiment, so the post-mortem sampling occurred at various times during the experiment, not at the end. Figure 102 shows the results for the Coarse mix. Only the Coarse mix sections with high air-voids content (06 and 26) show aging (hardening) similar to that observed for the Fine mix, previously shown in Figure 30, although most of the Fine mixes were sampled at the end of the entire WesTrack experiment and therefore were in place in the pavement for a longer period of time. This can be seen in Figure 102, where the second letter in the designation indicates the air-void content and the first letter indicates the asphalt content, with L meaning Low target value, M meaning Medium, and H meaning High. The section with high AC content and low air voids (Section 25 HL) shows a doubling of the modulus, which is rather surprising, especially considering that it was removed and replaced after the first year of trafficking.

This is not confirmed by the shear tests, also performed after one year of trafficking. Shear tests after the first year of trafficking were done on six coarse sections. For Section 25 (HL) the shear modulus decreases slightly (3 percent). For the other sections the agreement with the change in resilient modulus from indirect tensile testing is quite good, as evidenced by Figure 103, which shows the ratio of the modulus measured post mortem to the initial modulus, for both the indirect tensile tests and the shear tests.

Figure 103. Ratio of post-mortem modulus to initial modulus.

An attempt was made to use tests on untrafficked material to estimate the coefficients of Equation 25. The parameters from the untrafficked cores result in greater prediction of rutting than was the case when trafficked cores were used, particularly if the section had high as-constructed air-voids. When the as-constructed air-voids are high, the constant height of the RSST-CH doesn't permit the initial rapid early densification that occurred under trafficking. This suggests that RSST-CH tests should be run on specimens with air-void contents that would be expected after initial trafficking.

A K value of 0.8 was used (versus a K of 0.9 for Fine and Fine Plus mixes). For some of the RSST-CH tests the difference between the two test samples was such that it was not possible to fit a single relationship to the results, using "Solver." These tests were fitted individually and the parameters were determined as the mean values.

No shear tests on trafficked material were available for test sections 24CMM2 and 26CLH.

3.5.2 Section 05CMM1

Table 22. Summary of Input Values for Section 05CMM1

Modulus	α	β	γ	δ	aT	A	VTS
AC	1.9542	-0.8059	0.8059	2.000	1.300	10.0406	-3.680
Unbound	*Eo*	*Stiffness factor*	*Power on load*	*Estart*			
AB	298 MPa	0.57	0.6	211 MPa			
Subgrade	63 MPa	0	-0.2	63 MPa			
Aging	*AgeA*	*AgeB*					
AC	0.1703	-0.0048					
Fatigue	*A*	α	β	γ	δ		
AC	0.1202	0.4293	2.2150	1.1075	0.3666		
Rutting	*A*	α	β	γ	*dVoids*		
AC	51.39	0.215	1.03	1	3.1		

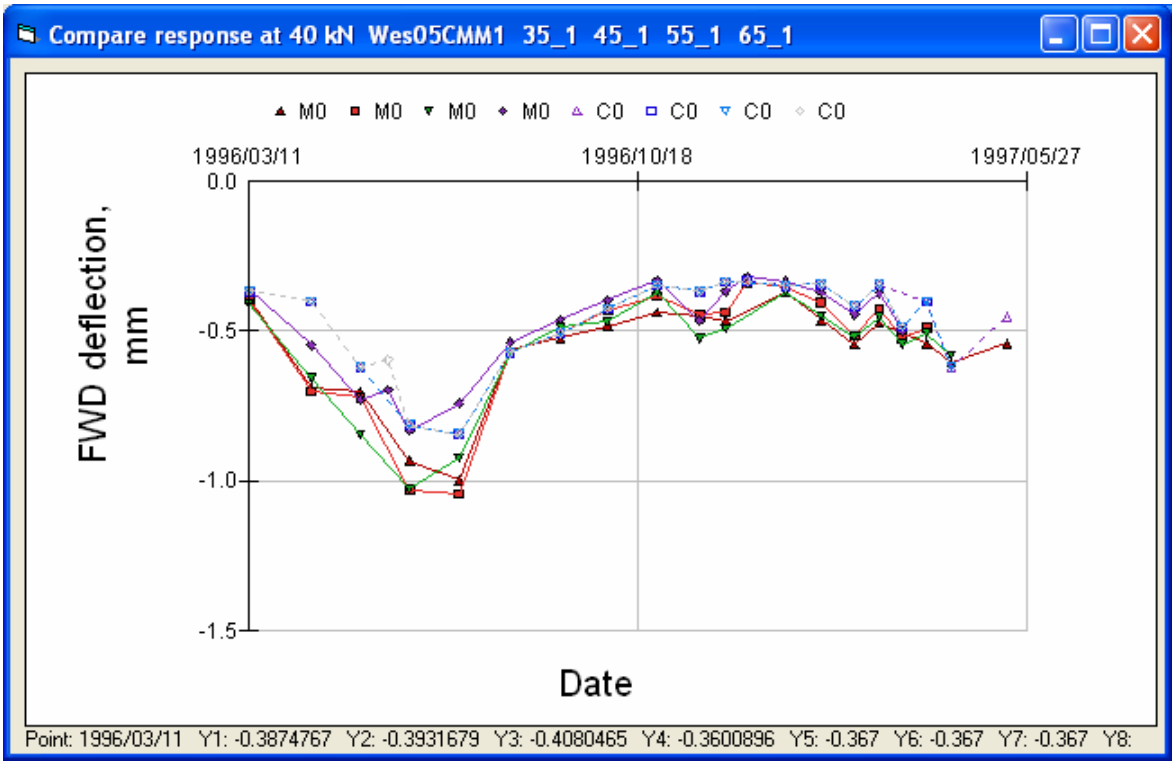

Figure 104. FWD deflections at Section 05 (in wheelpath, geophone under load plate).

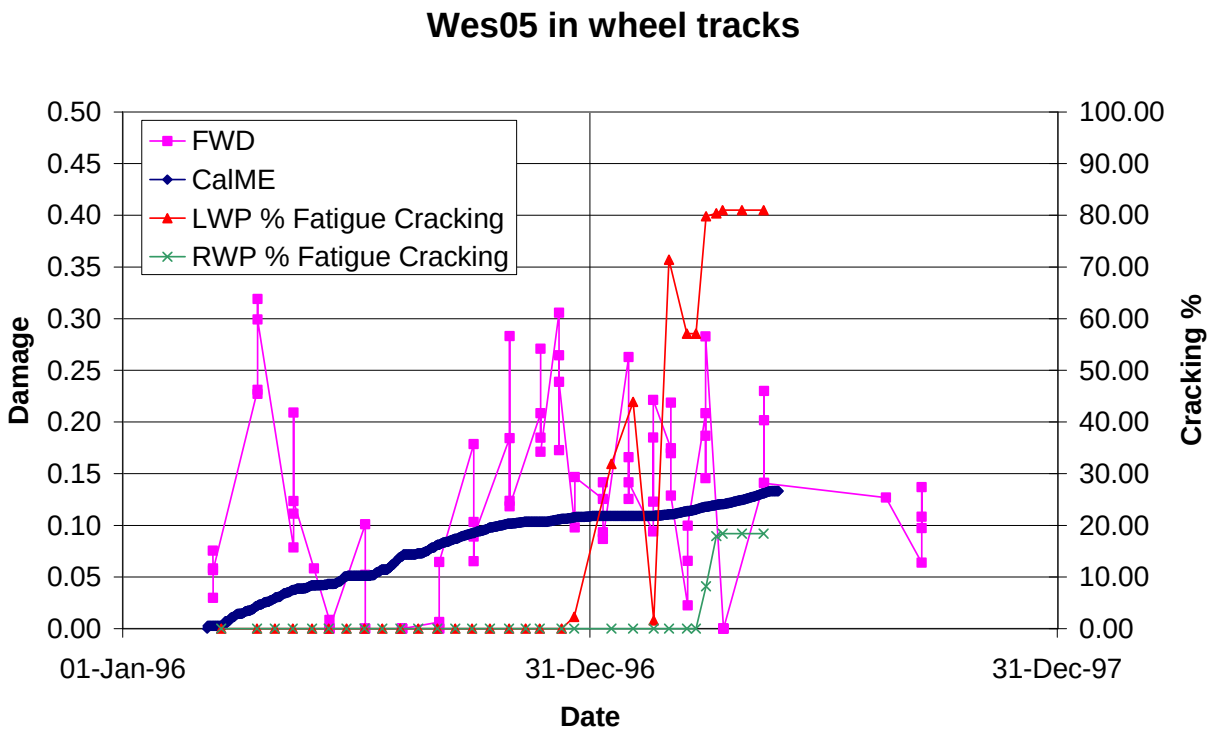

Figure 105. Damage in wheelpath of Section 05 (LWP = left wheelpath, RWP = right wheelpath).

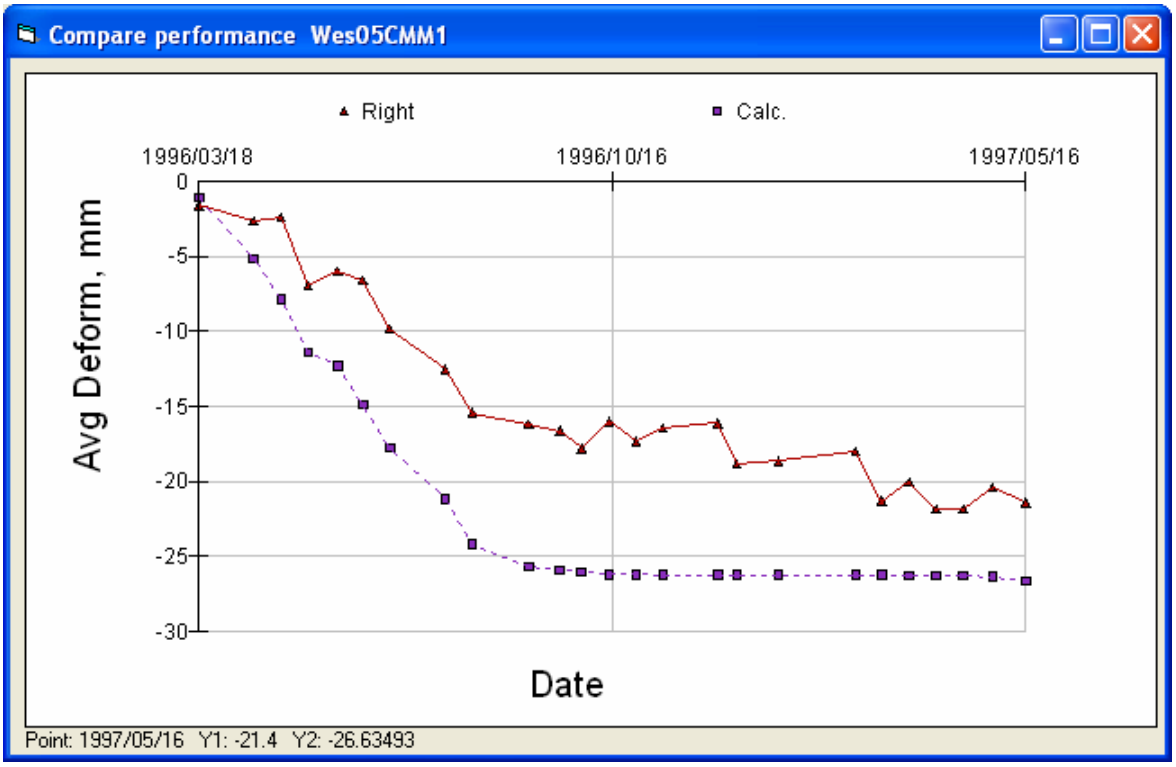

Figure 106. Down rut in right wheelpath at Section 05.

This section had significant early rutting that required that the pavement in this section be removed prior to the end of the experiment.

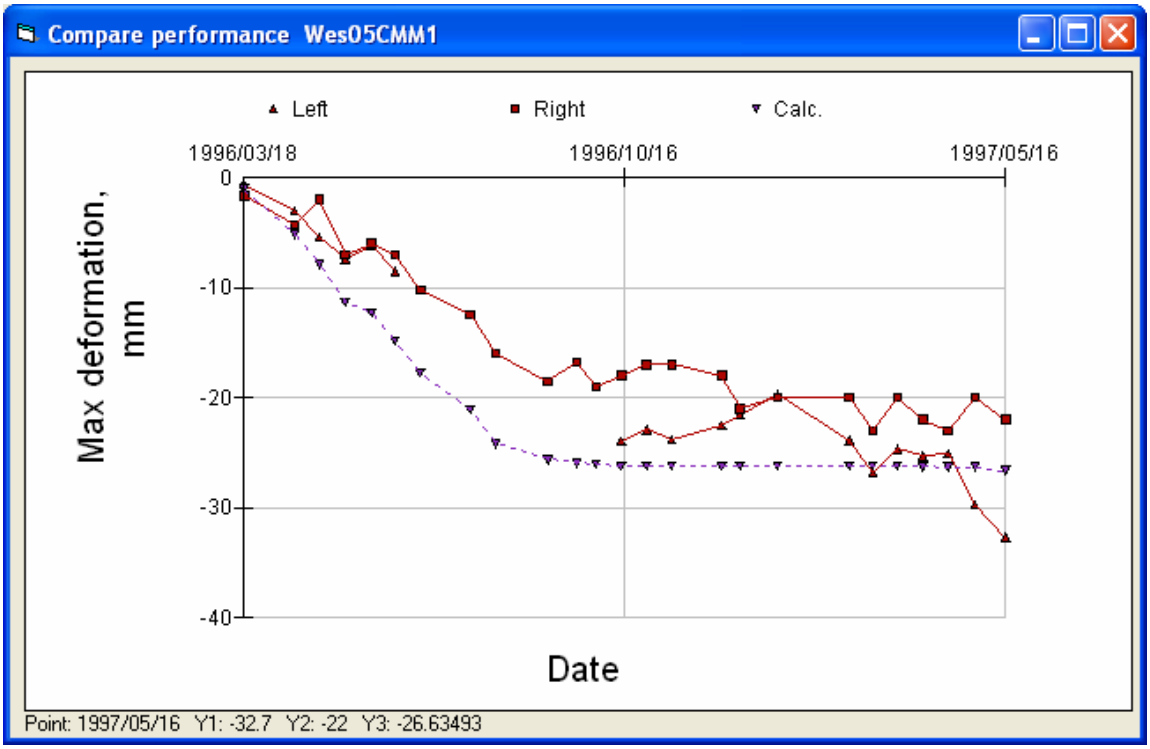

Figure 107. Maximum rutting in left and right wheelpaths at Section 05.

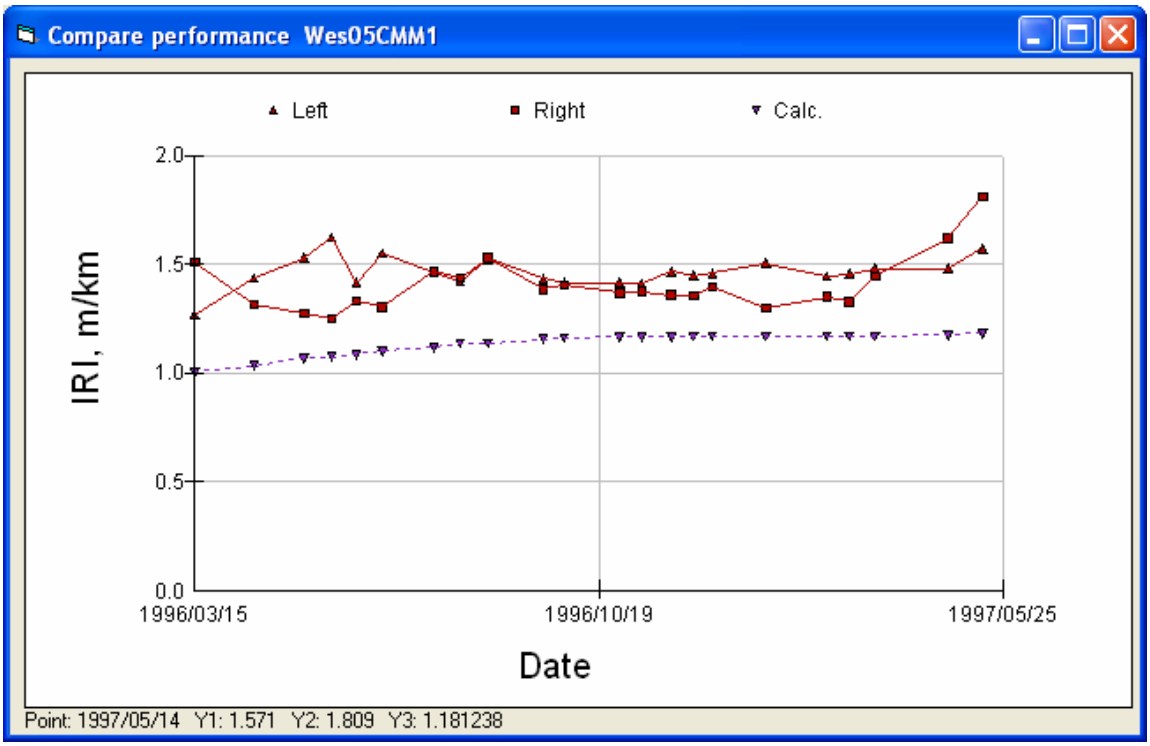

Figure 108. IRI in left and right wheelpaths at Section 05.

3.5.3 Section 06CMH

Table 23. Summary of Input Values for Section 06CMH

Modulus	*α*	*β*	*γ*	*δ*	*aT*	*A*	*VTS*
AC	1.9031	-0.8059	0.8059	2.000	1.300	10.0406	-3.680
Unbound	*Eo*	*Stiffness factor*	*Power on load*	*Estart*			
AB	106 MPa	0	0.6	106 MPa			
Subgrade	55 MPa	0	-0.2	55 MPa			
Aging	*AgeA*	*AgeB*					
AC	0.3135	-0.8493					
Fatigue	*A*	*α*	*β*	*γ*	*δ*		
AC	0.1407	0.4493	2.5804	1.2908	0.3837		
Rutting	*A*	*α*	*β*	*γ*	*dVoids*		
AC	53.1	0.237	1.03	1	4.4		

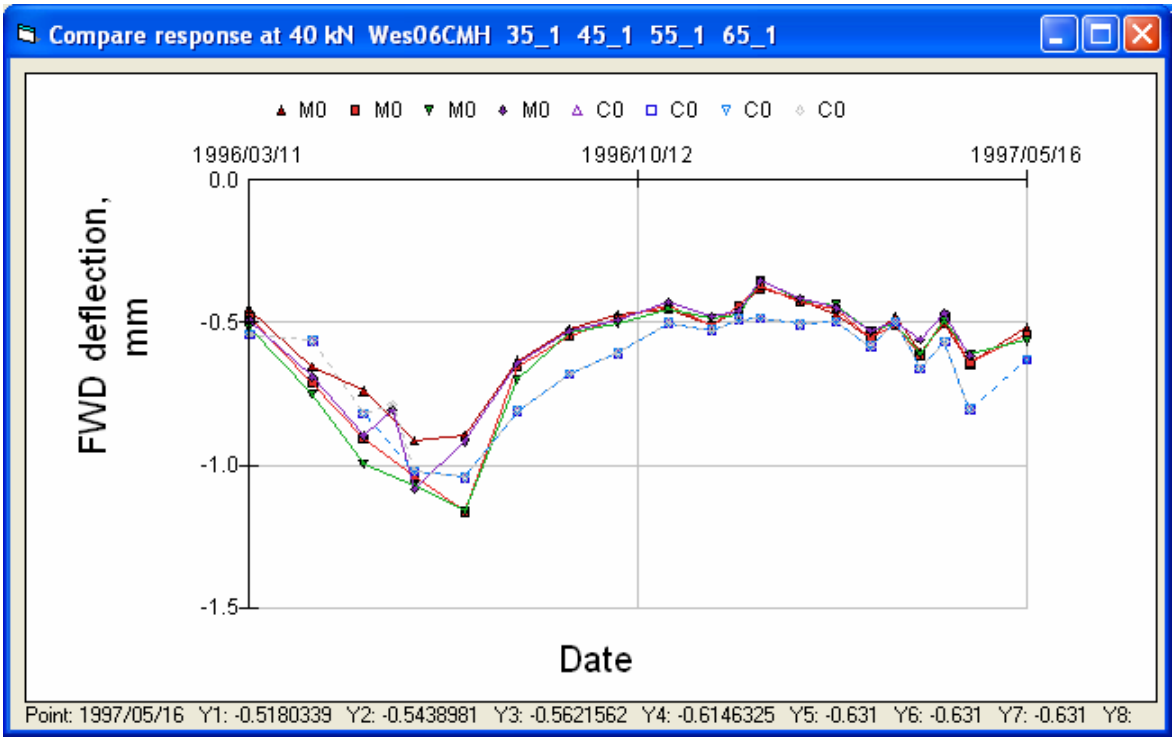

Figure 109. FWD deflections at Section 06 (in wheelpath, geophone under load plate).

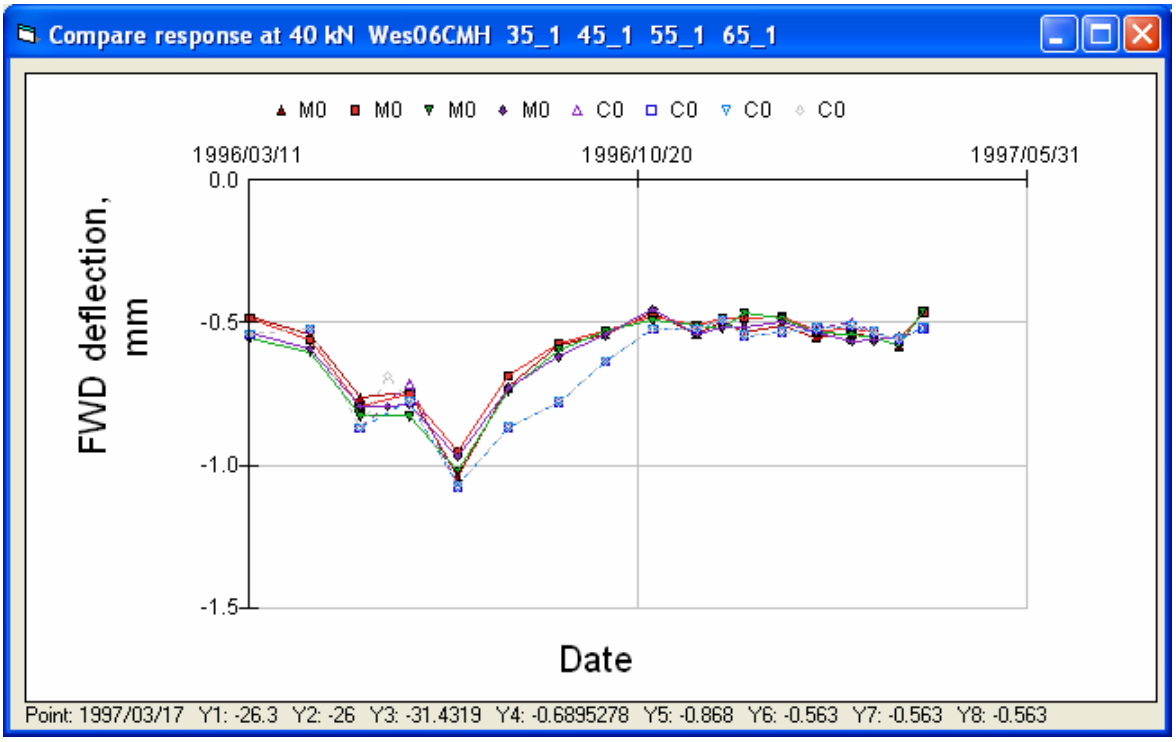

Figure 110. FWD deflections at Section 06 (between wheelpaths, geophone under load plate).

The FWD deflections between the wheelpaths were a little larger than in the wheelpath, toward the end of the experiment, as can be seen from Figure 110. This is contrary to what should be expected as the larger damage in the wheelpath should lead to larger deflections.

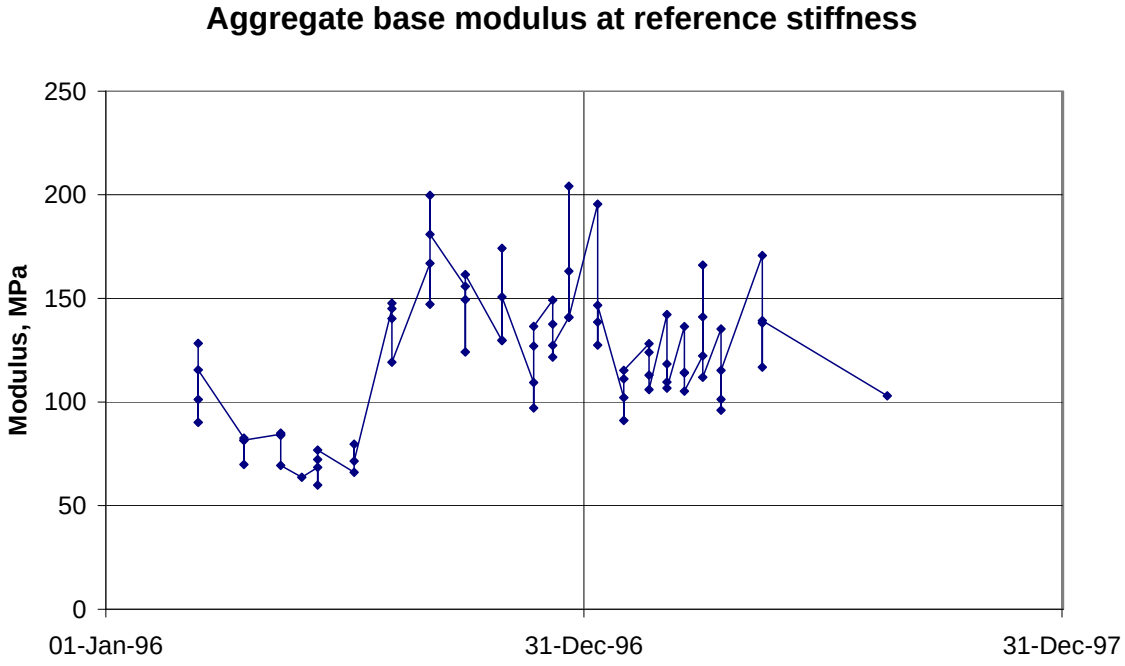

Figure 111. AB modulus in wheelpath at reference stiffness, backcalculated from FWD results.

Some of the discrepancy between the measured and calculated deflection may be partly due to the irregular changes in the modulus of the aggregate base in the wheelpath, seen in Figure 111.

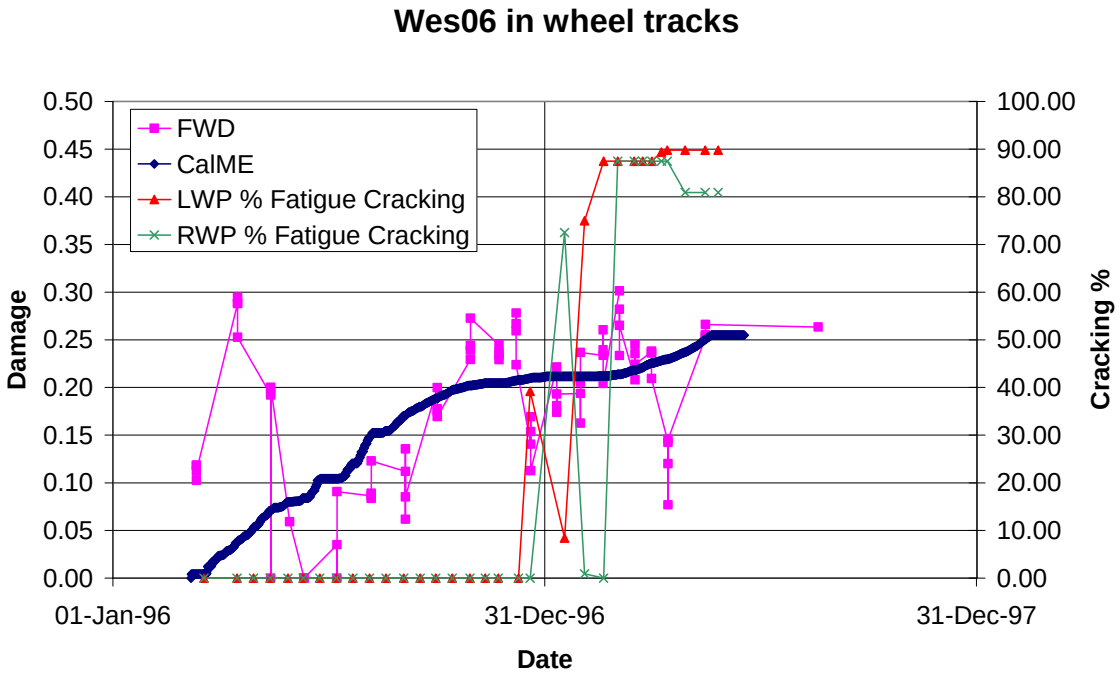

Figure 112. Damage in wheelpath of Section 06 (damage scale to 0.5) (LWP = left wheelpath, RWP = right wheelpath).

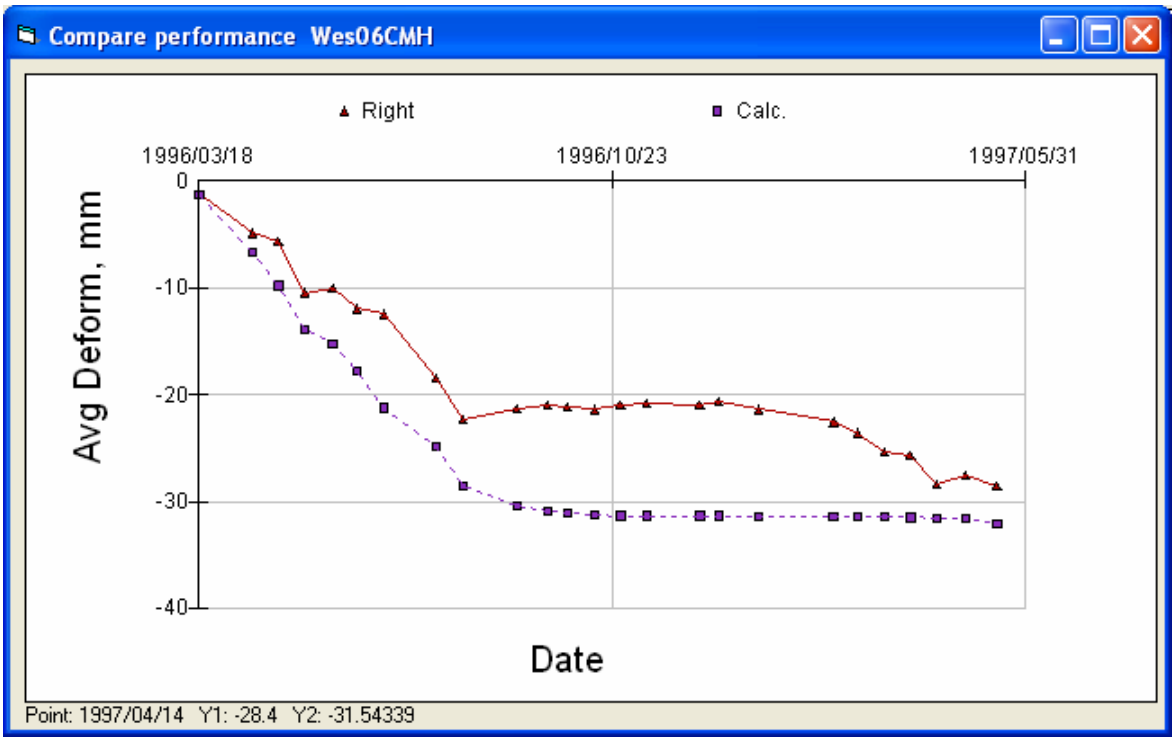

Figure 113. Down rut in right wheelpath at Section 06.

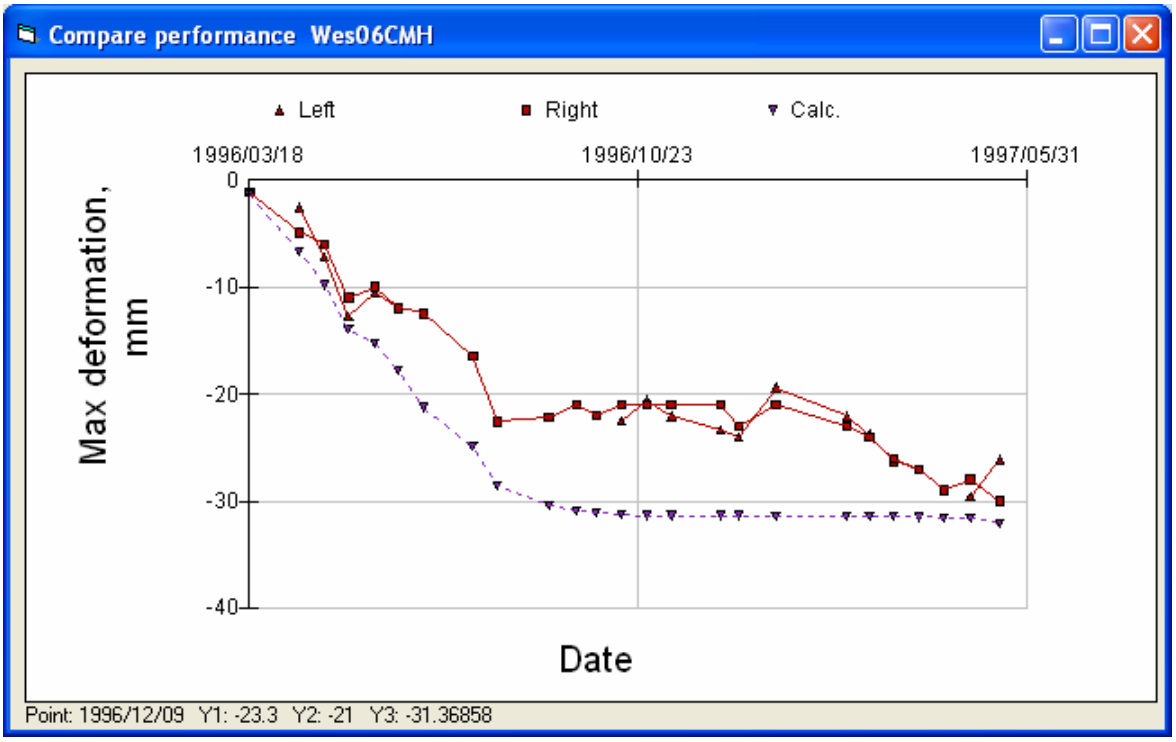

Figure 114. Maximum rutting in left and right wheelpaths at Section 06.

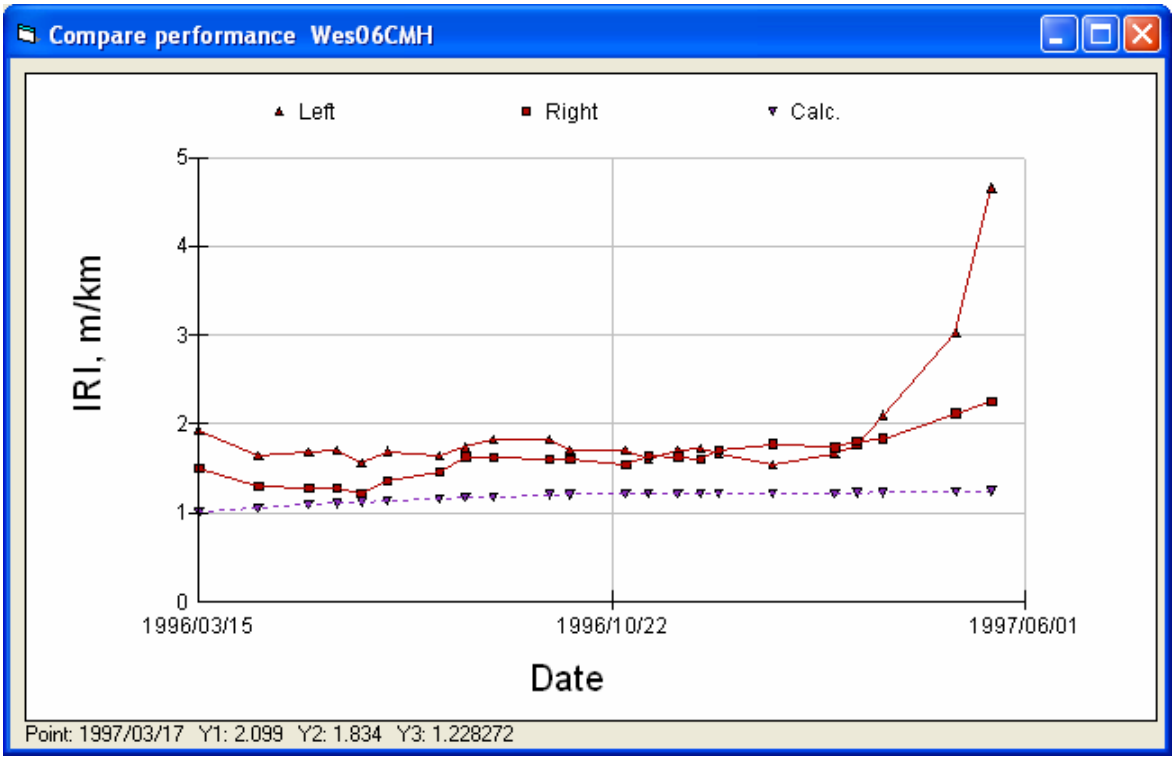

Figure 115. IRI in left and right wheelpaths at Section 06.

3.5.4 Section 07CHM

Table 24. Summary of Input Values for Section 07CHM

Modulus	*α*	*β*	*γ*	*δ*	*aT*	*A*	*VTS*
AC	2.1461	-0.6447	0.6447	2.000	1.300	10.0406	-3.680
Unbound	*Eo*	*Stiffness factor*	*Power on load*	*Estart*			
AB	256 MPa	0.52	0.6	202 MPa			
Subgrade	61 MPa	0	-0.2	61 MPa			
Aging	*AgeA*	*AgeB*					
AC	0.1963	-0.1582					
Fatigue	*A*	*α*	*β*	*γ*	*δ*		
AC	0.0508	0.5907	3.6182	1.8091	0.5045		
Rutting	*A*	*α*	*β*	*γ*	*dVoids*		
AC	155.67	0.315	1.03	1	2.7		

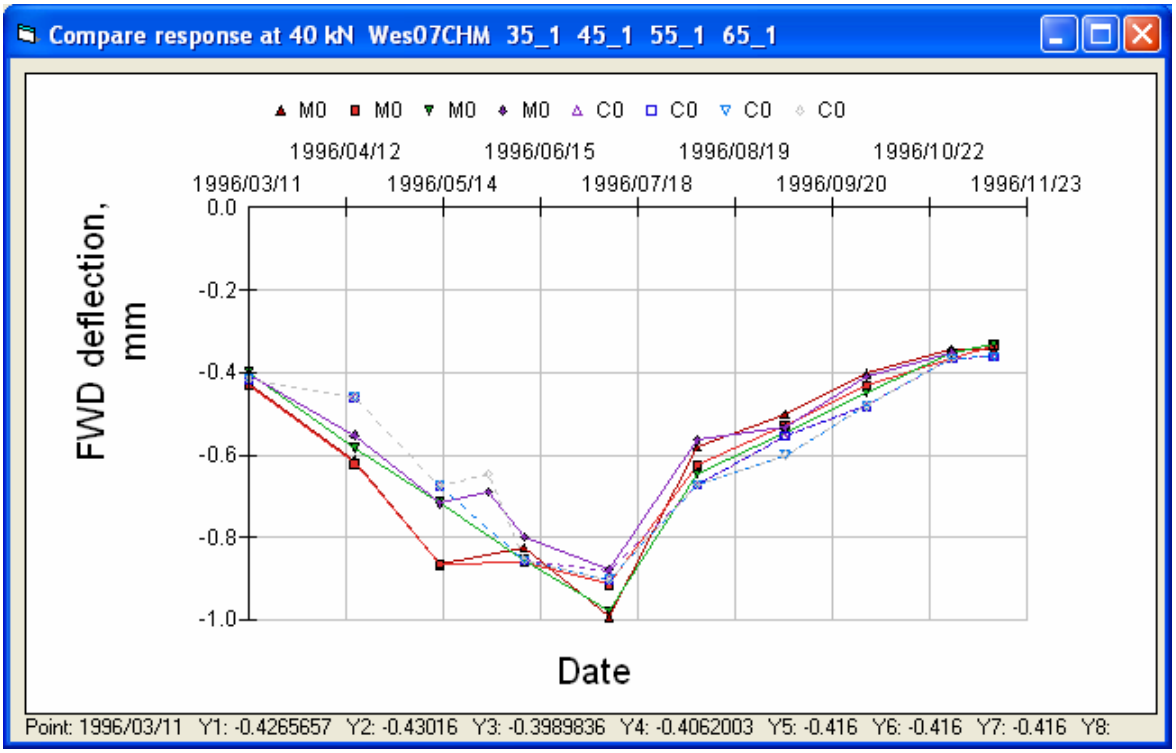

Figure 116. FWD deflections at Section 07 (in wheelpath, geophone under load plate).

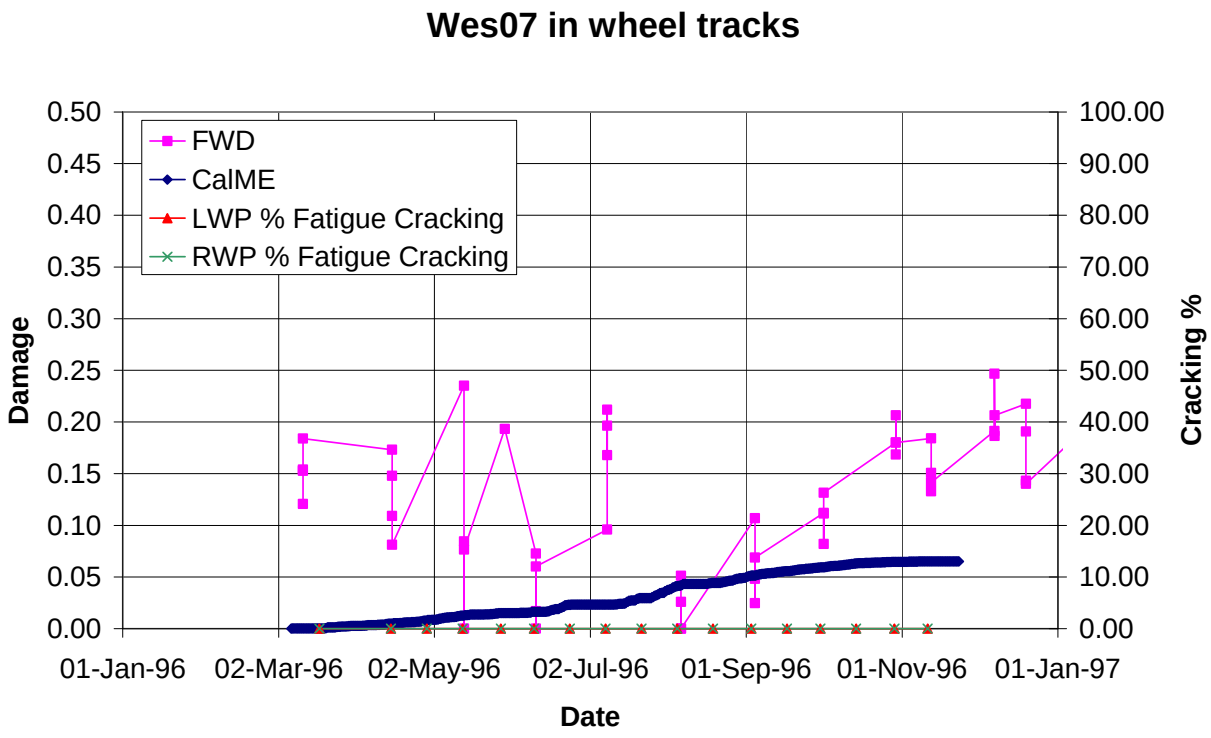

Figure 117. Damage in wheelpath of Section 07 (LWP = left wheelpath, RWP = right wheelpath).

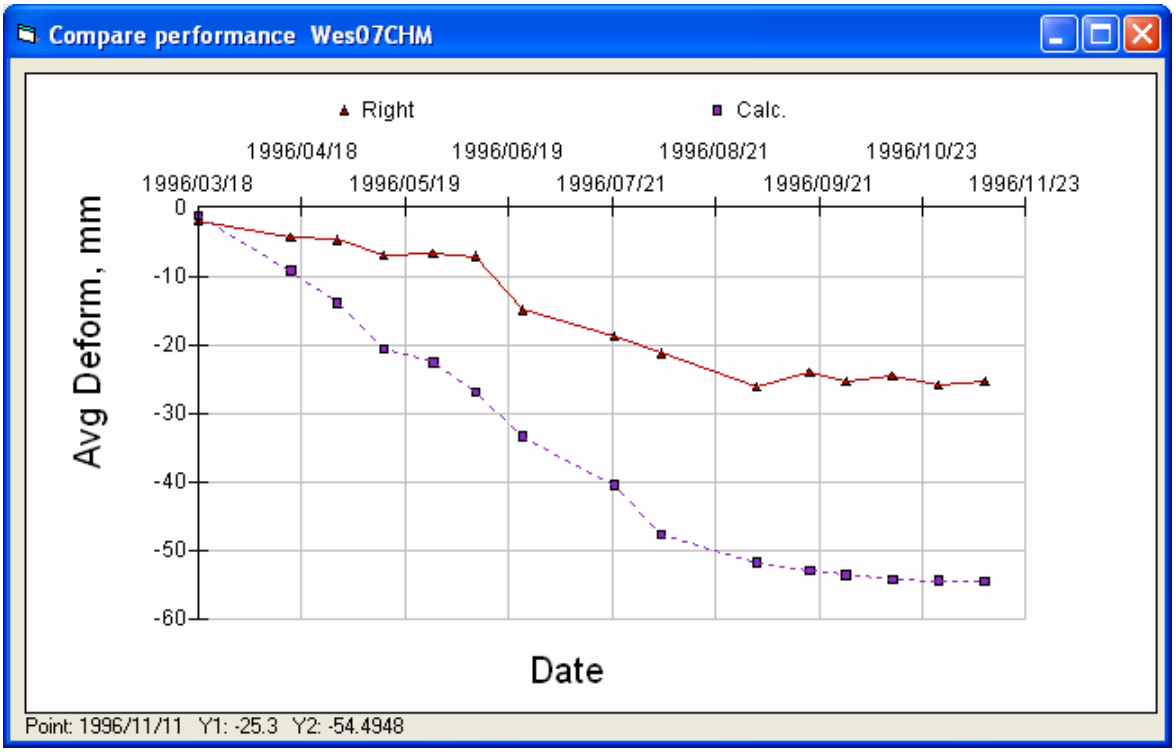

Figure 118. Down rut in right wheelpath at Section 07.

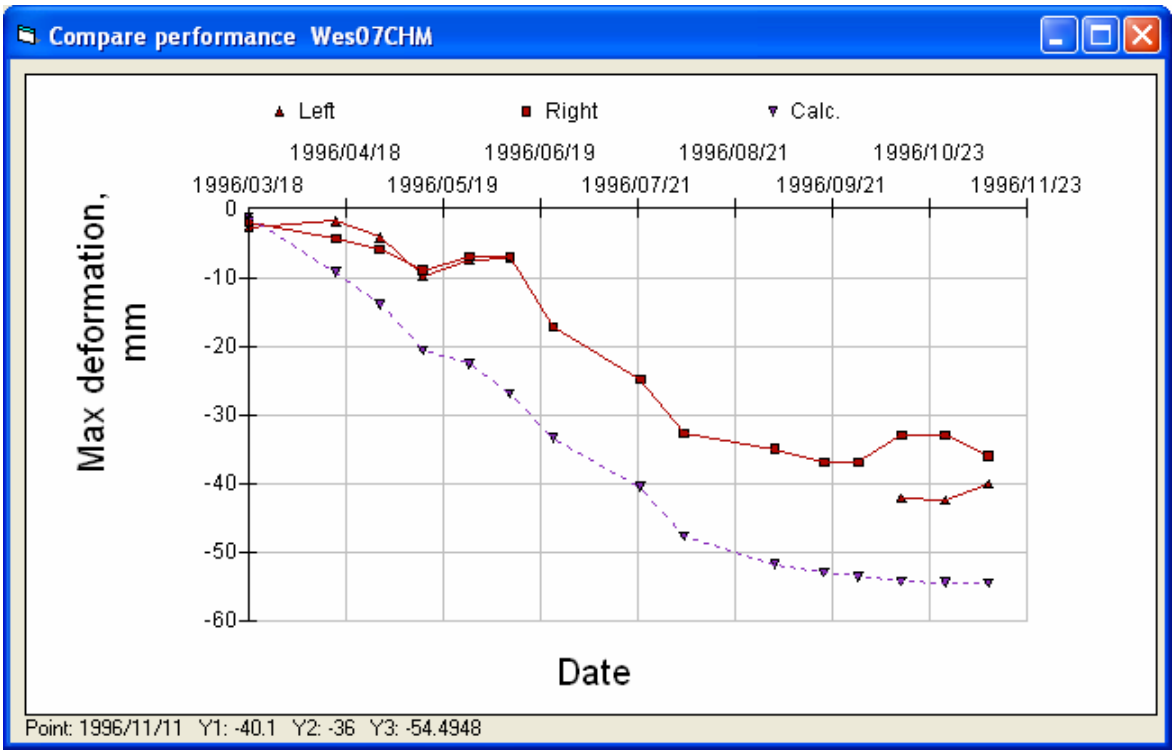

Figure 119. Maximum rutting in left and right wheelpaths at Section 07.

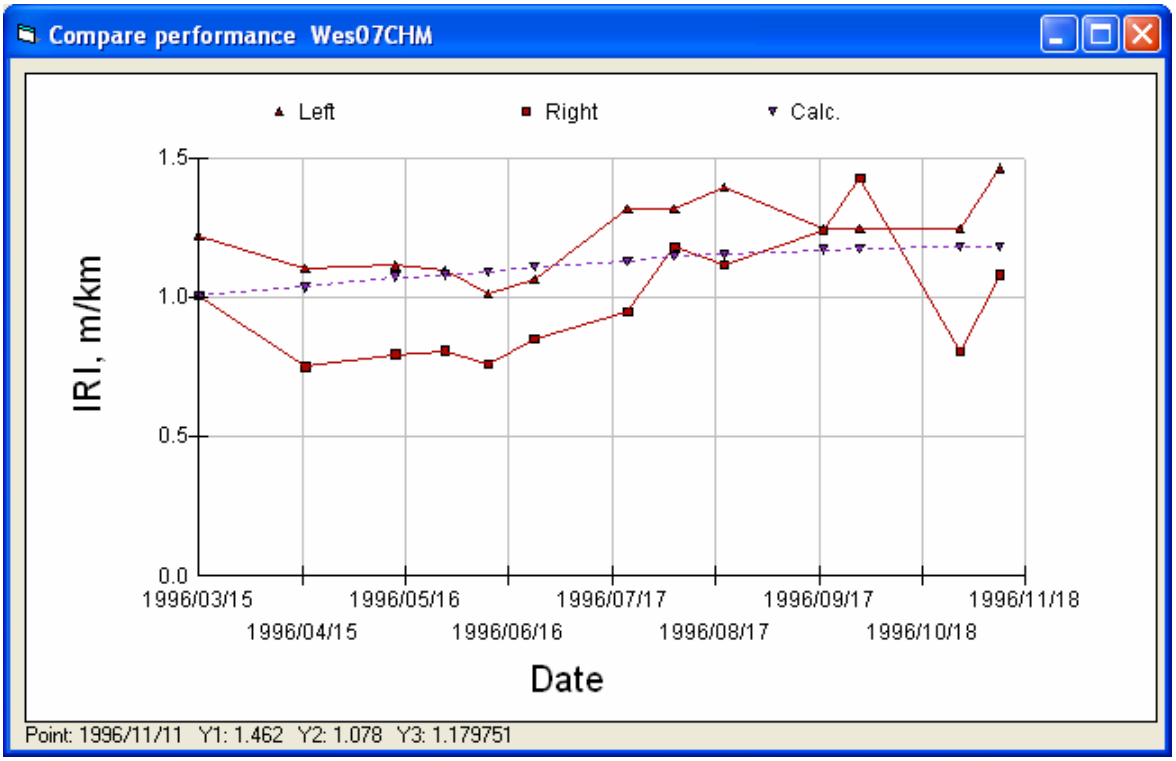

Figure 120. IRI in left and right wheelpaths at Section 07.

3.5.5 Section 08CLM

Table 25. Summary of Input Values for Section 08CLM

Modulus	*α*	*β*	*γ*	*δ*	*aT*	*A*	*VTS*
AC	2.2041	-0.4145	0.4145	2.000	1.300	10.0406	-3.680
Unbound	*Eo*	*Stiffness factor*	*Power on load*	*Estart*			
AB	104 MPa	0	0.6	104 MPa			
Subgrade	57 MPa	0	-0.2	57 MPa			
Aging	*AgeA*	*AgeB*					
AC	0.0592	0.6509					
Fatigue	*A*	*α*	*β*	*γ*	*δ*		
AC	0.0393	0.4726	2.4236	1.2118	0.4036		
Rutting	*A*	*α*	*β*	*γ*	*dVoids*		
AC	39.78	0.234	1.03	1	3.0		

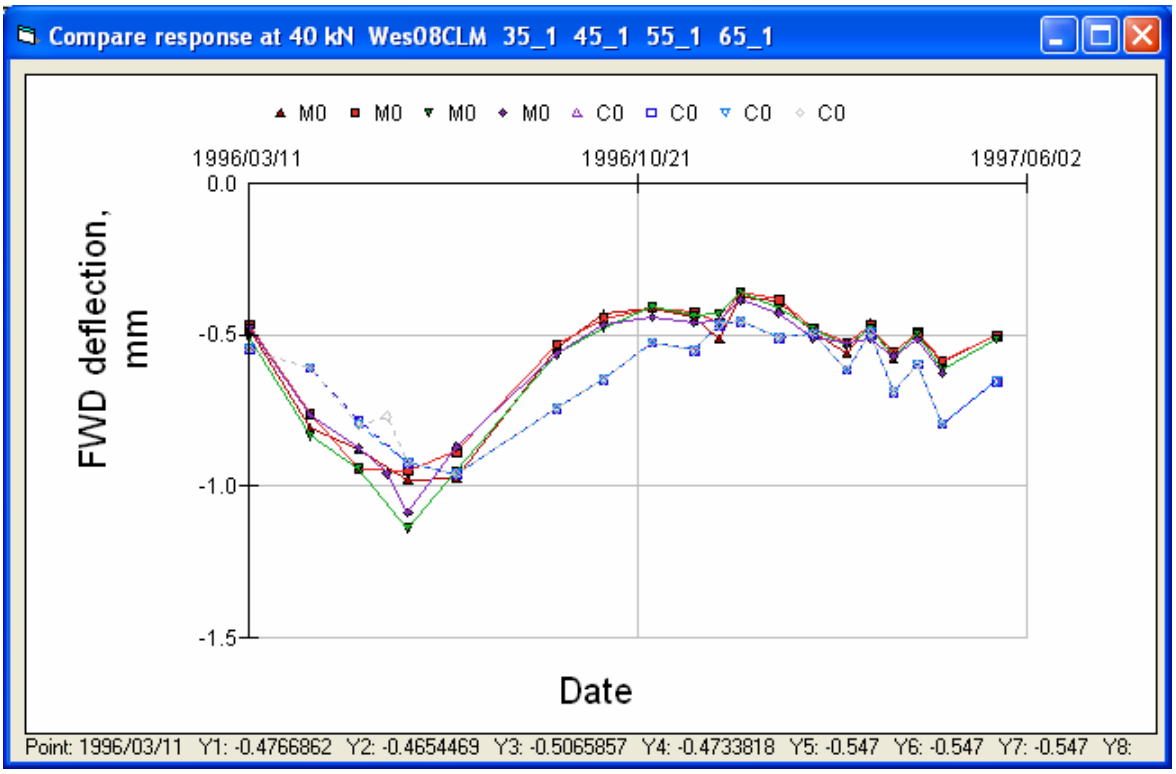

Figure 121. FWD deflections at Section 08 (in wheelpath, geophone under load plate).

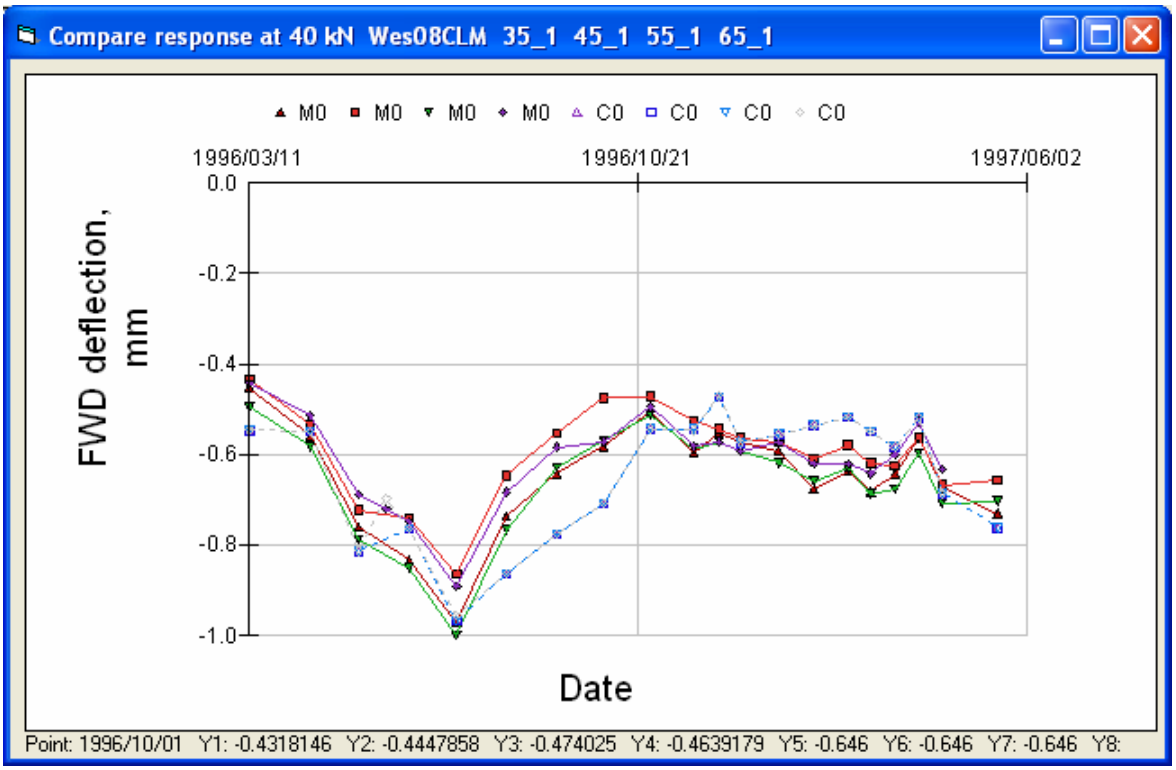

Figure 122. FWD deflections at Section 08 (between wheelpath, geophone under load plate).

During the last part of the experiment the fatigue damage is apparently larger between the wheelpaths than in the wheelpath, for Section 08. The mean difference between measured and calculated deflections between the wheelpaths was -8 µm and the RMS was 80 µm, where the corresponding values for the wheelpath (Table 40) were -55 µm and 107 µm, respectively.

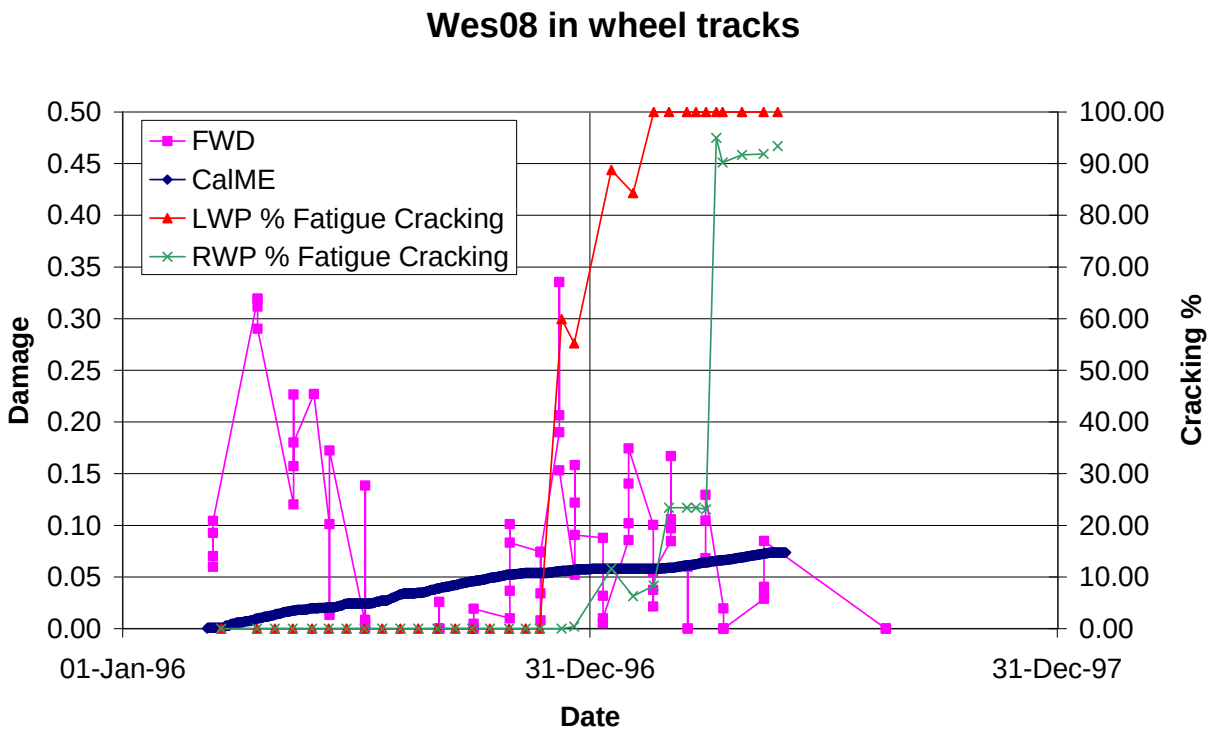

Figure 123. Damage in wheelpath of Section 08 (LWP = left wheelpath, RWP = right wheelpath).

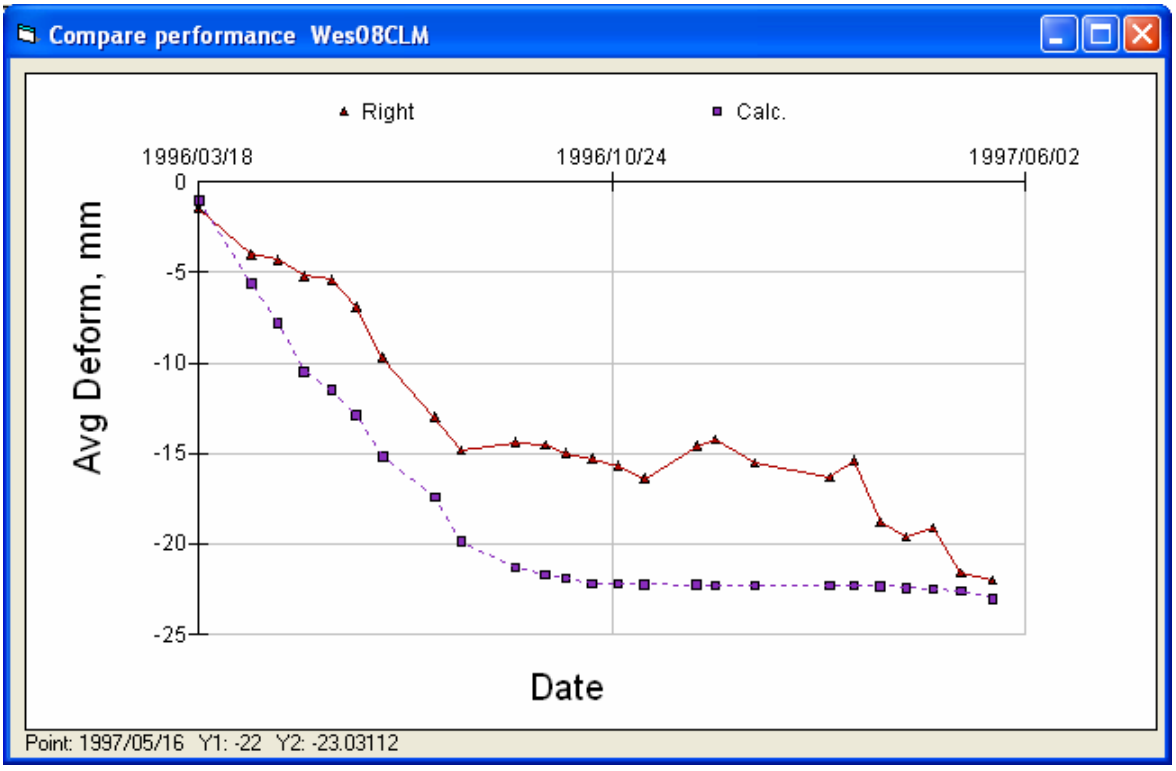

Figure 124. Down rut in right wheelpath at Section 08.

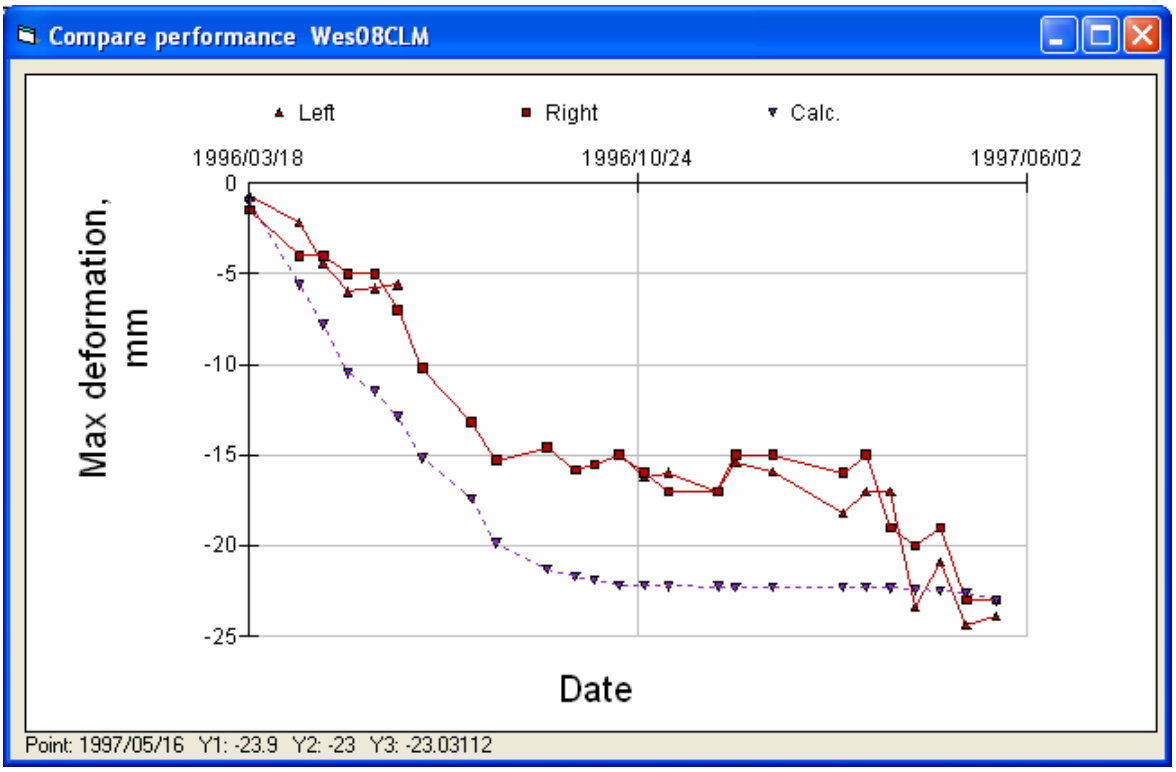

Figure 125. Maximum rutting in left and right wheelpaths at Section 08.

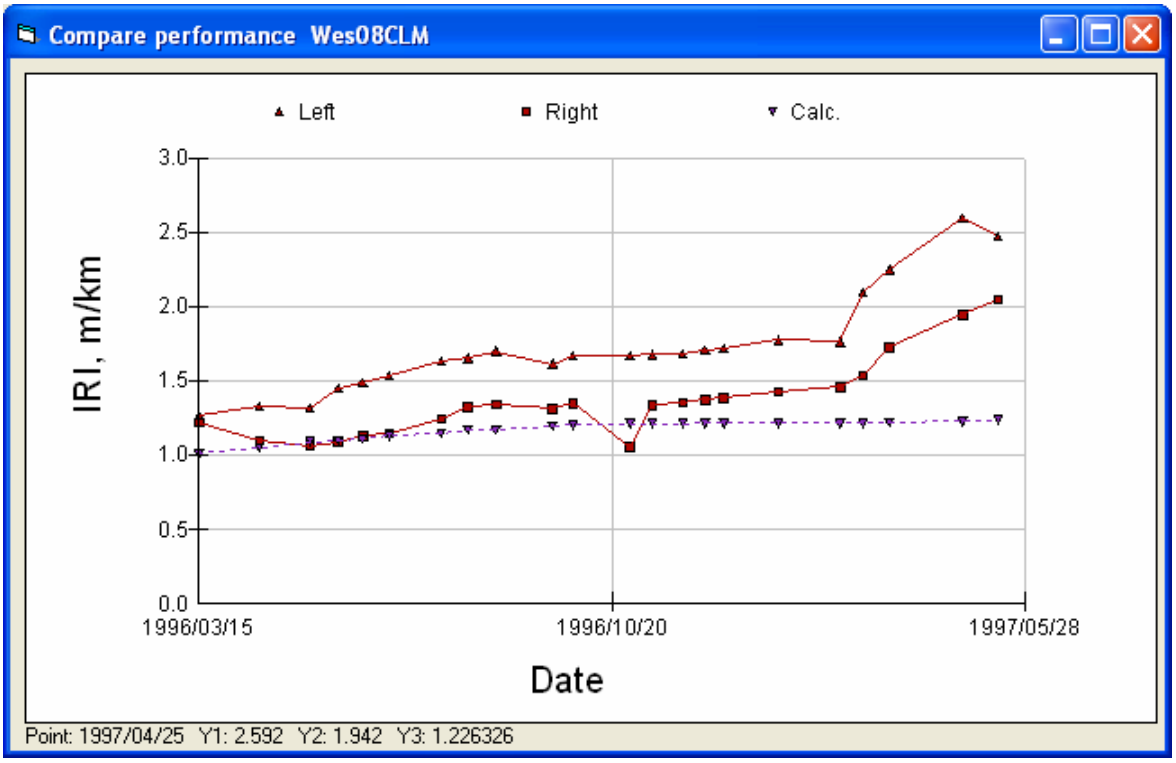

Figure 126. IRI in left and right wheelpaths at Section 08.

3.5.6 Section 23CML

Table 26. Summary of Input Values for Section 23CML

Modulus	*α*	*β*	*γ*	*δ*	*aT*	*A*	*VTS*
AC	2.2041	-0.9786	0.756	2.000	1.300	10.0406	-3.680
Unbound	*Eo*	*Stiffness factor*	*Power on load*	*Estart*			
AB	192 MPa	0.56	0.6	164 MPa			
Subgrade	67 MPa	0	-0.2	67 MPa			
Aging	*AgeA*	*AgeB*					
AC	0	1					
Fatigue	*A*	*α*	*β*	*γ*	*δ*		
AC	0.0289	0.4847	2.6027	1.3013	0.4139		
Rutting	*A*	*α*	*β*	*γ*	*dVoids*		
AC	16.65	0.196	1.03	1	2.1		

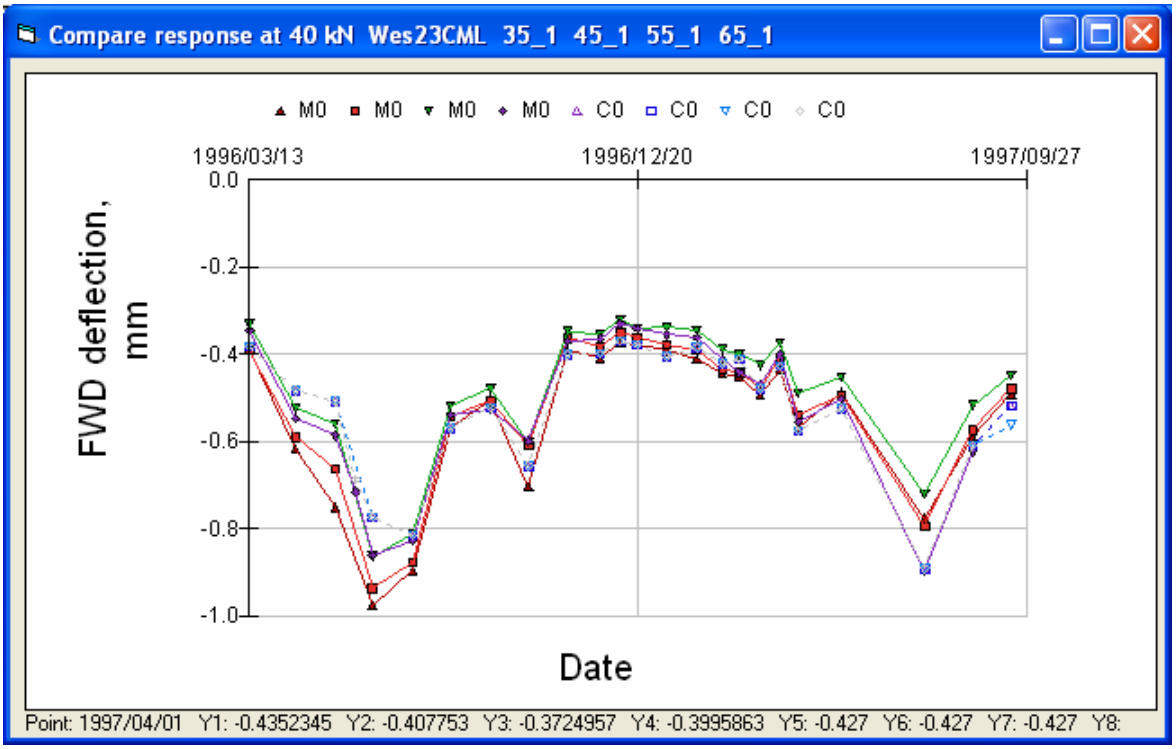

Figure 127. FWD deflections at Section 23 (in wheelpath, geophone under load plate).

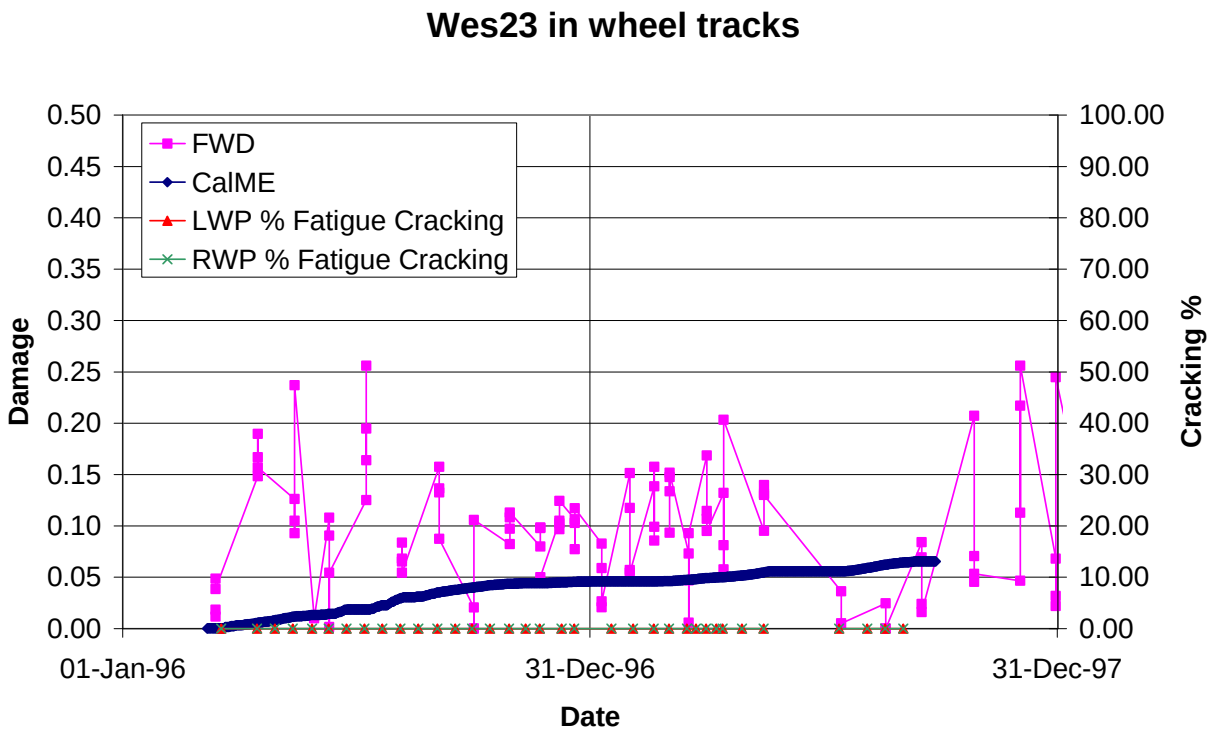

Figure 128. Damage in wheelpath of Section 23 (LWP = left wheelpath, RWP = right wheelpath).

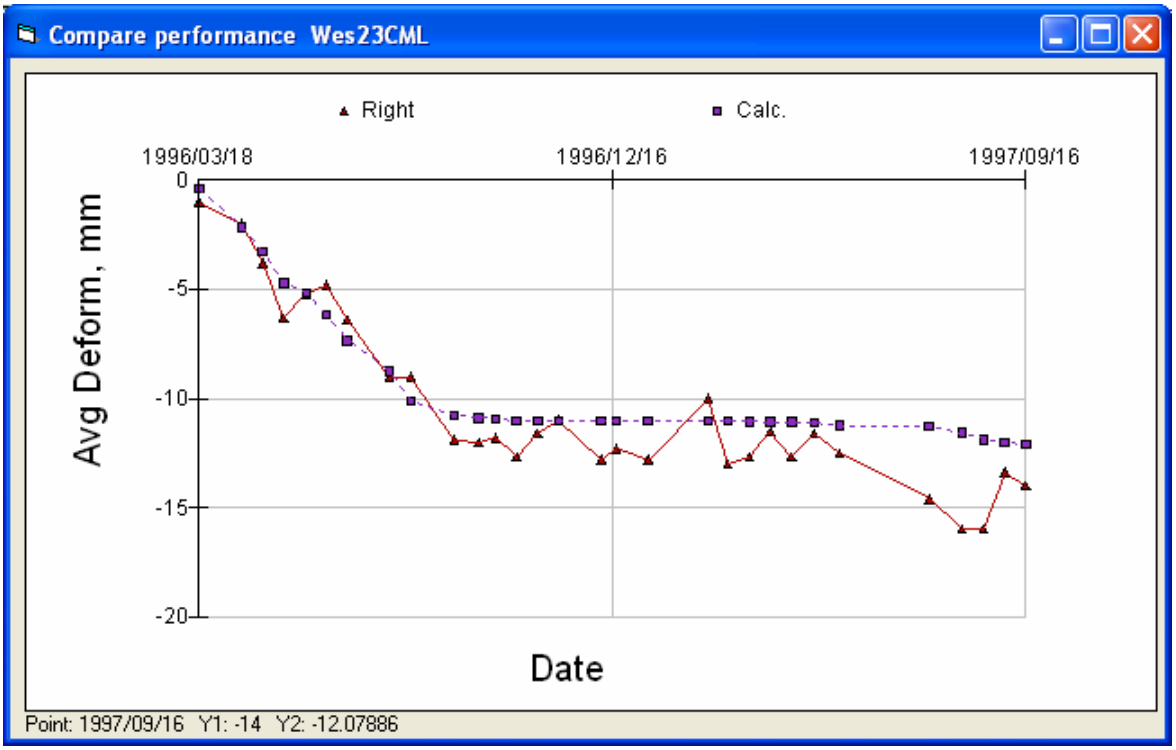

Figure 129. Down rut in right wheelpath at Section 23.

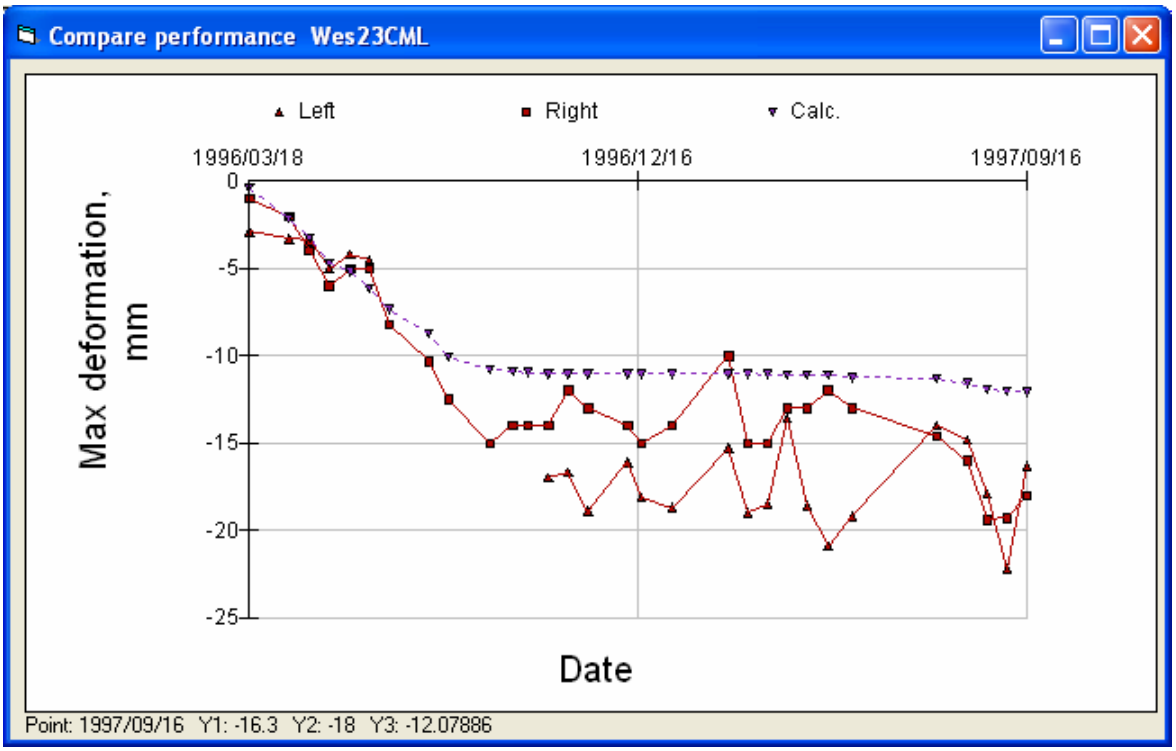

Figure 130. Maximum rutting in left and right wheelpaths at Section 23.

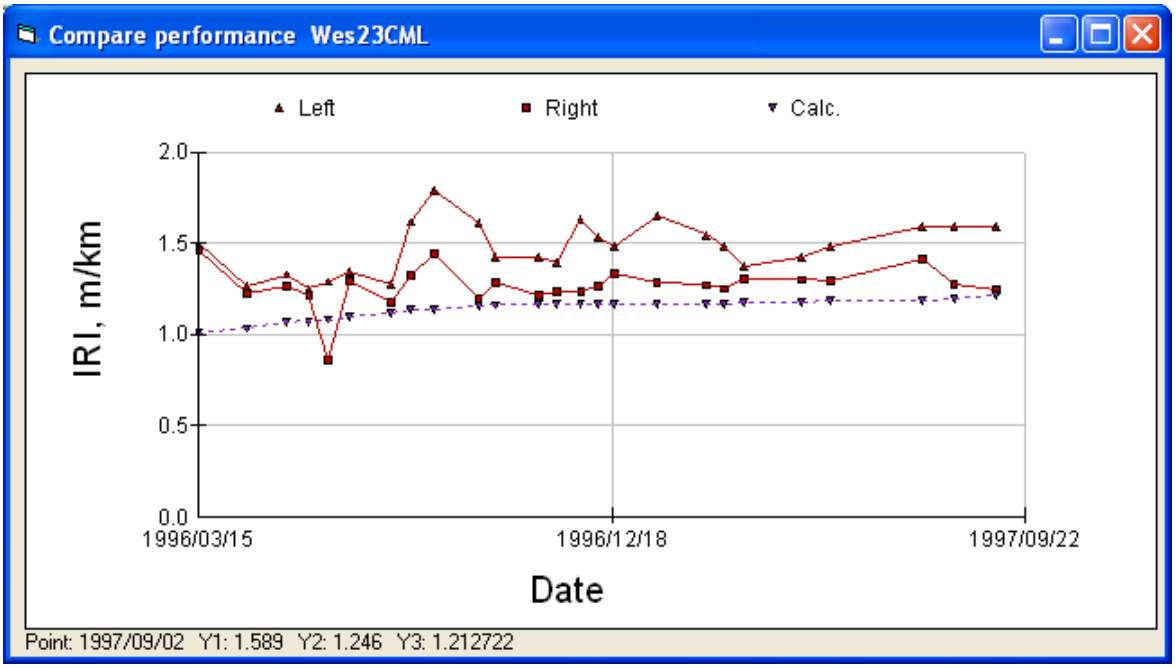

Figure 131. IRI in left and right wheelpaths at Section 23.

3.5.7 Section 24CMM2

Table 27. Summary of Input Values for Section 24CMM2

Modulus	*α*	*β*	*γ*	*δ*	*aT*	*A*	*VTS*
AC	1.9031	-1.2894	0.8059	2.000	1.300	10.0406	-3.680
Unbound	*Eo*	*Stiffness factor*	*Power on load*	*Estart*			
AB	129 MPa	0.45	0.6	112 MPa			
Subgrade	57 MPa	0	-0.2	57 MPa			
Aging	*AgeA*	*AgeB*					
AC	0.1181	0.3034					
Fatigue	*A*	*α*	*β*	*γ*	*δ*		
AC	0.0354	0.6175	3.8604	1.9302	0.5273		
Rutting	*A*	*α*	*β*	*γ*	*dVoids*		
AC					3.0		

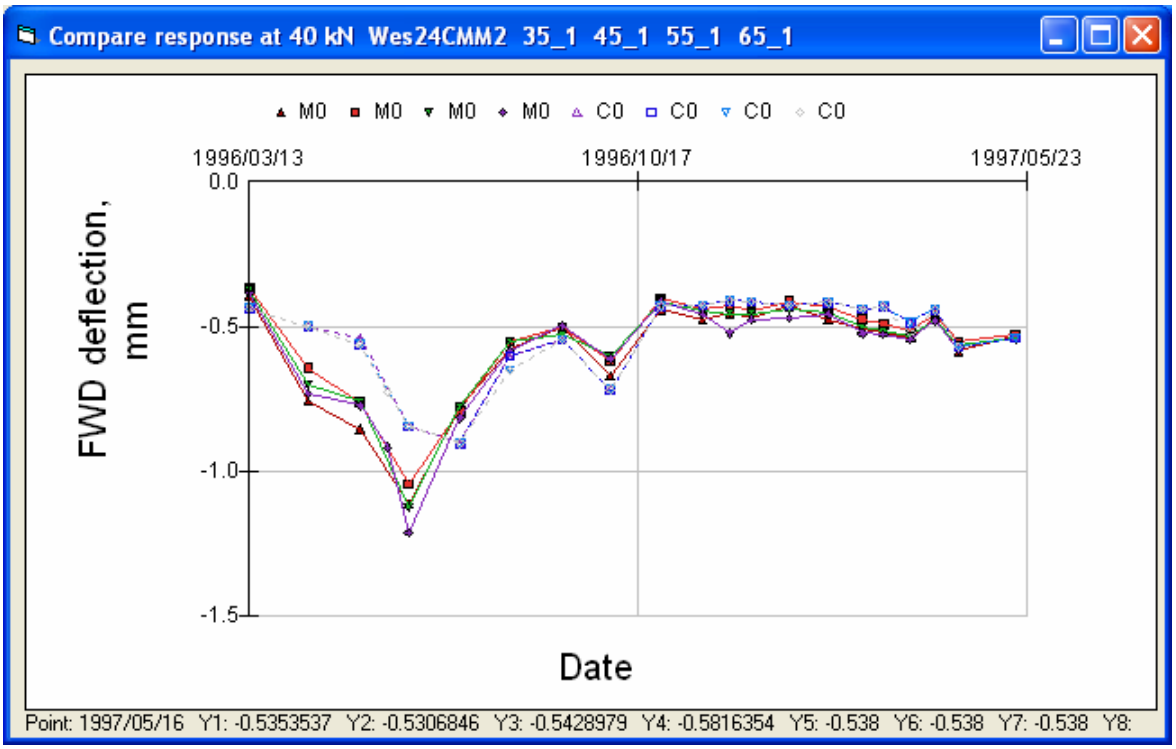

Figure 132. FWD deflections at Section 24 (in wheelpath, geophone under load plate).

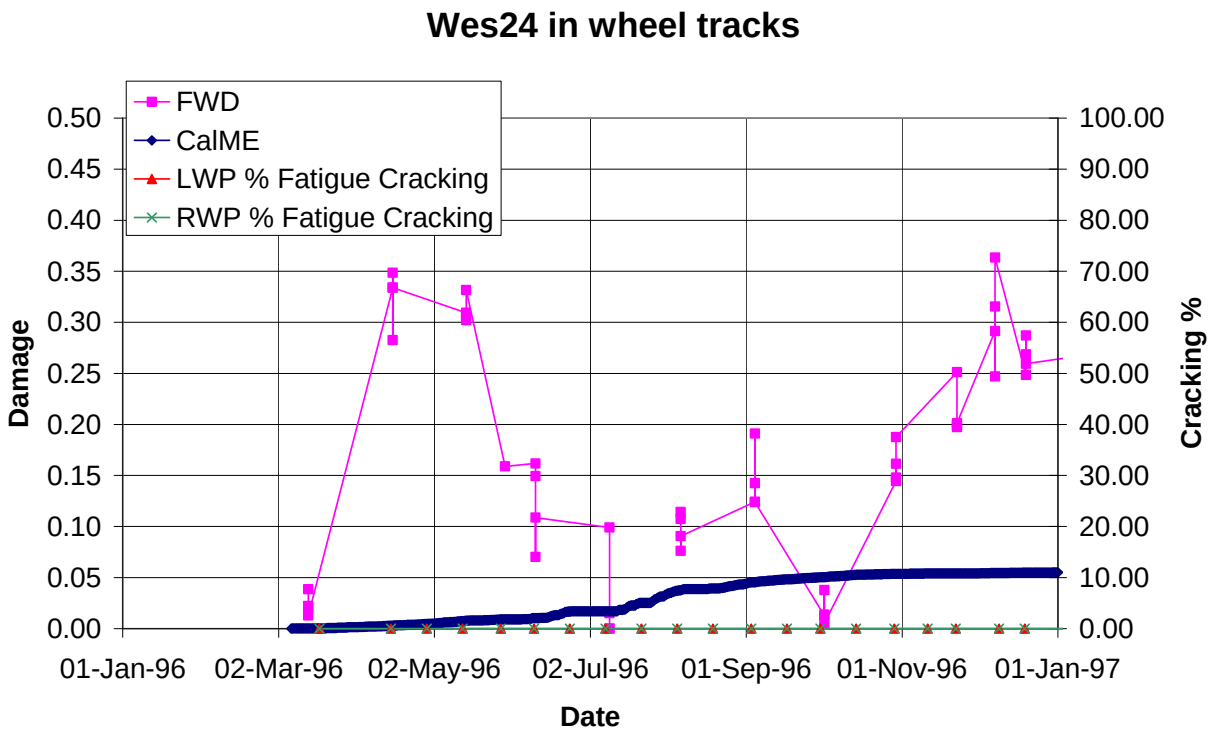

Figure 133. Damage in wheelpath of Section 24 (LWP = left wheelpath, RWP = right wheelpath).

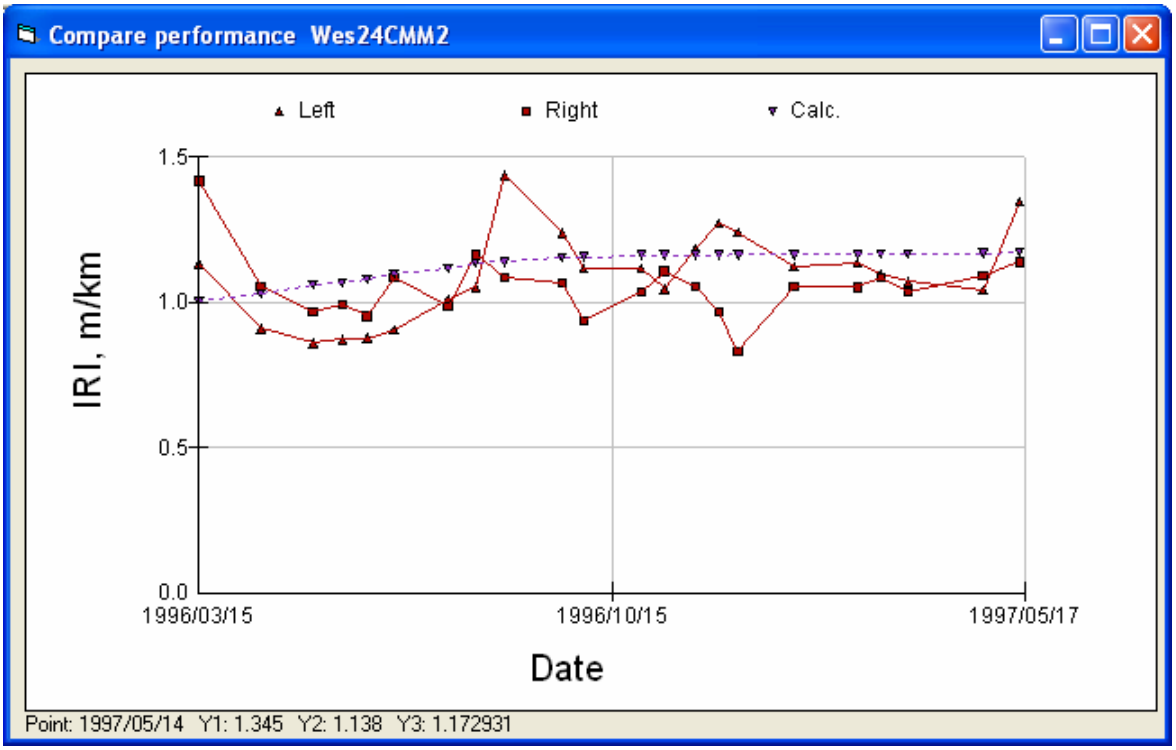

Figure 134. IRI in left and right wheelpaths at Section 24.

3.5.8 Section 25CHL

Table 28. Summary of Input Values for Section 25CHL

Modulus	*α*	*β*	*γ*	*δ*	*aT*	*A*	*VTS*
AC	2.0000	-1.2894	0.8059	2.000	1.300	10.0406	-3.680
Unbound	*Eo*	*Stiffness factor*	*Power on load*	*Estart*			
AB	204 MPa	0.43	0.6	173 MPa			
Subgrade	76 MPa	0	-0.2	76 MPa			
Aging	*AgeA*	*AgeB*					
AC	0.3033	-0.7892					
Fatigue	*A*	*α*	*β*	*γ*	*δ*		
AC	0.0821	0.3367	1.2840	0.6420	0.2876		
Rutting	*A*	*α*	*β*	*γ*	*dVoids*		
AC	64.89	0.275	1.03	1	1.5		

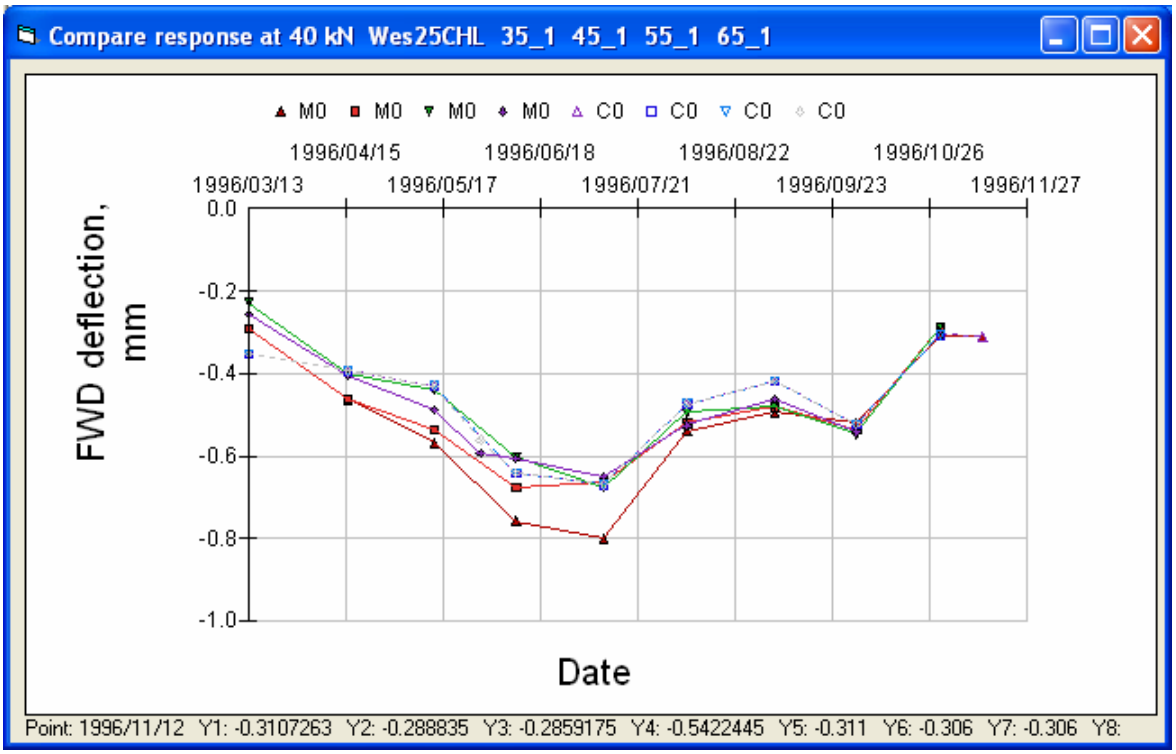

Figure 135. FWD deflections at Section 25 (in wheelpath, geophone under load plate).

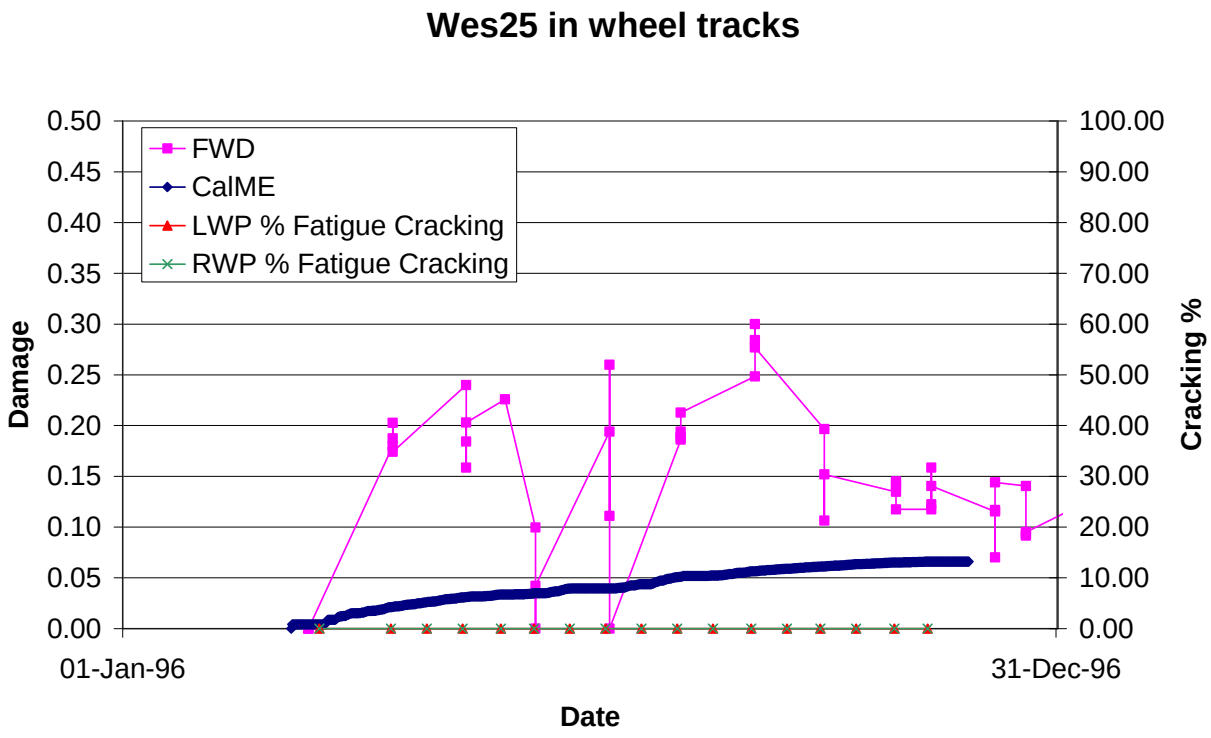

Figure 136. Damage in wheelpath of Section 25 (LWP = left wheelpath, RWP = right wheelpath).

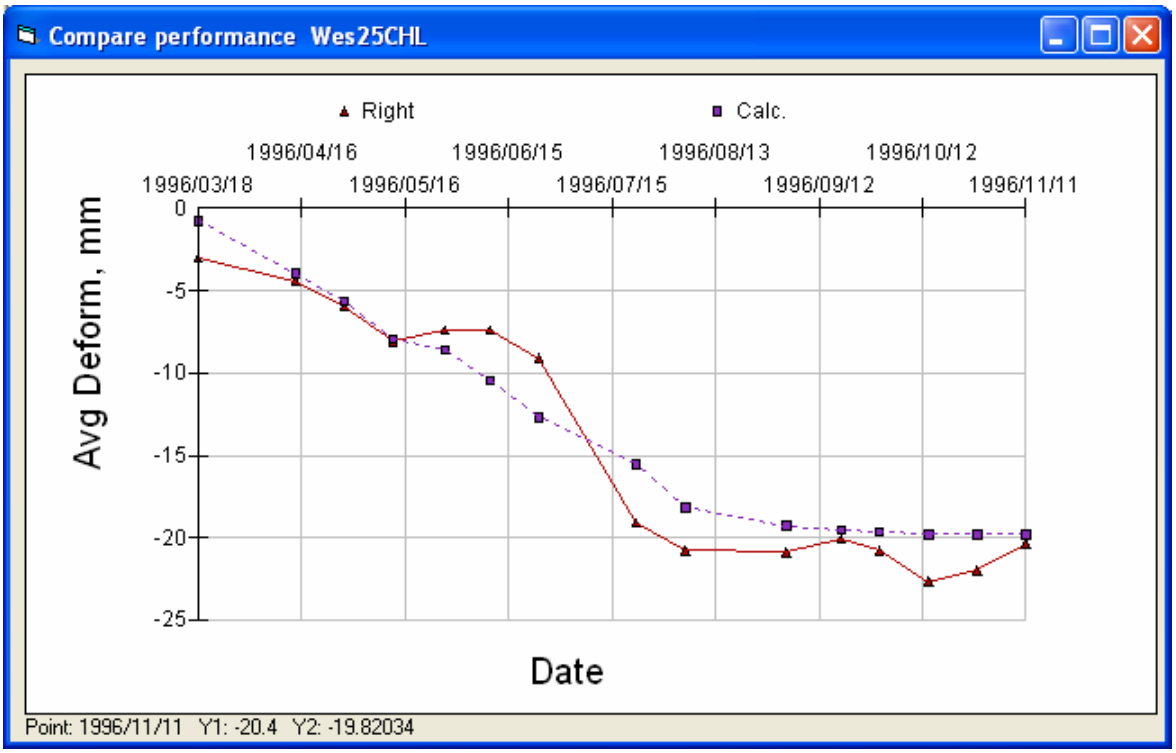

Figure 137. Down rut in right wheelpath at Section 25.

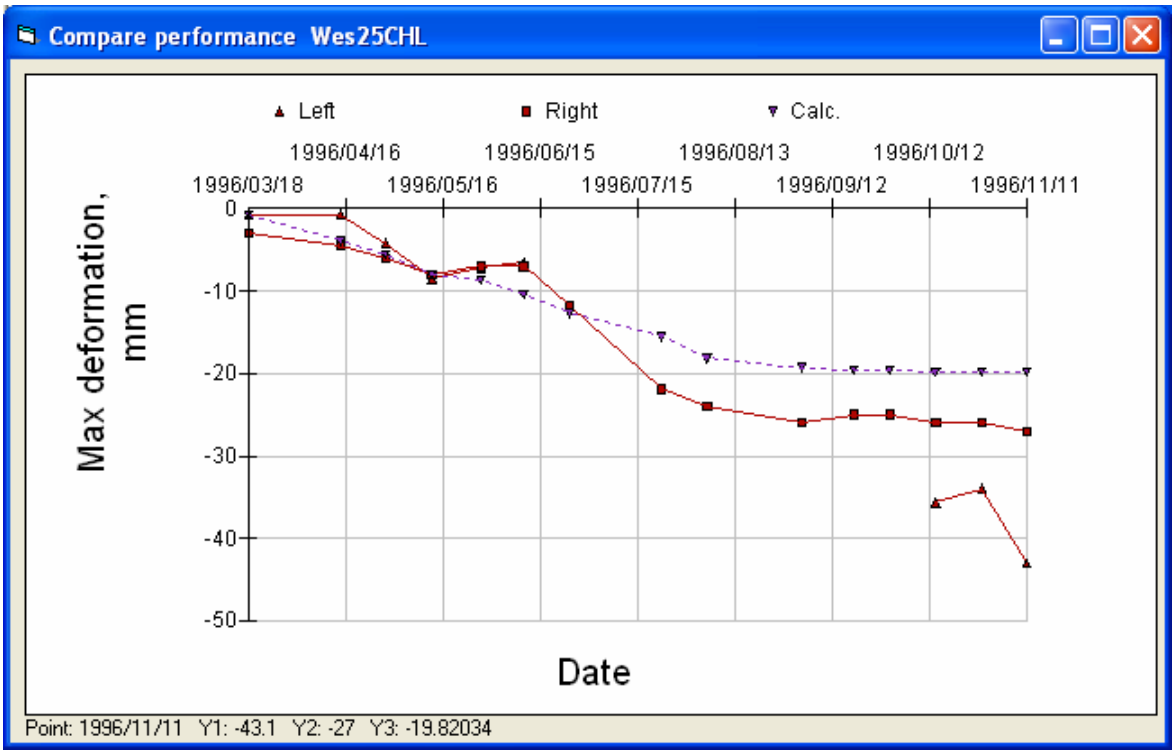

Figure 138. Maximum rutting in left and right wheelpaths at Section 25.

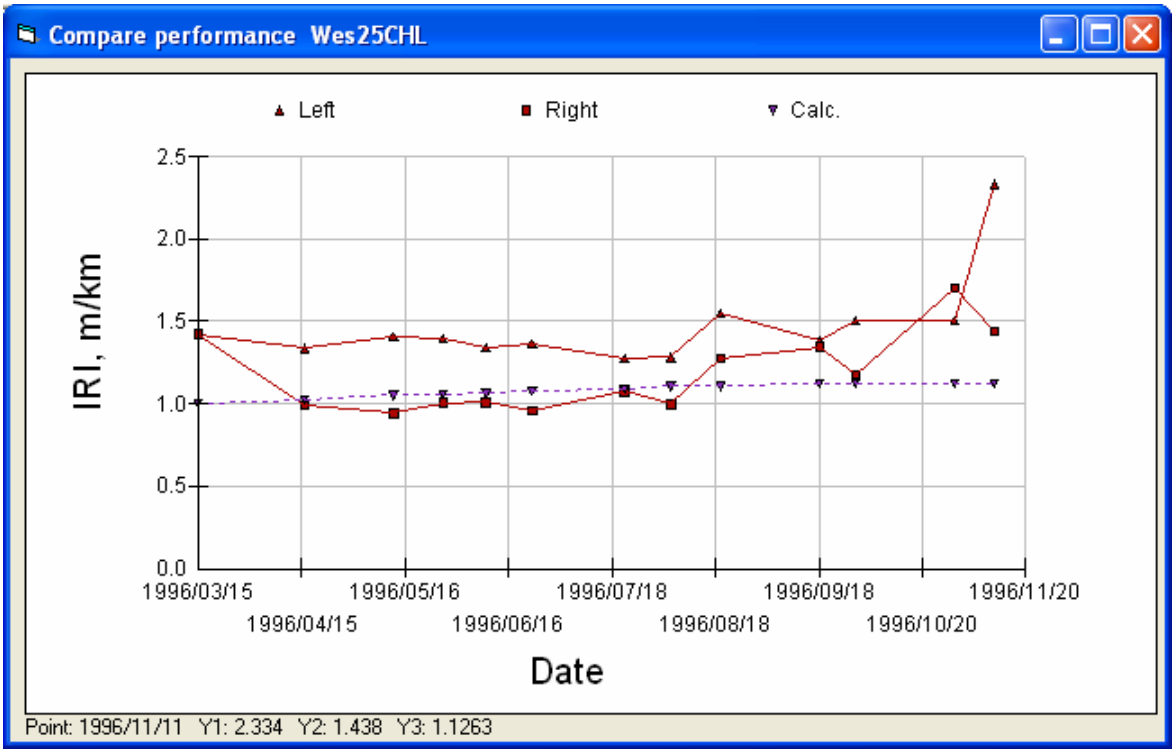

Figure 139. IRI in left and right wheelpaths at Section 25.

3.5.9 Section 26CLH

Table 29. Summary of Input Values for Section 26CLH

Modulus	*α*	*β*	*γ*	*δ*	*aT*	*A*	*VTS*
AC	1.6990	-1.2434	0.6908	2.000	1.300	10.0406	-3.680
Unbound	*Eo*	*Stiffness factor*	*Power on load*	*Estart*			
AB	106 MPa	0.17	0.6	95 MPa			
Subgrade	56 MPa	0	-0.2	56 MPa			
Aging	*AgeA*	*AgeB*					
AC	0.1962	-0.1573					
Fatigue	*A*	*α*	*β*	*γ*	*δ*		
AC	0.1202	0.5818	3.1148	1.5574	0.4968		
Rutting	*A*	*α*	*β*	*γ*	*dVoids*		
AC					4.3		

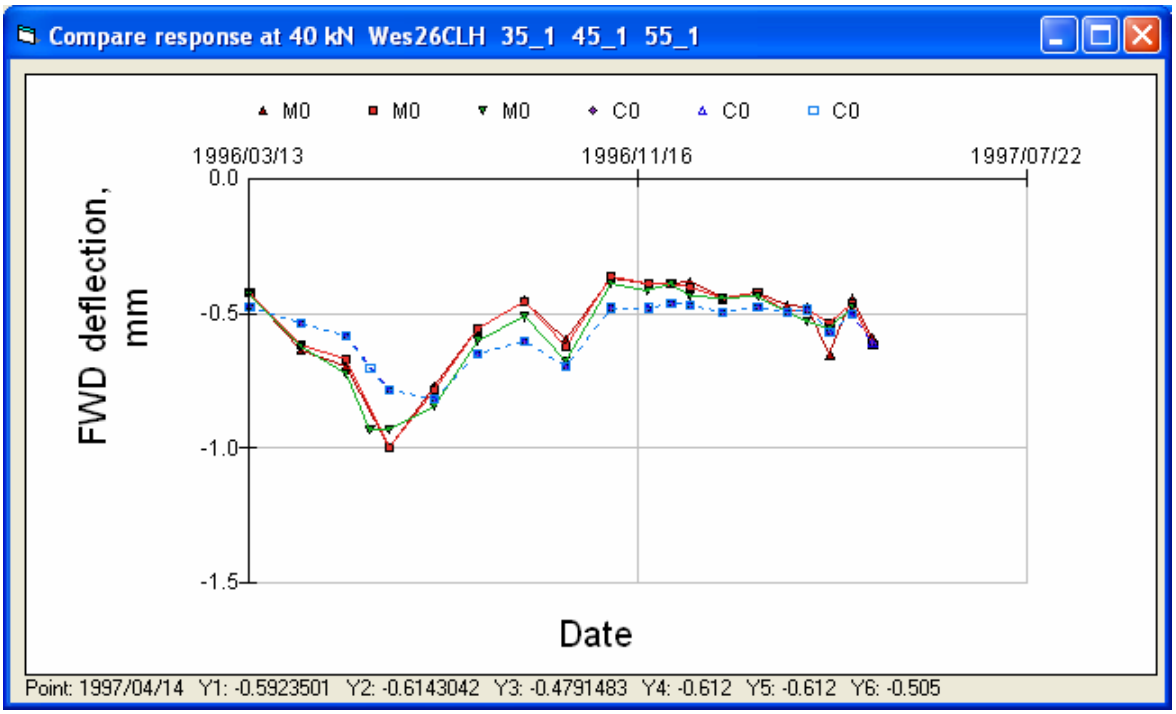

Figure 140. FWD deflections at Section 26 (in wheelpath, geophone under load plate).

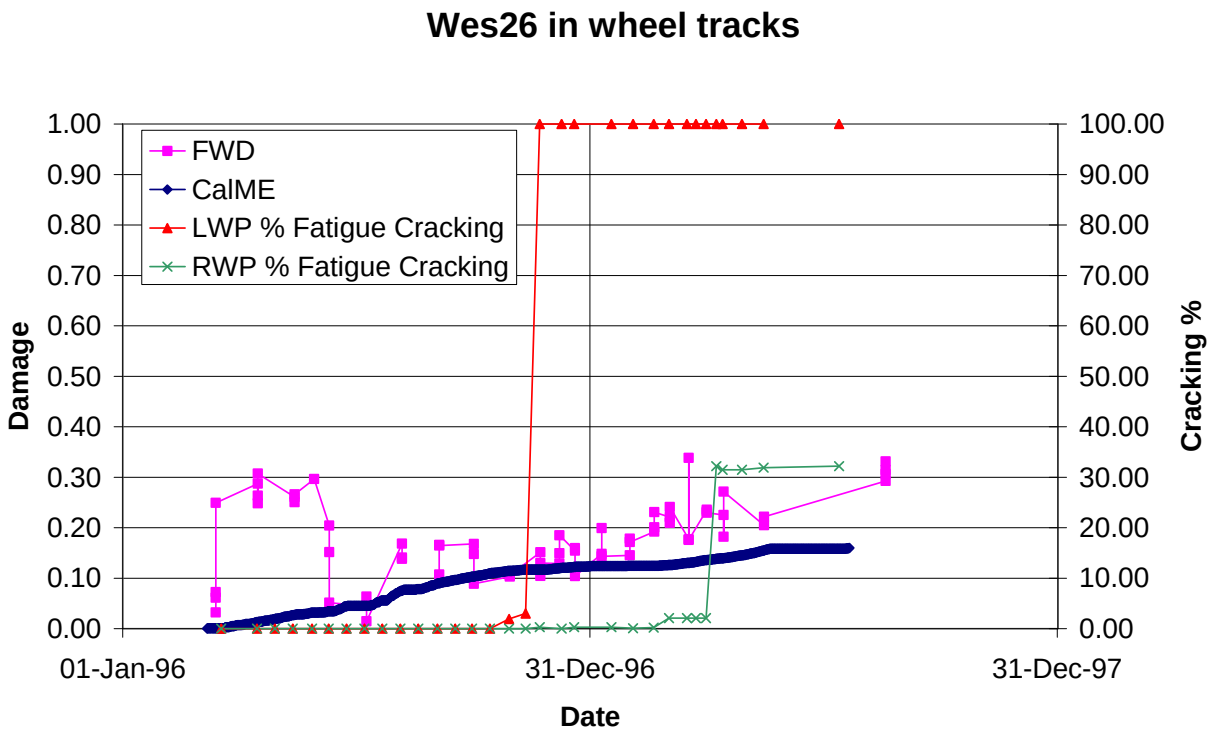

Figure 141. Damage in wheelpath of Section 26 (LWP = left wheelpath, RWP = right wheelpath).

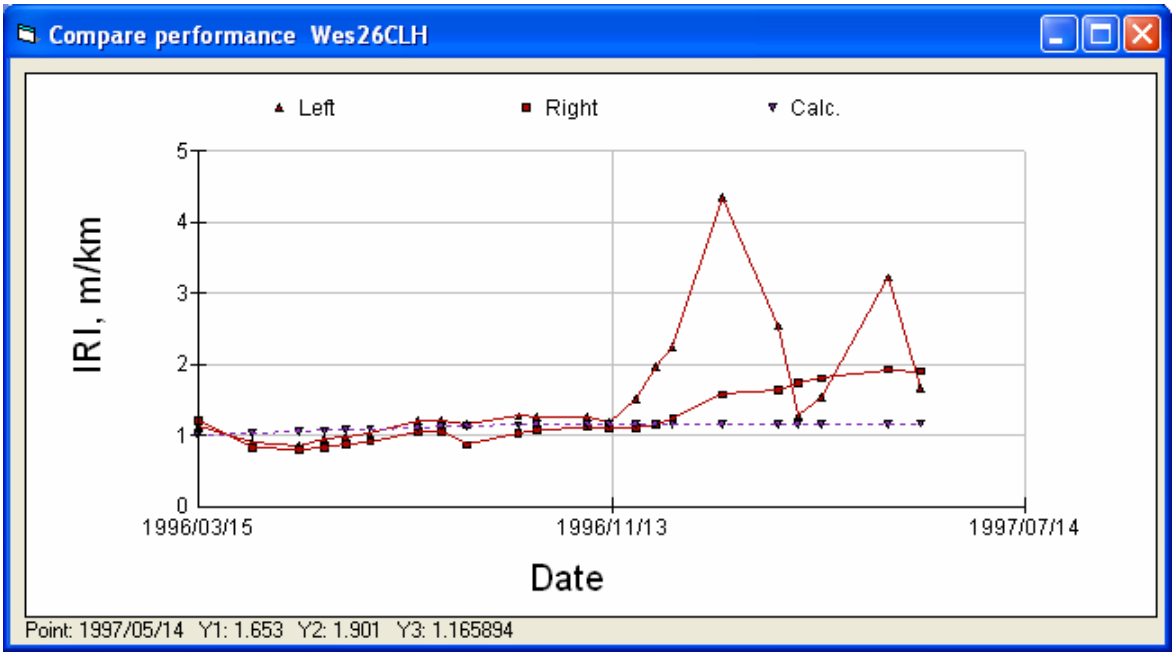

Figure 142. IRI in left and right wheelpaths at Section 26.

3.6 Fine Plus Mix Sections

3.6.1 Notes on Simulations of Fine Plus Mix Sections

For each of the WesTrack sections simulated, a table shows the input values in the *CalME* database used for the simulation of that section, followed by plots comparing measured and calculated FWD deflections, damage and fatigue cracking, rutting, and IRI.

Development of input values, analysis, and plotting of results for the Fine Plus sections is the same as for the Fine and Coarse mixes.

Indirect tensile tests performed by the University of Nevada, Reno, showed a considerable increase in modulus over time, as shown in Figure 143.

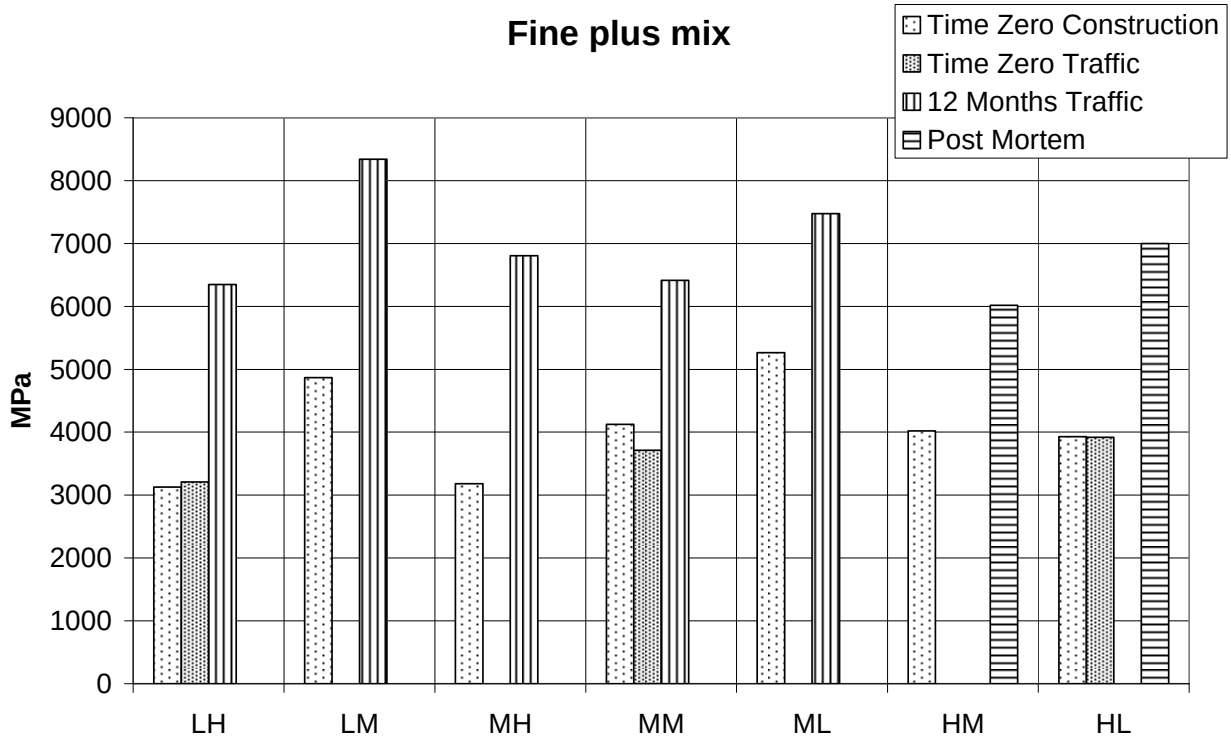

Figure 143. Mean Resilient Moduli of Fine Plus mix, at different points in time.

The increase in modulus over time was confirmed by RSST-CH tests done on the untrafficked mix and Post Mortem as shown in Table 30, where Gpm is the shear modulus from the test on the post-mortem core and Go is from the core taken before trafficking.

Table 30. Hardening from Shear Tests, Fine Plus Mix

Mix	Gpm/Go
LH	2.65
LM	1.62
MH	1.80
MM	2.24
ML	1.12
HM	NA
HL	NA

Post mortem tests were not done for the Fine Plus mixes with a high binder content as they failed within the first year of the experiment. These are sections 09PHL2, 13PHM, and 21PHL1.

3.6.2 Section 09PHL2

Table 31. Summary of Input Values for Section 09PHL2

Modulus	*α*	*β*	*γ*	*δ*	*aT*	*A*	*VTS*
AC	2.0000	-1.2434	0.8059	2.000	1.300	10.0406	-3.680
Unbound	*Eo*	*Stiffness factor*	*Power on load*	*Estart*			
AB	245 MPa	0.41	0.6	150 MPa			
Subgrade	68 MPa	0	-0.2	68 MPa			
Aging	*AgeA*	*AgeB*					
AC	0.1752	-0.0339					
Fatigue	*A*	*α*	*β*	*γ*	*δ*		
AC	0.0530	0.4899	2.4289	1.2144	0.4184		
Rutting	*A*	*α*	*β*	*γ*	*dVoids*		
AC					1.2		

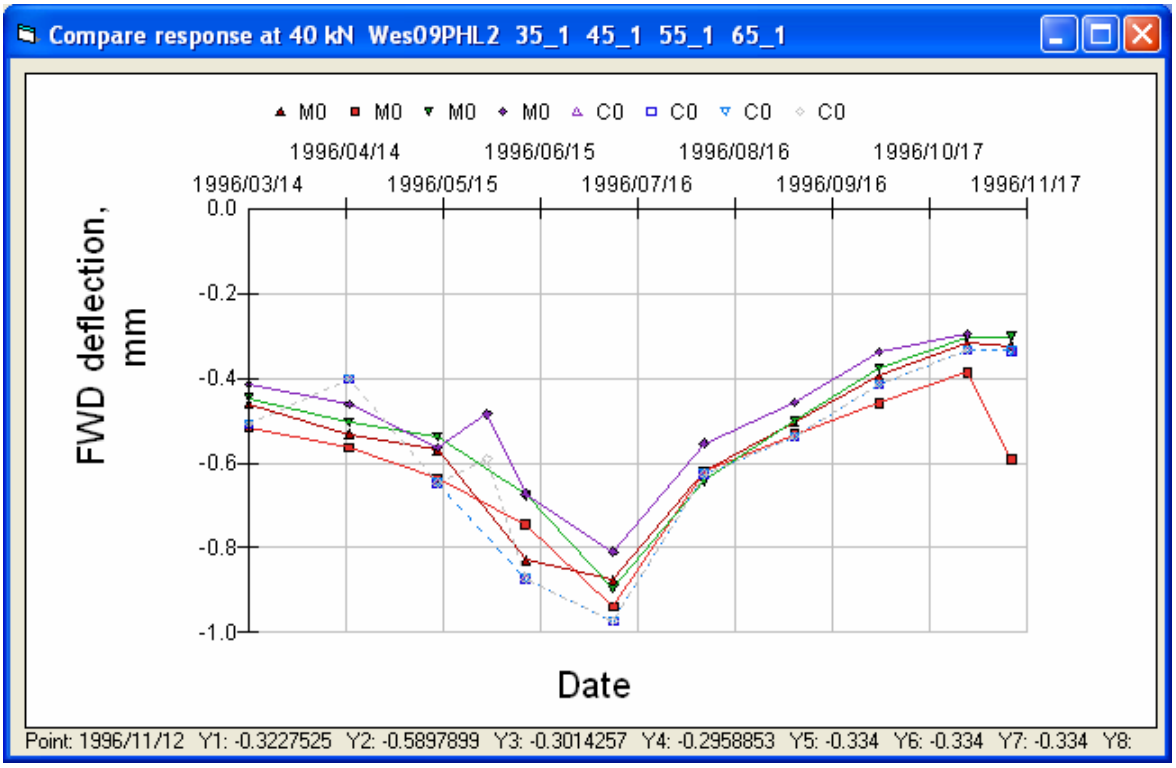

Figure 144. FWD deflections at Section 09 (in wheelpath, geophone under load plate).

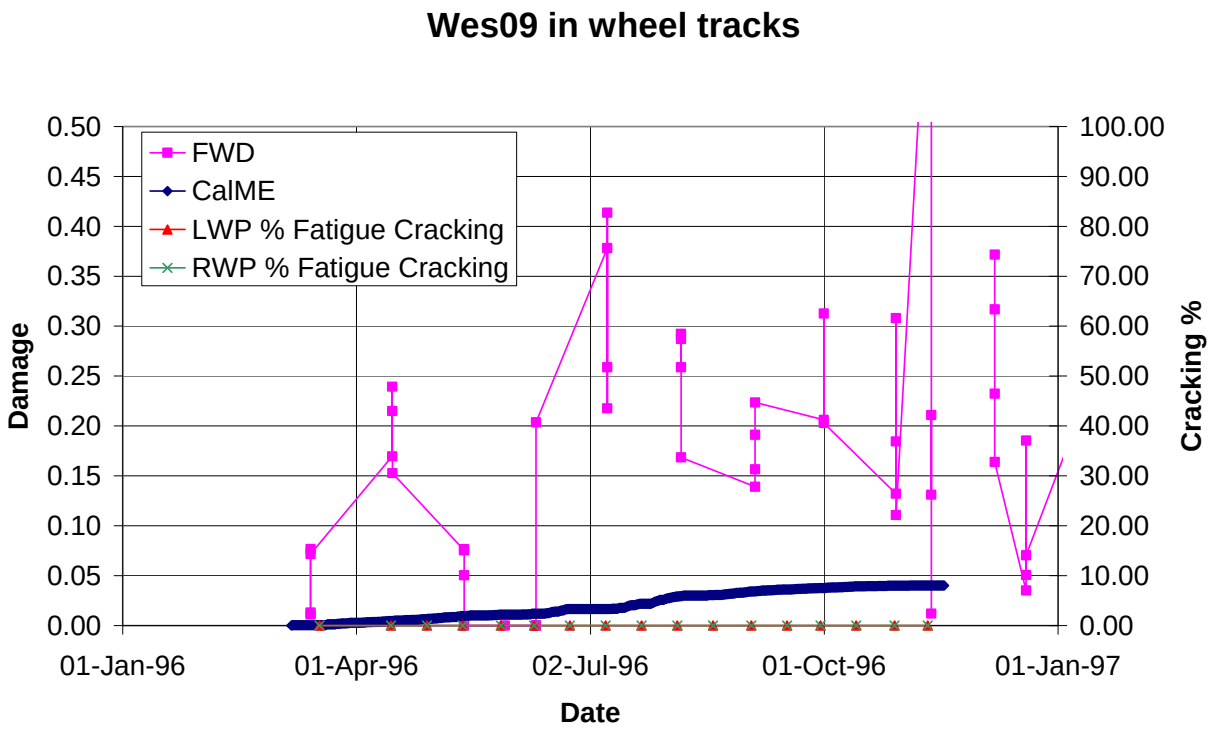

Figure 145. Damage in wheelpath of Section 09 (LWP = left wheelpath, RWP = right wheelpath).

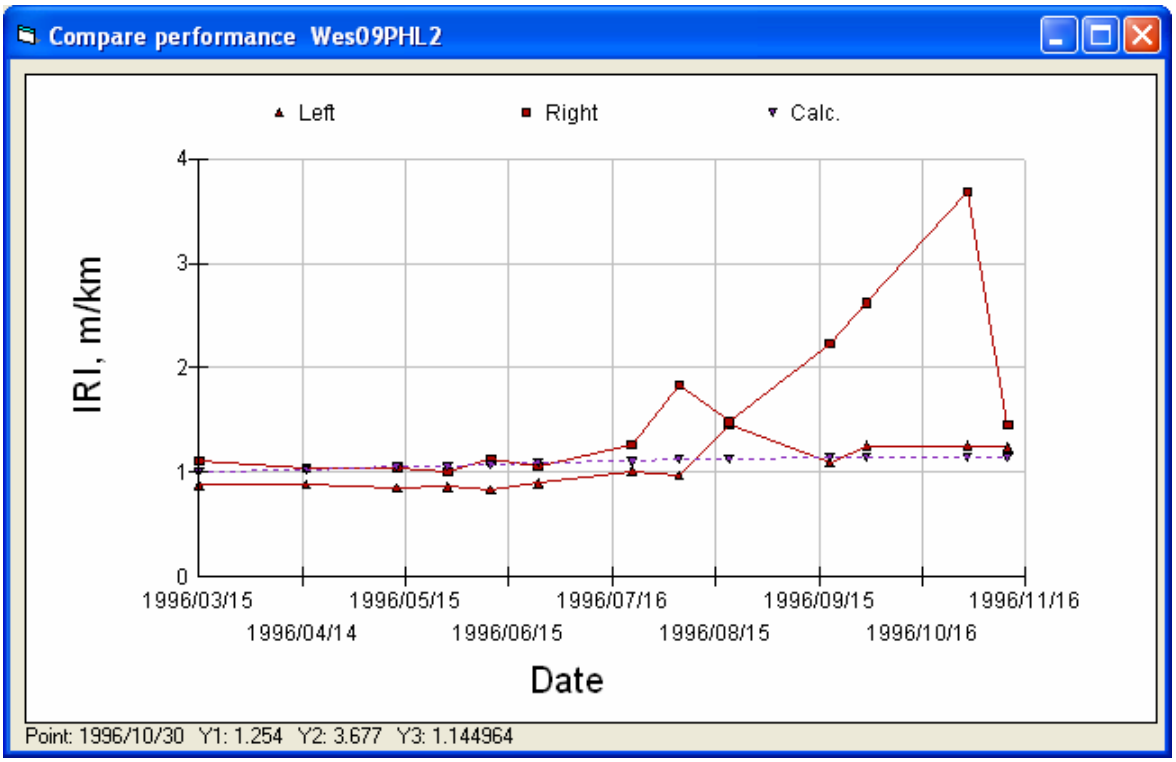

Figure 146. IRI in left and right wheelpaths at Section 09.

3.6.3 Section 10PLH

Table 32. Summary of Input Values for Section 10PLH

Modulus	*α*	*β*	*γ*	*δ*	*aT*	*A*	*VTS*
AC	1.6990	-1.2089	0.8059	2.000	1.300	10.0406	-3.680
Unbound	*Eo*	*Stiffness factor*	*Power on load*	*Estart*			
AB	230 MPa	0.43	0.6	178 MPa			
Subgrade	70 MPa	0	-0.2	70 MPa			
Aging	*AgeA*	*AgeB*					
AC	0.3074	-0.8158					
Fatigue	*A*	*α*	*β*	*γ*	*δ*		
AC	0.4675	0.4886	1.7461	0.8731	0.4172		
Rutting	*A*	*α*	*β*	*γ*	*dVoids*		
AC	10.89	0.1116	1.03	1	4.4		

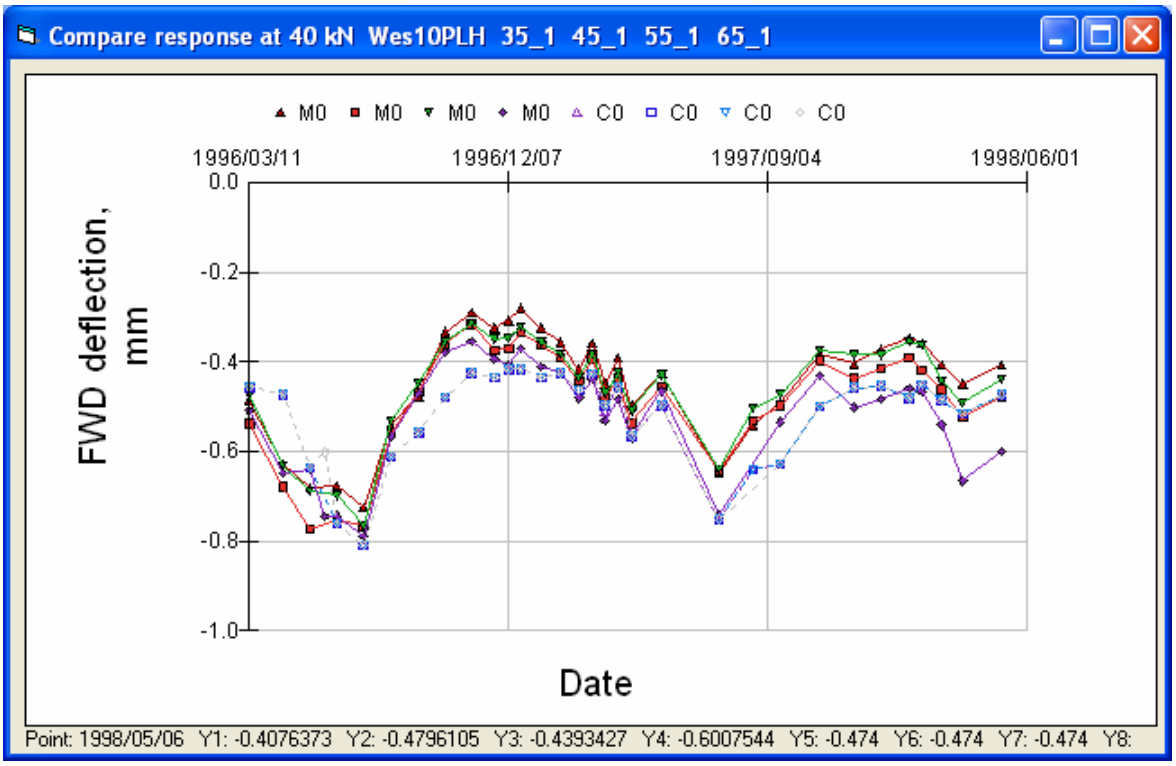

Figure 147. FWD deflections at Section 10 (in wheelpath, geophone under load plate).

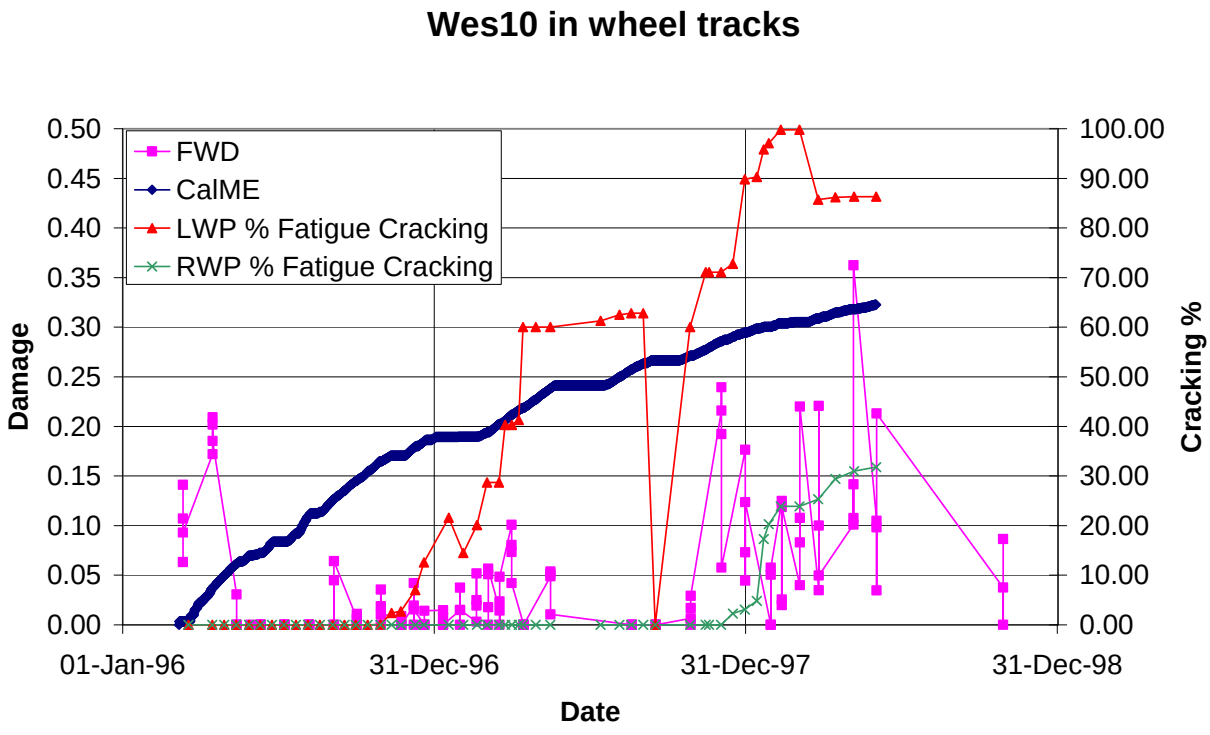

Figure 148. Damage in wheelpath of Section 10 (LWP = left wheelpath, RWP = right wheelpath).

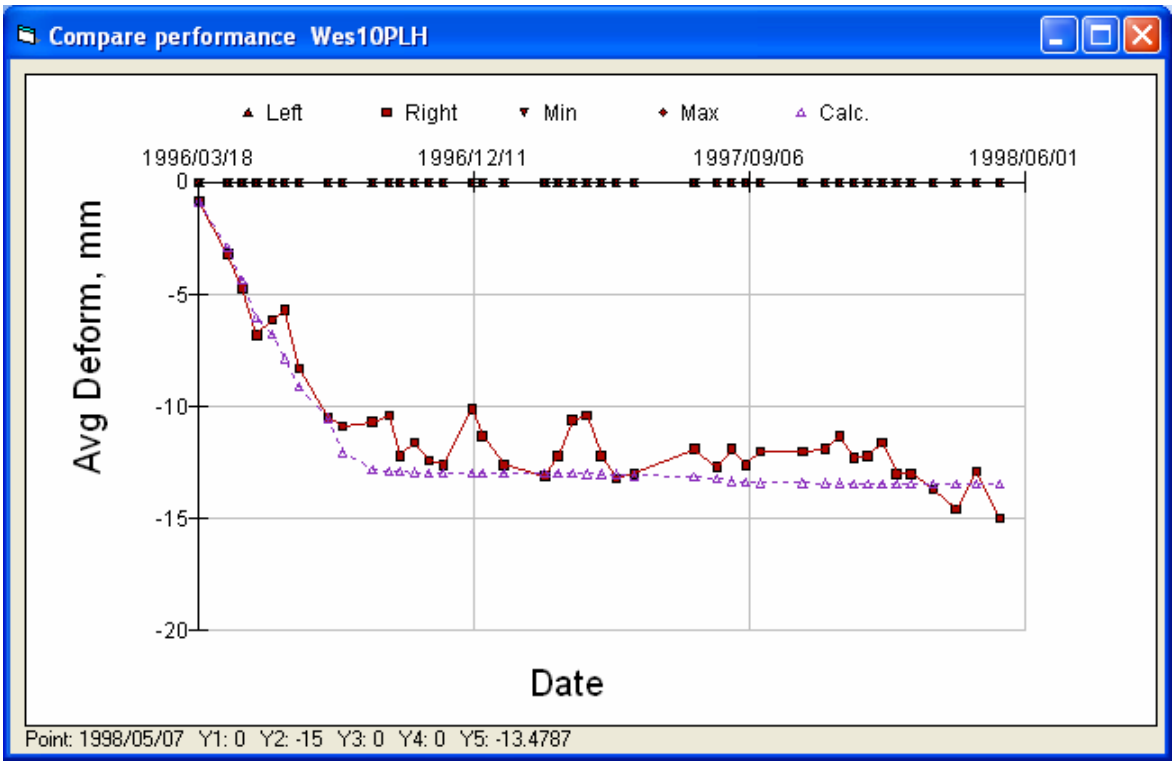

Figure 149. Down rut in right wheelpath at Section 10.

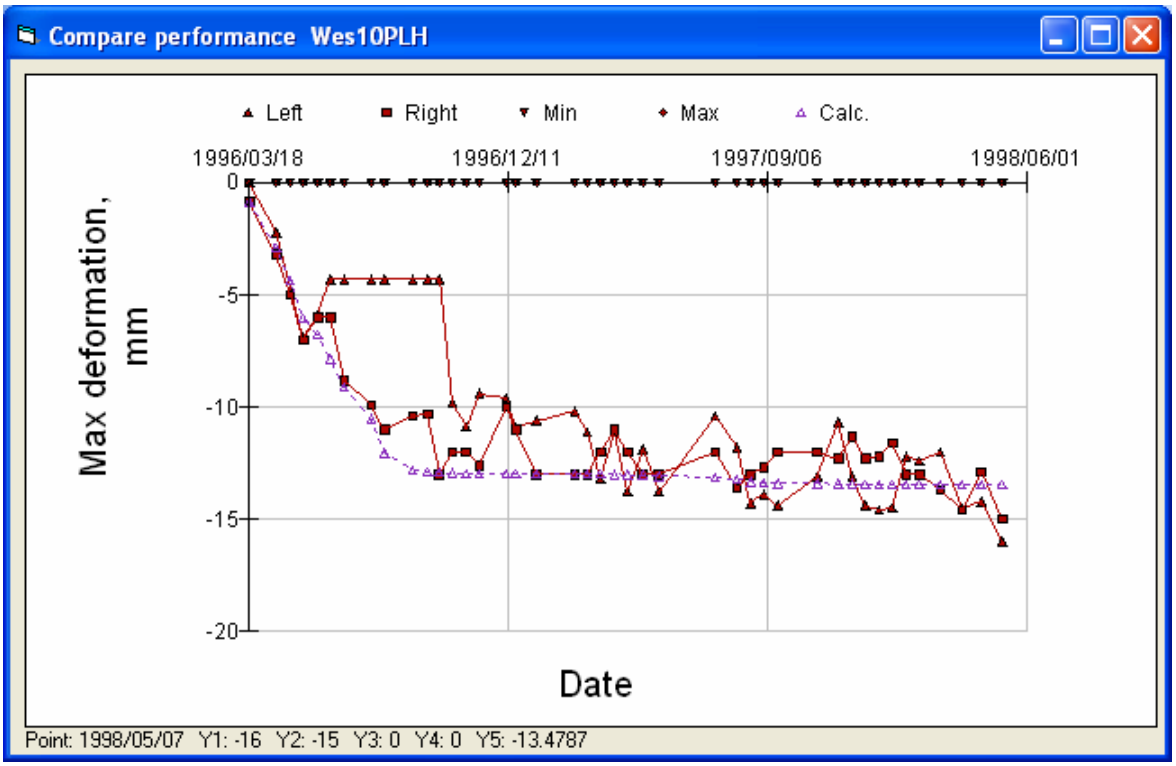

Figure 150. Maximum rutting in left and right wheelpaths at Section 10.

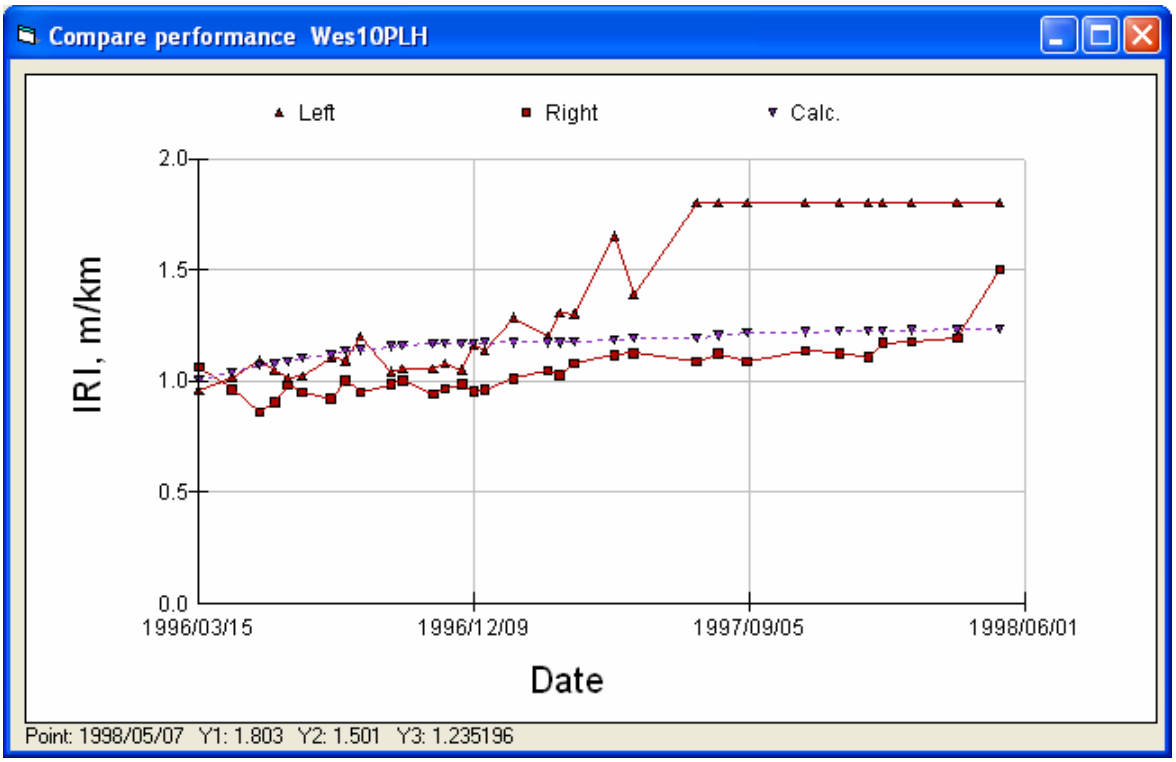

Figure 151. IRI in left and right wheelpaths at Section 10.

3.6.4 Section 11PMM2

Table 33. Summary of Input Values for Section 11PMM2

Modulus	*α*	*β*	*γ*	*δ*	*aT*	*A*	*VTS*
AC	2.0414	-0.9210	0.4605	2.000	1.300	10.0406	-3.680
Unbound	*Eo*	*Stiffness factor*	*Power on load*	*Estart*			
AB	328 MPa	0.61	0.6	170 MPa			
Subgrade	79 MPa	0	-0.2	79 MPa			
Aging	*AgeA*	*AgeB*					
AC	0.2008	-0.1848					
Fatigue	*A*	*α*	*β*	*γ*	*δ*		
AC	0.0987	0.5406	2.4804	1.2404	0.4616		
Rutting	*A*	*α*	*β*	*γ*	*dVoids*		
AC	6.4202	0.1383	1.03	1	2.7		

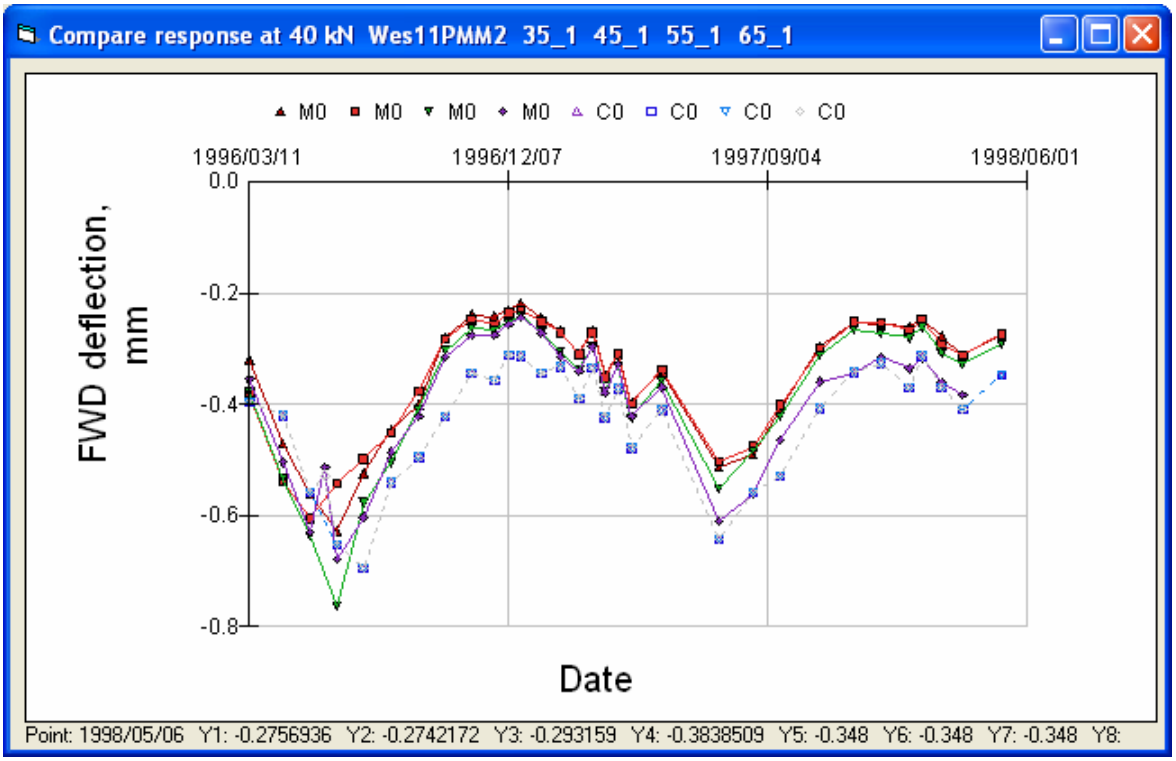

Figure 152. FWD deflections at Section 11 (in wheelpath, geophone under load plate).

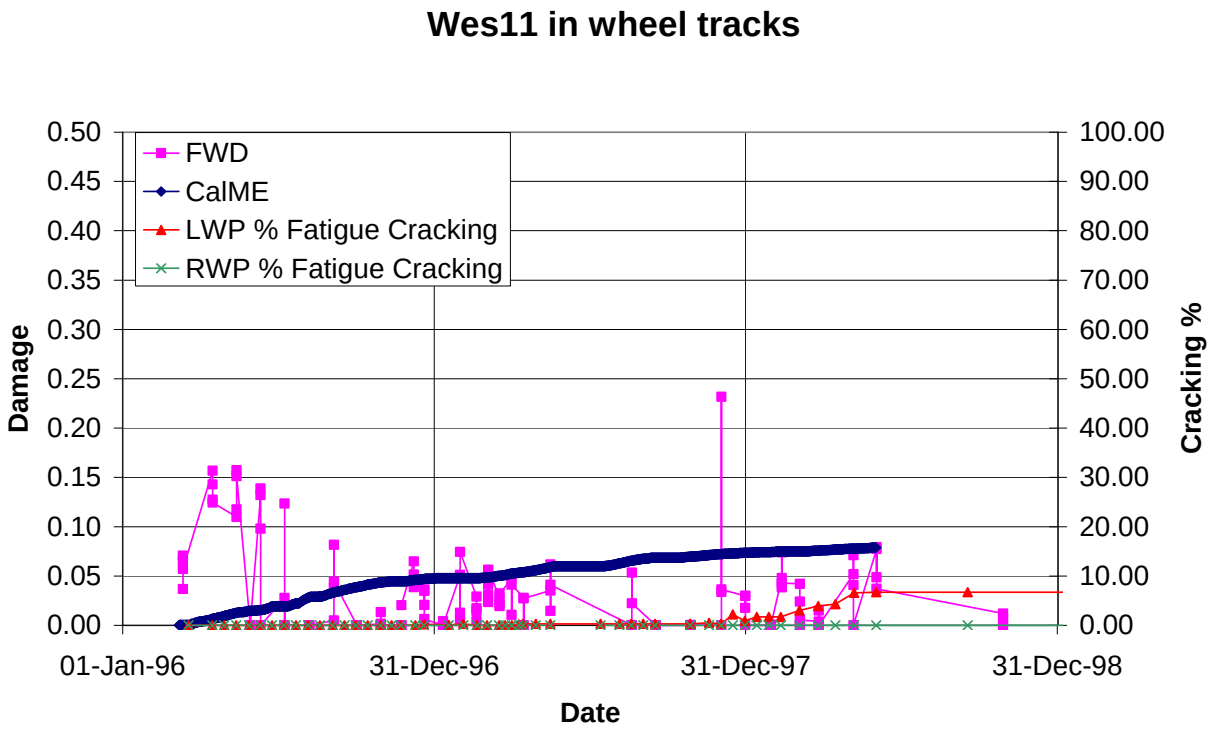

Figure 153. Damage in wheelpath of Section 11 (LWP = left wheelpath, RWP = right wheelpath).

Figure 154. Down rut in right wheelpath at Section 11.

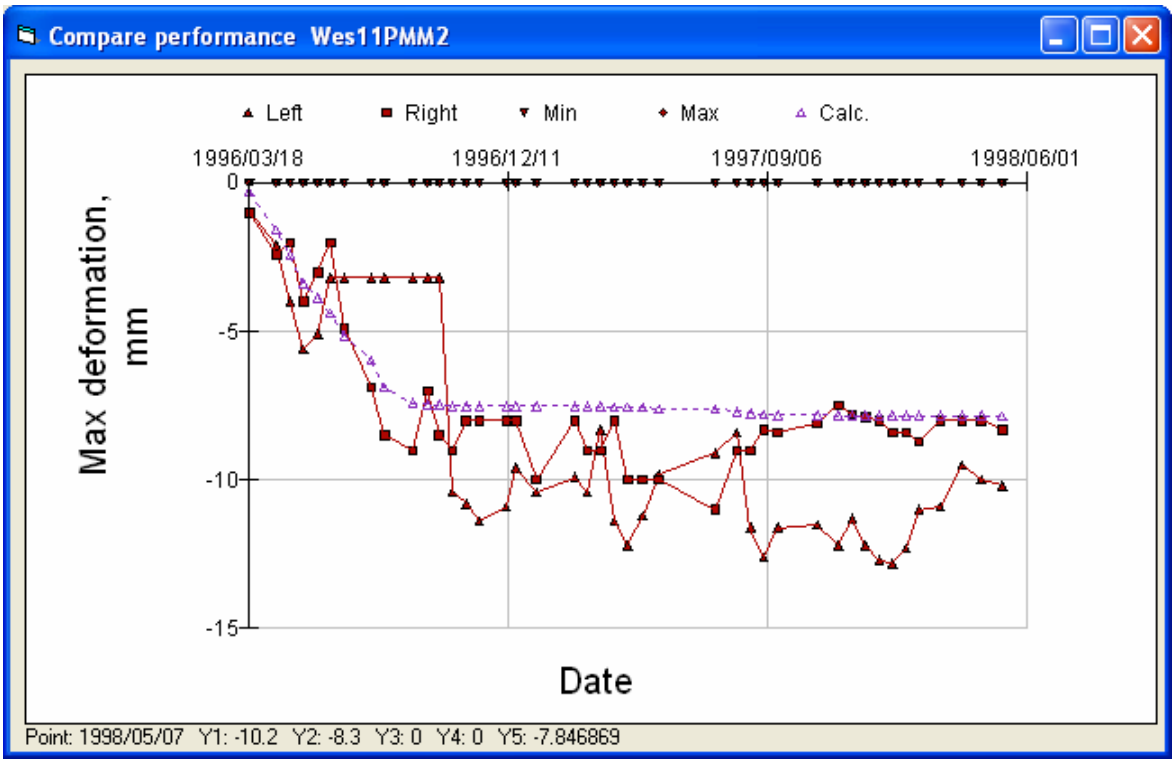

Figure 155. Maximum rutting in left and right wheelpaths at Section 11.

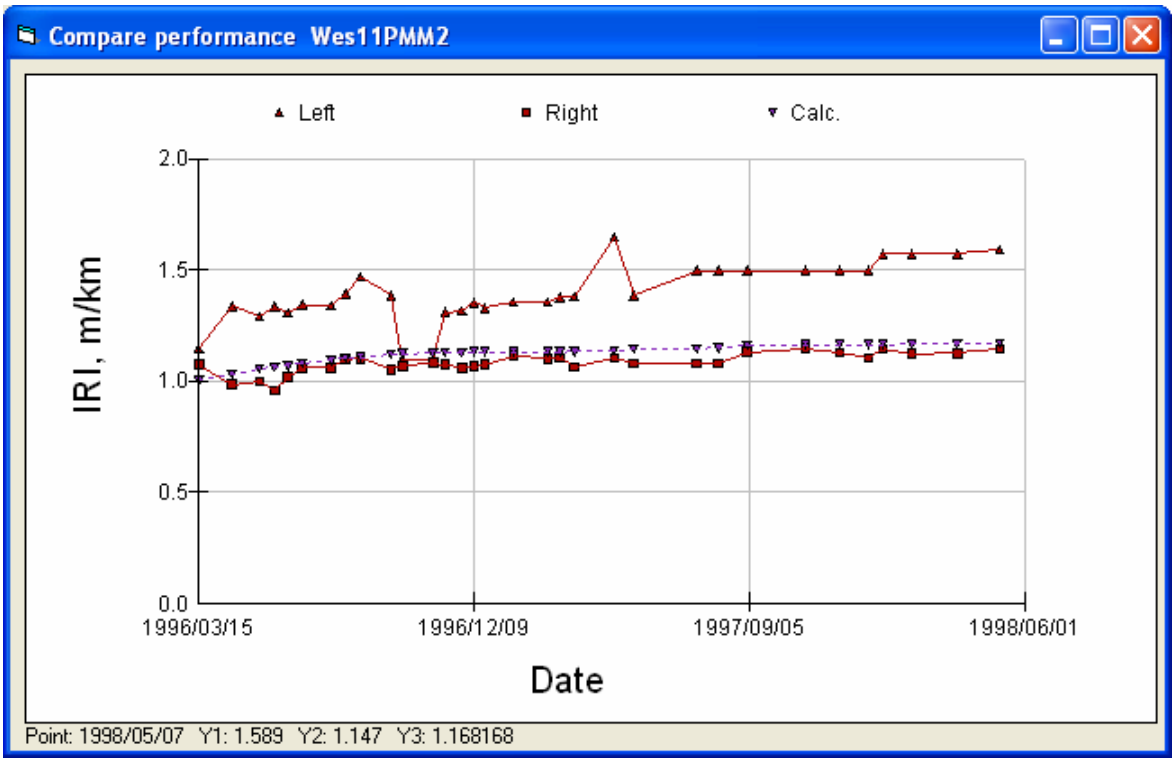

Figure 156. IRI in left and right wheelpaths at Section 11.

3.6.5 Section 12PML

Table 34. Summary of Input Values for Section 12PML

Modulus	*α*	*β*	*γ*	*δ*	*aT*	*A*	*VTS*
AC	2.1761	-0.9210	0.5756	2.000	1.300	10.0406	-3.680
Unbound	*Eo*	*Stiffness factor*	*Power on load*	*Estart*			
AB	319 MPa	0.65	0.6	190 MPa			
Subgrade	75 MPa	0	-0.2	75 MPa			
Aging	*AgeA*	*AgeB*					
AC	0.1792	-0.0576					
Fatigue	*A*	*α*	*β*	*γ*	*δ*		
AC	0.0983	0.4614	2.1221	1.0606	0.3941		
Rutting	*A*	*α*	*β*	*γ*	*dVoids*		
AC	12.02	0.2019	1.03	1	1.3		

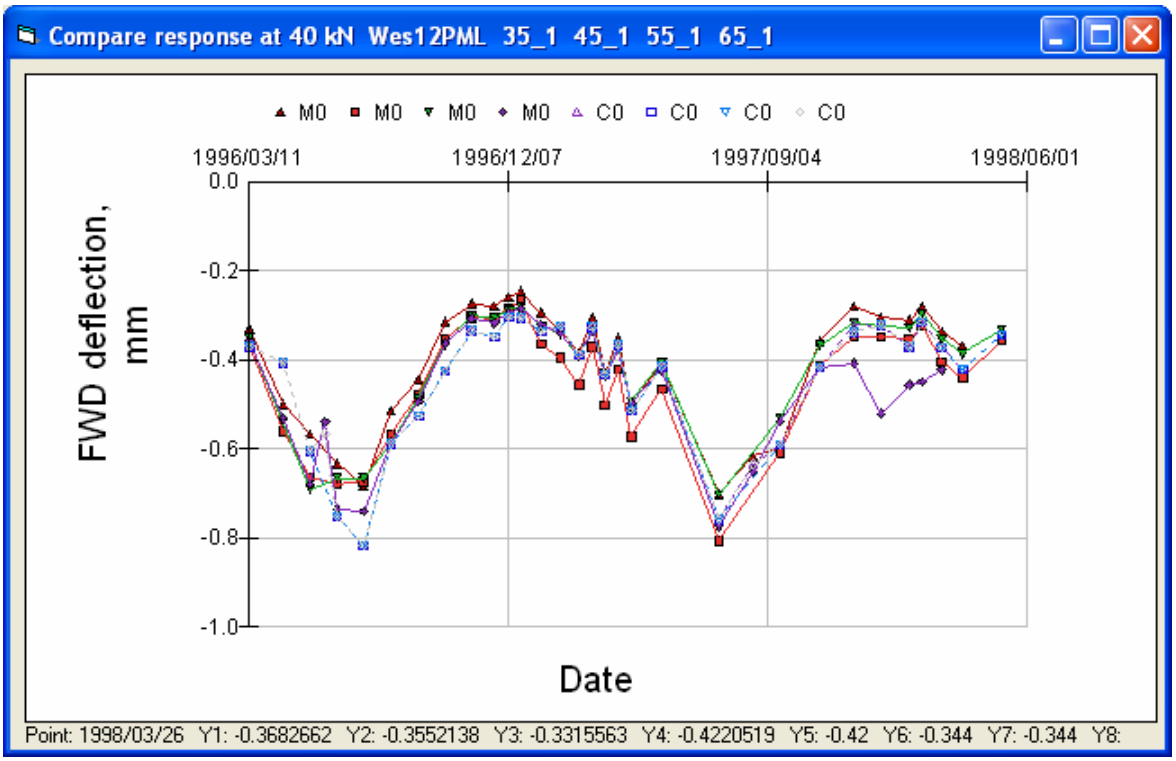

Figure 157. FWD deflections at Section 12 (in wheelpath, geophone under load plate).

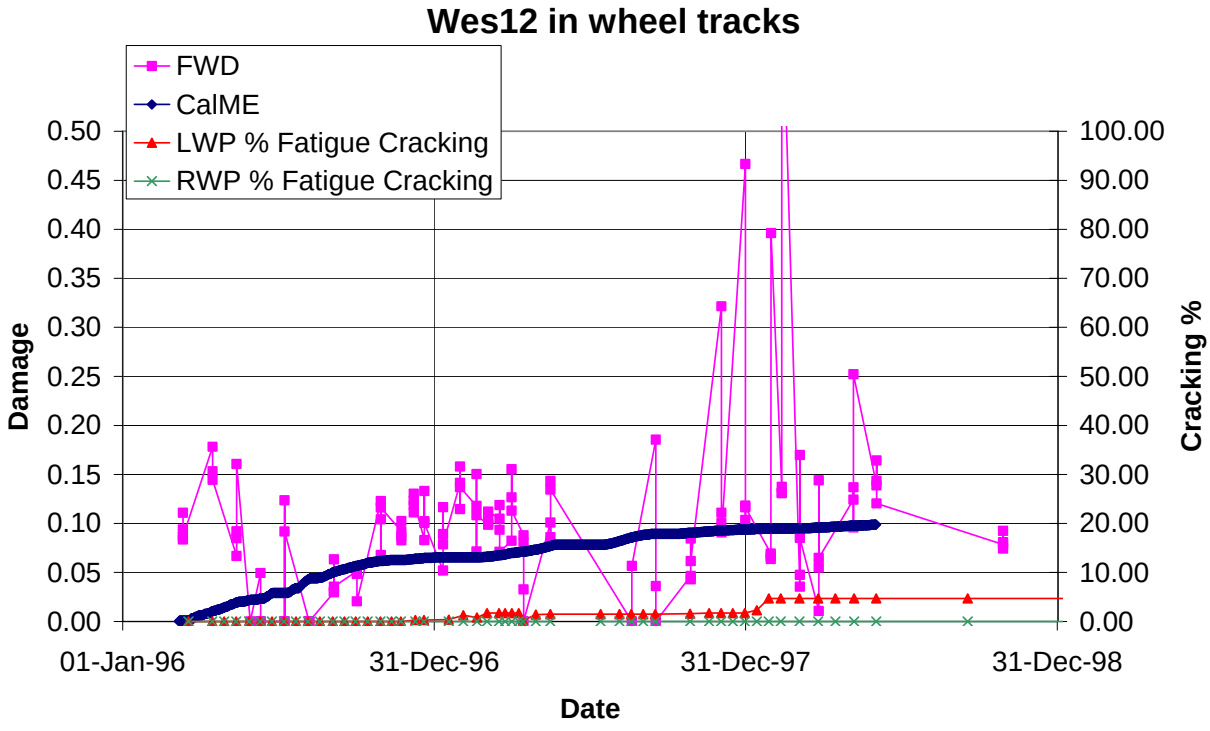

Figure 158. Damage in wheelpath of Section 12 (LWP = left wheelpath, RWP = right wheelpath).

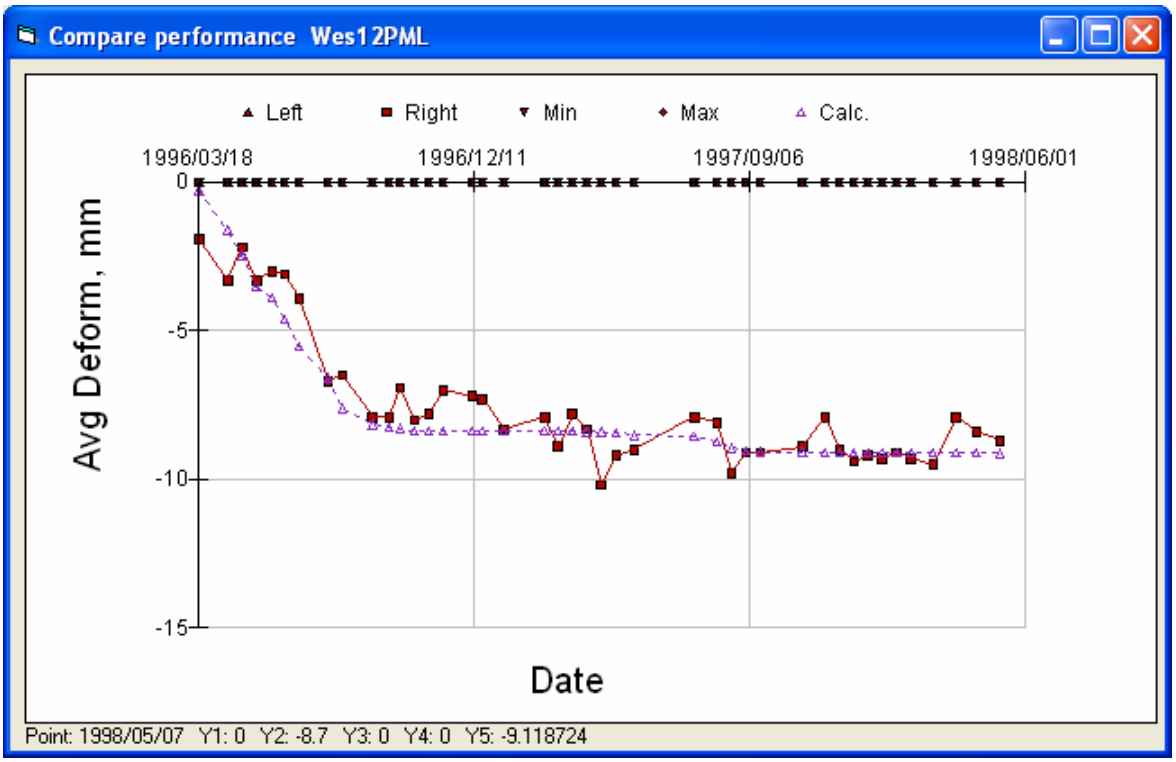

Figure 159. Down rut in right wheelpath at Section 12.

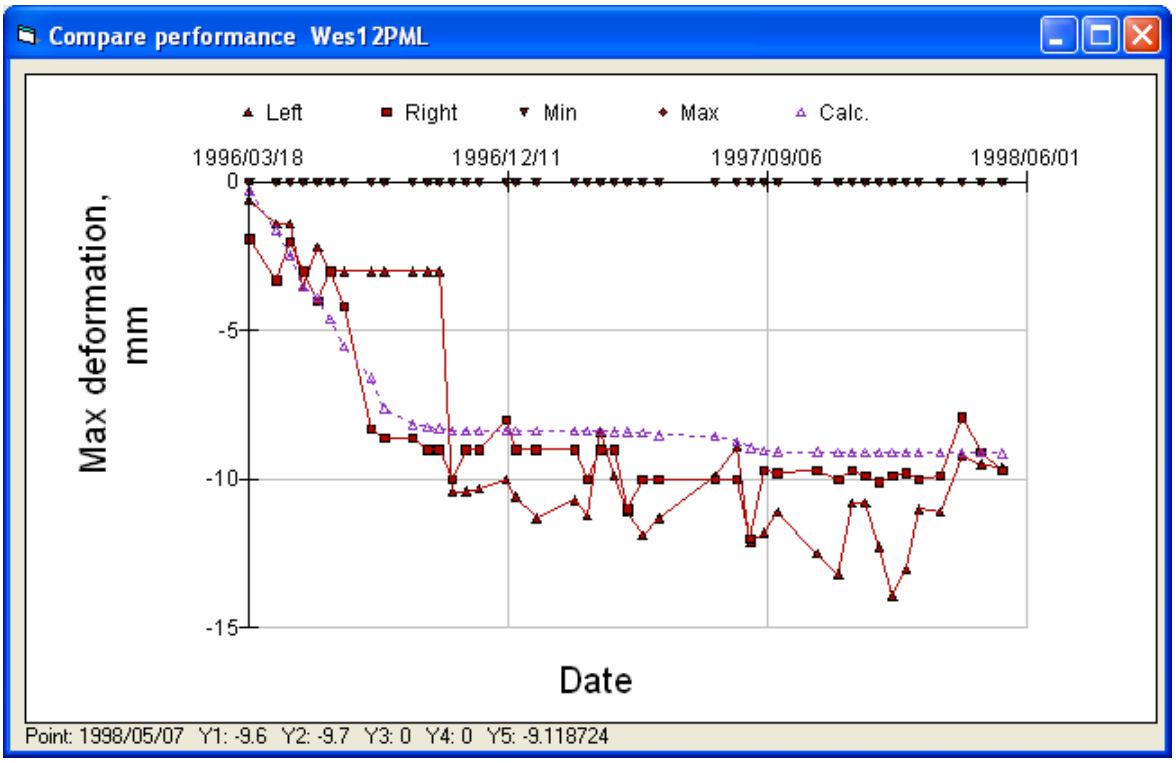

Figure 160. Maximum rutting in left and right wheelpaths at Section 12.

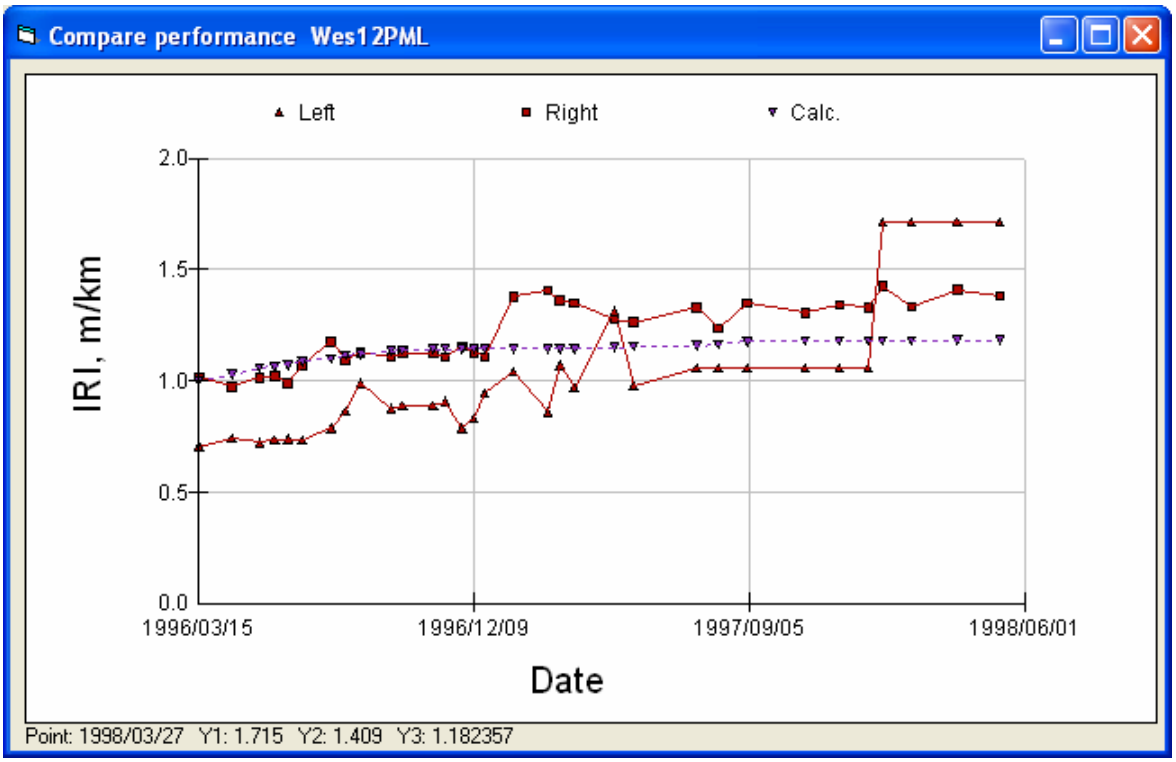

Figure 161. IRI in left and right wheelpaths at Section 12.

3.6.6 Section 13PHM

Table 35. Summary of Input Values for Section 13PHM

Modulus	*α*	*β*	*γ*	*δ*	*aT*	*A*	*VTS*
AC	1.9031	-1.2664	0.5756	2.000	1.300	10.0406	-3.680
Unbound	*Eo*	*Stiffness factor*	*Power on load*	*Estart*			
AB	244 MPa	0.57	0.6	170 MPa			
Subgrade	72 MPa	0	-0.2	72 MPa			
Aging	*AgeA*	*AgeB*					
AC	0.2010	-0.1856					
Fatigue	*A*	*α*	*β*	*γ*	*δ*		
AC	0.1763	0.4471	1.7853	0.8926	0.3818		
Rutting	*A*	*α*	*β*	*γ*	*dVoids*		
AC					2.2		

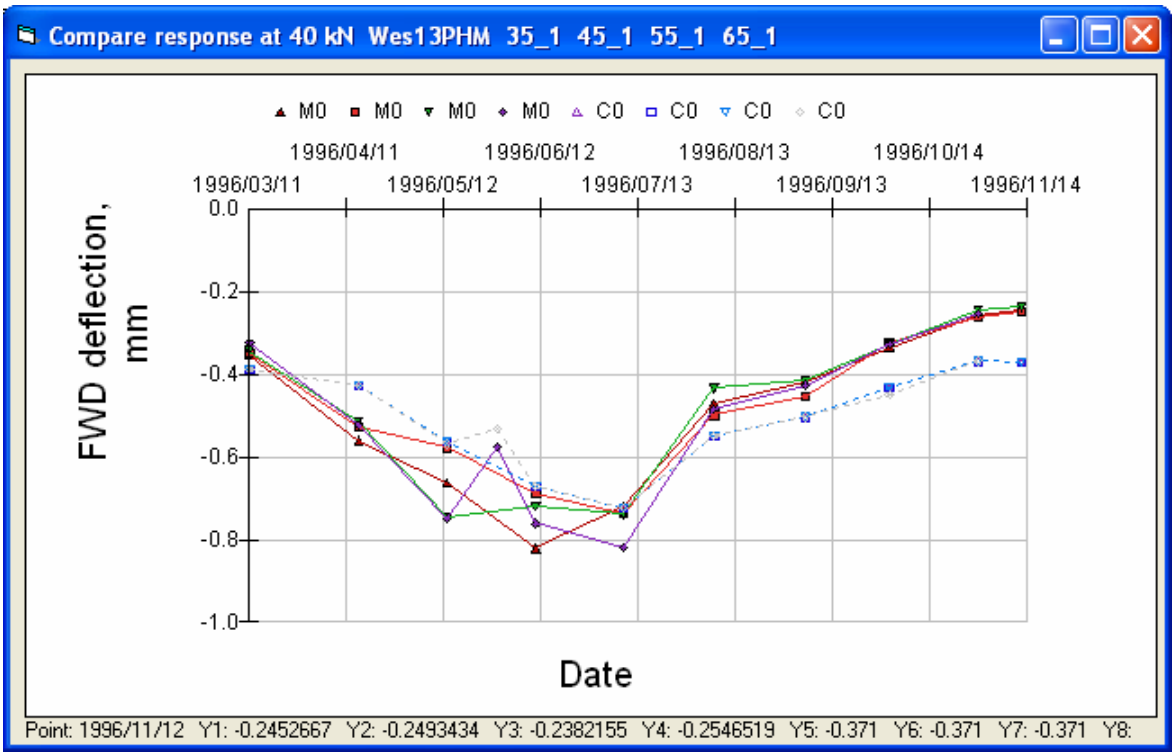

Figure 162. FWD deflections at Section 13 (in wheelpath, geophone under load plate).

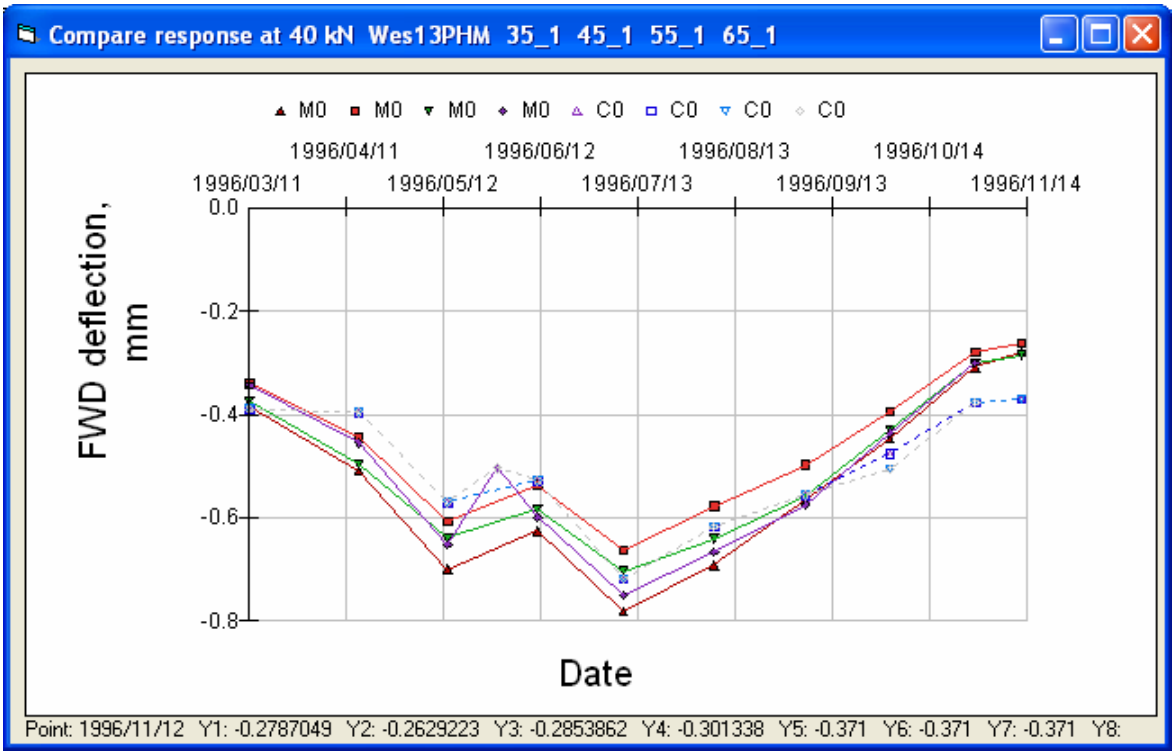

Figure 163. FWD deflections at Section 13 (between the wheelpaths, geophone under load plate).

The deflections measured between the wheelpaths are a little larger than the deflections measured in the right wheelpath for Section 13.

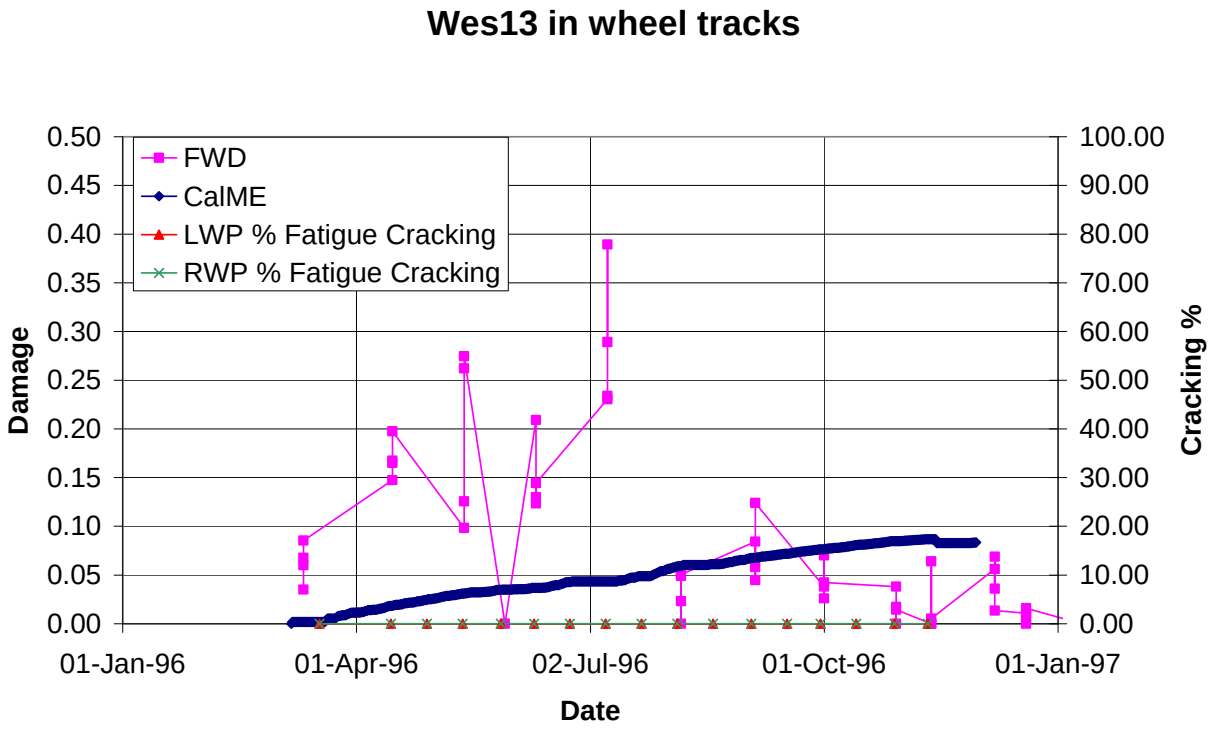

Figure 164. Damage in wheelpath of Section 13 (LWP = left wheelpath, RWP = right wheelpath).

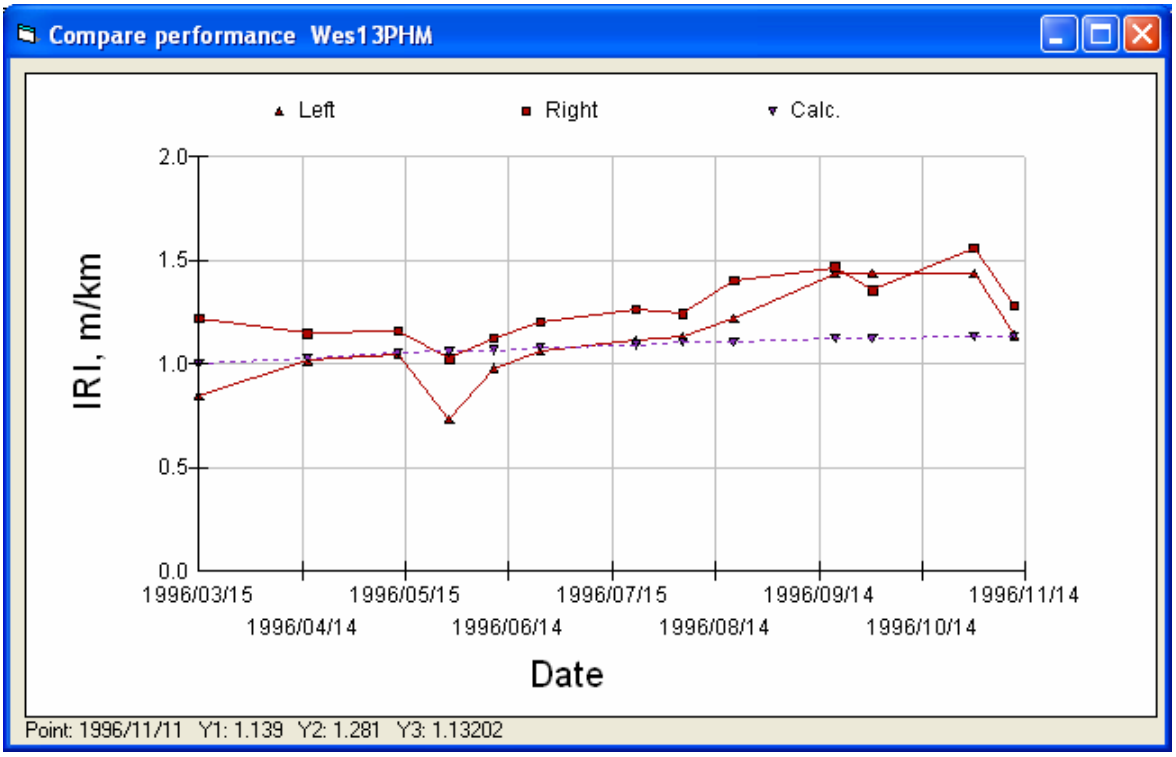

Figure 165. IRI in left and right wheelpaths at Section 13.

3.6.7 Section 19PMM1

Table 36. Summary of Input values for Section 19PMM1

Modulus	*α*	*β*	*γ*	*δ*	*aT*	*A*	*VTS*
AC	2.0792	-1.0362	0.6908	2.000	1.300	10.0406	-3.680
Unbound	*Eo*	*Stiffness factor*	*Power on load*	*Estart*			
AB	207 MPa	0.49	0.6	150 MPa			
Subgrade	88 MPa	0	-0.2	88 MPa			
Aging	*AgeA*	*AgeB*					
AC	0.2369	-0.3979					
Fatigue	*A*	*α*	*β*	*γ*	*δ*		
AC	0.1293	0.5252	2.8116	1.4058	0.4485		
Rutting	*A*	*α*	*β*	*γ*	*dVoids*		
AC	6.573	0.1006	1.03	1	2.6		

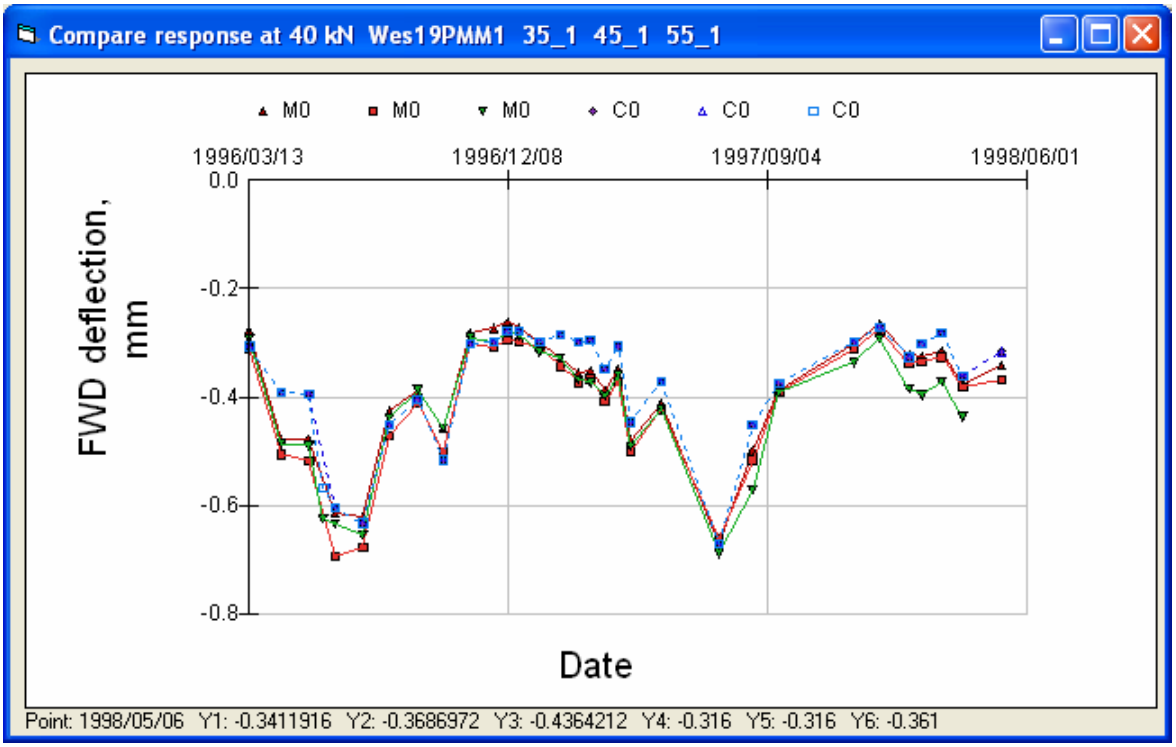

Figure 166. FWD deflections at Section 19 (in wheelpath, geophone under load plate).

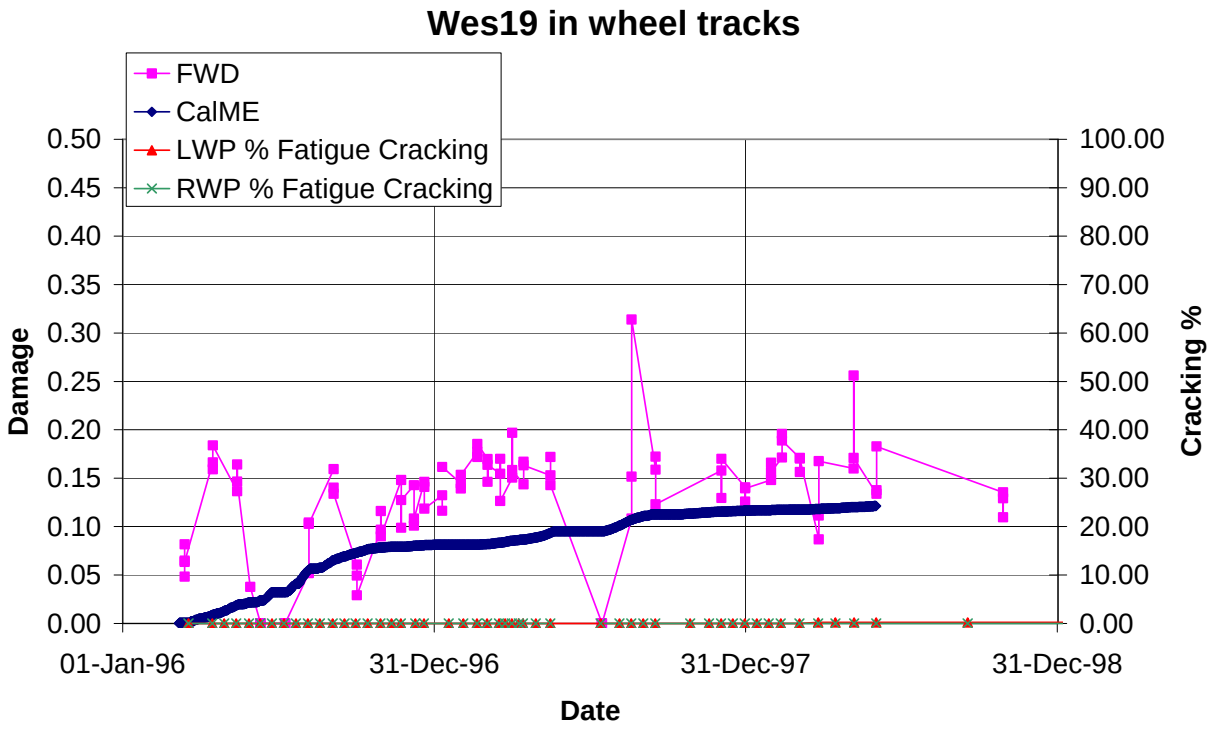

Figure 167. Damage in wheelpath of Section 19 (LWP = left wheelpath, RWP = right wheelpath).

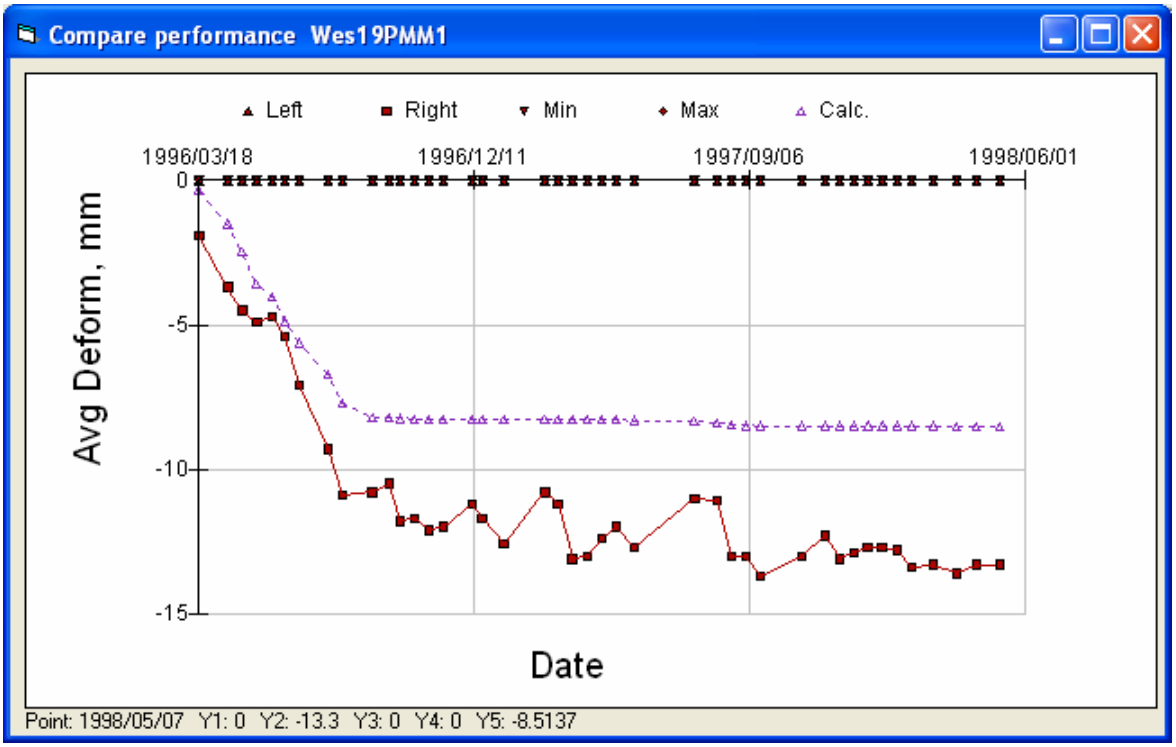

Figure 168. Down rut in right wheelpath at Section 19.

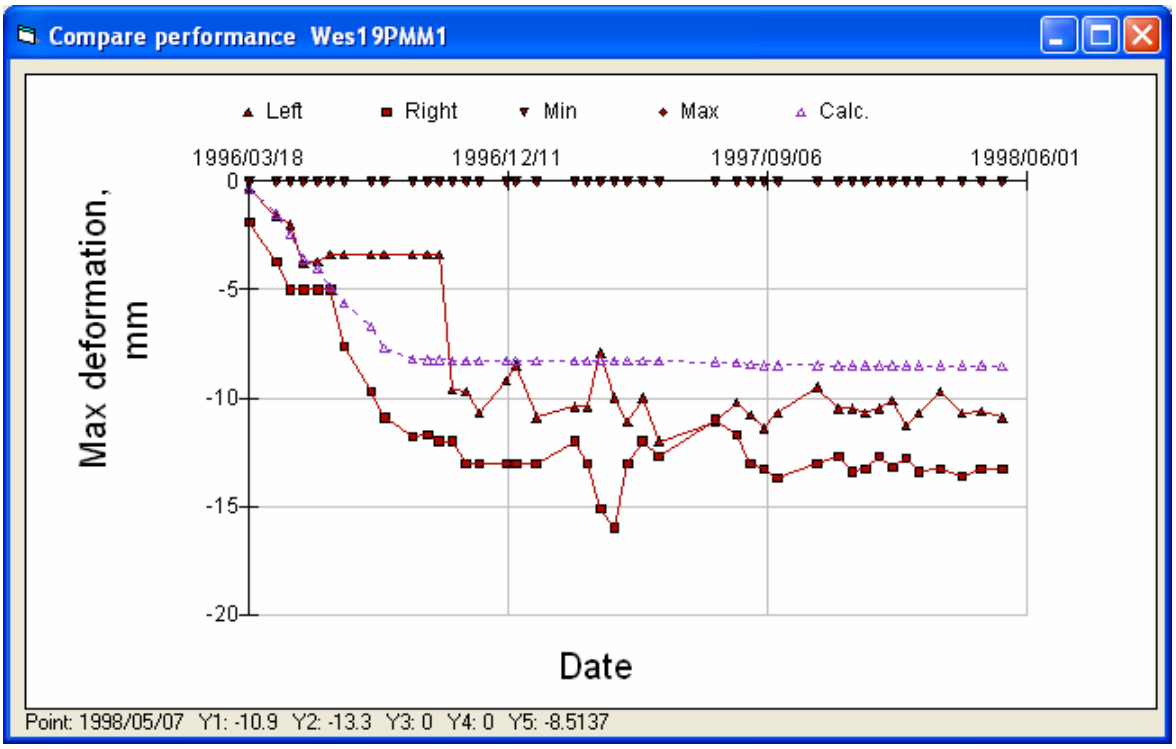

Figure 169. Maximum rutting in left and right wheelpaths at Section 19.

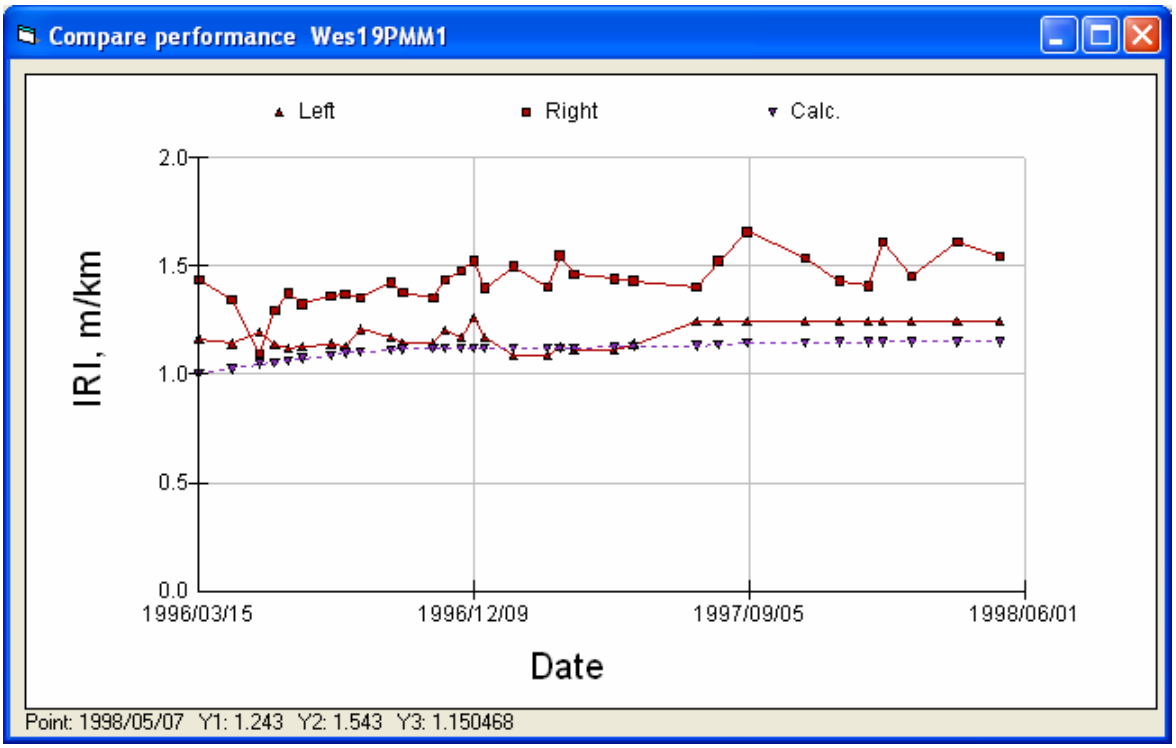

Figure 170. IRI in left and right wheelpaths at Section 19.

3.6.8 Section 20PMH

Table 37. Summary of Input Values for Section 20PMH

Modulus	*α*	*β*	*γ*	*δ*	*aT*	*A*	*VTS*
AC	1.9031	-1.0362	0.6908	2.000	1.300	10.0406	-3.680
Unbound	*Eo*	*Stiffness factor*	*Power on load*	*Estart*			
AB	181 MPa	0.50	0.6	110 MPa			
Subgrade	75 MPa	0	-0.2	75 MPa			
Aging	*AgeA*	*AgeB*					
AC	0.3284	-0.9378					
Fatigue	*A*	*α*	*β*	*γ*	*δ*		
AC	0.1909	0.4366	2.0895	1.0488	0.3728		
Rutting	*A*	*α*	*β*	*γ*	*dVoids*		
AC	8.451	0.1052	1.03	1	3.5		

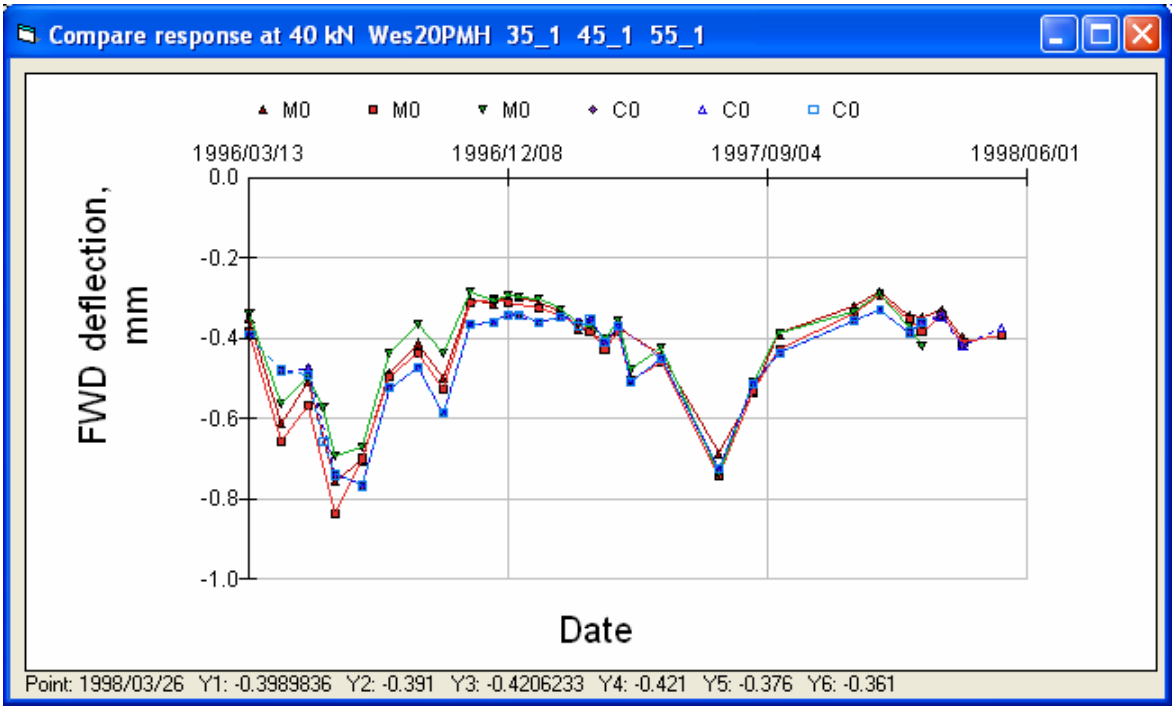

Figure 171. FWD deflections at Section 20 (in wheelpath, geophone under load plate).

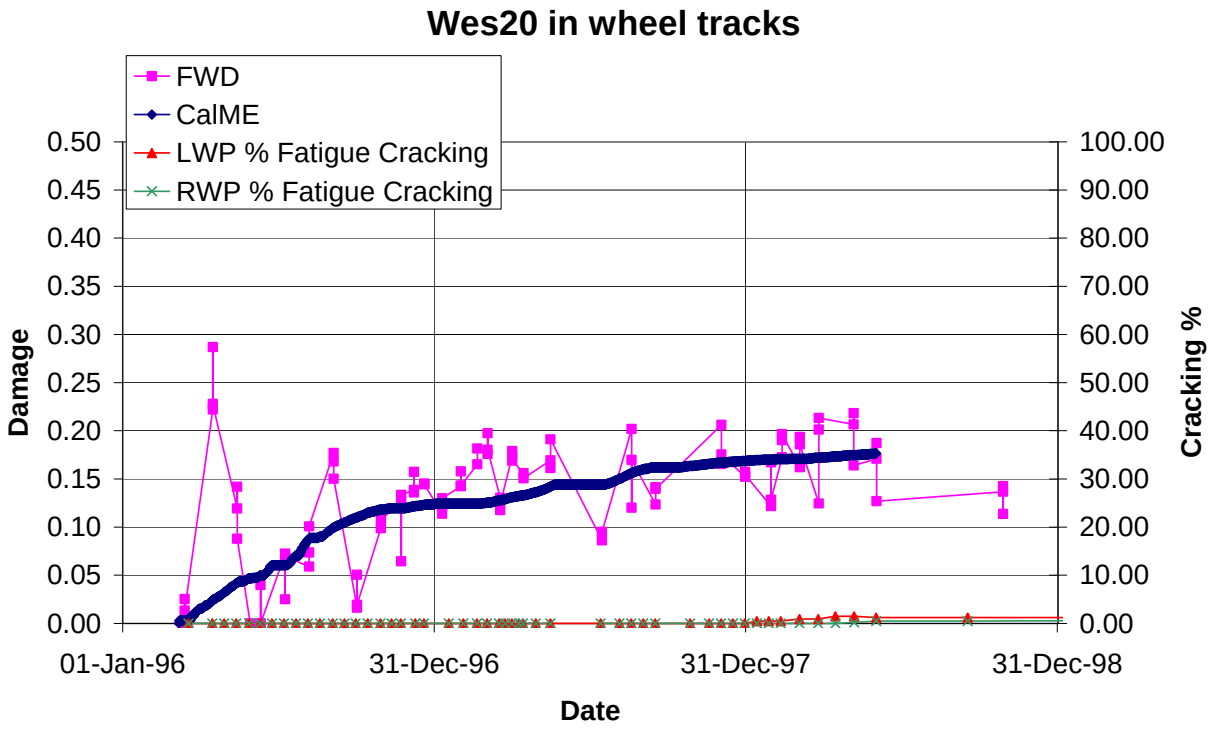

Figure 172. Damage in wheelpath of Section 20 (LWP = left wheelpath, RWP = right wheelpath).

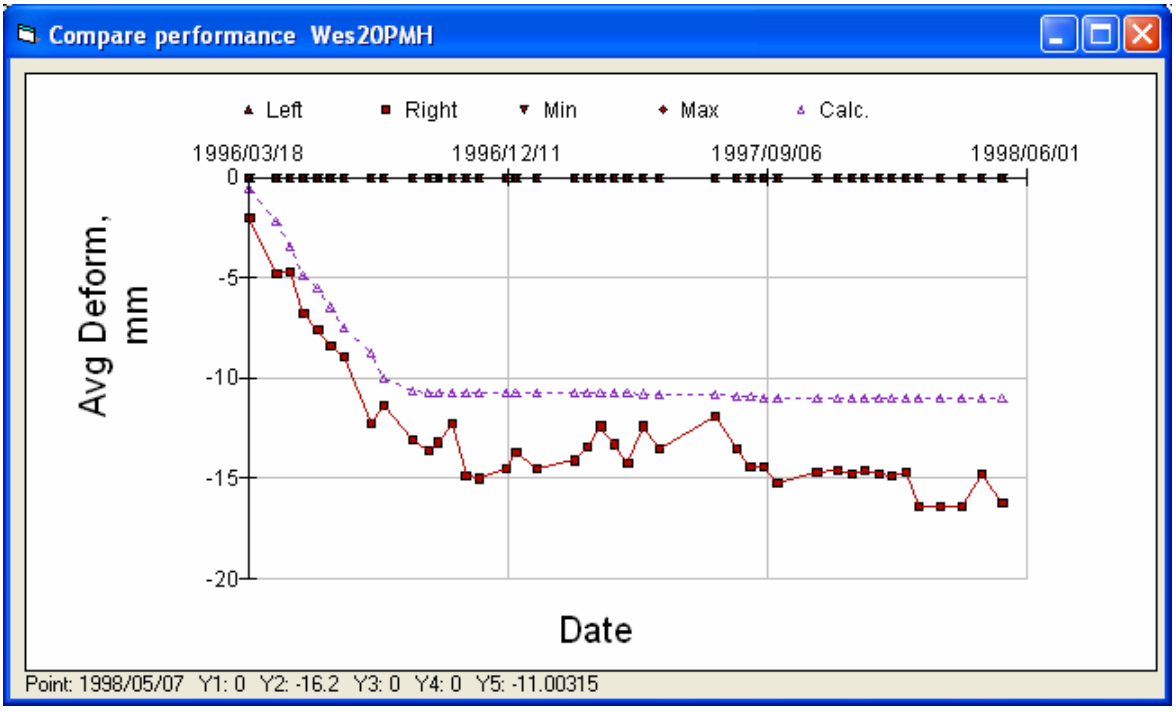

Figure 173. Down rut in right wheelpath at Section 20.

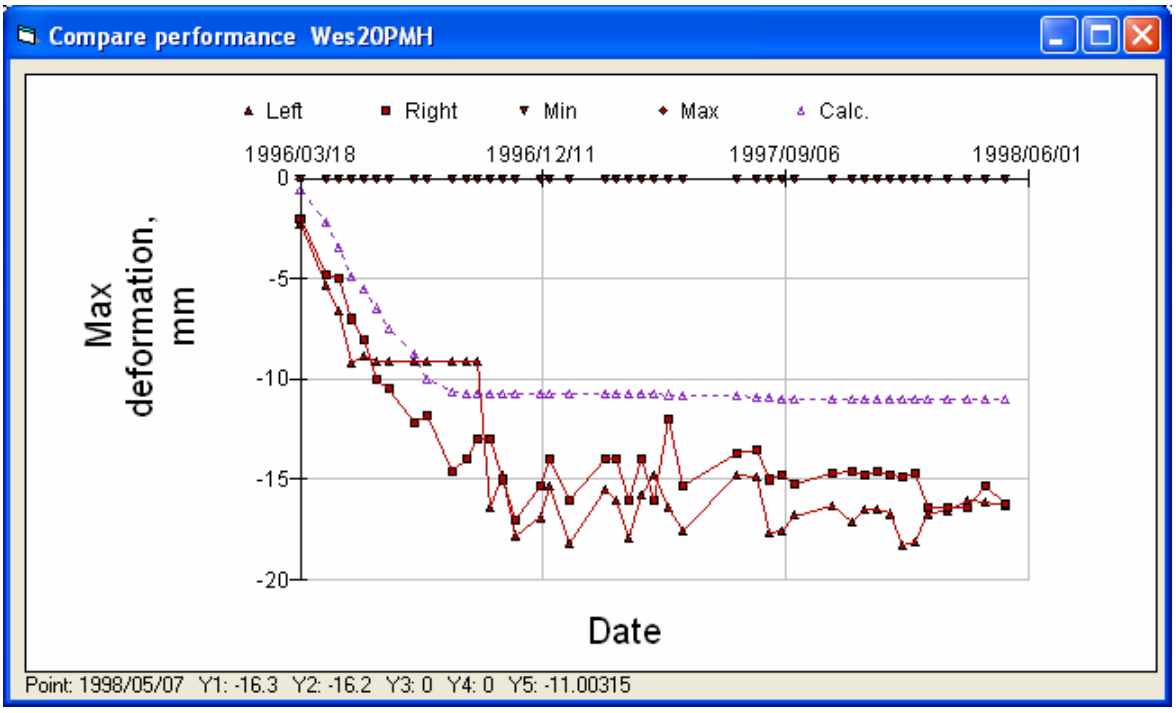

Figure 174. Maximum rutting in left and right wheelpaths at Section 20.

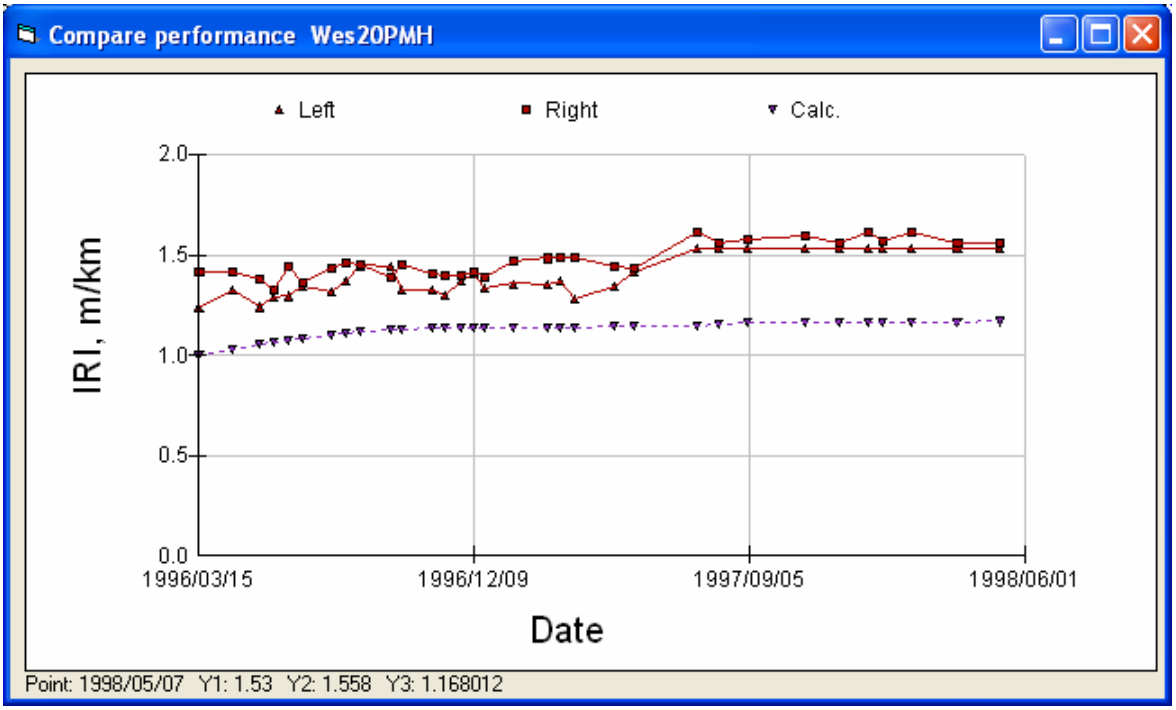

Figure 175. IRI in left and right wheelpaths at Section 20.

3.6.9 Section 21PHL1

Table 38. Summary of Input Values for Section 21PHL1

Modulus	*α*	*β*	*γ*	*δ*	*aT*	*A*	*VTS*
AC	2.1461	-1.0362	0.6908	2.000	1.300	10.0406	-3.680
Unbound	*Eo*	*Stiffness factor*	*Power on load*	*Estart*			
AB	245 MPa	0.46	0.6	175 MPa			
Subgrade	89 MPa	0	-0.2	89 MPa			
Aging	*AgeA*	*AgeB*					
AC	0.3196	-0.8855					
Fatigue	*A*	*α*	*β*	*γ*	*δ*		
AC	0.0498	0.4781	2.7813	1.3906	0.4083		
Rutting	*A*	*α*	*β*	*γ*	*dVoids*		
AC					1.3		

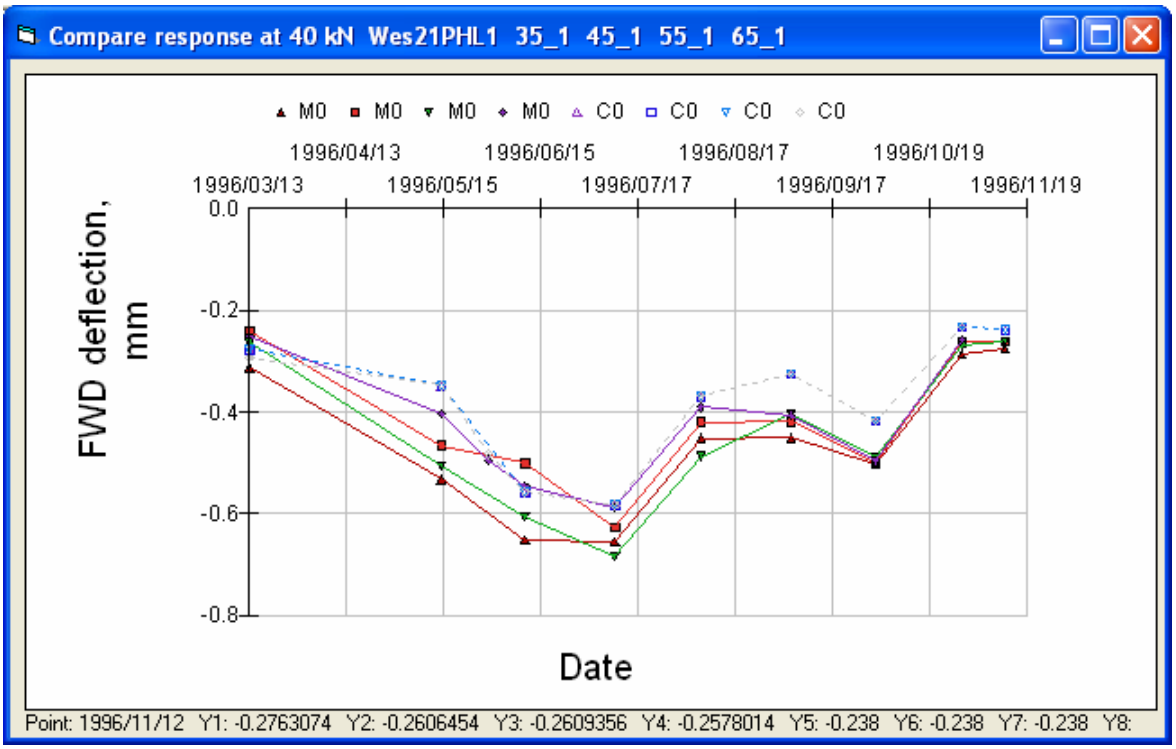

Figure 176. FWD deflections at Section 21 (in wheelpath, geophone under load plate).

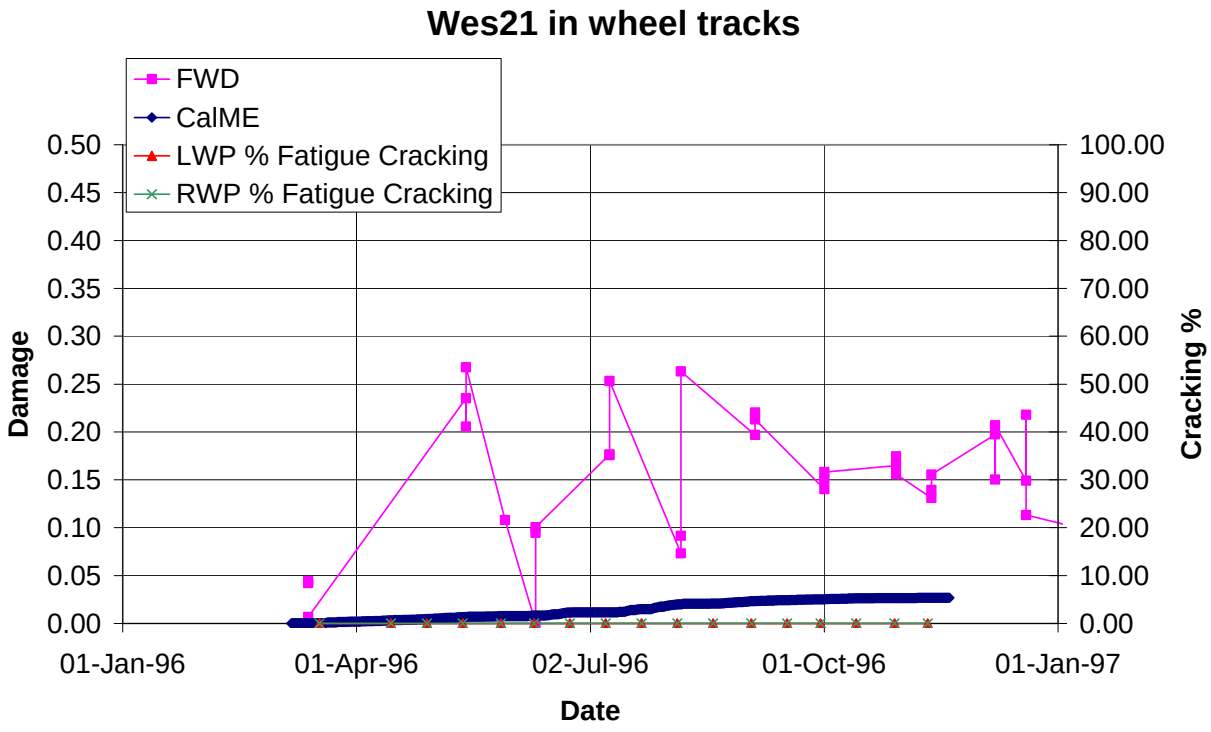

Figure 177. Damage in wheelpath of Section 21 (LWP = left wheelpath, RWP = right wheelpath).

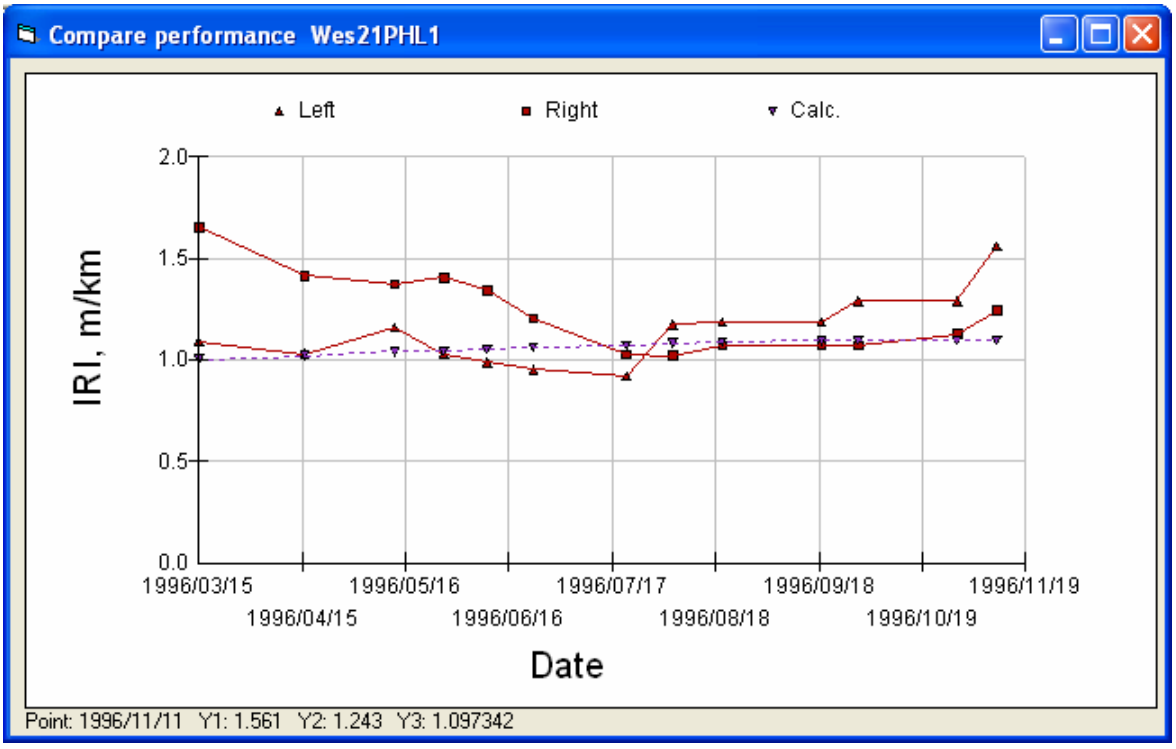

Figure 178. IRI in left and right wheelpaths at Section 21.

3.6.10 Section 22PLM

Table 39. Summary of Input Values for Section 22PLM

Modulus	*α*	*β*	*γ*	*δ*	*aT*	*A*	*VTS*
AC	2.0792	-1.0362	0.6908	2.000	1.300	10.0406	-3.680
Unbound	*Eo*	*Stiffness factor*	*Power on load*	*Estart*			
AB	257 MPa	0.64	0.6	170 MPa			
Subgrade	94 MPa	0	-0.2	94 MPa			
Aging	*AgeA*	*AgeB*					
AC	0.2568	-0.5151					
Fatigue	*A*	*α*	*β*	*γ*	*δ*		
AC	0.1378	0.4667	2.2338	1.1169	0.3985		
Rutting	*A*	*α*	*β*	*γ*	*dVoids*		
AC	14.77	0.2262	1.03	1	2.9		

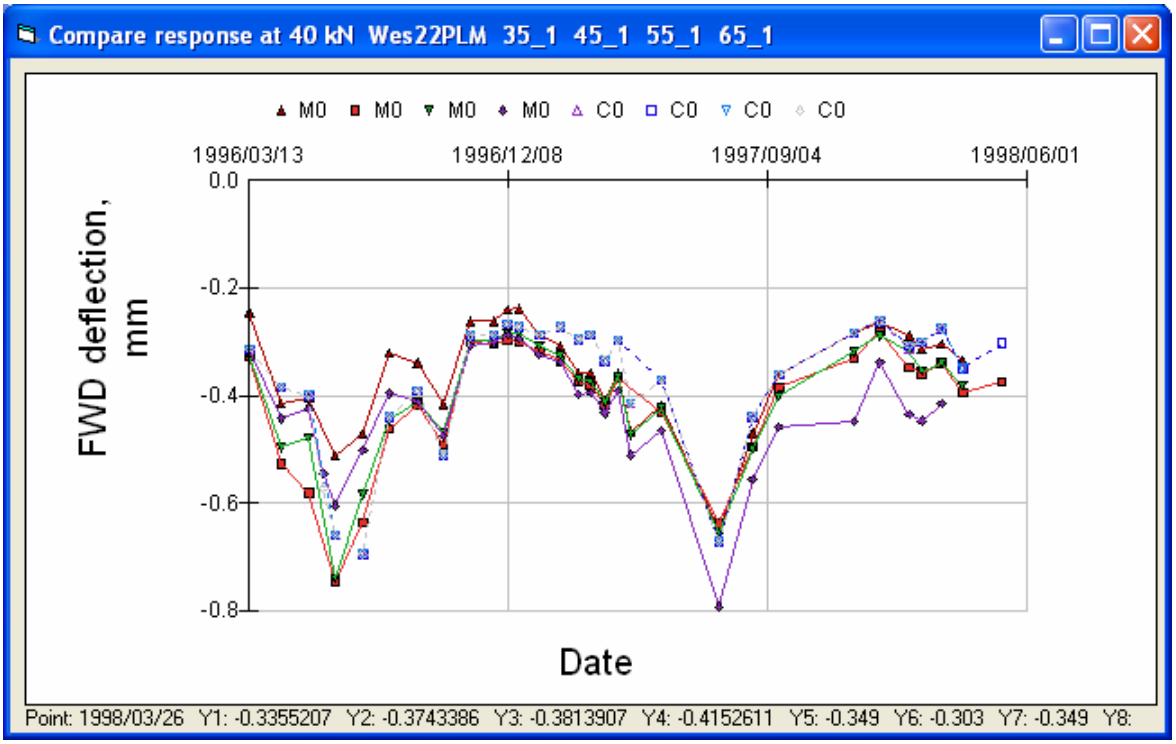

Figure 179. FWD deflections at Section 22 (in wheelpath, geophone under load plate).

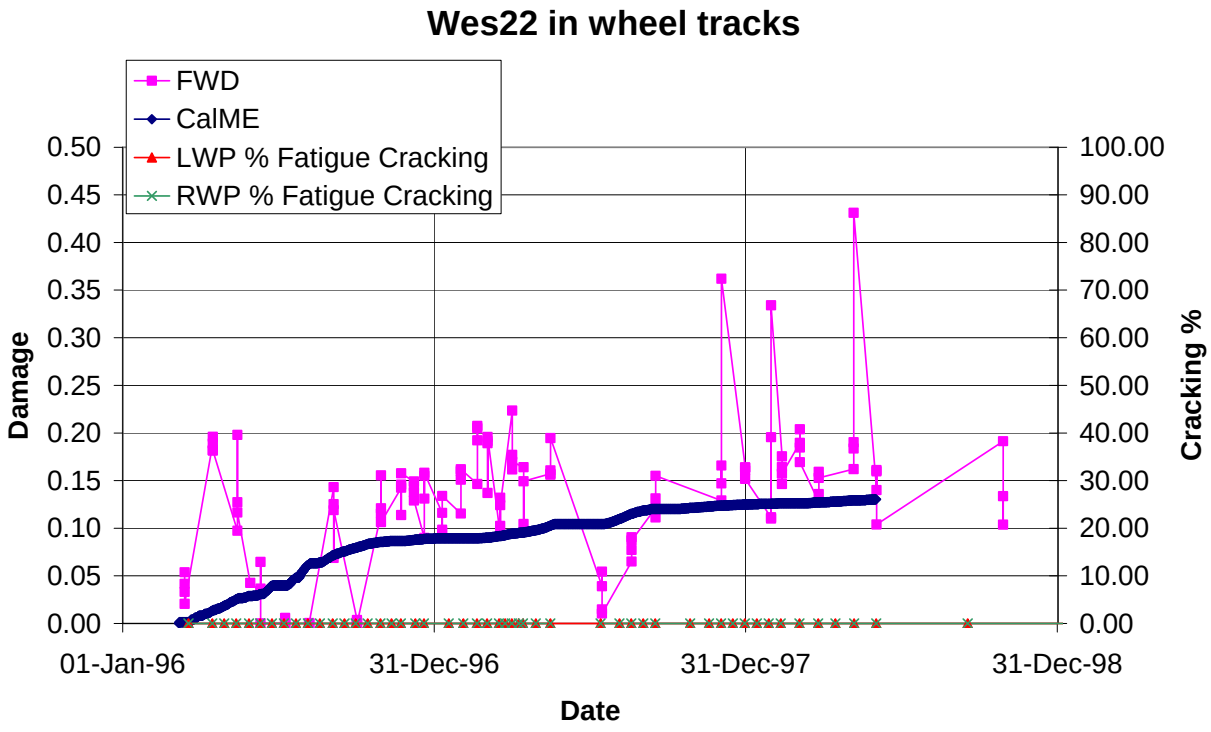

Figure 180. Damage in wheelpath of Section 22 (LWP = left wheelpath, RWP = right wheelpath).

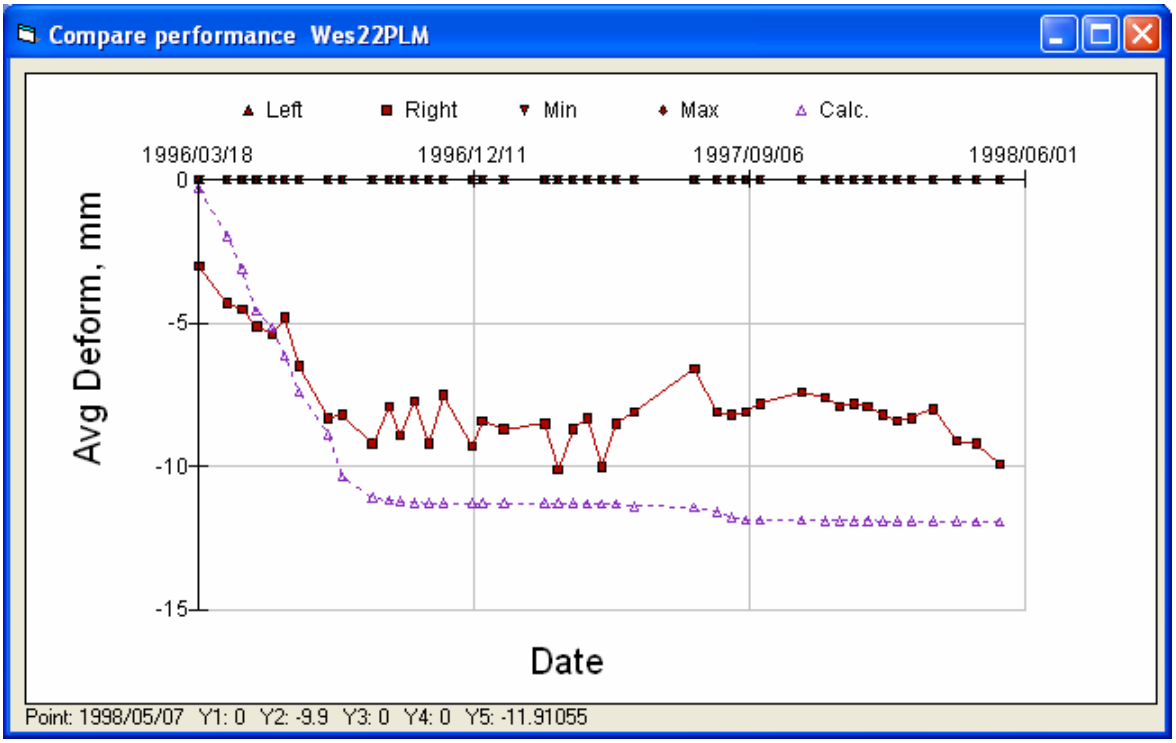

Figure 181. Down rut in right wheelpath at Section 22.

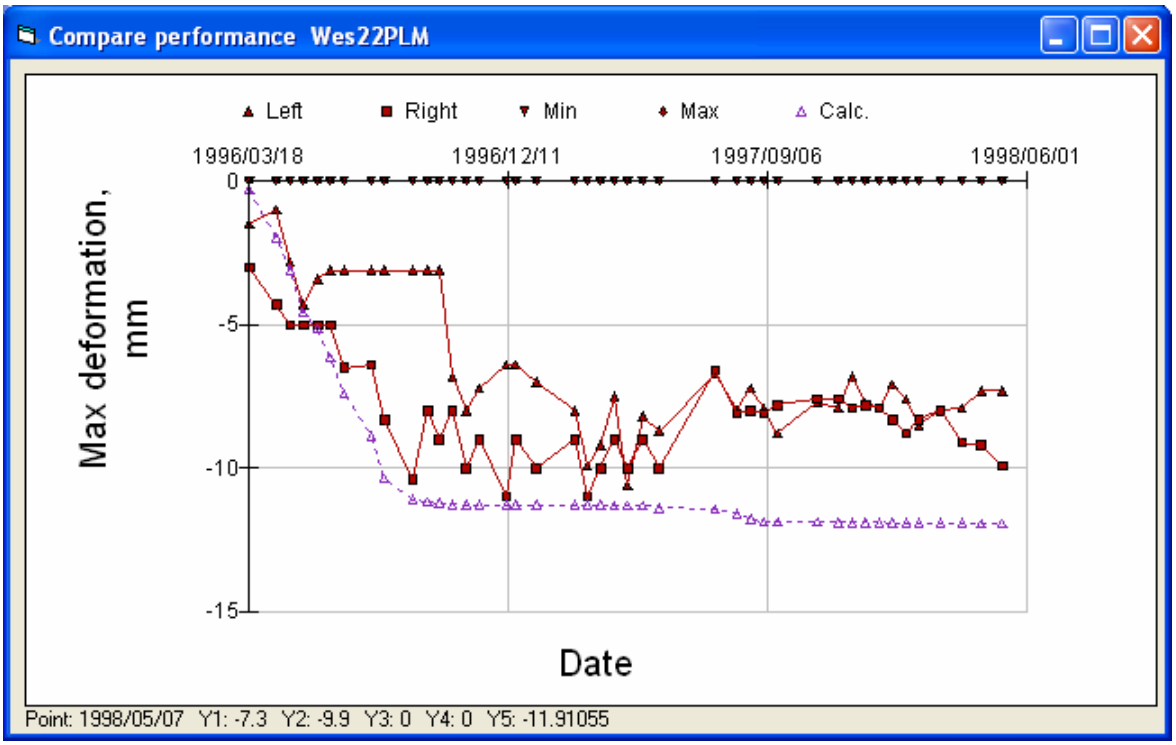

Figure 182. Maximum rutting in left and right wheelpaths at Section 22.

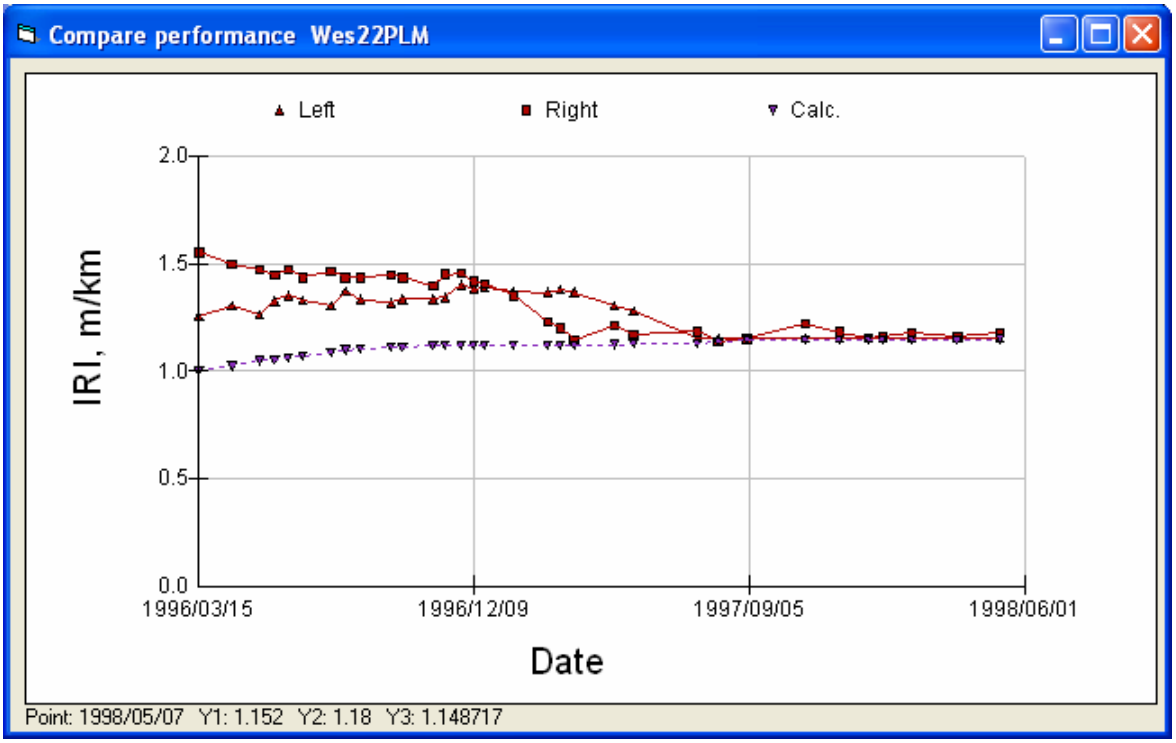

Figure 183. IRI in left and right wheelpaths at Section 22.

4 Summary of *CalME* Incremental-Recursive Procedure Results

4.1 Deflection Response

The agreement between the measured and calculated responses on the WesTrack sections, in terms of the deflection under the load plate of the FWD, is seen to be very good in most cases. The calculated deflections are a function of the following factors which are considered in *CalME* of:

- The estimated asphalt temperature during the FWD test,
- The asphalt modulus-versus-reduced time relationship,
- The moduli of the unbound materials (aggregate base and subgrade),
- The hardening of the asphalt material as a function of post compaction and aging , and
- The damage to the asphalt caused by fatigue.

The measured deflections will be a function of the actual asphalt temperature during the FWD tests, the contact between the FWD loading plate and the pavement surface, as well as of the position of the test.

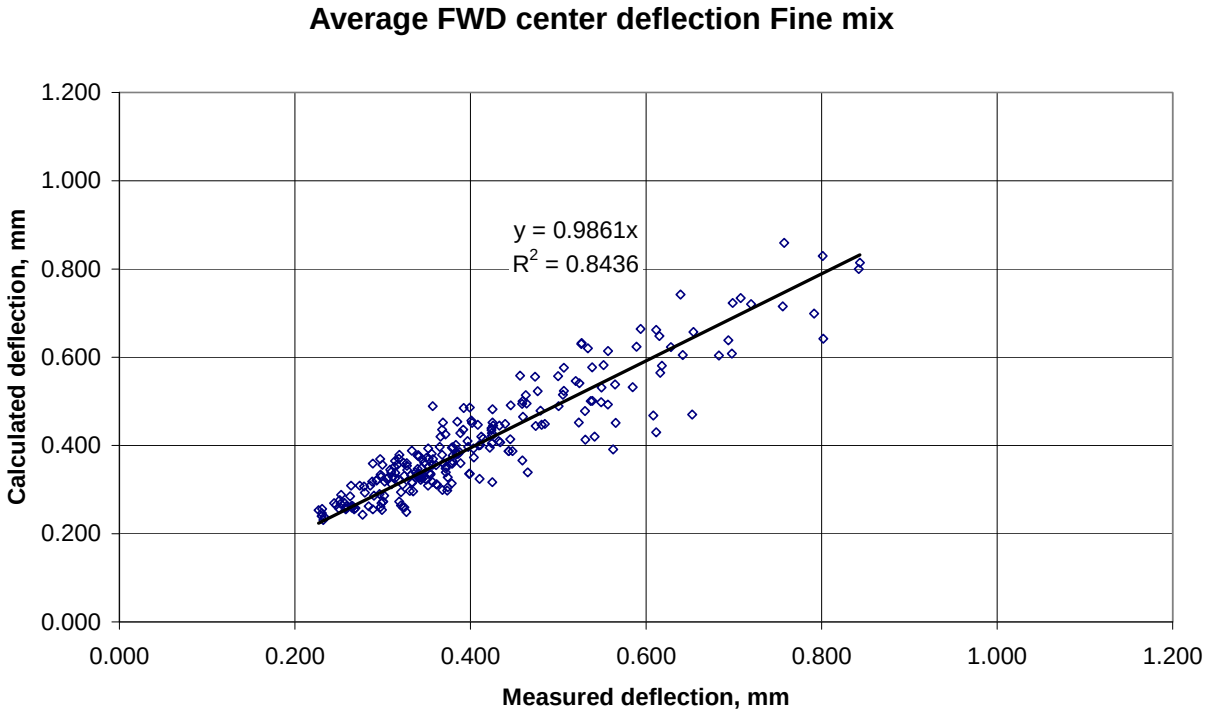

Figure 184. Measured and calculated center deflections on Fine mix sections.

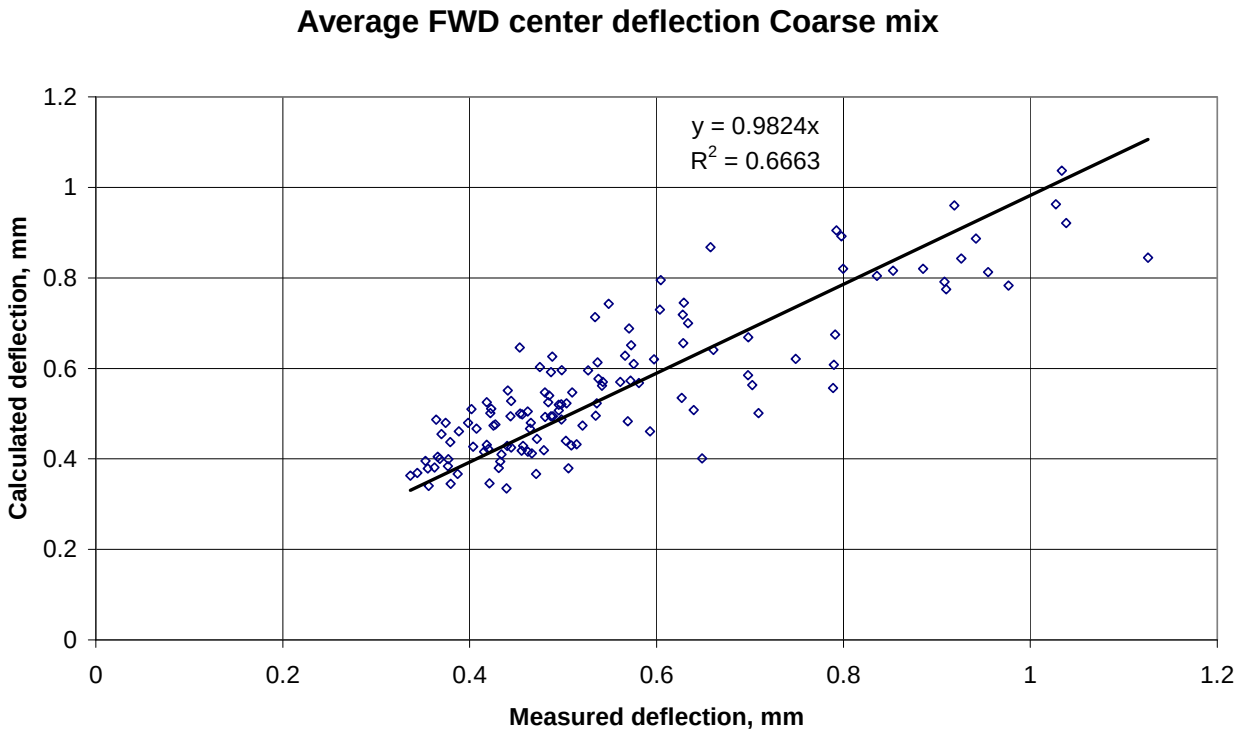

Figure 185. Measured and calculated center deflections on Coarse mix sections.

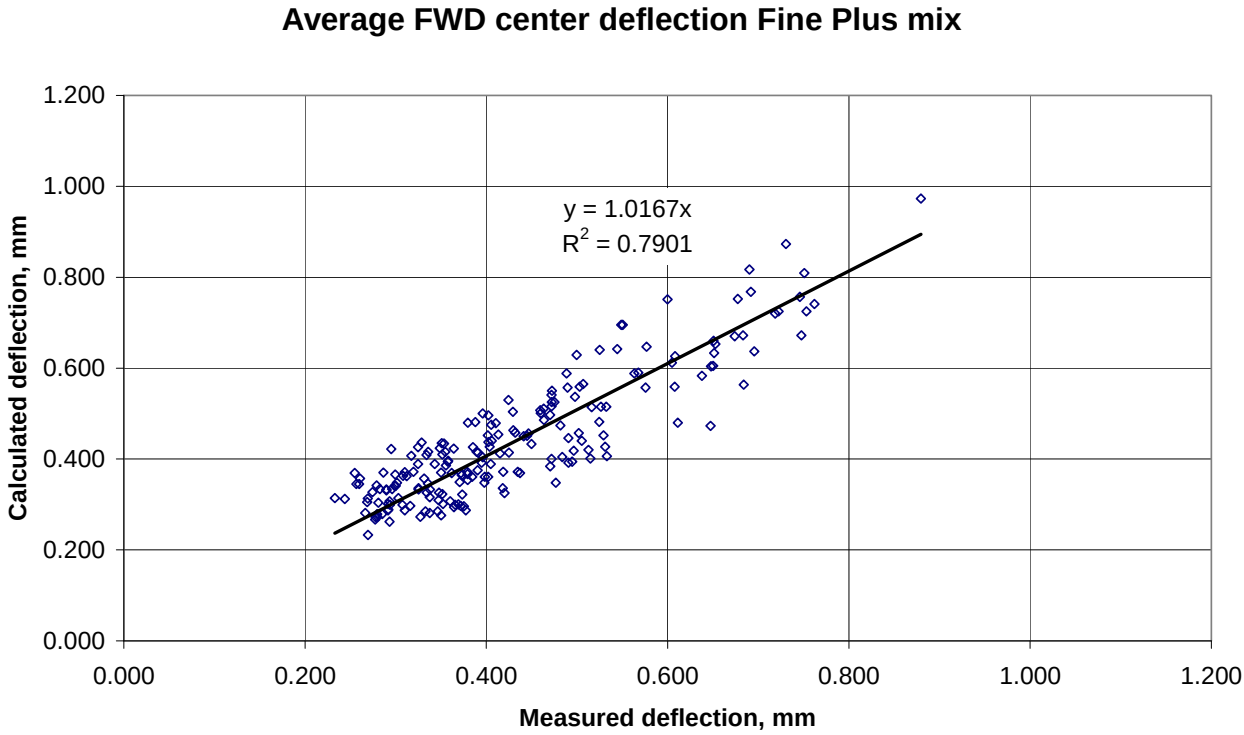

Figure 186. Measured and calculated center deflections on Fine Plus mix sections.

Figure 184, Figure 185, and Figure 186 show the average deflection at the center of the FWD loading plate, calculated for each section and each monitoring session. Only tests done at a chainage of 30 m or higher were used, in order to avoid the transition sections.

For the Fine mix sections the standard error of estimate is 50 μm, for the Coarse mix sections 103 μm, and for the Fine Plus mix sections 60 μm. For the Fine mix and the Fine Plus mix these values are similar to the standard deviations of the measured values for a single monitoring session on one test section. In other words, the difference between measured and calculated values is similar to the scatter in the measured values. For the Coarse mix the standard error of estimate is somewhat higher.

Table 40 shows the differences between the measured values as well as the differences between the measured and calculated values. The measured values are mostly based on four FWD tests within the section, although a few sections had only three tests. The mean difference between the measured center deflections is the mean of the absolute values given in μm (micron, 10^{-6} m). RMS is the Root Mean Square value, also in μm. For the differences between measured and calculated deflections a positive mean difference indicates that the measured deflection was (numerically) larger than the calculated deflection, and vice versa.

In most cases the differences between the measured and the calculated deflections are not much larger than the differences between the measured deflections.

The RMS values are also shown in Figure 188.

Table 40. Measured and Calculated Deflection Differences

		Measured Values		Measured vs Calculated	
Section	**Mix**	**Mean dif.**	**RMS**	**Mean dif.**	**RMS**
1	FMM1	36	42	5	42
2	FLM	29	33	-17	47
3	FLH1	46	52	-27	72
4	FML	51	57	20	52
5	CMM1	61	70	75	94
6	CMH	39	46	-53	105
7	CHM	54	66	-1	89
8	CLM	31	36	-55	107
9	PHL2	57	66	-36	77
10	PLH	56	66	-40	82
11	PMM2	34	39	-63	79
12	PML	43	52	-9	51
13	PHM	37	43	-10	90
14	FHM	37	41	-3	37
15	FMM2	15	17	-12	32
16	FLH2	16	17	-11	39
17	FMH	33	37	43	57
18	FHL	18	21	27	34
19	PMM1	24	26	30	41
20	PMH	44	51	-18	45
21	PHL1	44	49	58	73
22	PLM	62	75	27	68
23	CML	43	49	-3	52
24	CMM2	29	34	39	83
25	CHL	48	56	41	58
26	CLH	28	32	-21	74

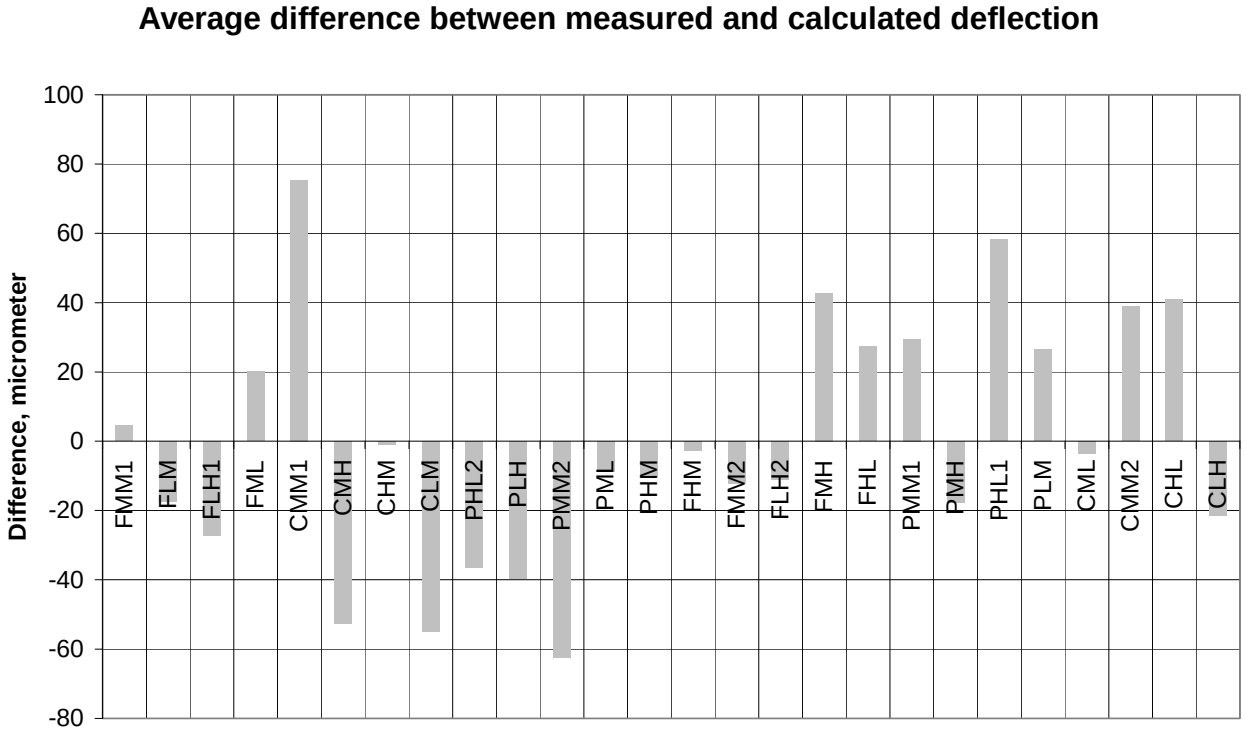

Figure 187. Deflection difference versus mix type.

Figure 187 shows the average difference between measured and calculated deflections in μm versus mix type. For comparison it may be noted that the average standard deviation on the measured deflections was 30 μm and the maximum average standard deviation for each section was 50 μm.

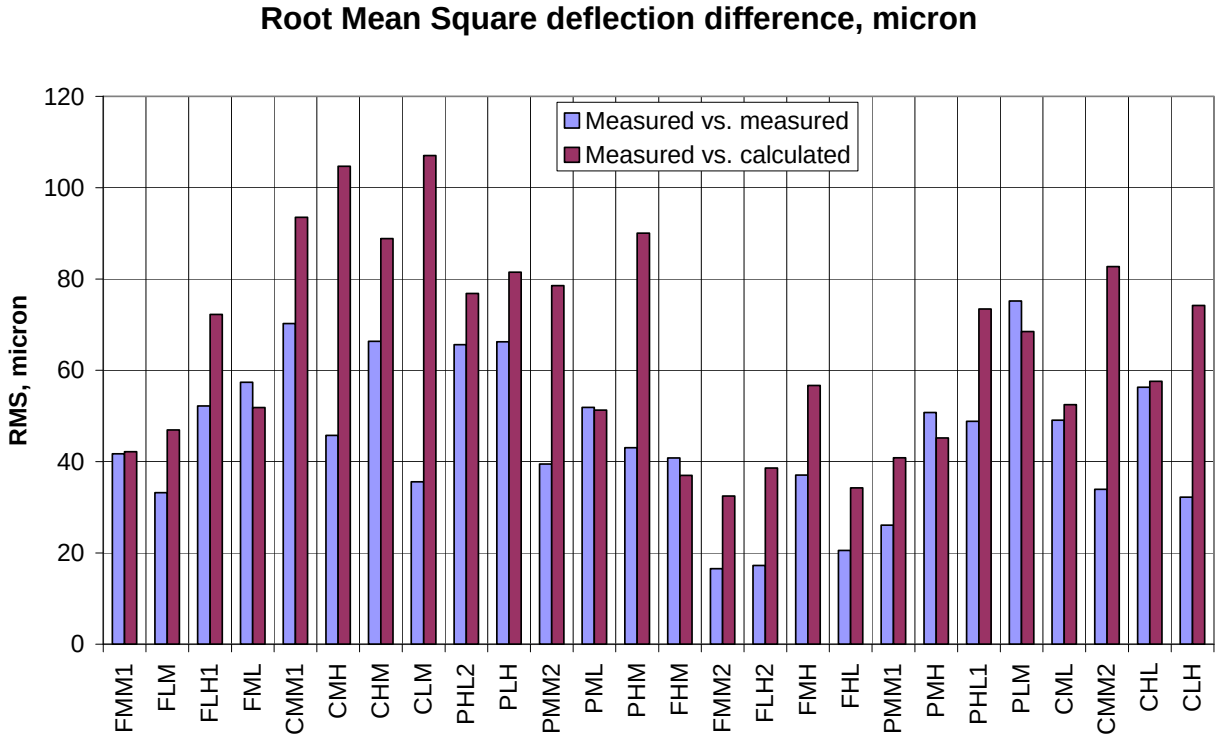

Figure 188. Comparison of RMS differences within measured and between measured and calculated response.

Figure 188 compares the Root Mean Square (RMS) differences between the measured deflections to the RMS differences between the measured and calculated values. The average RMS for the measured deflections is 45 μm and it is 65 μm for the difference between measured and calculated deflections.

4.2 Damage and Cracking

Figure 189 compares the damage, ω, predicted by *CalME*, based on the laboratory fatigue data, to the damage estimated from the FWD tests in the right wheelpath. As explained above the FWD backcalculated asphalt moduli were corrected for the effects of (estimated) temperature and hardening, due to aging and decrease in air-voids content. The difference between the adjusted modulus and the modulus calculated from the modulus versus reduced time model was then assumed to be due to damage. Decrease in modulus was converted to damage using Equation 24.

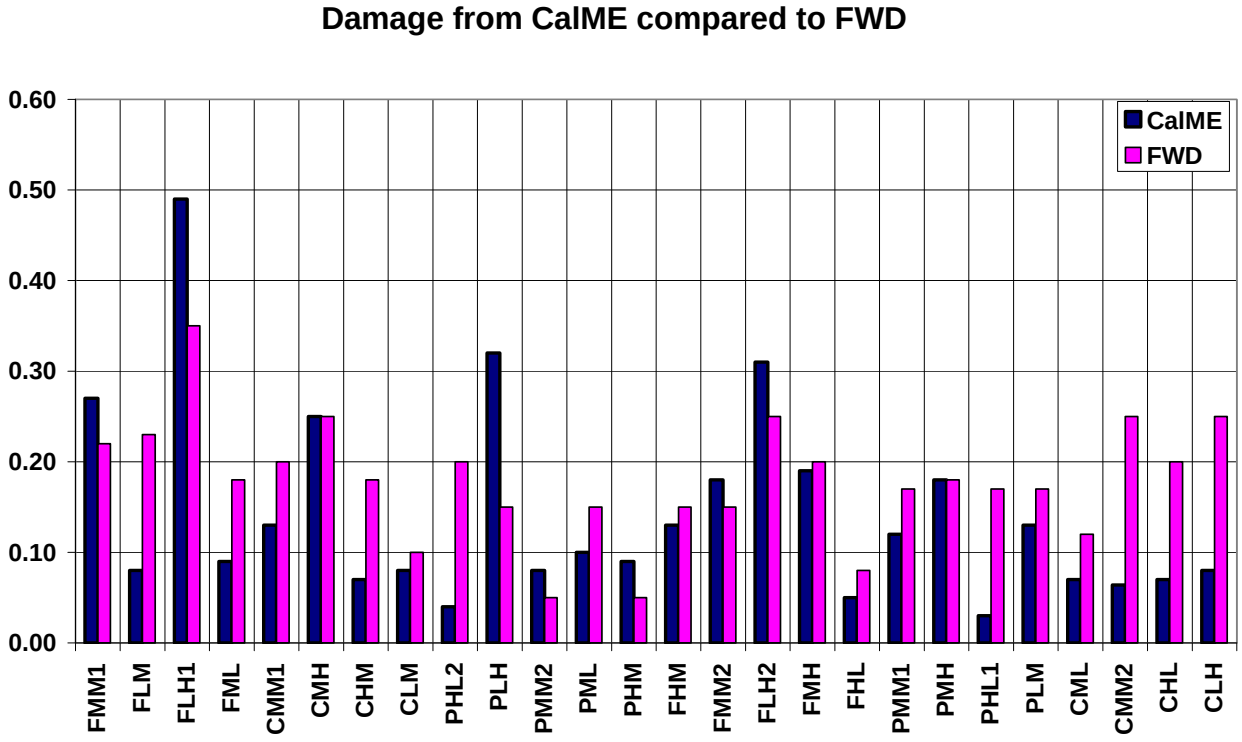

Figure 189. Damage predicted by CalME compared to damage estimated from FWD tests.

On average the Fine, Coarse, and Fine Plus mixes all have less damage predicted by *CalME* than estimated from the FWD. The Coarse mix shows the largest difference, with the FWD estimated damage being 2.2 times that of the *CalME* predicted damage, even though the shift factor used for the Coarse mix was 5, compared to 15 for the other two mixes. For the Fine and the Fine Plus mixes the ratio is 1.3 and 2.0, respectively. This indicates that the shift factor of 15 is too large, and that it probably should be a function of mix type. This is quite reasonable as the influence of rest periods on the fatigue life is likely to be different for different mixes.

There is also some indication that mixes with a high binder content should have a lower shift factor than mixes with a low binder content, and that mixes with a low air-voids content should have a lower shift factor than mixes with a high air-void content. This would indicate that the asphalt under in situ loading is less affected by the binder and air-void content than in the laboratory fatigue tests, but it should be recalled that the uncertainties on the damage estimated from the FWD tests are very large.

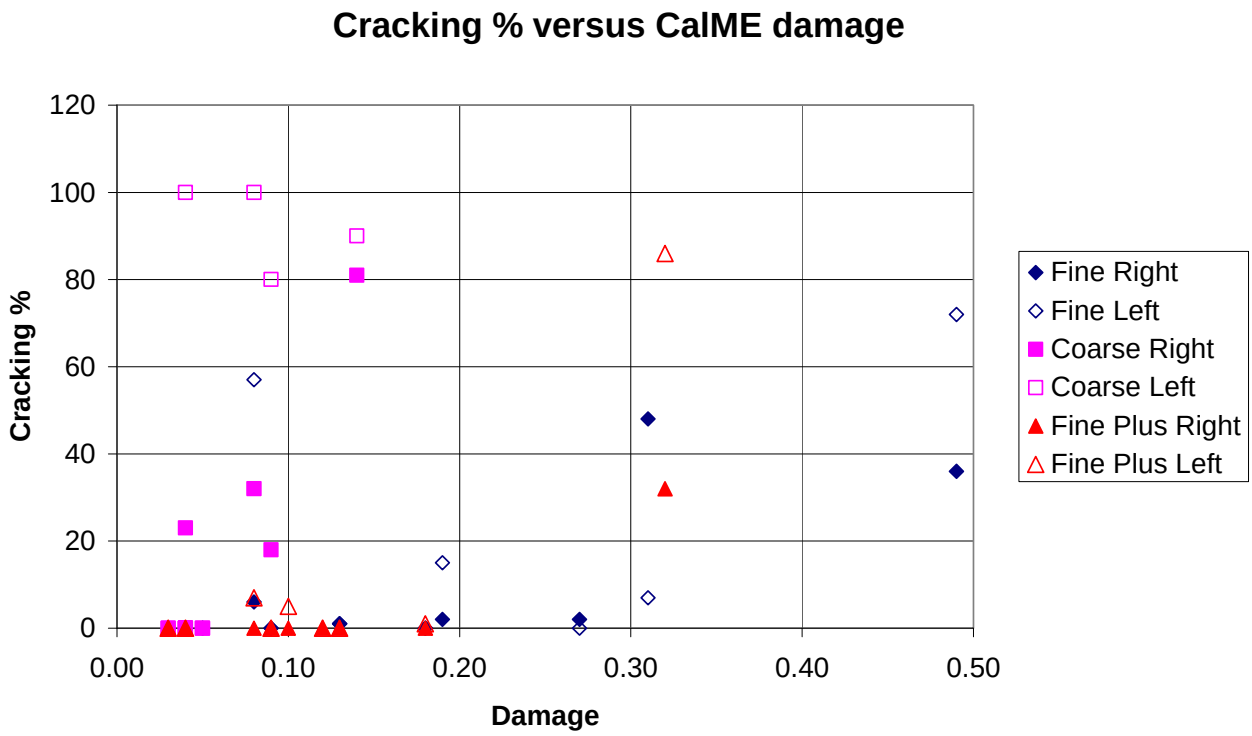

Figure 190. Cracking in left and right wheelpaths as a function of damage predicted by CalME.

The cracking versus damage shown in Figure 190 also indicates that even the shift factor of 5 was too large for the Coarse mix. As noted above the cracking is generally higher in the left wheelpath than in the right wheelpath, where the FWD tests were carried out.

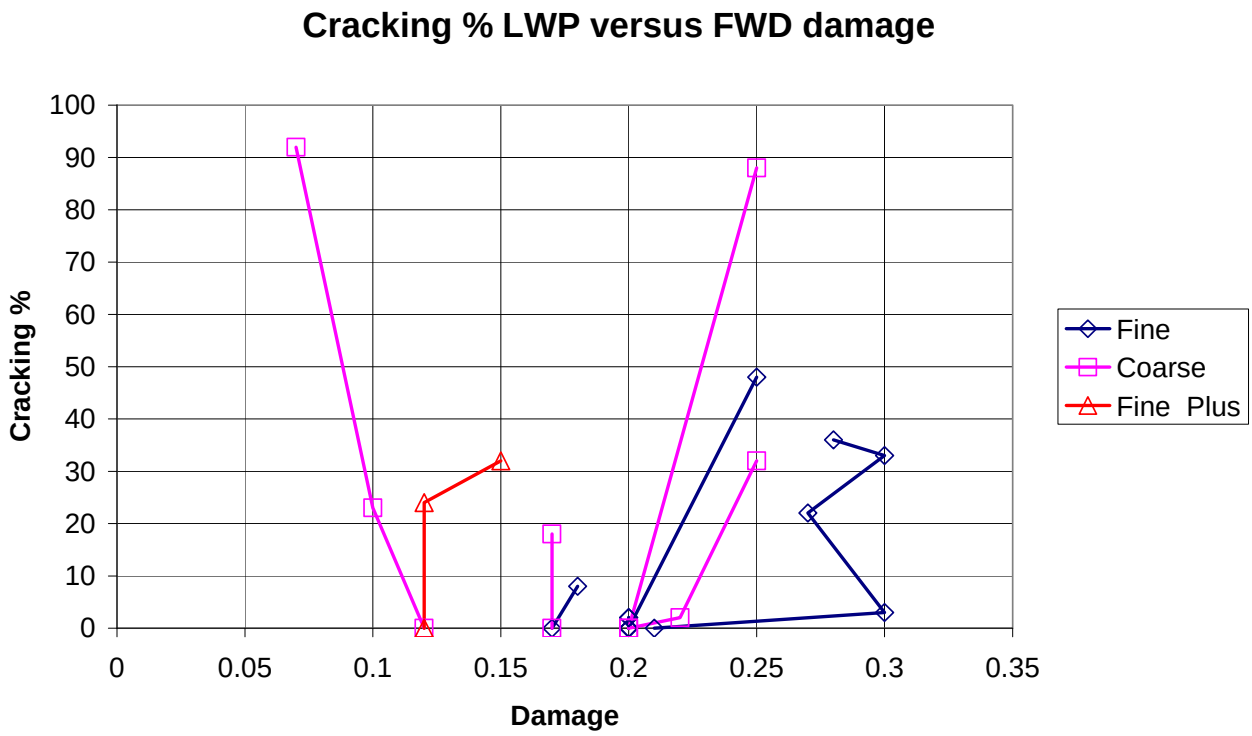

Figure 191. Cracking in right wheelpaths versus damage estimated from FWD tests.

Figure 191 shows the relationship between the damage calculated from FWD tests and the observed cracking in the right wheelpath. In some cases an increase in cracking is associated with a decrease in the calculated damage.

4.3 Permanent Deformation

Table 41shows the mean difference between the measured down rut in the right wheelpath and the predicted permanent deformation using all of the historical data, as well as the RMS value, both in mm.

A positive mean difference implies that the calculated permanent deformation was numerically larger than the measured down rut.

For comparison it may be noted that the difference between the rutting in the right and the left wheelpaths was often 3–4 mm with an RMS value of 4–5 mm.

Table 41. Difference Between Measured and Calculated Permanent Deformation (mm)

Section	Mix	Mean Dif.	RMS
1	FMM1	2.7	3.1
2	FLM	4.7	5.1
3	FLH1	2.8	3.2
4	FML	0.7	2.5
5	CMM1	6.9	7.4
6	CMH	6.9	7.5
7	CHM	20.0	22.1
8	CLM	5.0	5.5
10	PLH	0.8	1.3
11	PMM2	-0.2	0.8
12	PML	0.2	0.8
14	FHM	-1.5	1.8
15	FMM2	1.7	2.1
16	FLH2	3.1	3.6
17	FMH	1.4	1.7
18	FHL	-0.1	1.0
19	PMM1	-3.5	3.7
20	PMH	-3.1	3.3
22	PLM	2.4	3.0
23	CML	-1.0	1.7
25	CHL	-0.7	2.1

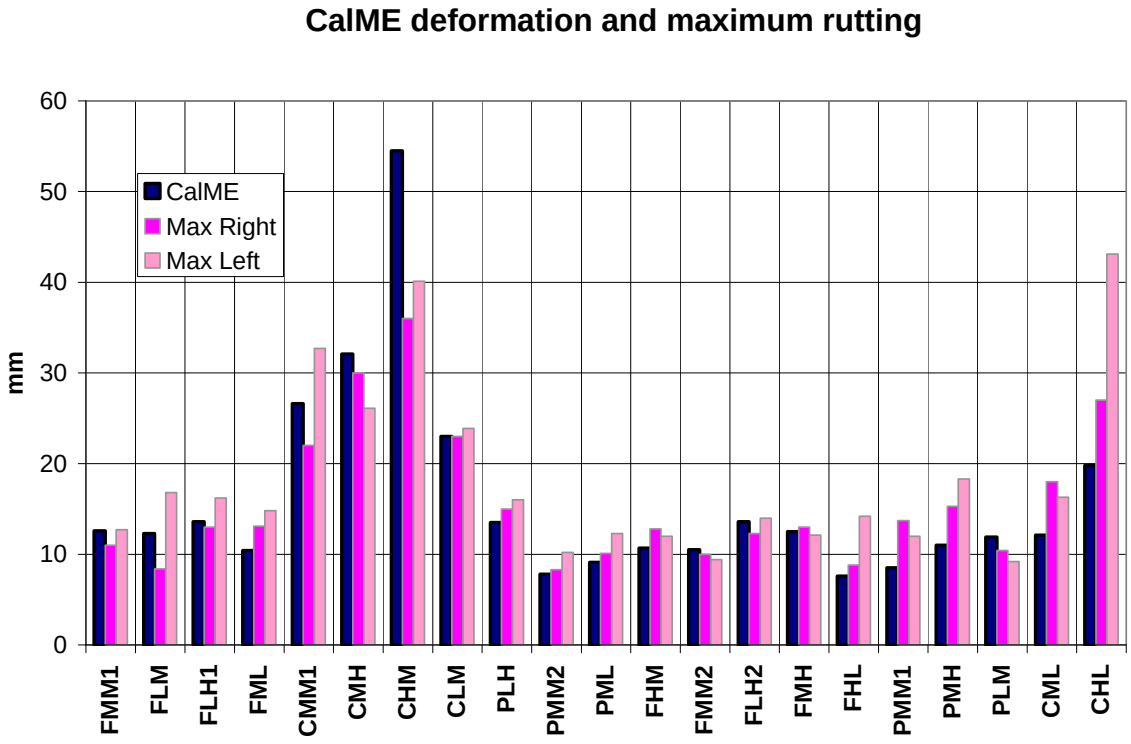

Figure 192. CalME deformation and maximum rutting in right and left wheelpaths.

Figure 192 shows the final permanent deformation calculated by *CalME* (for the right wheelpath) and the maximum rutting recorded for the right and left wheelpaths, which is not necessarily at the end of the experiment. The average values are: *CalME* 15.9 mm, right wheelpath 15.8 mm, and left wheelpath 18.2 mm.

5 References

1. Ullidtz, P., Harvey, J., Tsai, B.-W., and Monismith, C. "Calibration of Incremental-Recursive Flexible Damage Models in CalME Using HVS Experiments." Research Report UCPRC-RR-2005-06, University of California Pavement Research Center, Davis and Berkeley, June, 2006. (FHWA No.: F/CA/RR/2006/49).
2. NCHRP "Guide for Mechanistic-Empirical Design of New and Rehabilitated Pavement Structures." National Cooperative Highway Research Program, Report 1-37A, March 2004. *http://www.trb.org/mepdg/guide.htm*
3. Epps, J., et al, "Recommended Performance-Related Specification for Hot-Mix Asphalt Construction: Results of the WesTrack Project." Report 455, National Cooperative Highway Research Program, Transportation Research Board, Washington, DC, 2002.
4. Monismith, C. L., Deacon, J. A., and Harvey, J. T. "WesTrack: Performance Models for Permanent Deformation and Fatigue." Report to Nichols Consulting Engineers, Chtd., Pavement Research Center, Institute of Transportation Studies, University of California, Berkeley, 2000.
5. Dynatest. http://www.dynatest.com/software/elmod_5.htm. 2005.
6. Barker, W.R., Brabstone, W.N. and Chou, Y.T. "A General System for the Structural Design of Flexible Pavements." Proceedings, The Fourth International Conference on the Structural Design of Asphalt Pavements, Ann Arbor 1977.
7. Shook, J. F., Finn, F. N., Witczak, M. W., and Monismith, C.L. "Thickness Design of Asphalt Pavements – The Asphalt Institute Method." Proceedings of the 5th International Conference on the Structural Design of Asphalt Pavements, Vol. 1, Delft, 1982, pp. 17–43.
8. Tsai, B.-W., Harvey, J. T., and Monismith, C. L. "WesTrack Fatigue Performance Prediction Using Miner's Law." Transportation Research Record: Journal of the Transportation Research Board, No. 1809, TRB, National Research Council, Washington, D.C., 2002, pp. 137–147.
9. Larson, G. and B. Dempsey. EICM Software. Enhanced Integrated Climatic Model Version 3.0 (EICM). Urbana, Illinois: University of Illinois. 2003.
10. Witczak, M.W. and Fonseca, O.A. "Revised Predictive Model for Dynamic (Complex) Modulus of Asphalt Mixtures." Transportation Research Record 1540, Transportation Research Board, 1996.
11. Harvey, J., Guada, I., Monismith, C., Bejarano, M., and F. Long, "Repeated Simple Shear Test for Mix Design: A Summary of Recent Field and Accelerated Pavement Test Experience in California," International Society for Asphalt Pavements, 9th International Conference, Copenhagen, Denmark, 17-22 August, 2002, Volume I, Paper 1:7-7.
12. Deacon, J. A, Harvey, J. T., Guada, I., Popescu, L., and Monismith, C.L. "Analytically Based Approach to Rutting Prediction," Transportation Research Record 1806, Washington D.C., 2002.
13. Ullidtz, P. "Simple Model for Pavement Damage." Transportation Research Record, Journal of the Transportation Research Board, No. 1905, TRB, National Academies, Washington, D.C., 2005, pp. 128–137.

6 Appendix: Parameter Values Used in the Simulations

6.1 Modulus of DGAC as a Function of Temperature and Loading Time

The modulus of intact asphalt is determined from:

$$\log(E_i) = \delta + \frac{\alpha}{1 + \exp(\beta + \gamma \log(tr))}$$

$$tr = lt \times \left(\frac{visc_{ref}}{visc} \right)^{aT}$$

$$\log(\log(visc\, cPoise)) = A + VTS * \log(t_K)$$

The values of A = 10.0406 and VTS = -3.68 were used for all sections. t_K is temperature in ºK. $visc_{ref}$ is the viscosity at the reference temperature. The reference loading time was lt = 0.015 sec. The reference modulus is in MPa. The reference temperature was 15.4ºC.

6.1.1 Fine Mix

Projectname	δ	β	γ	aT	Reference Modulus
Wes01FMM1	2	-0.6908	0.6908	1.3	6613
Wes02FLM	2	-0.8289	0.5526	1.3	6215
Wes03FLH1	2	-0.6908	0.6908	1.3	4637
Wes04FML	2	-1.0362	0.6908	1.3	7745
Wes14FHM	2	-1.0362	0.6908	1.3	7745
Wes15FMM2	2	-1.0362	0.6908	1.3	6563
Wes16FLH2	2	-0.8842	0.5526	1.3	5470
Wes17FMH	2	-0.6447	0.6447	1.3	5264
Wes18FHL	2	-0.8842	0.5526	1.3	7328

6.1.2 Coarse Mix

Projectname	δ	β	γ	aT	Reference Modulus
Wes06CMH	2	-0.8059	0.8059	1.3	5319
Wes05CMM1	2	-0.8059	0.8059	1.3	5918
Wes07CHM	2	-0.6447	0.6447	1.3	7032
Wes08CLM	2	-0.4145	0.4145	1.3	4811
Wes23CML	2	-0.9786	0.5756	1.3	8870
Wes24CMM2	2	-1.2894	0.8059	1.3	6162
Wes25CHL	2	-1.2894	0.8059	1.3	7601
Wes26CLH	2	-1.2434	0.6708	1.3	5076

6.1.3 Fine Plus Mix

Projectname	δ	β	γ	aT	Reference Modulus
Wes09PHL2	2	-1.2434	0.8059	1.3	9634
Wes10PLH	2	-1.2089	0.8059	1.3	3889
Wes11PMM2	2	-0.921	0.4605	1.3	5521
Wes12PML	2	-0.921	0.5756	1.3	8128
Wes13PHM	2	-1.2664	0.5756	1.3	6733
Wes19PMM1	2	-1.0362	0.6908	1.3	7745
Wes20PMH	2	-1.0362	0.6908	1.3	5359
Wes21PHL1	2	-1.0362	0.6908	1.3	8910
Wes22PLM	2	-1.0362	0.6908	1.3	7745

6.2 Hardening/Aging of DGAC

The modulus after d days, $E(d)$, is found from:

$$E(d1) = E(d0) \times \frac{AgeA \times \ln(d1) + AgeB}{AgeA \times \ln(d0) + AgeB}$$

6.2.1 Fine Mix

Projectname	AgeA	AgeB
Wes01FMM1	0.2770	-0.6354
Wes02FLM	0.1912	-0.1279
Wes03FLH1	0.3840	-1.2656
Wes04FML	0.2792	-0.6471
Wes14FHM	0.2885	-0.7021
Wes15FMM2	0.2657	-0.5502
Wes16FLH2	0.3458	-1.0401
Wes17FMH	0.3497	-1.0632
Wes18FHL	0.1120	0.3391

6.2.2 Coarse Mix

Projectname	AgeA	AgeB
Wes05CMM1	0.1703	-0.0048
Wes06CMH	0.3135	-0.8493
Wes07CHM	0.1963	-0.1582
Wes08CLM	0.0592	0.6509
Wes23CML	0.0000	1.0000
Wes24CMM2	0.1181	0.3034
Wes25CHL	0.3033	-0.7892
Wes26CLH	0.1962	-0.1573

6.2.3 Fine Plus Mix

Projectname	AgeA	AgeB
Wes09PHL2	0.1752	-0.0339
Wes10PLH	0.3074	-0.8138
Wes11PMM2	0.2008	-0.1848
Wes12PML	0.1792	-0.0576
Wes13PHM	0.2010	-0.1856
Wes19PMM1	0.2369	-0.3979
Wes20PMH	0.3284	-0.9378
Wes21PHL1	0.3196	-0.8855
Wes22PLM	0.2568	-0.5151

6.3 Moduli of Unbound Layers

For the aggregate base the modulus is a function of the stiffness of the asphalt, calculated from:

$$E_{AB} = E_{ref} \times \left(1 - \left[1 - \frac{S}{3500^3}\right] \times Stiffness\ \ factor\right)$$

$$S = h_{AC}^3 \times E_{AC}$$

E2 is the modulus of the aggregate base and E3 the modulus of the subgrade. Moduli are in MPa.

Projectname	E2.Modulus	Stiffness Factor	E3.Modulus
Wes01FMM1	210	0.65	70
Wes02FLM	184	0.42	70
Wes03FLH1	158	0.60	69
Wes04FML	228	0.47	82
Wes05CMM1	211	0.47	82
Wes06CMH	106	0.00	55
Wes07CHM	202	0.52	61
Wes08CLM	104	0.00	57
Wes09PHL2	150	0.58	68
Wes10PLH	178	0.43	70
Wes11PMM2	170	0.61	79
Wes12PML	190	0.65	75
Wes13PHM	178	0.57	70
Wes14FHM	176	0.40	95
Wes15FMM2	151	0.43	89
Wes16FLH2	129	0.43	77
Wes17FMH	142	0.64	75
Wes18FHL	286	0.57	100
Wes19PMM1	150	0.49	88
Wes20PMH	110	0.50	75
Wes21PHL1	175	0.46	89
Wes22PLM	170	0.64	94
Wes23CML	164	0.56	67
Wes24CMM2	112	0.45	57
Wes25CHL	173	0.43	76
Wes26CLH	98	0.17	56

6.4 Damage Function for DGAC

The modulus of damaged the asphalt is determined from:

$$\log(E) = \delta + \frac{\alpha \times (1-\omega)}{1+\exp(\beta+\gamma\log(tr))}$$

$$\omega = A \times MN^{\alpha} \times \left(\frac{\mu\varepsilon}{200\ \mu strain}\right)^{\beta} \times \left(\frac{E}{3000\,MPa}\right)^{\gamma} \times \left(\frac{E_i}{3000\,MPa}\right)^{\delta}$$

MN is the number of load applications in millions.

6.4.1 Fine Mix

Projectname	A	α	β	γ	δ
Wes01FMM1	0.3253	0.4872	2.0678	1.0339	0.4161
Wes02FLM	0.1047	0.4470	2.2666	1.1333	0.3817
Wes03FLH1	0.6447	0.5289	2.1371	1.0685	0.4517
Wes04FML	0.1170	0.4746	2.8603	1.4301	0.4053
Wes14FHM	0.1677	0.4010	1.6609	0.8305	0.3424
Wes15FMM2	0.2117	0.4436	1.9107	0.9554	0.3788
Wes16FLH2	0.3825	0.4738	2.0600	1.0300	0.4046
Wes17FMH	0.2350	0.4481	1.9743	0.9871	0.3826
Wes18FHL	0.0812	0.4741	2.0304	1.0452	0.4049

6.4.2 Coarse Mix

Projectname	A	α	β	γ	δ
Wes06CMH	0.1407	0.4493	2.5804	1.2902	0.3837
Wes05CMM1	0.1202	0.4293	2.0215	1.1075	0.3666
Wes07CHM	0.0508	0.5901	3.6182	1.8091	0.5045
Wes08CLM	0.0393	0.4726	2.4236	1.2118	0.4036
Wes23CML	0.0289	0.4847	2.6027	1.3013	0.4139
Wes24CMM2	0.0354	0.6175	3.8604	1.9302	0.5273
Wes25CHL	0.0821	0.3367	1.2840	0.6420	0.2876
Wes26CLH	0.1202	0.5818	3.1148	1.5574	0.4968

6.4.3 Fine Plus Mix

Projectname	A	α	β	γ	δ
Wes09PHL2	0.0530	0.4899	2.4289	1.2144	0.4184
Wes10PLH	0.4675	0.4886	1.7461	0.8731	0.4172
Wes11PMM2	0.0987	0.5406	2.4804	1.2404	0.4616
Wes12PML	0.0983	0.4614	2.1221	1.0606	0.3941
Wes13PHM	0.1763	0.4471	1.7853	0.8926	0.3818
Wes19PMM1	0.1293	0.5252	2.8116	1.4058	0.4485
Wes20PMH	0.1909	0.4366	2.0895	1.0448	0.3728
Wes21PHL1	0.0498	0.4781	2.7813	1.3906	0.4083
Wes22PLM	0.1378	0.4667	2.2338	1.1169	0.3985

6.5 Permanent Deformation of DGAC

The permanent deformation (down rut) of the DGAC is calculated from:

$$rd_{AC}\ mm = \sum_{i=1}^{3} K \times h_i \times A \times MN^{\alpha} \exp\left(\frac{\beta \times \tau}{resp_{ref}}\right) \times \left(\gamma_i^e\right)^{\gamma}$$

$$\gamma_i^e = \frac{\tau}{2 \times G_i}$$

h_i is the thickness of layer i in mm, MN is the number of load applications in millions, τ is the shear stress at the edge of a tire and a depth of 50 mm, and G_i is the shear modulus of layer i. The DGAC layer is subdivided into three layers with thicknesses from top to bottom of 25 mm, 50 mm, and 25 mm (no permanent deformation is attributed to depths larger than 100 mm).

The constant β was 1.03, γ was 1, and $resp_{ref}$ was 0.1 MPa.

6.5.1 Fine Mix

Projectname	$K \times A$	α
Wes01FMM1	11.02	0.1350
Wes02FLM	12.59	0.1430
Wes03FLH1	10.90	0.0958
Wes04FML	11.92	0.0460
Wes14FHM	11.38	0.1434
Wes15FMM2	9.79	0.1508
Wes16FLH2	13.66	0.1322
Wes17FMH	9.31	0.1269
Wes18FHL	12.02	0.1890

6.5.2 Coarse Mix

Projectname	$K \times A$	α
Wes05CMM1	41.11	0.215
Wes06CMH	42.48	0.237
Wes07CHM	124.54	0.315
Wes08CLM	31.82	0.224
Wes23CML	13.32	0.196
Wes25CHL	51.91	0.275

6.5.3 Fine Plus Mix

Projectname	$K \times A$	α
Wes10PLH	9.805	0.1116
Wes11PMM2	5.778	0.1383
Wes12PML	12.440	0.2254
Wes19PMM1	5.916	0.1006
Wes20PMH	7.606	0.1052
Wes22PLM	13.300	0.2262

6.6 Permanent Deformation of Unbound Layers

The permanent deformation of the unbound layers were calculated from:

$$dp\ mm = A \times MN^{\alpha} \times \left(\frac{\mu\varepsilon}{1000\ \mu strain} \right)^{\beta} \times \left(\frac{E}{40\ MPa} \right)^{\gamma}$$

A was 0.8 mm for aggregate base and 1.1 mm for subgrade. α = 0.333, β = 1.333, and γ = 0.333 were used for both layers.